Development of a Novel Hybrid Field and Zone Fire Model

Daniel John Burton

August 2011

School of Computing and Mathematical Science,

The University of Greenwich,

Park Row,

Greenwich SE10 9LS

DECLARATION

I certify that this work has not been accepted in substance for any degree, and is not concurrently being submitted for any degree other than that of Doctor of Philosophy (PhD) being studied at the University of Greenwich. I also declare that this work is the result of my own investigations except where otherwise identified by references and that I have not plagiarised the work of others.

_____

Daniel Burton

_____

Dr Angus Grandison (First Supervisor)

_____

Dr Mayur Patel (Second Supervisor)

ACKNOWLEDGEMENTS

Research is what I'm doing when I don't know what I'm doing.

~Wernher Von Braun

ABSTRACT

This thesis describes the design and implementation of a novel hybrid field/zone fire model, linking a fire field model to a zone model. This novel concept was implemented using SMARTFIRE (a fire field model produced at the University of Greenwich) and two different zone models (CFAST which is produced by NIST and FSEG-ZONE which has been produced by the author during the course of this work). The intention of the hybrid model is to reduce the amount of computation incurred in using field models to simulate multi-compartment geometries, and it will be implemented to allow users to employ the zone component without having to make further technical considerations, in line with the existing paradigm of the SMARTFIRE suite.

 In using the hybrid model only the most important or complex parts of the geometry are fully modelled using the field model. Other suitable and less important parts of the geometry are modelled using the zone model. From the field model's perspective the zone model is represented as an accurate pressure boundary condition. From the zone model's perspective the energy and mass fluxes crossing the interface between the models are seen as point sources.

The models are fully coupled and iterate towards a solution ensuring both global conservation along with conservation between the regions of different computational method. By using this approach a significant proportion of the computational cells can be replaced by a relatively simple zone model, saving computational time. The hybrid model can be used in a wide range of situations but will be especially applicable to large geometries, such as hotels, prisons, factories or ships, where the domain size typically proves to be extremely computationally expensive for treatment using a field model. The capability to model such geometries without the associated mesh overheads

could eventually permit simulations to be run in 'faster-real-time', allowing the spread of fire and effluents to be modelled, along with a close coupling with evacuation software, to provide a tool not just for research objectives, but to allow real time incident management in emergency situations.

Initial 'proof of concept' work began with the development of one way coupling regimes to demonstrate that a valid link between models could allow communication and conservation of the respective variables. This was extended to a two-way coupling regime using the CFAST zone model and results of this implementation are presented. Fundamental differences between the SMARTFIRE and CFAST models resulted in the development of the FSEG-ZONE model to address several issues; this implementation and numerous results are discussed at length. Finally, several additions were made to the FSEG-ZONE model that are necessary for an accurate consideration of fire simulations.

The test cases presented in this thesis show that a good agreement with full-field results can be obtained through use of the hybrid model, while the reduction in computational time realised is approximately equivalent to the percentage of domain cells that are replaced by the zone calculations of the hybrid model.

CONTENTS

TABLES AND FIGURES

'step' temperature profile.

seconds.

approaches.

seconds.

1. Introduction

1.1 The need for a hybrid model

In the United Kingdom, fire caused 328 recorded fatalities during the period between April 2009 and March 2010, with 8,500 non fatal casualties [DCLG2010]. The economic cost of fire during 2008, in England alone, has been estimated at £8.3 billion [DCLG2011]. Worldwide, it has been suggested that every year an occurrence of 7-8 million fires cause 80,000 deaths and 500,000-800,000 injuries [Brushlinsky2006]. The very nature of fire implies that these injuries and costs are arguably quite preventable. Regulation attempts to improve these statistics through the prevention of fire incidence and spread (material and construction standards) and by attempting to improve the outcome of fire occurrence through prescriptive methods (building and fire alarm/protection codes). Such regulations will naturally depend on an existing level of knowledge of the numerous factors that can affect such situations, but evidence and data to support these decisions are not easily obtained.

The destructive nature of fire means that post-occurrence determination of the cause of a fire is often an extremely difficult task to perform. Such information also gives little indication of the intermediate dynamics involved between ignition and the final outcome, and fire experiments performed to gain a deeper understanding of these dynamics are prohibitively expensive to carry out. Fire modelling has been developed to address these issues, and to allow a greater understanding of fire and its effects to be gained. These models have increased in complexity with the progression of technology and

the increase in available computational resources and there are two methodologies in widespread use today, zone modelling and field modelling.

Zone modelling has the longer history of the two approaches since the significant simplifications made in its formulation were suited to the limited resources available in early computing systems, but despite these simplifications it has been demonstrated that the results obtained from zone model simulations can have a commendable level of accuracy, depending on the intended use of the results (as long as the assumptions of the zone model remain valid in the respective application area). Zone models have also been developed over time to include additional considerations, such as species concentrations and radiation, which further increase their applicability. Still, as computing power increased so did the opportunity to utilize the more complex field models which directly address the physics of fluid flows, as opposed to the zone model's empirical understanding in simple compartments, therefore providing considerably more accurate results along with a deeper understanding of the dynamics involved.

Since their conception, fire field models have been extensively developed to include further phenomena and considerations that improve their accuracy and applicability, whilst simultaneously increasing the complexity of the physics models involved . In combination with the large types of cases that require simulation, for example ships and hotels, this complexity means that field modelling still requires computational resources that can prove inhibitive to most potential users of such models. The most restrictive factor is the time required to run such simulations with repeat experiments, such as those involved in parametric testing, likely to be unfeasible. It has also been suggested [Esmaeilz.2011] that G.H. Moore's famous law, which has been verified over the last fifty years and predicts a doubling in computing power (number of transistors) every two years, is likely to be invalidated in the near future as power supply issues (be they processor fabrication issues, frequency limitations, excessive heat dissipation etc.) become more apparent at ever smaller scales. Parallel and/or multicore implementations can mitigate some

of these limitations although such treatments are not trivial in a CFD environment.

It is therefore important to focus a portion of the research performed in the area to methods of optimising the performance of field models to maximise their intended use, as sources of understanding of fire situations. In this manner the hybrid field/zone fire model discussed in this thesis provides a method of reducing the computational requirements of fire simulations whilst maintaining the level of accuracy and understanding gained by allowing the continued use of the field model, ensuring that such a methodology can remain at the forefront of technology.

1.2 Research Questions

The context of the present work and the main research questions relate to the connection of field and zone codes in a single model, whether this is possible, whether it is valid to do so, and whether it can provide speed ups in computational time. This leads to further questions,

- Why is speed so important? – As with any piece of software, low execution time is naturally a favorable quality, but fast performance has benefits above and beyond convenience for fire engineering. The research side of fire science would benefit from the numerous runs and parametric-testing that a faster simulations capability could offer. Commercially, users would be less tempted to choose possibly invalidating simplifications to case setups for the sake of timely runs. Also "super-real-time" speedups with coupled CFD/evacuation software will become a possibility, allowing for incidence management in emergency situations.
- How will the speed up be obtained? – The hybrid model will allow the replacement of suitably simple portions of the CFD domain using an equivalent zone model. Because the zone model has an almost negligible run time in comparison to the CFD model, this should result

in a reduction in time equal to that previously required by the replaced compartment. It is therefore important that the hybrid model makes a minimum of additional requirements on the solution regime to realise such speed-ups.

- What will be the magnitude of the speed-up? – As mentioned above, the speed-up will be closely related to the proportion of the compartments being replaced with the zone model. In reality there are many inter-related factors that will affect this time, but a reasonable expectation for an efficient hybrid model would be a speed-up close to the proportion of domain, on a cell basis, that is being replaced.

- What rooms will be suitable for treatment with the zone model? – Future modifications are a possibility, but the assumptions of zone models are generally applicable to rooms of constant cross sectional area (normal to vertical). Further model considerations that are dependent on room surfaces, such as radiation and convective cooling, will tend to limit the applicability to cuboid rooms. Additionally, the absence of momentum and intra-room flows means that there is a limit on the aspect-ratio of compartments at which the instant layer assumption of zone models becomes invalid; this is most obvious for corridors which will experience a progressively longitudinal layer as time goes on. It is questionable if the zone model will be applicable to rooms beyond these fundamental shapes, although more complex geometries, such as L-shaped rooms, may be addressable through the use of multiple adjacent zones.

- How will the hybrid model be used? – The advantage of combining a zone model with the existing SMARTFIRE field model is that use can be made of knowledge and tools that are previously available. The hybrid model should be implemented in such a way that any extra consideration required of an end-user is minimized. Due to the nature of the zone model, the addition of these compartments to the simulation geometry should be at least as simple as the corresponding CFD compartment. The final hybrid model should also not be seen as a isolated modelling paradigm, but should be seen as a possible optimization that can be used in addition to other modelling

techniques. A foreseeable use of the hybrid model would be in a dynamic sense, where a CFD compartment can be converted to a zone compartment mid-simulation, and can revert back to full CFD treatment, if conditions dictate the need.

- What are the specifics of the implementation? – There are numerous considerations to be made over the specifics of the implementation itself, such as
  - o How are the models joined?
  - o Where are the models joined?
  - o How do they communicate?
  - o How are they coupled/iterated/solved?

Along with questions of the results obtained,

  - o Do they display good agreement with a full-field simulation?
  - o Can any discrepancies be explained by the simplifications being made?
  - o Is the expected speed-up being realised?
  - o Are the results provided by the hybrid model of sufficient quality when taking into account the reduction computational time obtained?

These questions are discussed further in the relevant sections of the thesis.

1.3 Structure of the thesis

Chapter 2 – Background and Literature review

The fundamentals of both field and zone fire modelling are discussed, highlighting both the advantages and disadvantages of the different methodologies. The case for the hybrid model is put forward and previous and related work performed in this area is examined and reviewed.

Chapter 3 - Zone and Field Fire Modelling

The zone and field models are discussed in detail with a derivation of the equations used and implementation specifics.

Chapter 4 – Hybrid Fire Model

The hybrid model is discussed in detail, looking at the reasons for its use along with the expected limits of its performance. The hybrid model is formulated and the details of its implementation are laid out.

Chapter 5 – CFAST/SMARTFIRE Hybrid Model

Initial work focussed on the development of a hybrid model combining the CFAST zone model with the SMARTFIRE field model. The specific details of the implementation are discussed and two test cases are examined.

Chapter 6 – FSEG-ZONE/SMARTIRE Hybrid Model

The reasons behind the need for a custom zone model, FSEG-ZONE, are discussed. The details behind the formulation of the new model are laid out along with the implementation specifics. Various cases are examined to test both the performance and validity of the new model.

Chapter 7 – Extending the FSEG-ZONE model

The basic FSEG-ZONE model discussed in chapter 6 is extended to include various phenomena of interest in a fire situation. The additional model capabilities are demonstrated through several test cases of interest.

Chapter 8 – Conclusions and Further Work

Conclusions are drawn on the results presented in this thesis. Further avenues of model extension and improvement are discussed.

2. Background and Literature Review

2.1 CFD modelling

Computational Fluid Dynamics models attempt to model the physics of fluid flow through a discretisation of the problem domain, and in general consider the Navier-Stokes set of equations [Patankar1980] along with various modifications and additions allowing for the inclusion of phenomena such as turbulence and radiation. Milne-Thomson reports that initial forays into CFD modelling using a much simpler equation set were made over 80 years ago [Milne1973], but understandably were extremely limited in their application due to the extremely limited computing power available at that time.

The partial differential equations defining the variables of interest cannot in general be solved analytically, but must instead be solved numerically by discretisation [Patankar1980]. Discretisation leads to the creation of a number, thousands to perhaps many millions, of computational control volumes or cells to represent the solution within the computational domain. The discretisation process creates a large number of cells and, for explicit formulations, a large amount of iterations are required to achieve a converged solution for each time step of the calculation; in turn many time steps are required to solve whole transient problems.

Due to the above requirements to ensure converged and stable solutions, CFD models make high requirements on computational resources [Chow1995]. The

values of certain quantities are required for each of these volumes which places a requirement on the amount of memory (RAM) available to the model, also the solution procedure results in the consideration of sizeable matrices which places an even greater requirement on the processing power of the machine [Galea1989]. Considerations such as turbulence require much finer meshes and therefore many times more available memory for an accurate treatment [Boris1992]; this is especially true for trans/super-sonic flows although such regimes are generally not necessary in fire field models. Model extensions such as radiation that are not strictly part of the Navier-Stokes set, but are solved in parallel with them, can potentially add a great deal of extra computation tothe basic model unless various optimizations are made [Hostikka2006]. Despite this, thermal radiation can become a dominant form of heat transfer in real fires and therefore its inclusion is important in order for the model to provide results that are in reasonable agreement with reality. Various radiation models exist, with those that provide more accurate results tending to be more computationally expensive.

The use of CFD modelling for simulating fires began over 25 years ago [Rosten1983] [Markatos1984] [Chow1995] [Cox1995] [Jia1997] [Rubini1997] [McGrattan2001] and has become increasingly popular, having been used extensively over the years in modelling a large catalogue of fire situations [SIMCox1992] [Yan2001] [Luo1994] [Luo1996] [Wang2001] [Jia2006] [Yeoh2003] [Liu2002] [Gutierrez 2009] [Abanto2007] allowing greater insight into the fire dynamics involved than afforded by earlier models. As with CFD in general, a disadvantage with its use in fire modelling is the time necessary to run the models [Chow1995], and there are a number of potential ways of reducing runtimes for CFD based fire simulations. Parallel Processing has been applied to fire modelling to reduce run times [Grandison2003] [Grandison2007], and although these have been successful many engineers may not have access to more than a single computer. Despite this, newer machines are based on dual/quad core architectures and a method of parallelisation is possible in this framework (this is also applicable to graphical processor units (GPUs) that can have many hundreds of cores). Another methodology for reducing runtime is to make use of group solvers

[Hurst2004]; in combining cells/regions into logical groups, it is possible to significantly reduce computational requirements by setting solver criteria on a group by group basis. In this way, regions requiring less computation can be lowered in priority, allowing computational effort to be focused as required. A further method of reducing runtimes which is discussed in this thesis is through the implementation of a hybrid field/zone model where segments of the CFD domain are replaced by the zone model with the aim of achieving a significant speed up in the solution procedure.

Of great importance in fluid dynamics is the role turbulence plays both in transport/mixing and energy transfer [Versteeg2007]. Turbulence is present in practically all fluid flows of interest to an engineer, and therefore its inclusion in a CFD model is imperative. The nature of turbulence, with its random fluctuations (or at least seemingly random) and its occurrence over many time and length scales and in three dimensions, results in great difficulties when attempting to model it. Short of performing a direct numerical solution which requires a very high resolution of cell size, which is generally unfeasible for all but the smallest cases, a deterministic representation is not an option. As is common with phenomena of a stochastic nature, turbulence can be addressed by considering an average fluid velocity, along with corresponding deviations from this mean. Work on scientifically accounting for turbulence began in the 19th century when Reynolds first proposed this idea of considering the motion of a fluid to be composed of mean and relative (random) components [Reynolds1894].

Since the second component is random, its cumulative effect is zero, and therefore it is valid to consider the mean component of the motion. Substituting this 'two-part' representation of the velocity into the Navier-Stokes equations results in a new set of equations which, despite being very similar to the original system, includes a number of new unknown terms [Wilcox1994]. These terms are referred to as Reynolds stresses, in recognition of his original work in this area, and are properties of the flow itself as opposed to the more familiar viscous stresses that depend on the viscosity of

the fluid. These Reynolds stresses are present in the momentum equation of the mean flow, therefore the turbulent fluctuations, despite being random and summing to zero, actually affect the mean flow and cause it to be different to the corresponding flow were turbulence not accounted for. The existence of the Reynolds stresses means that the number of unknowns in the system exceeds the number of equations, and the majority of work performed in the area of turbulence modelling is concerned with determining these unknown values.

One method of addressing these unknowns is the 'two-equation' $k - \epsilon$ model [Wilcox1994], which is implemented in SMARTFIRE. Use is made of the method first suggested by Boussinesq [Boussinesq1877] of regarding the transfer of momentum caused by the Reynolds stresses to be caused by an 'eddy-viscosity', similar in nature to the usual viscous stresses. Doing so allows transport equations for the turbulent kinetic energy k and dissipation rate ϵ to be formed, and these are solved along with the remainder of the Navier-Stokes system.

Another method of separating the velocity components is by directly resolving the larger scales of turbulence as far as the cell resolution dictates, while again relying on an 'eddy-viscosity' representation to model the remaining smaller scale motions. Such methods are referred to as Large Eddy Simulations (LES), and are based on work originally performed by Smagorinsky in 1963 [McGrattan1998]. The LES method has been found to perform better than the two-equation methods so long as a sufficiently refined resolution is used [Emmerich1998], yet such requirements will tend to significantly increase the computational overheads of a model.

The simulation of fire brings with it extra considerations which may be of significant interest to the fire engineer. The simplest of these is the transport of gaseous species, either the fundamental fuel, oxidant and product concentrations, or the more specific toxic species released through combustion and pyrolysis, such as carbon monoxide, hydrochloric acid or hydrogen

cyanide. Generally it is these species that represent the greatest danger to building occupants [Babrauskas1991][Babrauskas1995], as opposed to direct damage from heat, and since the fundamental aims of performing fire simulations are to assess building design safety, or retrospective examination of previous cases, the consideration of these threats is paramount to a full analysis.

By the nature of the Navier-Stokes equations, the transport of these species is almost a trivial matter, especially if simplifying assumptions are made that allow a basic mass or volume fraction treatment to be used. The difficulty then of including such phenomena is the actual creation of such species, in modelling the chemical and physical processes that result in the model source terms [Pitts1995][Purser2003]. The accurate treatment is limited by the mesh and time-steps used by the model, since the actual reactions can happen on length and time scales significantly smaller than those considered [YWFW2005]. There are of course methods of simplifying procedures such as assuming infinitely fast one step chemistry thereby allowing the use of a mixture fraction [Xue2001][Chen2011][Wang2007][Yeoh1995]. Although this method can provide accurate results of simple fuel/oxidant/product concentrations it prevents any detailed consideration of the formation of other species, soot production or flame extinction. The mixture fraction concept has been extended to allow the modelling of these factors [Floyd2009] yet this still remains a significant simplification over the actual chemistry involved. Much more advanced models of combustion have been developed [Lecocq2011] [Wade2004] yet such complications add greatly to the already prohibitive costs of using a CFD model, especially in the relatively large domain of interest to a fire engineer.

For this reason many CFD models allow fires to be represented by a simple heat (enthalpy) source, neglecting combustion altogether. Despite this such simulations have provided acceptable results when compared to data obtained from actual compartment fire experiments [Kerrison1994][Kerrison1994b][Wang2001]. Clearly, despite the improved

accuracy provided by the more complex models a compromise between precision and computational requirements is a very real consideration when performing fire simulations. The development of more complex models is a necessary occurrence since situations will exist that are simply not open to treatment by the simpler methods, e.g. cases where the combustion chemistry has a large effect on the flow dynamics or where fire proliferation and suppression are to be modelled [Hadjisoph.2005]. Also, computing power naturally increases over time meaning that such compromises will become redundant since the more complex models will be executed in acceptable time frames. Despite this, a recent paper [Esmaeilz.2011] argues that actual performance increases in the near future are likely to be below that expected from G. E. Moore's famous law [Moo1965] due to difficulties in supplying power to the ever smaller scales involved in transistor and processor development. In this way, complex model additions should obviously never be discounted simply due to their computational requirements since they become increasingly viable as technology progresses, but at the same time model optimisations still need to be researched to ensure that CFD remains useful as a current commercial tool. The work performed by Grandison et al. [Grandison2003][Grandison2007] in developing a parallel implementation of a fire field model has great importance in this regard since distributing the computational requirements over several machines has the potential to circumvent these limitations.

It must be remembered that apart from the rich theory being developed for CFD modelling and its application to fire simulation, outside of a research environment the final product is extremely practical in its nature. The models not only have to perform within realistic timeframes, but the end users must at least have the option to use validated simplifications, rather than potentially making their own to achieve acceptable runtimes; these users come from a wide range of professions and will generally not be well versed in CFD.

2.2 Zone Modelling

Zone modelling was first incepted over 50 years ago with the development of simple single-layer models [Kawagoe1958] [Babrauskas1978] [Quintiere1977]. These were expanded to dual-layer [Thomas1963] [Babrauskas1981] [Pape1981] [McCaffrey1981] and multi compartment models [Tanaka1980] [Jones1985], and have been used to model a number of different scenarios [Nelson1991] [Peacock1993] [Bukowski1996] [Chow1995] [Chow1996] [Dembsey1995] [Lee2010]. Despite its age, zone modelling is still in widespread use today with a vast number of users undaunted by its apparent shortcomings, or with most users simply willing to compromise on these issues for the advantages it brings as a methodology [Spearpoint2003] [Spearpoint2006] [SFPE2010]. The extensive nature of its use can, in part, be attributed to its intrinsic ease of setup and use, meaning that a large number of users which would otherwise need specialist training and/or a sufficiently qualified background can generally pick up such a model and quickly perform fire simulations with validated and trustworthy results without such requirements [SFPE2010]. This extends the zone model's scope of use to those professionals who may not have a scientific or computational background, but who still have an interest in the simulation of fire situations e.g. architects, fire investigators and those involved in regulatory bodies and policy making.

The zone model's ease of setup and use stems from the style of input that the model requires [Peacock2008]; compartments are defined by their three dimensions only (width, height and depth), and in general location and aspect have no bearing on the simulation. Momentum is not solved within a zone model [Jones1992], therefore flow within a room is not accounted for. Connections between rooms are themselves defined similarly but in addition require the declaration of the two rooms that they connect. In this manner the setting up of a building plan often reduces to the case of providing three numbers for the dimensions of each room, and four numbers for each planar connection (two for dimensions and two indicating the rooms being connected); no indication of where rooms are in relation to one another need

be provided. In essence these objects are entirely virtual, with cases that are spatially impossible in three dimensions being valid inputs. Finally fires and heat sources are defined by their heat and species release rates which can be constant, table defined or based on functions such as being proportional to the square of time [Peacock2008]. Considering this, zone model input files generally consist of a series of configuration commands and numbers which all have meaningful physical significance; the only difficulty faced by the user in compiling such a file is found in addressing the particular format that a zone model may use. This difficulty can be entirely circumvented by the provision of a user interface that prompts the user for these values and then proceeds to automatically create the file with the required formatting [Peacock2008].

The underlying assumption of zone models is that a room can be divided into a number of distinct horizontal zones or layers, and the temperature, density and other attributes (e.g. product concentrations) are assumed to be uniform within each layer at any point in time i.e. the layers are fully mixed. In a large amount of experimental data, gases within rooms in a fire situation have been seen to stratify into these distinct layers[Peacock1993][Jones2001], and while these values are rarely in reality uniform the variations through the layer, compared with those between the layers, are small enough to be assumed negligible. Due to the foremost stratification taking place between the existing ambient 'cold' air and the fire affected 'hot' gases, a two layer zone model is in general seen to be a valid assumption allowing the capture of sufficiently accurate transient data; an accepted error of ten percent in the height of the interface between the two layers is commonly quoted [Steckler1982] [Quintiere1984][Jones2009]. The variables for these layers are calculated from sets of ordinary differential equations derived from conservation equations of mass and energy, in turn ensuring physically realistic results. The particular choice of differential equations used is a central difference between the various zone models that are available. These disparities exist to address numerical issues such as convergence speed and stability of the solvers used; the final results obtained should of course be the same regardless of the equation set being considered.

This zone methodology can in theory be applied to a building design with any number of different cuboid shaped rooms and interconnections (horizontal portals between same floor rooms, vertical portals connecting rooms above and below each other, or virtual venting systems which can connect any two rooms regardless of their proximity), and each room can in turn be connected to the external section of the domain which is usually taken to be the 'outside' in similar ways. The handling of these connections between the rooms and any interactions that may occur are governed by the movements of mass, energy and species through these portals, with species fluxes being dependent on the flow of gases between the rooms. The modelling of the flow is open to different treatments, but in general the flow through a section of the interface will depend on the pressure differential existing at that point, along with the densities of the gases either side; usually this equates to a power law between the flow velocity and pressure differentials with the most popular representation being Bernoulli's principle which pertains to the square root case [Emmons1989].

As mentioned above, zone models do not solve a momentum equation of any kind and therefore do not address fluid flow or convection (the flow calculated at the interface between rooms is merely an average flux acting on a plane in space that satisfies a balance as opposed to representing the actual flow across a doorway). It is also the case, that due to the lack of spatial variation in compartments, diffusion is largely absent. There is no scope for diffusion within layers due to their assumed uniformity, the single place where diffusion can be addressed is at the interfaces between uniform objects, i.e. where layers meet walls, ceilings, floors and each other, but once again the quantity calculated will be an averaged value across the entire interface and is therefore limited in its accuracy. As a consequence of zone models lacking any handling of convection, and being severely limited in their treatment of diffusion, any physical phenomena that rely on these transport forces are not simulated by the basic zone model assumptions; it is at this point that the disadvantages of the zone methodology become apparent.

Of principle interest in fire simulations is the transient development of conditions within the domain. Further analyses, such as structural failure or safe egress times, rely on being able to accurately provide solutions at various points in time as opposed to finding the steady 'equilibrium' state. Transient variations are inextricably linked to spatial variations in time, and to neglect these would be to deny a large portion of the fire modelling subject matter. Phenomena such as corridor creep, where hot gases entering a corridor do not instantly form a layer covering its entire length but do so gradually over time, can be the governing conditions that dictate the results in large sections of the domain.

Zone models do make provisions for these phenomena, but because the data required for an accurate representation isn't calculated they make use of empirical relations that have been developed through experimental work [Jones2001]; examples include complex empirical equations that attempt to model turbulent shedding as the plume rises from a fire source, or treatment of corridor creep through empirical relations over floor area and roots of temperature ratios [Jones2009]. Obviously the scope of experiments is severely limited due to costs and resources, and can never realistically address the huge variation of possible room sizes and layouts. As an example, a common coefficient is the constriction coefficient [Jones2009] which attempts to address the resistance caused by the shape and size of an orifice on flow passing through it. This coefficient is present in most relationships that depend on such flows and the value assigned to it is usually found by averaging the results gained from numerous experiments; for this reason these empirical coefficients apply to no cases in particular, introducing them may introduce significant errors before the simulation even begins.

Despite these problems zone models continue to be popular with models such as CFAST [Jones2009] and BRANZFIRE [Wade2004] still in widespread use. Work is continuously being done to improve the empirical sections of the models, both by providing a choice of relations to use depending on situation, and by bringing phenomena previously unaccounted for within the scope of

the model. Advanced models such as CFAST have been developed to include phenomena such as corridor flow, shaft flow, ceiling jets, radiation models, combustion species concentrations, sprinkler systems, mechanical venting with filtration and simplified momentum consideration[Jones1992]; inclusions that mean zone modelling remain pertinent to fire science almost 40 years after its inception.

2.3 Hybrid Modelling

A limited body of work has previously been published on the development of hybrid fire models. In 1991 Xu et al. [Xu1991] developed a hybrid field and zone model (HFAZM) to simulate smoke transport in a single storey, multi-room building. (It should be noted that the consideration of smoke in the models discussed herein is not made as an individual species, but is limited to simply defining the zone upper-layer to be a smoke-layer; in this way the presence of smoke and hot gases are equivalent.) Additionally, Xu et al. only considered two dimensional field compartments, but the HFAZM model was extended to consider three dimensions by Wang and Fan in 1996 [Wang1996].

Around the same time as the first HFAZM model, Fan et al. [Fan1992] developed a hybrid field-zone-network (FZN) model. The numerics of the FZN model were further developed by Fan & Wang (field model PDEs) [Fan1997] and Yao et al. (zone model ODEs) [Yao1999] who in 1999 improved the solution routine of the zone portion of the model through basing it on a volume correction method. Since modern computing power is more than sufficient with regards to zone modelling, whether an additional network component in a hybrid field-zone model is currently of any benefit is questionable. Network models are one dimensional in nature and lack the layers that make the zone model applicable to fire situations. Still, network models can indeed be useful in situations where the assumption of totally mixed compartments is valid. One interesting factor of network models is that their formulation and assumptions allow a simple conservation of momentum to be considered [Colella2010], although the validity of this is

restricted to the simple 'block-flow' that results from the absence of variation between locations due to vertical displacement. The above conservation is also questionable where connecting vents between locations are smaller than the cross-sectional area, e.g. doorways in walls, and whether it remains applicable at the interface with higher resolution models is uncertain. Despite these issues there is certainly potential to consider a corresponding treatment within the hybrid zone model, see chapter 8.

For field and zone models, Yao et al. [Yao1999] suggested that specifying boundary conditions at a doorway, the natural interface between models, was a very difficult task. They circumvented this issue by actually extending the field model a short distance into the zone compartment, 'establishing a free boundary condition' [Yao1999]. The paper itself is more concerned with performing some basic verification of the FZN model than validating against other data. The first test case considers a field modelled fire room, connected to the exterior through a corridor, which is modelled using three individual zone sections. The results are compared to data gained from an experiment performed for the same setup, although the range of temperatures observed are fairly low (maximum experimental temperature was approximately 40°C). The basic trends are captured, such as progressive heating of the successive zone sections of the corridor, yet quantitatively the results are not favourable. Considering the low temperatures throughout the domain, the average error between model temperatures (~8°C) is significant. Yao et al. attribute this to the fact that the FZN model does not include heat transfer between the gas and walls, which is likely to cause an appreciable difference. Despite the layer height being an important quantity in zone modelling no comparisons are made in the test cases and the 2nd test case simply reports the FZN model data from a larger geometry without making any comparisons; the authors acknowledge the 'verification' nature of the paper along with the need for further comparisons with experimental results, and the inclusion of additional phenomena (e.g. radiation, combustion) in the model. Verification refers to the evaluation of whether the model has been implemented correctly, in line with the intent of the developers, this is in comparison to validation, in which the performance of the final (verified)

model is judged in relation to a benchmark; in the case of fire simulations this bench mark is physical reality, and validation refers to the capability of the model to represent this physical reality.

Most recently Hua et al. [Hua2005] developed a hybrid model based on the HFAZM model. The solution of the zone portion of the model was again improved, this time being based on a pressure correction method. The previous volume correction was re-cast in terms of the actual mass fluxes which in turn depend on the pressure distributions in neighbouring zone compartments. This resulted in a system of equations in terms of the new pressure correction, with the aim of improving the numerics of the solution routine, and Hua et al. were able to model the interface between field and zone models along the actual doorway. The paper also claimed to be the first instance of considering two field modelled compartments separated by a zone domain, along with being the first to consider a two-storey geometry, although this should follow a consistent treatment of hydrostatic pressure between models.

The first test case in Hua et al. is similar to the first case seen in Yao et al. where a field modelled fire room is connected to the exterior by a zone corridor, with Hua et al. using four zone segments to span this section; again, the level of comparisons is limited. The field modelled fire room is compared between full field and hybrid models, although this is done in a purely visual manner. Hua et al. state that there is good agreement, but of concern is a stark contrast between the flow dynamics seen in the two rooms. In the full field simulation it appears as though the fire plume contains turbulent motions with visible vortices; in contrast the hybrid fire room contains a laminar plume. It is apparent towards the end of the paper that this is because the full-field simulation is not performed by the hybrid model (by only considering field compartments), but has been performed using a third party code (Fluent). This suggests that the hybrid model developed by Hua et al. considers two modelling methodologies combined in a single hybrid model, as opposed to the alternative hybrid possibility where the aim is to combine

two separate and individual models. The difference is subtle, yet the former type circumvents some inherent issues of the latter involving consistency between the models (e.g. solver employed, step size, coupling, variable units).

The comparisons made are for layer height alone, and for the full field case this value is obtained by noticing that the largest gradient in temperature occurs at approximately 60°C and that therefore any gas hotter than this forms part of the upper layer. Despite this fairly subjective criterion, the hybrid model does appear to agree well with the full field results, although the resolution of this field data is unexpected considering its visual basis. Hua et al. find that the results towards the end of the simulation, where pseudo-steady state is reached, provide the best comparisons.

The second test case simply extends the first to consider two storeys, where a second field compartment is used to model a shaft compartment that connects two zone corridors on different floors (fire room/1st floor corridor/shaft/second floor corridor/exterior). No comparisons are made for this case, with the hybrid results simply being presented in isolation. The authors comment favourably on the delay seen in a layer developing in the zone corridor segments on the upper floor in comparison to the lower corridor, although this is likely to be caused simply by the fluid having to traverse the field modelled shaft.

Hua et al. make the first mention of any speed up realised from the use of a hybrid model, with regards to the first test case. Although the hybrid model was not used to provide any full field results, the timings are in relation to such a simulation since the authors rightly state it would be unfair to compare the hybrid model to a third party code 'from different developers, and run on different computer platforms' [Hua2005]. The timings are reported as less than an hour for a full zone simulation, 3.5 hours for a hybrid simulation, and 20 hours for a full field simulation, resulting in a 82.5% saving for the hybrid model. The paper does not discuss the cell budgets used in the simulations, but on a volume basis the hybrid model removes 8/11 of

the geometry (~73%) which would suggest a super-linear saving (over unity). Here super-linear simply refers to the situation where the percentage improvement in performance (computational time) is observed to exceed that which is expected when based on a preliminary consideration of the savings being made by model adjustments (domain cells); the cause of such an occurrence can be due to many factors, for instance cache effects.

Not directly related to hybrid field-zone fire models are hybrid field-zonal models used in the study of building ventilation [Wang2007]. Despite the expected similarities it seems as if little is to be gained for fire modelling by consideration of these models. The zonal models used are in effect numerous network models since they introduce resolution solely in the horizontal direction, as opposed to the vertical layers of a true fire zone model. A requirement of these zonal models is that at least one zone is connected to another of constant pressure, otherwise the solution of inter-zone flow will be singular [Wang2007]. The constant pressure zone can indeed be the exterior at ambient conditions, yet such a model is naturally unsuitable for the treatment of 'closed' geometries, where a zone(s) may exist in isolation from others and have no direct link to the outside.

Another variation on the hybrid fire model has been suggested by Galaj [Galaj2009], yet again the similarities with a field-zone model are limited. The numerous cells of a field simulation are used, but each cell is considered to be a separate zone with the flows between cells/zones calculated as such. Clearly this is a great simplification since the complex Navier-Stokes equations are avoided, yet whether such a method can provide results significantly better than a zone model, that warrant the extra effort involved, is unknown. Such a model may likely be seen as a 'step back' considering the large number of phenomena that CFD has been developed to include. It is reported that the model is still under development.

Finally, some related work has been performed by Colella with the results from previously published papers, along with additional developments,

collected and reported in a PhD thesis [Colella2010] where he develops a hybrid field-network model for use in the simulation of tunnel fires. Due to the dimensions of tunnels (lengths can be measured in km), CFD modelling proves to be much more inhibitive than in standard 'compartment' fire cases. Still, the sheer length of these structures means that flows have ample time to mix, or at least become somewhat steady, and therefore the use of a simple network model can be valid in sections situated some distance from the fire source. Regardless, the single values of pressure and temperature reported by a network 'node' can be a significant limitation and will fail to represent in an accurate manner any situation with variation not in the longitudinal direction.

Essentially the work considers three varieties of simulation: steady ventilation flows, steady fire flows and time dependent (transient) fire flows. For the first situation, where a fan provides the source of ventilation, the hybrid field-network model provides reasonable results against a full CFD simulation, although the size of field domain required as a percentage of the tunnel needs to be relatively high (300m of a 1.5km tunnel) to achieve acceptable errors (~1%). The comparisons are made for two tunnel types, both circular and flat bottomed profiles, with the modelling performing better for the circular type. The time taken by the hybrid model is claimed to be two orders of magnitude less than a full CFD simulation (a 99% saving despite only replacing 66% of the domain) yet no actual values are reported.

For the steady fire flow situation the field domain is also relatively large (400m of a 1.2km tunnel), yet more critical is the necessity of performing preliminary simulations over a range of configurations to ascertain a suitable value. For field domains less than 200m long, deviations of 25% in temperature and 40% in velocity are observed compared to a full field simulation. As to be expected, accurate results appear harder to achieve for larger fire (heat) sources. The full CFD simulations are reported to take between 48 and 72 hours, with the hybrid simulations taking between 2- 4 hours (a 96% saving in time compared to replacing just 66% of the domain.

Finally, for a transient fire situation the same tunnel has been used as in the previous case, therefore the previous analysis of field domain length has been used to decide on a 300m long field domain (since the author notes that good results have been observed for hybrid interfaces placed 20 times the tunnel diameter away from the fire source, or 150m; the total size is 300m since the field domain is centred on the fire). The hybrid field-network model appears to capture realistic transient results, yet unfortunately no comparisons are made with a full CFD simulation. Additionally, because of this, no comparisons in run times can be made, with the author mentioning that this would be unfeasible considering that such full field simulations take in the region of three months to complete. The model developed by Colella is certainly of interest in tunnel modelling, but despite the significant, almost unrealistic savings in time, such a model is unlikely to perform well in general room fire situations since the flow variations will fail to reach a significantly uniform level for valid use of the network model. In compartment fires the zone model rooms still need to provide an accurate representation since their close proximity to the fire means their effect will be more critical than the simple pressure node values provided by a network model in a tunnel setting.

3. Zone and Field Fire Models

3.1 Zone Modelling

Despite all the drawbacks of zone models, there is one simple reason above all others why they are still in widespread use today, even in circles that have the resources required to run the more advanced models, and this is their sheer speed. With zone models taking mere seconds to complete all but the largest simulations, it is generally true that more time is spent on initial setup than in obtaining the results from the computation. The low requirement on computational power stems from the fact that the model is based on a set of ordinary differential equations that are relatively simple to solve. The size of the solution vector to be calculated is proportional to the number of compartments in the simulation; the factor being the number of variables being solved. In basic simulations without species concentrations, this vector can have as little as $6r$ elements, r being the number of rooms, and the interdependency between the majority of these variables is generally quite small. For example, the initial ODEs are known to be stiff with regard to pressure, meaning that small changes in this variable can have a large destabilizing effect on the solution; however, layer temperature and density variations have a comparatively gentle effect on numerical stability, with large differences being comfortably handled. Also, as most pairs of rooms are generally unconnected, the corresponding variables tend to have a reduced impact on each other due to them not being in direct contact, further promoting stability of the solution. Due to these properties and with a small enough time step the solution of these equations can be performed explicitly, i.e. by using the last calculated values for variables rather than attempting to solve them all simultaneously at the same point in time through iteration. In

this way the solver can step forward in time over these small time steps without having to consume resources in iterating the solution for convergence; the use of a solver capable of varying time steps means that as conditions permit the time step can be increased, significantly improving computational time. These qualities mean that the solution of zone models do not require powerful processors or large memory resources for acceptable run times, in fact they can be comfortably utilized by anyone in possession of a personal computer built within the last ten years.

3.1.1 Zone Formulation

Each of the 2 layers has variables as follows (with $i = U$ or L for upper or lower respectively),

$$\text{Mass} - m_i$$

$$\text{Volume} - V_i$$

$$\text{Density} - \rho_i$$

$$\text{Temperature - } T_i$$

the compartment as a whole also has,

$$\text{Pressure - } P$$

making for a total of eleven variables. It's possible to reduce the dimension of the problem to that of four unconstrained variables by using the following seven constraints; remembering that the first three are each used twice, once for each layer:

$$\rho_i = \frac{m_i}{V_i} \tag{3.1.1}$$

$$P = R\rho_i T_i \tag{3.1.2}$$

$$E_i = c_V m_i T_i \tag{3.1.3}$$

$$V = V_U + V_L \tag{3.1.4}$$

where c_V and c_P are the specific heat content of the fluid at constant volume and pressure respectively, and are related by the universal gas constant $R = c_P - c_V$; also used is the ratio of the specific heats, $\gamma = \dfrac{c_P}{c_V}$.

Four further equations are now required to allow calculation of a unique solution, and these are taken from the conservation equations of mass and energy (enthalpy) for the two layers. Because of the nature of the Zone model, where the fire mass release rate is defined by the user, the two mass conservation equations are simply of the form:

$$\frac{dm_i}{dt} = \dot{m}_i \tag{3.1.5}$$

The energy conservation equation comes from the first law of thermodynamics which states that 'the change in internal energy of a system

is equal to the heat added to the system minus the work done by the system.'
The instantaneous heat added to a layer equates to its rate of increase of
enthalpy, $\dot{h}_i$, giving,

$$\frac{dE_i}{dt} = \dot{h}_i - P\frac{dV_i}{dt} \qquad (3.1.6)$$

$$\Rightarrow \quad \frac{dE_i}{dt} + P\frac{dV_i}{dt} = \dot{h}_i \qquad (3.1.7)$$

(where $P\dfrac{dV_i}{dt}$ represents the work done in compressing the volume, i.e. 'force
times distance')

These eleven equations mean it is now possible to find a unique solution to
each problem; one zone model that uses these present equations is called
FIRST [Mitler1987] (originating from the HARVARD V method) but CFAST
[Peacock2008] uses four alternative equations, namely differential equations
for volume, pressure, and the two layer temperatures; these are derived
below.

Pressure equation

Using the initial constraints for layer i,

$$\frac{dE_i}{dt} = \frac{d(c_i m_i T_i)}{dt} = \frac{d(c_V \rho_i V_i T_i)}{dt} = \frac{d(c_V \frac{P}{R} V_i)}{dt} = \frac{c_V}{R} \cdot \frac{d(PV_i)}{dt} \qquad (3.1.8)$$

and on summing the energy equations for both layers,

$$\dot{h}_U + \dot{h}_L = \frac{c_V}{R}\left(\frac{d(PV_U)}{dt} + \frac{d(PV_L)}{dt}\right) + P\left(\frac{dV_U}{dt} + \frac{dV_L}{dt}\right) \qquad (3.1.9)$$

The compartment volume, $V = V_U + V_L$, is constant therefore $\dfrac{dV_U}{dt} = -\dfrac{dV_L}{dt}$, giving:

$$\frac{R}{c_V}\left(\dot{h}_U + \dot{h}_L\right) = V\frac{dP}{dt} \qquad (3.1.10)$$

$$\Rightarrow \frac{dP}{dt} = \left(\frac{1}{V}\right)\left(\frac{c_P}{c_V} - 1\right)\left(\dot{h}_U + \dot{h}_L\right) \qquad (3.1.11)$$

and finally,

$$\frac{dP}{dt} = \left(\frac{\gamma - 1}{V}\right)\left(\dot{h}_U + \dot{h}_L\right) \qquad (3.1.12)$$

Volume equation

Again using the energy equation as for pressure,

$$\frac{c_V}{R} \cdot \frac{d(PV_i)}{dt} + P\frac{dV_i}{dt} = \dot{h_i} \qquad (3.1.13)$$

$$\Rightarrow \frac{d(PV_i)}{dt} + (\gamma - 1).P\frac{dV_i}{dt} = (\gamma - 1)\dot{h_i} \qquad (3.1.14)$$

$$\Rightarrow \left(P\frac{dV_i}{dt} + V_i\frac{dP}{dt} \right) + (\gamma - 1).P\frac{dV_i}{dt} = (\gamma - 1)\dot{h_i} \qquad (3.1.15)$$

$$\Rightarrow V_i\frac{dP}{dt} + \gamma P\frac{dV_i}{dt} = (\gamma - 1)\dot{h_i} \qquad (3.1.16)$$

and finally,

$$\frac{dV_i}{dt} = \frac{1}{\gamma P}\left[(\gamma - 1)\dot{h_i} - V_i\frac{dP}{dt} \right] \qquad (3.1.17)$$

Energy equation

Eliminating the $\dfrac{dV_i}{dt}$ term from the energy equation gives,

$$\frac{dE_i}{dt} + P\left[\frac{1}{P\gamma}\left[(\gamma - 1)\dot{h_i} - V_i\frac{dP}{dt} \right] \right] = \dot{h_i} \qquad (3.1.18)$$

$$\Rightarrow \frac{dE_i}{dt} + \left(1 - \frac{1}{\gamma}\right)\dot{h}_i - \frac{V_i}{\gamma}\cdot\frac{dP}{dt} = \dot{h}_i \tag{3.1.19}$$

and finally,

$$\frac{dE_i}{dt} = \frac{1}{\gamma}\left(\dot{h}_i + V_i\frac{dP}{dt}\right) \tag{3.1.20}$$

Density equation

Using $\rho_i = {m_i}/{V_i}$, the quotient rule $\left({u(t)}/{v(t)}\right)' = {v\dot{u} - u\dot{v}}/{v^2}$, and

$\frac{dV_i}{dt} = \frac{1}{\gamma P}\left[(\gamma - 1)\dot{h}_i - V_i\frac{dP}{dt}\right]$ from above gives,

$$V_i^2\frac{d\rho_i}{dt} = V_i\dot{m}_i - \frac{m_i}{P\gamma}\left((\gamma - 1)\dot{h}_i - V_i\frac{dP}{dt}\right) \tag{3.1.21}$$

$$\Rightarrow V_i\frac{d\rho_i}{dt} = \dot{m}_i - \frac{\rho_i}{R\rho_i T_i\gamma}\left((\gamma - 1)\dot{h}_i - V_i\frac{dP}{dt}\right) \tag{3.1.22}$$

$$\Rightarrow V_i\frac{d\rho_i}{dt} = \dot{m}_i - \frac{\gamma}{RT_i\gamma}\dot{h}_i + \frac{1}{RT_i\gamma}\dot{h}_i + \frac{V_i}{RT_i\gamma}\cdot\frac{dP}{dt} \tag{3.1.23}$$

$$\Rightarrow \frac{d\rho_i}{dt} = \frac{1}{V_i RT_i \gamma}\left(RT_i \gamma \dot{m}_i - \gamma \dot{h}_i + \dot{h}_i + V_i \frac{dP}{dt} \right) \tag{3.1.24}$$

$$\Rightarrow \frac{d\rho_i}{dt} = \frac{(\gamma-1)c_V}{V_i RT_i c_P}\left(\frac{c_P RT_i \dot{m}_i}{c_V(\gamma-1)} - \frac{c_P}{c_V(\gamma-1)}\dot{h}_i + \frac{1}{(\gamma-1)}\dot{h}_i + \frac{V_i}{(\gamma-1)}.\frac{dP}{dt} \right) \tag{3.1.25}$$

Noticing that $R = c_P - c_V \Rightarrow \frac{R}{c_V} = (\gamma - 1)$,

$$\Rightarrow \frac{d\rho_i}{dt} = \frac{1}{V_i T_i c_P}\left(c_P T_i \dot{m}_i - \dot{h}_i + \frac{V_i}{(\gamma-1)}.\frac{dP}{dt} \right) \tag{3.1.26}$$

and finally,

$$\frac{d\rho_i}{dt} = -\frac{1}{c_P V_i T_i}\left(\left(\dot{h}_i - c_P \dot{m}_i T_i\right) - \frac{V_i}{(\gamma-1)}.\frac{dP}{dt} \right) \tag{3.1.27}$$

Temperature equations

Again using the quotient rule and $T_i = \dfrac{P}{R\rho_i}$ gives,

$$\frac{dT_i}{dt} = \frac{d}{dt}\left(\frac{P}{R\rho_i}\right) = \frac{1}{R}\left[\frac{\rho\frac{dP}{dt} - P\frac{d\rho_i}{dt}}{\rho_i^2}\right] \qquad (3.1.28)$$

eliminating $\frac{d\rho_i}{dt}$ by using the previous differential equation gives,

$$\frac{dT_i}{dt} = \frac{1}{R\rho_i^2}\left[\rho_i\frac{dP}{dt} + \frac{P}{c_P T_i V_i}\left(\left(\dot{h}_i - c_P\dot{m}_i T_i\right) - \frac{V_i}{(\gamma-1)}\cdot\frac{dP}{dt}\right)\right] \qquad (3.1.29)$$

$$\Rightarrow \frac{dT_i}{dt} = \frac{1}{R\rho_i^2}\left[\rho_i\frac{dP}{dt} + \frac{R\rho_i T_i}{c_P T_i V_i}\left(\left(\dot{h}_i - c_P\dot{m}_i T_i\right) - \frac{V_i}{(\gamma-1)}\cdot\frac{dP}{dt}\right)\right] \qquad (3.1.30)$$

$$\Rightarrow \frac{dT_i}{dt} = \frac{1}{R\rho_i}\cdot\frac{dP}{dt} + \frac{1}{c_P\rho_i V_i}\left(\left(\dot{h}_i - c_P\dot{m}_i T_i\right) - \frac{V_i}{(\gamma-1)}\cdot\frac{dP}{dt}\right) \qquad (3.1.31)$$

$$\Rightarrow \frac{dT_i}{dt} = \frac{1}{c_P\rho_i V_i}\left(\left(\dot{h}_i - c_P\dot{m}_i T_i\right) + \left(\frac{c_P V_i}{R} - \frac{V_i}{(\gamma-1)}\right)\cdot\frac{dP}{dt}\right) \qquad (3.1.32)$$

and noting that,

$$\frac{c_P}{R} - \frac{1}{(\gamma-1)} = \frac{1}{\left(1-\frac{1}{\gamma}\right)} - \frac{1}{(\gamma-1)} = \frac{\gamma-2+\frac{1}{\gamma}}{\gamma-1-\frac{\gamma}{\gamma}+\frac{1}{\gamma}} = 1$$

finally gives,

$$\frac{dT_i}{dt} = \frac{1}{c_P \rho_i V_i} \left(\left(\dot{h}_i - c_P \dot{m}_i T_i \right) + V_i . \frac{dP}{dt} \right)$$ (3.1.33)

3.1.2 Full zone model equation set

$$\rho_U = \frac{m_U}{V_U} \quad , \quad \rho_L = \frac{m_L}{V_L}$$ (3.1.34)

$$P = R\rho_U T_U \quad , \quad P = R\rho_L T_L$$ (3.1.35)

$$E_U = c_V m_U T_U \quad , \quad E_L = c_V m_L T_L$$ (3.1.36)

$$V = V_U + V_L$$ (3.1.37)

$$\frac{dP}{dt} = \left(\frac{\gamma - 1}{V} \right) \left(\dot{h}_U + \dot{h}_L \right)$$ (3.1.38)

$$\frac{dV_U}{dt} = \frac{1}{\gamma P} \left[(\gamma - 1) \dot{h}_U - V_U \frac{dP}{dt} \right]$$ (3.1.39)

$$\frac{dT_U}{dt} = \frac{1}{c_P \rho_U V_U} \left(\left(\dot{h}_U - c_P \dot{m}_U T_U \right) + V_U \cdot \frac{dP}{dt} \right)$$

(3.1.40)

$$\frac{dT_L}{dt} = \frac{1}{c_P \rho_L V_L} \left(\left(\dot{h}_L - c_P \dot{m}_L T_L \right) + V_L \cdot \frac{dP}{dt} \right)$$

(3.1.41)

3.2 Field Modelling

Field modelling is more mathematically complex than its zone modelling counterpart, and is based on the actual physics of the fluid flow [Patankar1980]. Due to its reduced reliance on empiricism, the range of applicability is generally far greater for the field modelling approach compared to that of the zone model. In fire field modelling, the fluid flow is governed by a set of three-dimensional partial differential equations. This set consists of the continuity equation, the momentum equations in three space dimensions, the energy equation, the user equations for mass and mixture fraction, and the equations for the turbulence model; in this case the k-ε model which incorporates buoyancy modification. These equations are all based on the principle of conservation of various key quantities, the most elementary being the conservation of mass which is discussed below.

3.2.1 Conservation of Mass

Consider the volume in figure 3-1, where attention is focussed on a single direction. This volume is a fixed region of space through which a fluid flows. At any instant in time, fluid may be crossing the faces of the volume which can result in a net change of fluid mass within this region of space.
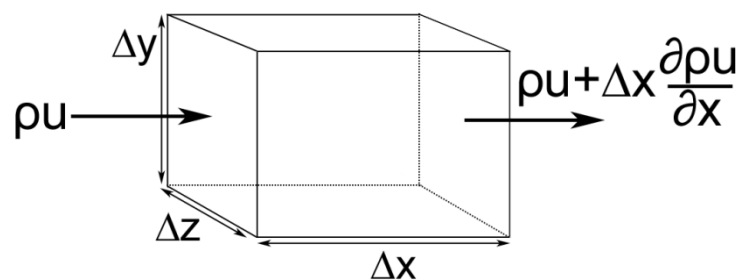
Figure 3-1. Control volume with fluxes at the x-faces.

The fluid crossing the left face is simply the velocity at this face multiplied by the fluid density and the face area, $A\rho u$. This flux is varying in the direction under consideration at a rate $\partial \rho u / \partial x$, and since the faces are separated by a distance Δx, the flux at the right face is $A(\rho u + \Delta x . \partial \rho u / \partial x)$. The net accumulation of mass due to these two faces is then

$$A\left(\rho u - \rho u - \Delta x \frac{\partial \rho u}{\partial x}\right) = -\Delta x \Delta y \Delta z \frac{\partial \rho u}{\partial x} \qquad (3.2.1)$$

Repeating this for the remaining directions, the net change in fluid mass within the volume due to flow across the faces is then

$$-\Delta x \Delta y \Delta z \left(\frac{\partial \rho u}{\partial x} + \frac{\partial \rho v}{\partial y} + \frac{\partial \rho w}{\partial z}\right) = -V\nabla.(\rho \bar{U}) \qquad (3.2.2)$$

Since mass is conserved and can neither be created nor destroyed, this flow across faces is the sole means of changing the mass inside the volume which is increasing at a rate $\partial \rho V / \partial t$, meaning

$$\frac{\partial \rho}{\partial t} + \nabla.(\rho \bar{U}) = 0 \qquad (3.2.3)$$

which is the conservation equation for mass, or the continuity equation. The first term is the transient term, giving the rate of change of a quantity over time. The second term is the convection term which represents changes due to the velocity field of the fluid.

3.2.2 Conservation of a General Variable

For other quantities, excepting mass and momentum – which are handled separately - a further method of transport is possible, i.e. diffusion. If a gradient exists in a scalar fluid variable ϕ, then diffusion will serve to spread this value from areas of higher concentrations – due to particle motions. The efficiency at which this is done will vary according to the quantity under consideration but is proportional to the gradient in question such that the flux across the left face in figure 3-1 due to diffusion will be $-A\Gamma_\phi \, \partial\phi/\partial x$, where Γ_ϕ is the conduction coefficient for ϕ. As for velocity above, the gradient will have changed over a distance Δx such that the net increase in ϕ due to diffusion in the x direction is given by

$$-A\left(\Gamma_\phi \frac{\partial\phi}{\partial x} - \Gamma_\phi \frac{\partial\phi}{\partial x} - \Delta x \frac{\partial}{\partial x}\left(\Gamma_\phi \frac{\partial\phi}{\partial x}\right)\right)$$

$$= \Delta x \Delta y \Delta z \frac{\partial}{\partial x}\left(\Gamma_\phi \frac{\partial\phi}{\partial x}\right) \qquad (3.2.4)$$

Repeating for the remaining directions, the net change in ϕ over the volume due to diffusion will be

$$\Delta x \Delta y \Delta z \left(\frac{\partial}{\partial x}\left(\Gamma_\phi \frac{\partial\phi}{\partial x}\right) + \frac{\partial}{\partial y}\left(\Gamma_\phi \frac{\partial\phi}{\partial y}\right) + \frac{\partial}{\partial z}\left(\Gamma_\phi \frac{\partial\phi}{\partial z}\right)\right)$$

$$= V\nabla.\left(\Gamma_\phi \nabla\phi\right) \qquad (3.2.5)$$

The full governing conservation equation for general variable ϕ can then be written as

$$\frac{\partial \rho \phi}{\partial t} + \nabla. (\rho \overline{U} \phi) = \nabla. (\Gamma_\phi \nabla \phi) + S_\phi \qquad (3.2.6)$$

where the source term S_ϕ represents an opportunity for addition or removal of ϕ over the volume.

3.2.3 The Momentum Equation

The momentum equation is built up by consideration of different forces acting on the volume, such as pressure, viscous forces and gravity. The viscous stresses themselves are unknowns that need to be modelled for a full representation. The Navier-Stokes equations result from the substitution into the momentum equation of a particular representation of the viscous stresses that in turn depend on two viscosities, the dynamic viscosity μ and the second viscosity λ. This results in a considerable number of terms that do not fit satisfactorily in the general conservation equation in (3.2.6). Instead the equation is rearranged to fit the form of the general equation, and the additional terms are lumped into the source term, giving

$$\frac{\partial \rho u_i}{\partial t} + \nabla. (\rho \overline{U} u_i) = \nabla. (\mu \nabla u_i) - \frac{\partial P}{\partial x_i} + S_{u_i} \qquad (3.2.7)$$

3.2.4 The Energy Equation

The energy equation describes the conservation of all types of energy within the volume: thermal energy, kinetic energy and potential energy. The energy is transported by the usual convection and diffusion terms, but now forces performing work on the fluid, as well as the fluid performing its own work, also varies the energy. Similar to the momentum equation, these forces

include the compression due to pressure, surface and volume deformations from the velocities along with the effect of gravity and further considerations.

SMARTFIRE uses the enthalpy form of the energy equation, which has had the kinetic and potential energy components removed such that the value solved for is simply the enthalpy of the fluid, from which the temperature is more easily obtained. The energy equation is again arranged in the form of the general equation with remaining terms included in the source term if required,

$$\frac{\partial \rho h}{\partial t} + \nabla.(\rho \bar{U} h) = \nabla.\left(\left(\frac{k}{C_P} + \frac{\rho v_t}{\sigma_T}\right) \nabla h\right) + S_h \qquad (3.2.8)$$

3.2.5 Turbulence Modelling

Turbulence is an important consideration for any fluid flow, providing significant opportunity for energy and momentum transfer through efficient mixing and variations in effective viscosity. For any general CFD simulation, although especially for the large domains used in fire modelling, available computational resources dictate mesh sizes that are significantly larger than those required to resolve turbulent flow. Methods have been developed to include turbulent properties of flows without having to resort to such prohibitive measures [Wilcox1994], although anything less than a direct numerical simulation will always be an approximation. The majority of methods are based on averaging fluid properties such that the random component is removed, allowing the governing equations to be solved instead for the mean values of the flow. Products of random terms average to non-zero amounts and their effect must still be included through further introduced terms. More advanced methods such as large eddy simulation [Wilcox1994][Emmerich1998] resolve the larger proponents of the turbulent component, but then model the smaller scales that tend to be more uniform in comparison. In this case the governing equations are solved for a filtered

value which has had smaller scales removed, resolving all flows above this level. The smaller scales are then considered through further modelling requirements.

SMARTFIRE uses a two equation averaging technique where extra equations for turbulent kinetic energy k and turbulent dissipation rate ε are solved. These take the form

$$\frac{\partial k}{\partial t} + \nabla.(\rho \bar{U} k) = \nabla.\left(\left(\mu_l + \frac{\rho v_t}{\sigma_k}\right)\nabla k\right) + P + G - \rho\varepsilon \tag{3.2.9}$$

$$\frac{\partial \varepsilon}{\partial t} + \nabla.(\rho \bar{U} \varepsilon) = \nabla.\left(\left(\mu_l + \frac{\rho v_t}{\sigma_\varepsilon}\right)\nabla \varepsilon\right)$$
$$+ \frac{\varepsilon}{k}\left[C_{1,\varepsilon}\left(P + C_3 max(G,0)\right) - C_{2,\varepsilon}\rho\varepsilon\right] \tag{3.2.10}$$

with turbulent production rate

$$P = 2\rho v_t\left[\left(\frac{\partial u}{\partial x}\right)^2 + \left(\frac{\partial v}{\partial y}\right)^2 + \left(\frac{\partial w}{\partial z}\right)^2\right]$$
$$+ \rho v_t\left[\left(\frac{\partial u}{\partial y} + \frac{\partial v}{\partial x}\right)^2 + \left(\frac{\partial u}{\partial z} + \frac{\partial w}{\partial x}\right)^2\right.$$
$$\left. + \left(\frac{\partial w}{\partial y} + \frac{\partial v}{\partial z}\right)^2\right] \tag{3.2.11}$$

and buoyancy modification term

$$G = g\nu_t \frac{\partial \rho}{\partial y} \qquad (3.2.12)$$

The turbulent viscosity is calculated as

$$\nu_t = C_\mu \frac{k^2}{\varepsilon} \qquad (3.2.13)$$

All model constants in the equations above are adjustable, but have default values based on both a considerable amount of empirical research and comparisons with experimental results in many application areas; the default values used in SMARTFIRE are

$$\sigma_k = 1\,, \qquad \sigma_\varepsilon = 1.22\,, \qquad C_{1,\varepsilon} = 1.44, \qquad C_{2,\varepsilon} = 1.92, \qquad C_3 = 1, \qquad C_\mu = 0.09$$

3.2.6 Radiation Modelling

Since radiation can be such a significant transfer mechanism of heat in a fire situation, its inclusion in the model is necessary for an accurate treatment. Different models for the radiation exist with varying complexities, although any models attempting to make a true representation of the nature of radiation add a great deal to the computational requirements of the CFD model. In SMARTFIRE the radiation can be modelled using either a radiosity model, a six-flux radiation model or a multiple-ray radiation model.

Six-Flux Radiation Model

The six flux model only considers fluxes in the axis directions, and because of this the model does not provide an accurate representation of radiation fluxes on specific locations. Despite this its use does allow the energy loss from a fire

source due to radiation to be taken into consideration. Use of the model introduces six further conservation equations,

$$\frac{dI}{dx} = -(\alpha + s)I + \alpha E + \frac{s}{6}(I + J + K + L + M + N) \qquad (3.2.14\text{a})$$

$$\frac{dJ}{dx} = (\alpha + s)J - \alpha E + \frac{s}{6}(I + J + K + L + M + N) \qquad (3.2.14\text{b})$$

$$\frac{dK}{dy} = -(\alpha + s)K + \alpha E + \frac{s}{6}(I + J + K + L + M + N) \qquad (3.2.14\text{c})$$

$$\frac{dL}{dy} = (\alpha + s)L - \alpha E + \frac{s}{6}(I + J + K + L + M + N) \qquad (3.2.14\text{d})$$

$$\frac{dM}{dz} = -(\alpha + s)M + \alpha E + \frac{s}{6}(I + J + K + L + M + N) \qquad (3.2.14\text{e})$$

$$\frac{dN}{dz} = (\alpha + s)N - \alpha E + \frac{s}{6}(I + J + K + L + M + N) \qquad (3.2.14\text{f})$$

with absorption coefficient α, scattering coefficient s and black body equivalent radiosity E. The I, J, K, L, M and N are the radiosities in the six directions, e.g. I corresponds to the positive x direction, and N corresponds to the negative z direction. The contribution to the energy equation is through the use of an additional source term S_{rad}, where

$$S_{rad} = \alpha\big((I - E) + (K - E) + (M - E) + (J - E)$$
$$+ (L - E) + (N - E)\big)$$

(3.2.15)

Multiple-Ray Radiation Model

The multiple-ray model is not confined to axis directions and higher resolution can be attained by increasing the number of rays. In this way the true directionality of radiation can be accounted for, allowing opportunity for advanced phenomena such as flame spread to be modelled. If scattering is neglected, the governing equation is

$$\frac{d}{dl}I(\Omega, \mathrm{r}) = -\alpha I(\Omega, r) + \alpha I_b(r)$$

(3.2.16)

where I is the radiation intensity at position r in direction Ω, l is the path length, α is the absorption coefficient and I_b is the equivalent blackbody radiation intensity. Depending on how many rays are used the 4π steradians of possible angles are divided up between them, with weights assigned to the rays based on this partitioning.

3.2.7 Discretisation of the Conservation Equations

The partial differential equations defining the above quantities generally cannot be solved analytically due to their complexity and interdependence on one another. Instead the domain itself is partitioned into many thousands, if not millions, of control volumes (or cells), within which values are assumed to be uniform. The governing equations are then integrated over these small volumes, leading to a discretised system which is open to solution by certain numerical methods. Clearly, the larger these control volumes are the more of

an approximation the discretisation becomes; conversely, the smaller the volumes the more accurate the solution. Since the governing equations are based on conservation, this is always maintained regardless of the volume size. Despite this errors are introduced through having larger volumes since the infinitesimally true $dy = y' dx$ is no longer the case over finite distances. Higher order schemes can partly address this although the increase in accuracy may not warrant the additional effort.

3.2.7.1 Transient Term

Integrating the transient term over both time and the control volume gives

$$\int_V \int_t^{t+\Delta t} \frac{\partial (\rho \phi)}{\partial t} dt \, dV = [\rho \phi]_t^{t+\Delta t} \int_V dV \qquad (3.2.17)$$

$$\cong V_P \rho_P \, \phi_P - V_P \rho_P^0 \phi_P^0$$

where V_P is the volume of control volume P, and ρ_P and ϕ_P are the density and fluid variable throughout the volume. The first group of terms are the values presently being calculated, for the second group of terms superscript 0 signifies that the values are from the previous time step.

3.2.7.2 Convective Term

Integration of the convective term, and replacement of the volume integral with a surface integral by the divergence theorem gives

$$\int_t^{t+\Delta t} \int_V \nabla . (\rho \overline{U} \phi) dV \, dt = \int_t^{t+\Delta t} \int_S \rho n . (\overline{U} \phi) dS \, dt$$

$$= \Delta t \left[\sum_{faces} A_i \rho_i \phi_i (\bar{u}.n)_i \right] \tag{3.2.18}$$

where the sum is taken over the faces constituting the control volume; A_i, ρ_i and ϕ_i are the area, density and fluid variable respectively at face i; $(\bar{u}.n)_i$ is the dot-product of the velocity and normal to face i; and Δt is the time-step size. Since faces are located between neighbouring control volumes, the values of the corresponding variables at these locations are not immediately clear. One possible method is to assume variables take the value from the control volume at which the flow is originating; this is referred to as the *upwind* scheme. Other choices include taking interpolated values between control volume centres, linear or non-linear, with the particular choice dictated by the discretisation scheme being used.

3.2.7.3 Diffusion Term

Integration of the convective term and replacement of the volume integral with a surface integral by the divergence theorem gives

$$\int_{t}^{t+\Delta t} \int_{V} \nabla.\left(\Gamma_\phi \nabla \phi \right) dV \, dt = \int_{t}^{t+\Delta t} \int_{S} n.\left(\Gamma_\phi \nabla \phi \right) dS \, dt$$

$$= \Delta t \left[\sum_{faces} A_i \Gamma_{\phi,i} \frac{\partial \phi}{\partial x_j} \right] = \Delta t \left[\sum_{faces} A_i \Gamma_{\phi,i} \frac{\phi_n - \phi_P}{d_{nP}} \right] \tag{3.2.19}$$

where $\Gamma_{\phi,i}$ is the conductivity coefficient of ϕ at face i; ϕ_n and ϕ_P are the values at the centre of the neighbouring control volume and volume under consideration respectively, and d_{nP} is the distance between these two locations. The conductivity coefficient at a face can be calculated as

$$\Gamma_{\phi,i} = \frac{\Gamma_{\phi,n}\Gamma_{\phi,P}}{\beta_i\Gamma_{\phi,P} + (1-\beta_i)\Gamma_{\phi,n}} \tag{3.2.20}$$

which corresponds to a harmonic mean of volume values $\Gamma_{\phi,n}$ and $\Gamma_{\phi,P}$, with β_i being the ratio of the distance between face i and centre of volume n to the total distance between volume centres (see figure 3-2).
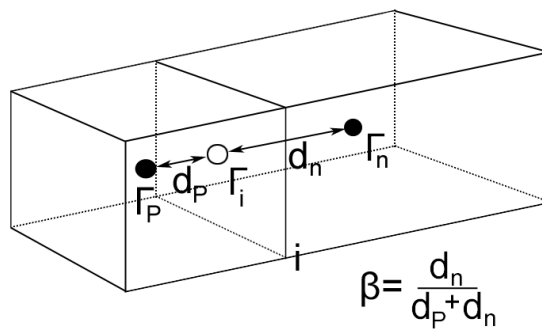
Figure 3-2. Interface conductivity coefficient.

3.2.7.4 Source term

The source term is linearised as follows

$$S_\phi = S_{\phi,C} + S_{\phi,P}\phi_P \tag{3.2.21}$$

where $S_{\phi,C}$ is the 'constant' part of S_ϕ and $S_{\phi,P}$ allows dependence of the source term on the value of ϕ_P; these terms can in turn depend on ϕ_P, allowing representation of non-linear relationships. Integration over the volume and time gives

$$\int_t^{t+\Delta t} \int_V S_{\phi,C} + S_{\phi,P}\phi_P \, dV \, dt = \Delta t V_P\left[S_{\phi,C} + S_{\phi,P}\phi_P\right]$$ (3.2.22)

3.2.7.5 Overall Scheme

$$V_P\rho_P \, \phi_P \; - V_P\rho_P^0\phi_P^0 + \Delta t\left[\sum_{faces} A_i\rho_i\phi_i(\bar{u}.n)_i\right]$$

$$= \Delta t\left[\sum_{faces} A_i\Gamma_{\phi,i}\frac{\phi_n - \phi_P}{d_{nP}}\right] + \Delta t V_P\left[S_{\phi,C} + S_{\phi,P}\phi_P\right]$$ (3.2.23)

$$\frac{V_P\rho_P \, \phi_P \; - V_P\rho_P^0\phi_P^0}{\Delta t}$$
$$= \sum_{faces} A_i\left(\Gamma_{\phi,i}\frac{\phi_n - \phi_P}{d_{nP}} - \rho_i\phi_i(\bar{u}.n)_i\right)$$
$$+ V_P\left[S_{\phi,C} + S_{\phi,P}\phi_P\right]$$ (3.2.24)

The general variables at the faces in the convective term are calculated based on the corresponding difference schemes being used. This results in a representation of the form

$$\phi_i = \alpha_i\phi_P + (1 - \alpha_i)\phi_n$$ (3.2.25)

Rearrangement of terms and grouping with respect to the n neighbouring volumes and 'centre' volume P allows (3.2.23) to be expressed in the following form

$$a_P \phi_P = \sum_n a_n \phi_n + b_P \qquad (3.2.26)$$

with

$$a_n = A_i \left(\frac{\Gamma_{\phi,i}}{d_{nP}} - (1 - \alpha_i)\rho_i(\bar{u}.n)_i \right) \qquad (3.2.27)$$

$$a_P = A_i \left(\frac{\Gamma_{\phi,i}}{d_{nP}} + \alpha_i \rho_i(\bar{u}.n)_i \right) + a_P^0 \rho_P - S_{\phi,P} V_P \qquad (3.2.28)$$

$$a_P^0 = \frac{V_P}{\Delta t} \qquad (3.2.29)$$

$$b_P = S_{\phi,C} V_P + a_P^0 \rho_P^0 \phi_P^0 \qquad (3.2.30)$$

As mentioned in section 3.3.6.2, one way of evaluating the density at the faces, ρ_i, is to assume upwind values where $\rho_i = \rho_P$ if the flow across the face is outwards from volume P, and $\rho_i = \rho_n$ if the flow is into the volume, from neighbour volume n. The remaining face variables also have to be evaluated by choosing values for the α_i terms corresponding to the scheme used.

3.2.8 Solution of the Discretised System

Consideration of equation 3.2.26 over all the control volumes to which the domain has been partitioned leads to a matrix equation of the form

$$A\bar{\phi} = \bar{b}$$

Vector b contains all terms that have been incorporated into the source term, such as the actual linearised source term or 'old' portions of the transient terms. Vector ϕ is composed of the values to solved for all volumes in the domain, i.e. the individual ϕ_P. The matrix A then contains all a_P and a_n terms, with the former falling on the diagonal, and the latter at corresponding locations either side of the diagonal, in the same row. This leads to a very 'sparse' matrix since the vast majority of elements are zero. For example, a regular decomposition of the domain into n cubes results in matrix rows n elements long of which only 7 are non-zero. The matrix is open to solution through any iterative method, yet the sparsity lends itself well to certain solution techniques that can be taken advantage of.

A solution technique commonly used is the successive over relaxation (SOR) method which iterates the cell values based on the most recently calculated values. In this way a value is updated as follows,

$$\phi_i^{(k+1)} = (1-r)\phi_i^{(k)} \qquad (3.2.31)$$

$$+ \frac{r}{a_P}\left(b_P - \sum_{j>i} a_j \phi_j^{(k)} - \sum_{j<i} a_j \phi_j^{(k+1)} \right)$$

Here the two sums correspond to values that have not been updated yet which must use the previous value $\phi_j^{(k)}$, and those that have been updated

before i, which can therefore use the newly calculated $\phi_j^{(k+1)}$. The relaxation factor allows the magnitude of updates to be controlled, either to prevent potential numerical instabilities $(0 \leq r < 1)$, or to speed up the convergence $(r > 1)$. The over-relaxation of the SOR method is generally reduced in fire CFD cases in favour of under-relaxation [Grandison2003] since the tight coupling between the equations is sensitive to pressure and density changes, requiring the higher numerical stability.

3.2.8.1 SIMPLE

The velocity and pressure fields are tightly coupled, with the pressure gradient appearing explicitly in the momentum equations. If the pressure field is known then a solution to the momentum equations can be found in the general manner, and vice versa. If instead both are unknowns as is the case with general CFD simulations, then the solutions of both must be found in an iterative manner, since changes in one field strongly affect the other. The SMARTFIRE solution procedure is formulated around the SIMPLE procedure outlined in [Patankar1980], which performs the solution in a given order,

1. Make an initial guess at the pressure field, P^*. Initial pressure fields may be everywhere zero, where intermediate fields may assume the last calculated values from the previous step.
2. The momentum equations are solved with regard to the guessed pressure field P^*, resulting in a velocity field comprising u^*, v^* and w^*.
3. Such an intermediate velocity field will result in an error in the continuity equation, corresponding to excess or shortage of mass. These errors are used in the pressure correction equation which is derived from the continuity equation, and gives a value for the pressure correction P' which will cause corresponding corrections to the velocities that address the mass errors.
4. Update the pressure field by the pressure corrections, $P^* \rightarrow P^* + P'$

5. Calculate corresponding u', v' and w' from the velocity correction equations which are derived from the momentum equation and apply the corrections, $u = u^* + u'$, $v = v^* + v'$ and $w = w^* + w'$.

6. The corrected velocity field is then used for the evaluation of the remaining equations.

7. The P^* from step 4 is now used as the initial guess in step 1.

The procedure is repeated until the relevant convergence tolerance is satisfied in the various equations.

3.2.8.2 Velocity correction

During the solution procedure, the SIMPLE pressure and velocity corrections become smaller as convergence is reached, meaning the assumption on which the velocity correction equation is based becomes valid. This assumption removes the effect of neighboring velocity corrections, leaving the velocity correction dependent only on the change in pressure gradient resulting from an applied pressure correction, such that

$$u_i' = \frac{A_i(P_P' - P_n')}{a_n} \qquad (3.2.32)$$

3.2.9 Boundary Conditions

Complete provision of the problem for a fire simulation requires consideration of the values attained by flow variables at boundaries of the domain, and the affect of their inclusion. The boundary conditions in the temporal dimension are satisfied through the use of correct initial conditions, which for most fire situations correspond to an ambient environment. Boundaries such as walls or symmetry patches are characterised by having zero velocity normal to these surfaces, although for wall surfaces there still remains the question of heat transfer. Of most interest to the present work are boundary conditions

for inlets and outlets, the usual representation for doorways, windows or other apertures when the domain does not extend past these openings.

Within SMARTFIRE, the boundary condition for an inlet consists of applied values for the velocities/convections on the faces contacting the boundary, and can therefore model both inflow and outflow regimes. Temperatures are also explicitly assignable on an inlet boundary condition meaning fluids of differing energy can be brought into the CFD domain, allowing representation of conditions other than ambient on the other side of such an inlet. An outlet boundary condition differs in that pressures/pressure-gradients are assigned to the faces as opposed to velocities but again this allows both inflow and outflow to occur, and in the same way as inlets temperatures can also be applied.

Further to values that are explicitly given by the user, the remaining variables must also be considered at the boundary, although treatment depends on the nature of the variable. Some variables are suited to being defined by a fixed value, such as $T_{boundary} = 400K$, or more generally by having their value ascertained in some manner that can vary, i.e. $\phi_{boundary} = f(T)$, with such conditions being referred as Dirichlet boundary conditions. Another way of describing a variable at a boundary is through specifying what value the derivative of the variable takes, i.e. $\frac{\partial \phi}{\partial n} = f(t)$, and such conditions are referred to as Neumann boundary conditions, these including the act of defining variable fluxes at such locations.

Since boundary conditions for inlets and outlets are by their nature approximations of the conditions at such locations, it is imperative that they are handled correctly since they can have a detrimental effect on the remainder of the domain. To reduce this problem, vents defined in SMARTFIRE are not modelled directly by a boundary condition, but instead cause the creation of an extended region of domain which is itself contained in a boundary condition relevant to the situation. In this way the pressure

boundary of an outlet is moved further away from the area of interest, decreasing the potential for it to affect results.

4. Hybrid Fire Model

This chapter discusses the reasoning behind the development of a hybrid field/zone model, along with any relevant issues that require consideration. Since this work describes the development of both SMARTFIRE/CFAST and SMARTFIRE/FSEG-ZONE hybrid models, the present discussion of implementation details will be limited to features that are common to both models. The chapters on the individual models themselves will go into further specific details.

4.1 Purpose of the Hybrid Model

The basic premise of a hybrid model is to combine the use of the two existing models (CFD and zone) to attempt to garner the benefits of each modelling approach, whilst implementing in such a way as to minimize their respective disadvantages. The CFD model would be used in primary compartments where accuracy of results is paramount, such as fire rooms and areas where further analysis requiring high resolution data is to be performed. It would also be used in rooms expected to contain phenomena that could not be accounted for satisfactorily by the zone model, e.g. corridor creep and the failure of gases to stratify in relatively tall volumes. Finally the CFD model would also be used in rooms containing complex flow qualities, such as significant turbulence, curl of the velocity field or anywhere that momentum driven flow is significant (e.g. due to forced/mechanical ventilation) which can have a significant effect on the simulation. The zone model would then be

used in the remaining rooms which still have a considerable impact on the simulation but are not subjected to the same scrutiny as the primary rooms; in full CFD simulations one option for representation of these secondary rooms is to remove them from the simulation by ignoring their existence and simply closing their doors.

Use of the zone model within these rooms would allow conclusions about the conditions within to be made, such as layer height and average temperature, which are extremely useful when performing evacuation modelling and risk analysis. Apart from allowing calculation of these room variables, including the secondary rooms in the simulation allows them to impart an effect on the remainder of the domain. For example, if the door to an empty room which is connected to a corridor with hot gases is suddenly opened, the room in very simplified terms will act as a sink, removing species from the corridor as the gases flow in (whilst simultaneously exchanging air at different temperatures). Removing these rooms from the simulation entirely would mean that this sink effect is never taken into account, resulting in a higher total enthalpy within the domain, along with over estimated temperatures and flows. This sink effect is also non linear in time as the changing conditions within these rooms cause the flows which depend on the cross interface pressure differentials to vary in non trivial ways. These rooms can also reach steady states when net flux becomes zero, at this point they cease to be sinks but still act to redistribute species between the cells on the interface. It is for these reasons that these secondary rooms are not easily accounted for in simple terms, despite their effects on the remainder of the domain appearing straightforward.

Even though a secondary room can have a discernible impact on results, it may still be deemed insignificant to the total flow and simulation being performed. The real strength of the hybrid model would be realised when the case in question contains many such rooms, insignificant in isolation but together having a very large cumulative effect. Environments especially suited to hybrid treatment would be large domains with numerous small

compartments such as those often found in hotels, prisons and maritime vessels. The abundance of rooms would mean their inclusion in the simulation is essential, but their size may not necessitate the accuracy of a field model. Also the increase in domain size by including these rooms within the field model may deem it unviable to do so when the corresponding increase in computational time and resources is taken into account.

When linking SMARTFIRE with CFAST, two independently validated models, any errors or inconsistencies will stem from how the interface is handled, both in the way it is represented within the models themselves and in how calculations and conversions are performed across it. Creation of the custom FSEG-ZONE model provides opportunity for the introduction of further errors and therefore it is paramount that the formulation is developed with care; regardless, it is still the interface that poses the most likely source of inconsistencies. Because the two models effectively have different inputs and outputs, it is a necessity to be able to convert between the different variables required in an accurate manner. The two models are both based on the various conservation equations, and so it is clearly a fundamental requirement that conservation is strictly adhered to over the interface.

4.2 Expectations of the Hybrid Model

The purpose of using a zone model to provide values for use on the boundary condition is clearly an attempt to provide as accurate a representation as possible of the original CFD room. This raises the question of which values are therefore required to simulate such an absent section of the CFD domain. Ideally, the boundary condition should provide all the variables that are considered by an individual CFD cell i.e. each and every variable/differential that is made use of in the CFD equations. The initial problem with this is that the zone model is essentially non-dimensional in that spatial variations are not accounted for further than the difference between layers. Dimensions are accounted for through distances, areas and volumes used in the zone calculations, yet this is done in an abstract fashion on an individual basis for

each occurrence, and where proximity is not an issue. This means that gradients do not exist within the zone model and are therefore not available for use on the boundary condition; it also prevents any treatment of momentum in a fashion that could provide a truly accurate representation of what would occur within the CFD room. The velocities calculated within a zone model find their basis in cross vent pressure differentials between rooms which are naturally one dimensional, this again means that velocity directions other than those normal to the hybrid interface are not considered by the zone model. The actual set of values used on the interface will vary with the hybrid implementation used, but essentially these come down to pressure, temperature and density when considering fluid flow and heat conduction. An extended model considering radiation, combustion and toxic species will also require the zone model to provide values of species mass fractions and fuel/oxidant mixture fraction as well as a representation of radiosity; these are discussed in chapter 7.

A further question of the hybrid model is just how accurate a representation of a CFD compartment is possible through the use of a zone model. Apart from exceptional cases, such as when the zone room may have been highly pressurised by a neighbouring section of the CFD domain which has since cooled down, it is the CFD domain that 'drives' the zone model in the sense that the zone acts simply as a passive accumulation/redistribution opportunity for the CFD flow. For normal cases, a closed zone compartment pressure will always lie somewhere between the minimum and maximum CFD values within the interface cells. The same is essentially true for temperature and density, where conservation, along with the fact that the zone considers average values, means that these values must lie within the extremes attained by the CFD cells on the interface. An open zone compartment that is itself vented to the exterior obviously allows opportunity for any accumulated energy and mass to escape; in this situation the values in the zone room can become less than those in the CFD interface cells, the lower bound then becoming the ambient conditions in the external part of the domain.

These two extremes happen to have a physical significance that can provide some kind of expectation of the limits of performance of the zone model. The first case, where the zone model effectively attains the same values as reported by the CFD cells, corresponds to a symmetry patch which itself is equivalent to a non-conducting wall where CFD flow is prevented from crossing the interface. The second case, where the zone model remains at the ambient values of the exterior, corresponds to an outlet fixed at the ambient pressure and provides no resistance to the CFD flow at the boundary.

In this way, using a hybrid model to replace a CFD compartment with a zone model can be expected to perform better than, and give results somewhere between, the two extreme options of either simply removing the CFD compartment and blocking the door with a wall or, removing the CFD compartment but allowing the door to remain as a vent to the exterior. In SMARTFIRE these extremes would correspond to a wall or outlet boundary patch.

Use of the zone model then becomes a method of trying to obtain the point/set of conditions between these two extremes that best represents the compartment being removed. Another way of looking at this range of conditions is that it monotonically corresponds to a continuous range of room sizes (volumes) from zero to infinity. As a room gets larger the effect of a source/flux gets proportionally less until at the limit of infinite volume the effect becomes zero, corresponding to the exterior which remains at ambient conditions for all time. Conversely, as a room becomes smaller, its resistance to any incoming flow becomes greater as the pressure increases quicker for a given flux; in the limit of a room of zero volume, any flow experiences an instant resistance which prevents it, corresponding in effect to a wall.

In this way, the effect that the inclusion of a zone model will have on the remainder of the CFD domain is fundamentally dependent on its volume. Since the volume is known, it is reasonable to expect a fairly accurate

replication of the effects of a CFD compartment on the remainder of the domain through replacement with a zone model.

Since the interface between the models is fundamentally dependent on the pressure value obtained from the zone model, this area is worthy of further discussion. The value of pressure used on the boundary condition consists of both the room pressure provided from the zone model along with a hydrostatic component. An equivalent neighbouring CFD compartment may have similar room pressure, yet the hydrostatic component will differ in that the continuously varying densities results in a continuous pressure distribution, compared to the two-piece linear profile in the zone model which results from uniform layer densities. This is an inherent weakness of the hybrid model, since no matter how accurate the implementation, the continuous pressure distribution is not representable. Since the flow between models is dictated by this pressure distribution, and that any room development is dependent on these flows, it is reasonable to expect this area to provide opportunity for discrepancy in the results. Conversely, this area will also prove to be a good test of the accuracy of the implementation, since if a two-piece linear pressure distribution can capture the general shape of the corresponding continuous distribution, this would require significant agreement between the remainder of the model terms.

4.3 Hybrid model implementation

This section considers the design and implementation of a novel hybrid field/zone model along with potential issues that need to be addressed. The intention is to combine the two separate models to take advantage of their various benefits whilst minimising the effects of their shortcomings. Use will be made of the CFD model's ability to supply accurate results in all situations, while the zone model's speed will be exploited to greatly reduce computational time in suitable areas of the domain. To achieve this, the field model will be used in regions where accuracy of results is paramount as well as in regions with complex/rapidly changing flow patterns and geometry. The

zone model can then be confidently used in the remaining geometry, which will be well suited to its methods. The focus of attention is the interface between the two models through which data will be passed and iterated, with the mechanism of the interface being invisible to the end user. It is intended that the end result will be a model that appeals to all individuals involved with practical fire engineering to whom time and efficiency are significant issues.

Within the field section of the hybrid model, the interface is modelled as a dynamic fixed pressure and temperature boundary condition, the values for which are obtained from the zone model results. This is performed by enhancing the CFD code's existing treatment of fixed-pressure boundary conditions, by allowing variation of pressure, temperature and density across the interface. Another vital difference centres on the fact that these values are generally varying over the iterations of each time step due to the coupled nature of the implementation whereas existing boundary conditions in the CFD code remain constant throughout these iterations and this has possible implications for the speed of convergence.

Within the zone model the interface is not visible per-se or modelled along with its own inter-compartment connections, but is simply implemented by creating a source/sink term in each layer to represent the net flow between the models. Within the CFAST zone model the internal room connections are in essence represented in a similar fashion, with the calculated doorway fluxes being converted into sources for mass, enthalpy and species to be deposited into their respective layers. A key difference is that CFAST's velocities are based on a simple Bernoulli pressure drop whereas CFD models solve the momentum equation resulting in more accurate fluxes. Theoretically the hybrid interface should perform as good as, if not better than, CFAST's own internal vents.

The pressure for the boundary condition is calculated from a hydrostatic pressure distribution similar to the treatment of pressure within the zone

model itself, and the applied temperatures and densities are calculated based on flow direction and height. When these values are applied on the boundary condition, and the CFD model is run for a single iteration, a flow is calculated across the interface. It is from this flow that the summed values to be communicated back to the zone model are found. At each cell-face lying on the boundary, the mass and enthalpy fluxes across the interface are calculated. These fluxes are grouped depending on which layer of the zone model they are depositing/extracting from, which in turn depends on the height of the current zone interface (layer) height, and are then applied to the appropriate layers as source/sink terms respectively.

In both directions there is an issue of converting the different forms of data the respective models use so that they can interact correctly. The field model provides as many sets of data as there are cells neighbouring the boundary condition in question (typically around 50 – 200 cells), whereas the zone model simply has two sets of values belonging to the upper and lower layers. When communicating data from CFD model to zone model, a simple sum will be used to reduce the resolution of the data to values for each of the two layers.

Passing fluxes from CFD to zone model as opposed to pressure ensures conservation across the interface; if instead pressure was passed from the CFD model, the calculation of fluxes for conversion to layer sources would have to be performed within the zone model itself. Clearly, the zone model calculation for fluxes is fundamentally different to that of the CFD model, and would result in discrepancies between the net flux leaving the CFD domain at the boundary and the net flux being accounted for by the sources within the zone model; this use of two representations of the fluxes would certainly result in the violation of conservation for all species involved.

In the other direction, from zone model to CFD, the difference between the models' calculation of fluxes is also the reason why pressure is passed for use

on the boundary. Since fluxes have to be calculated by at least one model it was a clear choice that the CFD model had to perform this task.

In this direction there is the issue of taking the sparse data of the zone model and applying it to the numerous cells at the interface. Consideration was made as to whether this data should be upscaled by fitting temperature and density profiles; this was ultimately decided against due to the possibility of failing to ensure conservation. Also, it was observed that inflows to the CFD domain generally come from the lower layer of the zone, which realistically has far less variation than the upper layer and room in general.
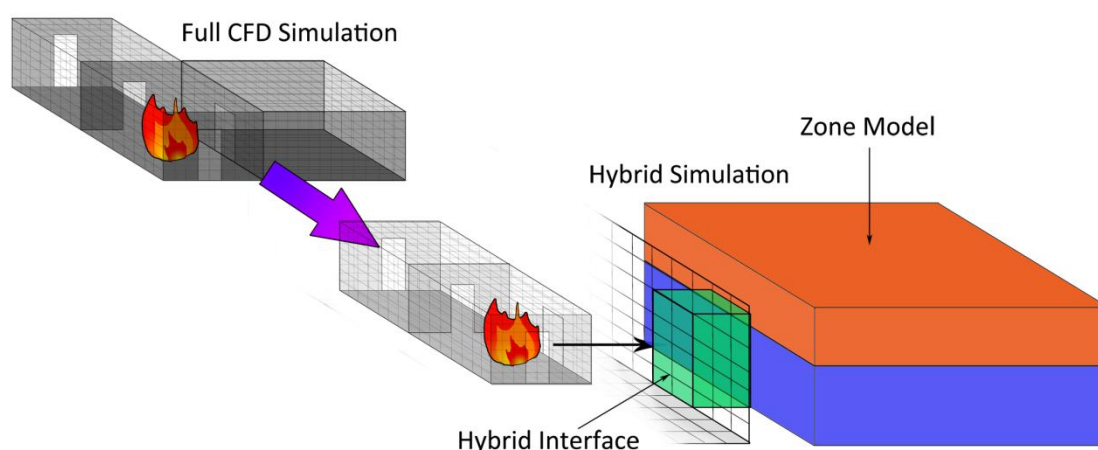
Figure 4-1. Using the Hybrid model to replace a room in a CFD simulation with a zone model

4.3.1 Pressure Boundary Condition

The hybrid interface is represented within the CFD model as a pressure boundary condition having variation in the vertical direction. Along with a value for pressure, accurate treatment of the hybrid interface also requires temperature and density to be declared at the boundary condition. These values are used to address convected quantities for flow entering the CFD domain from the zone model. Diffusion of heat is not considered through the hybrid interface, to ensure conservation this is also disabled in the CFD

model at the interface cell faces. This is unlikely to have any noticeable effect since air is naturally a relatively poor conductor and any diffusive component is likely to be swamped by the convective term.

The value of pressure assigned at any point on this interface consists of four components:

1. <u>The zone compartment floor level pressure (P_{room}) which is the value of pressure solved for within the zone model.</u> This equates to the total pressure within the room due to the enthalpy contained within and this value represents the notion of a room being 'pressurized'. Because the hydrostatic pressure manifests as a reduction with increasing height, this floor pressure is the highest value attained within the room. In this way it forms the basis for comparisons between rooms and differences in this value are the main driving force of flow.

2. <u>A hydrostatic term (P_{static}) representing the variation of pressure with height within the zone model.</u> The zone model lacks any variation in pressure throughout the rooms but the consequences of layers of differing depth, temperature and density need to be accounted for. Due to the absence of momentum and velocities, dynamic pressure is not represented in the zone model and a standard hydrostatic treatment is used. This treatment is extended to the interface.

3. <u>A pressure drop term ($P_{dynamic}$) representing the dynamic variation in pressure, due to flow speed, over the hydrostatic component.</u> The zone model pressure represents a static pressure where flow is assumed to have come to a state of rest; the CFD pressure contains an additional dynamic component depending on the speed of the flow and this needs to be represented at the hybrid interface. This drop term represents the pressure difference observed at a point on a streamline that comes to rest at the zone pressure value. It accounts for the pressure

gradient applying over the length of a streamline and not instantaneously at a point.

4. A pressure normalization term (P_{norm}) addressing the different representation of hydrostatic pressure within SMARTFIRE. Although the nature of hydrostatic pressure is equivalent in both models, the treatment within SMARTFIRE differs slightly in its representation. Because the pressure assigned to the boundary condition is effectively the zone models single means of effect, it is absolutely critical that pressure is handled consistently. For this reason it is required that the hydrostatic component P_{static} is now normalized to a representation equivalent to that within SMARTFIRE.

These four considerations result in the following representation for pressure on the boundary condition,

$$P = P_{room} + P_{static} + P_{dynam} + P_{norm} \tag{4.4.1}$$

with the individual components calculated as follows,

$$P_{room} = P_{zone} \tag{4.4.2}$$

where the value P_{zone} is taken directly from the solved room variable within the zone model;

$$P_{static} = \begin{cases} -g\rho_l h & : h \leq I \\ -g(\rho_l I + \rho_u(h - I)) & : h > I \end{cases} \tag{4.4.3}$$

where g is the acceleration due to gravity, ρ_l and ρ_u the lower layer and upper layer densities respectively, I the layer (interface) height within the zone room, and h being the height of the point on the interface at which the pressure is being calculated, taken to be the midpoint of the cell face being considered;

$$P_{dynam} = -\frac{\rho v^2}{2} \tag{4.4.4}$$

where ρ is the upwind density of the flow at this point and v is the component of velocity normal to the interface; and finally

$$P_{norm} = -2g\rho_{ref}\, h + P_{ref}\,(e^{\frac{g\rho_{ref}\, h}{P_{ref}}} - 1) \tag{4.4.5}$$

where ρ_{ref} and P_{ref} are the reference density and pressure respectively, taken from Smartfire with other variables defined as above.

4.3.2 Temperature and Density

Calculating the values of temperature and density to apply to the boundary condition in the CFD model is a straightforward matter; in contrast to hydrostatic pressure, temperature and density are handled consistently by both models.

Flow from CFD to zone

Due to the convected quantities being calculated from upwind variables, at faces where flow is leaving the CFD domain the values for temperature and pressure are assigned the values from the corresponding cell, i.e.

$$T_{boundary} = T_{cell} \qquad\qquad (4.4.6)$$

$$\rho_{boundary} = \rho_{cell} \qquad\qquad (4.4.7)$$

Flow from zone to CFD

Here the values of temperature and density at a face are taken from the layers in which the flow originates. Flow is assumed to have originated from the layer that shares its vertical displacement, i.e. the layer making contact with the face being considered. It is generally the case that the zone interface (layer) height falls midway along a face, causing both upper and lower layers to be in contact with the row of faces at that height. By using the midpoint of the face as the comparison height, this issue is consistently dealt with by assigning the layer that makes the majority of contact with each face. In this way,

$$T_{boundary} = \begin{cases} T_u & if \quad h > I \\ T_l & if \quad h \leq I \end{cases} \qquad\qquad (4.4.8)$$

$$\rho_{boundary} = \begin{cases} \rho_u & if \quad h > I \\ \rho_l & if \quad h \leq I \end{cases} \qquad\qquad (4.4.9)$$

where T_u and T_l are the upper and lower layer temperatures respectively obtained from the zone model, ρ_u and ρ_l are the upper and lower layer densities respectively, h is the vertical displacement of the midpoint of the face under inspection and I is the zone interface (layer) height.

4.3.3 Zone Model Sources

The calculations of the layer sources representing the interface fluxes within the zone model are relatively straightforward. The flux at each face is considered separately, and is assigned a layer that it is depositing or removing the species from depending on a set of rules. The flow variables are assigned upwind values corresponding to the domain from which the flow originates.

Flow from CFD to Zone

Here flux through a face is assigned the layer it deposits species to depending on the temperature of the flow through that face,

$$Layer = \begin{cases} upper & if & T \geq (T_u + T_{buff}) \\ lower & if & T \leq \quad T_l \end{cases} \qquad (4.4.10)$$

where T is the temperature of the flow, T_u and T_l are the temperatures of the upper and lower layers respectively of the zone compartment, and T_{buff} is a model parameter. The physical significance of this is that hot gases upon entering the zone room will rise due to buoyancy forming part of the upper layer, whereas cold gases will fall to the bottom of the room to become part of the lower layer. The T_{buff} term provides a way of buffering the development of the upper layer until the flow entering is sufficiently hot; one artefact of this is that a newly developed upper layer will seem to jump by T_{buff} degrees at the very beginning, although effects of this are negligible. For temperatures between these two values the flow is split with portions going to both the upper and lower layers as follows,

$$R_l = \frac{T_u - T}{T_u - T_l} \quad , \quad R_u = 1 - R_l \tag{4.4.11}$$

where R_l and R_u are the proportions of flow going to the lower and upper layers respectively. Flow with any temperature above ambient will be subject to buoyant forces upon entering the lower layer and could be assumed to be deposited entirely within the upper layer, although here proportional splitting provides a way of accounting for a portion of the rising hot gases to be assigned to the lower layer. This is realised physically when a portion of a rising plume is shed off due to the turbulent friction between a moving hot flow and static cold layer, or simply by the diffusion that occurs during the time it takes for the hot gases to reach the upper layer.

Once a layer is assigned the flux at a face is calculated using upwind cell values,

$$\dot{m}_i = \rho_i A_i v_i \tag{4.4.12}$$

$$\dot{h}_i = C_P \dot{m}_i T_i \tag{4.4.13}$$

Where $\dot{m}_i$ and $\dot{h}_i$ are the mass and enthalpy fluxes respectively at face i, ρ_i and T_i are the density and temperature within the cell corresponding to face i, A_i is the face area, v_i is the component of velocity normal to the interface, and C_P is the specific heat at constant pressure of the gas.

Flow from Zone to CFD

Here flux through a face is assigned the layer it removes species from depending on its vertical displacement compared to the zone layer height,

$$Layer = \begin{cases} upper & if \quad h_i > I \\ lower & if \quad h_l \leq I \end{cases} \qquad (4.4.14)$$

Where h_i is the height of the flow, taken to be the vertical displacement of the midpoint of face i, and I is the height of the interface in the zone compartment. The physical relationship to this is clear as species are to be removed from the layer at which the flow originates, the layer making contact with the face in question. The fluxes are calculated by simply taking the value of variables corresponding to the assigned layer, i.e.

$$\begin{aligned} \dot{m}_i &= \rho_u A_i v_i \\ \dot{h}_i &= C_P \dot{m}_i T_u \end{aligned} \quad if \quad layer = upper \qquad (4.4.15)$$

and

$$\begin{aligned} \dot{m}_i &= \rho_l A_i v_i \\ \dot{h}_i &= C_P \dot{m}_i T_l \end{aligned} \quad if \quad layer = lower \qquad (4.4.16)$$

where subscript u and l denote values are to be taken from the upper and lower layer respectively.

Forming source terms

Having now calculated the fluxes at each individual face on the interface, the source terms are formed by summing conditionally on the assigned layer to form net fluxes for each species and each layer,

$$\dot{m}_u = \sum_{i:\, layer\, =upper} \dot{m}_i \quad , \quad \dot{h}_u = \sum_{i:\, layer\, =upper} \dot{h}_i \qquad (4.4.17)$$

$$\dot{m}_l = \sum_{i:\, layer\, =lower} \dot{m}_i \quad , \quad \dot{h}_l = \sum_{i:\, layer\, =lower} \dot{h}_i \qquad (4.4.18)$$

4.3.4 Turbulence

The $k\text{-}\varepsilon$ turbulence equations require boundary conditions at the hybrid interface. For flow leaving the CFD domain the method is equivalent to that used within SMARTFIRE for outlets, where the boundary values are set equal to the cell values, i.e.

$$k = k_{cell} \quad , \quad \varepsilon = \varepsilon_{cell} \qquad (4.4.19)$$

For flow entering the CFD domain, the hybrid model uses a method similar to that used within SMARTFIRE for inlets. Modifications were required as values are uniform across an inlet, whereas hybrid interfaces generally report different values at each face on the boundary. The incoming flow at the doorway is first considered to allow the area and an area average value for incoming flow to be calculated. The mid points of the two flow directions are compared to allow estimation of the neutral plane, the height at which flow changes from inwards to outwards. From this the area and perimeter of the incoming flow can be found allowing turbulent kinetic energy and dissipation rate to be calculated by,

$$k = 0.002\bar{v}^2 \quad , \quad \varepsilon = \frac{\sqrt{k.e.^3}}{1.2AP} \qquad (4.4.20)$$

$$\bar{v} = \frac{\sum v_i A_i}{A} \qquad (4.4.21)$$

where k is the turbulent kinetic energy, ε is the dissipation rate, and A and P are the area and perimeter respectively of the incoming flow (see figure 4-2). $\bar{v}$ is taken as the area average of all incoming velocities v_i and corresponding individual face areas A_i.
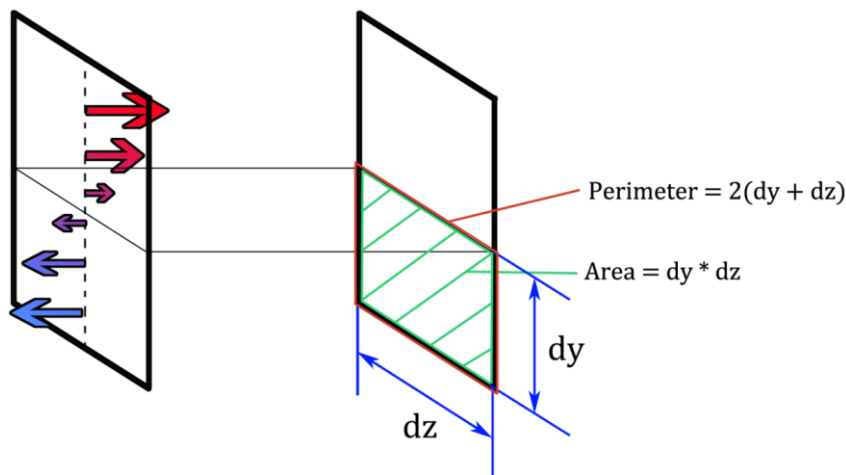
Figure 4-2. Diagram showing area and perimeter of incoming flow (right to left) for turbulence calculation.

4.4 The distinction between open and closed cases

It became apparent whilst testing the first implementations of the hybrid model, that the range of cases deemed suitable to having sections of the domain replaced by a zone model fell into two distinct categories, referred to herein as the 'open' and 'closed' cases. The fundamental difference is that for the open case, the room or section of building being replaced by the zone model has its own vent to the outside; in other words from any point in the

zone domain, it is possible to find a path to the external domain without having to first pass through any section of the CFD domain. The closed case on the other hand is characterised by the zone portion of the domain itself having no vent to the outside; any flow reaching the external domain, or any pressure release required by the zone section, would first have to pass through the hybrid interface into the CFD section. In essence, a domain having a link to the outside manifests itself as an opportunity for pressure release; this is due to the infinite nature of the exterior, meaning that despite net flows in or out the external pressure remains at the reference pressure throughout the simulation.

Ideally, any hybrid implementation should have no need to make such a distinction between the open and closed case, but the requirement stems from a key difference between the two models being used.

CFAST is an explicit model, which means that the formulation is based on the relationship between a particular variable being defined explicitly in terms of known (previous) values of the remaining variables, without consideration of any interdependency or feedback between the variables over the duration of the current time-step. For sufficiently small time-steps, during which the variables change by only small amounts, the explicit formulation is valid since the 'second-order' effects *between* variables tend to be smaller than the primary changes being considered (clearly, some systems fail to have this quality and are not immediately suitable for an explicit formulation). Also of concern to situations of fluid flow is the distance open to traversal by a 'packet' of fluid and whether the mesh used is sufficiently refined to capture such an occurrence; the Courant-Friedrichs-Lewy condition [Courant1928]   concerns such effects and places a mesh dependent requirement on the time-step size. These issues serve to constrain explicit formulations to relatively small time-steps.

SMARTFIRE on the other hand is an implicit model, such that each variable is defined in terms of the other unknown variables that are yet to be

calculated. In effect, this results in all variables being calculated simultaneously, at the same point in time, and therefore takes into account the interdependencies neglected by an explicit formulation. The simultaneous solution of multiple variables is addressed through iteration, where a solution is progressively obtained through repeated calculations. Although further model assumptions do in reality limit the time-step size, implicit formulations can be used over time-step lengths significantly greater than those that are required for explicit treatment.

Within SMARTFIRE the time step can be set to any required value, although convergence becomes an issue for larger time steps, and numerical stability a problem when dealing with steps smaller than 1×10^{-3} seconds due to the magnitude of the transient term; throughout this work the default time step size used within SMARTFIRE has been one second, other sizes are possible although, as is to be expected, larger time-steps generally require more computational effort to achieve the same level of convergence. Although smaller time steps tend to require less resources to converge, the reduction is not proportional to the increase in steps required to get to the same point in the simulation, e.g. the one hundred steps required to get to the one second mark with a 1×10^{-2} time step generally takes a great deal of time longer than the single step taken by a simulation with step size of one second. Due to this an optimum step size(s) will exist, although finding these is not a trivial matter; for the comparatively simple cases encountered in the course of this work the evidence suggest this optimum time step to certainly be larger than 0.1 seconds.

In contrast to this the DDASSL solver (Double-precision Differential Algebraic System Solver) [Brenan1989] within CFAST has, as is common with explicit solvers, a variable time step dependent on the rate of convergence. For steady simulations this step can be as large as a number of seconds, but for rapidly changing conditions, such as those found at the beginning of a simulation, the time step is often observed to be as small as 1×10^{-6} seconds as the solver attempts to address these issues within an

explicit framework. It is worth mentioning that although these larger time steps are possible within the zone model's solver, the tight coupling within the hybrid implementation means values being passed to the zone model are continuously changing, due to this the solver finds itself unable to increase the time step as it would for a full zone simulation.

These differences in step size cause the two types of simulation, namely open and closed, to behave in different manners. Phenomena that are non linear in time are addressed accurately by both models but results arrived at are not strictly equivalent due to the different paths taken. An assumption of both the used methods is that values apply over the length of a step i.e. results are not continuously varying in time but are discrete, with variables remaining constant over a time step. Because of this, phenomena acting on smaller time scales cannot be addressed directly but are taken into account by ensuring balance and conservation at the end of each time step. The higher temporal resolution of the zone model and its step size of $1\,\mathrm{x}\,10^{-6}$ means that these rapid phenomena are modelled more accurately in the sense that the transient behaviour can be better captured than with the linear approximations required by the use of larger time steps; for example, the equalization of pressure takes place at an extremely rapid rate, much quicker than the usual time step size typically used in CFD fire simulations.

As SMARTFIRE only performs a single time step for the thousands being performed by CFAST, the sources being applied within the zone model over these numerous steps remain constant because they are formed from the CFD fluxes. An increase of pressure within the zone room, from one CFAST step to the next, has no way of affecting these fluxes and sources. For the flux between two rooms to remain constant such as this, the pressure difference also needs to remain constant. In effect, passing constant sources is equivalent to telling CFAST that the pressure on the CFD side of the interface is changing at the same rate as the zone pressure. This leads to a feedback problem, with the expected instability and rapidly escalating growth of pressure over CFAST's time steps.

This is not a problem for open cases because the pressure has the ability to 'equalise' to the outside during the zone model time steps. The closed case on the other hand has no opportunity to do so, instead rapidly increasing in pressure until the next CFD time step, by which time the pressure contains a considerable error that only becomes worse as the procedure repeats.

4.5 Data Reduction

An important issue central to evaluating the performance of the hybrid model is the difference in data provided by the field and zone models. The field model provides values for every solved variable on a cell by cell basis, with even relatively small rooms being made up of many thousands of such cells. In comparison the zone model provides only two values for each variable, upper and lower layer versions, along with a layer height and compartment pressure. Although inherently less accurate, the small size of the zone data set is favourable for making comparisons without having to resort to the data visualization necessitated by the high resolution field model data.

The problems with a two layer data set are equivalent to those of zone models in general. For situations with strong stratification of gases, both zone models and the two layer data set provide a good representation of the compartment conditions. In conditions that inhibit stratification, the zone model will fail to capture such dynamics, providing invalid results in the form of a two layer data set. Even in possession of accurate results, the very reduction in data resolution required by a two layer representation will neglect some of the characteristic aspects that define the compartment conditions, greatly reducing the validity of such a method.

A new volume patch has been coded within SMARTFIRE which is set to fill the compartment that the data reduction method is to be used upon. At the end of each time step of the simulation, the methods discussed in this section are performed automatically and the results are printed to a table in an output file. In this way comparisons can be quickly and easily made between

CFD and hybrid results. This method may potentially have further use as a tool for obtaining reduced data that is more representative of the room conditions for export to secondary programs, such as the evacuation software EXODUS [Galea2004].

4.5.1 Layer Reduction

To make comparisons with the zone model possible, it is necessary to reduce the CFD data to an equivalent two layer data set, various methods have been suggested for obtaining such a data reduction. These methods originated for use on data obtained from thermocouple stacks in actual fire experiments and are therefore inherently suitable for application to CFD data due to the similarity between discrete data from probes and the data from individual CFD cells. Weaver [Weaver2000] compares three of these methods in a dual compartment setup for various HRRs and discuses their performances. The first method, termed the 'N% method', was suggested by Cooper et al. [Cooper1982] and calculates the layer height as the point at which the temperature over ambient is N% of the maximum temperature difference in the compartment at that time. Various values of N have been used although Cooper et al. found a value of 10% performed the best. The choice of N is clearly arbitrary, and even if the layer height was indeed related in some way to the maximum temperature variation, the relationship would be highly non-linear and certainly not remain constant.

The main problem with calculating a layer height for CFD data is what the layer actually signifies. For a zone model the layer is well defined since mass and enthalpy are added and removed from specific layers, allowing the total mass and energy of a layer to be known at every point of a simulation. The layer height is then simply the location at which these known layers find a balance within the compartment with regards to their individual volumes. In a CFD simulation such a distinction is not possible as fluid is not apportioned to layers as the simulation progresses; the layer is calculated retrospectively and therefore is open to interpretation.

The second method examined by Weaver [Weaver2000] is the maximum-slope method, and was suggested by Emmons [Emmons1989]. It locates the layer interface at the height at which the rate of change in temperature is greatest, see figure 4-3 below.
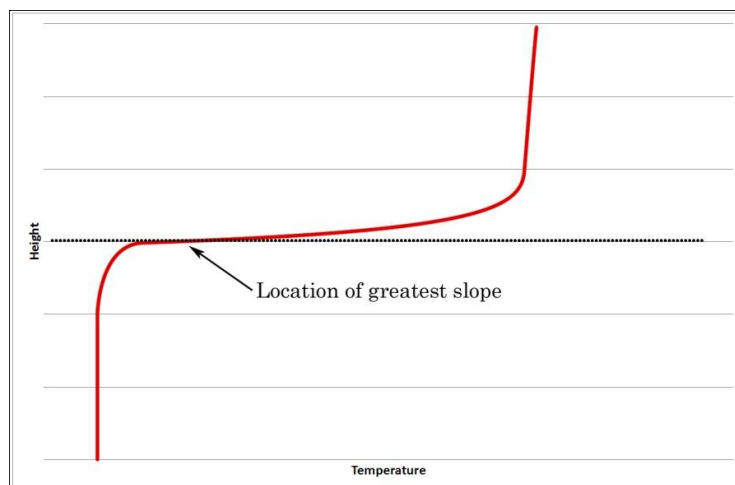
Figure 4-3. Layer location at maximum slope in temperature.
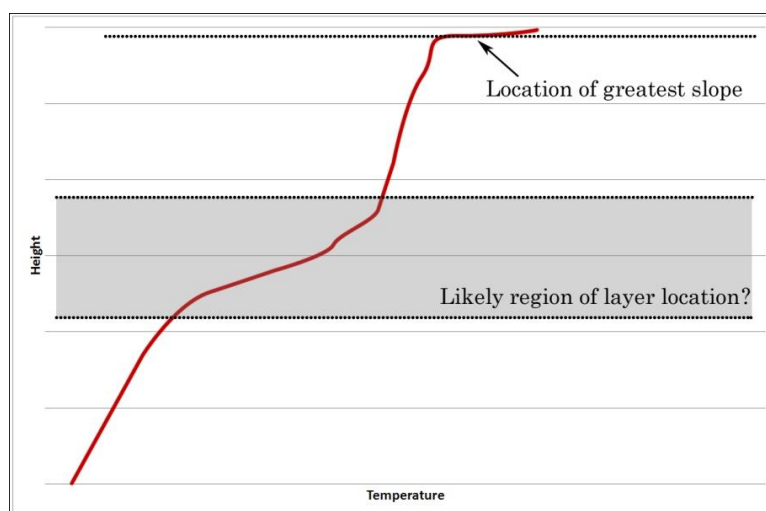
Figure 4-4. Situation unsuitable for treatment by the greatest slope method.

This appears to be consistent with the zone model representation of a layer since the temperature gradient would indeed be greatest at the interface between stratified layers. Despite this apparent agreement it must be remembered that the data provided by a CFD model can present variation invalidating a two layer assumption, and especially for initial periods of a simulation there is no guarantee that the maximum gradient of temperature will be situated anywhere near a sensible location for a layer height, see figure 4-4 above.

It can be argued that any hot fluid entering an ambient compartment will be deposited solely in the hot layer. In this way the lower layer will never deviate from ambient, and any location hotter than this ambient temperature will be considered to be part of the upper layer; this argument locates the layer at the height at which the temperature first varies (see figure 4-5)
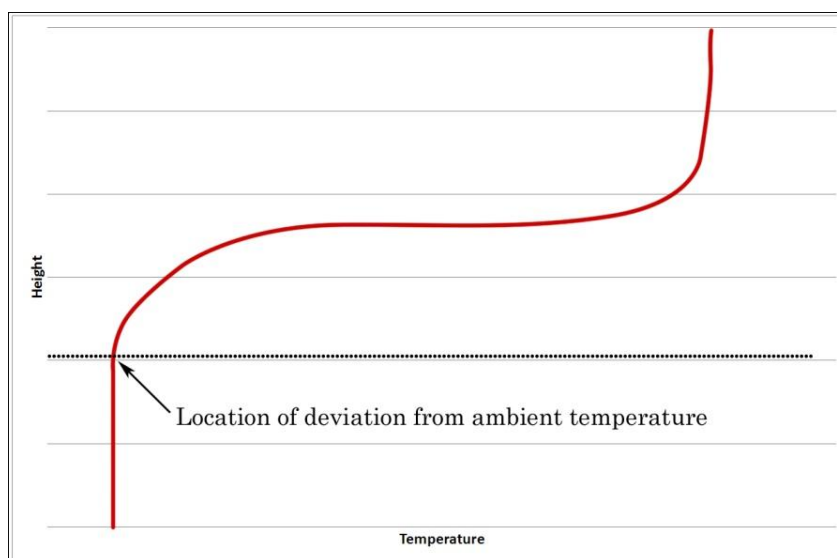
Figure 4-5. Layer location from assumption of ambient lower layer.

It is clear that despite defining the layer with respect to actual apportion of the fluid, the method will consistently report a relatively low layer.   Of

course, there will be instances when this is indeed the correct location of the layer height, yet in general, and especially after the initial periods of the simulation, the lower layer will experience some heating up which contradicts the above assumption.

The third method considered by Weaver [Weaver2000] is based on work by Quintiere et al. [Quintiere1984] and calculates the layer height and temperatures through two integral relationships. The equations themselves are discussed in section 4.6.2 below, but the method centres on having three unknowns (layer height and upper and lower layer temperatures) with two equations, meaning that one of the unknowns is first estimated allowing the remaining two to be directly calculated. Quintiere et al. suggest estimating the upper layer temperature as the average of the temperatures observed in the upper portion of the compartment. The reasoning is that the variation within the upper layer from these higher temperatures should be small, although again as seen in figure 4-4 this is in no way guaranteed. The estimated upper layer temperature then allows the lower layer temperature and layer height to be calculated.

Alternatively, an estimation can first be made of the lower layer temperature, again followed by calculation of the layer height and upper layer temperature through the equations. This method is used in the validation tests of the FDS field model [McGrattan2010], in a BRE international panel report [Miles2004] and by Keski-Rahkonen and Hostikka [Keski2002]. The first two assume the lower layer temperature to simply be the temperature observed at the lowest thermocouple probe/CFD cell; the third takes an average similar to that used by Quintiere et al. but for a number of the lowest probes/cells, although this number is not explicitly specified. The former method is used for comparisons in later sections; see the summary in section 4.6.10.

The above methods all rely on an amount of subjectivity, e.g. the choice of the N% parameter or the selection of probes/cells over which to make the initial temperature estimation. Due to this subjective nature, along with the

inherent inaccuracy of attempting to fit a two layer data set to a continuously varying distribution, it is to be expected that the data reductions performed will contain errors. These errors should be borne in mind during comparisons since discrepancies between the hybrid and field models may very well be attributed to them, as opposed to assuming that any disagreement between the models is caused solely by inaccuracies of the zone model. The imperfections of the layer reduction methods are of little importance in the general use of a hybrid model since they are used solely for comparisons during validation of the model.

4.5.2 Equivalency Method

The initial method presented in this section was first suggested by Quintiere et al. [Quintiere1984] and has been found to perform better than both the N% and greatest slope methods [Weaver2000] [Miles2004]. Janssens and Tran [Janssens1992] attempted to extend the treatment to consider the vent fluxes in addition to mass and energy equivalency, although the resulting calculation regime is both overly complex and difficult to solve. The addition of subjective 'rules' to ensure the solution (such as calculating upper layer temperature "from the average of all temperatures that are within 5% of the maximum temperature measured in the quiescent corner") reduce the validity of the method, and the consideration of neutral plane height limits its applicability to the present work; this extended formulation is not considered any further.

The method of Quintiere et al. works on the vertical distribution of temperature, and conserves mass within the room to provide estimations for layer height and upper and lower layer temperatures. Since a CFD compartment contains numerous cells in all three dimensions, it is first necessary to calculate an average vertical temperature distribution for the room as a whole. This is performed by converting each vertical layer of cells into a 'super cell' that spans both horizontal room dimensions, see figure 4-6;

the values assigned to such a super cell are volumised and mass averaged values calculated from the original layer of cells.
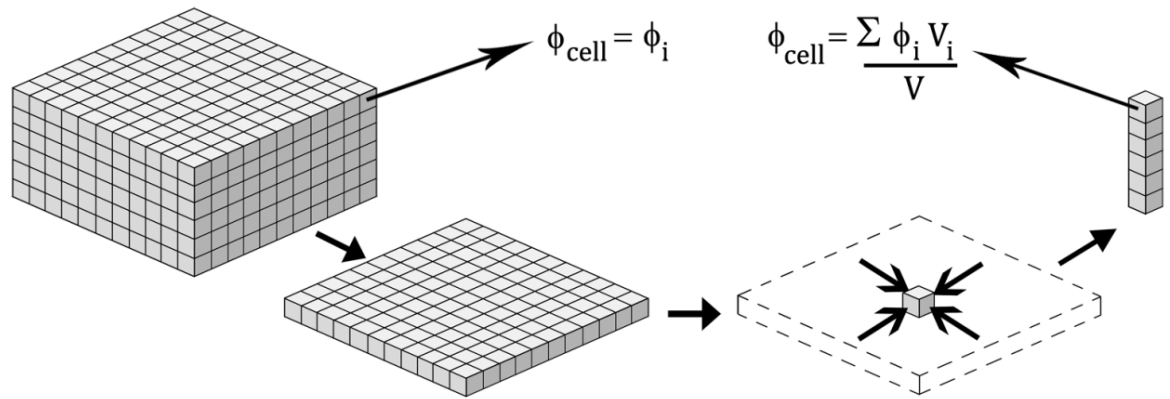
Figure 4-6. Reduction of each layer of cells into a single 'super cell' that assumes volumised averages for variable values.

The mass averaged temperature within a super cell is calculated by,

$$\overline{T_j} = \frac{\sum T_i \rho_i V_i}{\sum \rho_i V_i} \tag{4.6.1}$$

where $\overline{T_j}$ is the value for temperature in the super cell formed from layer j, $\sum \rho_i V_i$ is the total mass of layer j, T_i, ρ_i and V_i are the temperature, density and volume respectively of cell i and the sum is formed over all cells in the layer. Equation 4.6.1 is equivalent to calculating the temperature as the total enthalpy spread over the total mass of a super cell.

Quintiere et al. then define two integral relationships,

$$(h - I)\frac{1}{T_u} + I\frac{1}{T_l} = \int_0^h \frac{1}{T(z)} dz \equiv \sigma_1 \qquad (4.6.2)$$

and

$$(h - I)T_u + IT_l = \int_0^h T(z)dz \equiv \sigma_2 \qquad (4.6.3)$$

where h is the height of the room, $T(z)$ is the temperature at height z, I is the height of the layer interface to be found, and T_u and T_l are the temperatures in the upper and lower layers respectively. These relationships assign values to the layer variables to be calculated by conserving two quantities either side of the layer interface.

Equation 4.6.2 considers the reciprocal of temperature which, through the equation of state, is equivalent to considering the mass ($1/T$ can be replaced by ρ since the remaining terms are R, a constant which will therefore cancel from either side of the equation, and P, a value which sees very small relative variation, i.e. +/- $10Pa$ over $101325Pa$, and can therefore also be assumed to be constant). To satisfy 4.6.2 the temperatures, and therefore densities, of the two layer data set must equate to the total mass seen in the CFD vertical distribution, therefore conserving mass.

Equation 4.6.3 considers temperature itself although it has been noted that this does not correspond to any physical quantity [Janssens1992] [Weaver2000]. Keski-Rahkonen and Hostikka [Keski2002] also state this, but at the same time admit that it is actually quite close to a statement of enthalpy equivalency. In fact, the difference between (4.6.3) and enthalpy

equivalency is the absence of density from the equation, meaning higher temperatures will be over emphasised. The problem with including density in (4.6.3) is that the ρT term is equivalent to P/R, and as discussed for (4.6.2), this quotient remains almost constant. Taking account of the density in (4.6.3) whilst maintaining information in the relationship would mean reformulating over the density whilst taking account of small variations in the pressure, i.e. through consideration of the equivalent two-layer hydrostatic contribution. This would add a great deal of complexity to the method, yet without doing this (4.6.3) would simply reduce to equating the total compartment pressures between CFD data and the two layer data. The problem with using pressure as a comparison is that given such a P, $T\rho$ is constant, and $C_P T_1 \rho_1 = C_P T_2 \rho_2$ for any temperatures T_1 and T_2, meaning that any values for layer height and temperatures will satisfy such a constraint. Despite (4.6.3) not being an exact equivalency for enthalpy, it serves a similar purpose without having to resort to more complex measures.

For the present method, T_l is assumed to be the temperature observed in the lowest super cell. Once T_l is known the layer height and upper layer temperature can then be calculated from (4.6.2) and (4.6.3). Rearranging (4.6.3) for T_u and then substituting this into (4.6.2) gives

$$I = \frac{T_l(\sigma_1 \sigma_2 - h^2)}{\sigma_2 + \sigma_1 T_l^2 - 2T_l h} \tag{4.6.4}$$

The upper layer temperature is then calculated, not from the equivalencies discussed above, but instead through the integral

$$T_u = \frac{1}{(h - I)} \int_I^h T(z) dz \tag{4.6.5}$$

Prior to (4.6.5) the layer height I was only used for the two-layer data, and therefore until now the method made no requirement on the layer height being equivalent between the two data sets. Using (4.6.5) in place of (4.6.3) to calculate T_u now explicitly equates the layer height between the two sets of data.

For the hybrid model the above method is used solely to get the interface height from the data. The CFD model is afforded more vertical resolution than the usual thermocouple stack, also compartment-wide data is included in the above super-cells, as opposed to the data obtained from a stack solely originating from the specific vertical location at which it is situated. With the interface height given, the hybrid model can therefore calculate layer temperatures based on the actual mass and enthalpy above and below this height for the entire compartment, maintaining better conservation of enthalpy than 4.6.5 allows. Along with the super cell values of temperature, the mass and enthalpy are also summed, so too are variables such as pressure, smoke and toxic species for comparisons relevant to those sections of the model. In this way the layer temperatures are simply calculated as

$$T_u = \frac{\sum_{h \geq I} V_i \rho_i T_i C_P}{V_u \rho_u C_P} \quad , \quad T_l = \frac{\sum_{h < I} V_i \rho_i T_i C_P}{V_l \rho_l C_P} \tag{4.6.6}$$

where

$$V_u = \sum_{h \geq I} V_i \quad , \quad V_l = \sum_{h < I} V_i \tag{4.6.7}$$

$$\rho_u = \frac{\sum_{h \geq I} V_i \rho_i}{V_u} \quad , \quad \rho_l = \frac{\sum_{h < I} V_i \rho_i}{V_l} \tag{4.6.8}$$

and sums are taken over cells depending on their height; upper sums are taken for all cells whose lowest point is above the layer height I, lower sums are taken over all cells whose highest point is below the layer height. Cells that lay across the layer are also included in the above sums, but are simply split in proportion corresponding to the amount of cell over the layer to the amount of cell under. The pressure value calculated is a volumised average, similar to that for density above in (4.6.8) but taken for the compartment as a whole, and therefore independent of the layer height. The extra species are calculated in terms of layer mass fractions, which are calculated for general variable ϕ as

$$w_{\phi,u} = \frac{\sum_{h \geq I} V_i \rho_i w_{\phi,i}}{V_u \rho_u} \quad , \quad w_{\phi,l} = \frac{\sum_{h < I} V_i \rho_i w_{\phi,i}}{V_l \rho_l} \qquad (4.6.9)$$

where the mass fractions are with regard to layers, $w_{\phi,u}$ and $w_{\phi,l}$, and individual cells, $w_{\phi,i}$, and sums are taken as before.

4.5.3 Issue with equivalency method

The main issue with the equivalency method discussed above is that the integral relationships give two equations in three unknowns, leaving one of the layer height or temperatures to be estimated. Above, the lower layer temperature was assumed to be that observed in the lowest super cell, and this then allowed the layer height and upper layer temperature to be calculated. As mentioned earlier, assuming the lower layer to be 'ambient' does have a physical interpretation in the earlier stages of a simulation since any fluid hotter than this entering a compartment will become part of the upper layer. As a simulation progresses this assumption becomes dubious as the lower layer experiences heating through various means, e.g. mixing, conduction, entrainment or radiation.

The use of equation 4.6.6 to calculate layer temperatures provides opportunity for the lower layer to heat up, but the initial guess at T_l is almost certainly an underestimation, and in turn leads to an underestimation in the proceeding calculation of the layer height. Using equation 4.6.6 to find a revised T_l generally results in a higher value, although using this new value for a second calculation of the layer height poses problems. Looking at figure 4-7 it can be seen that for a monotonically increasing temperature distribution an increase in layer height leads to an increase in layer temperatures, and vice versa. This means that use of the revised T_l above to calculate a new layer height will simply result a higher value; this can in turn be used to find a second revised T_l greater than the previous, with this process repeating until the layer height is found to be at the top of the compartment.
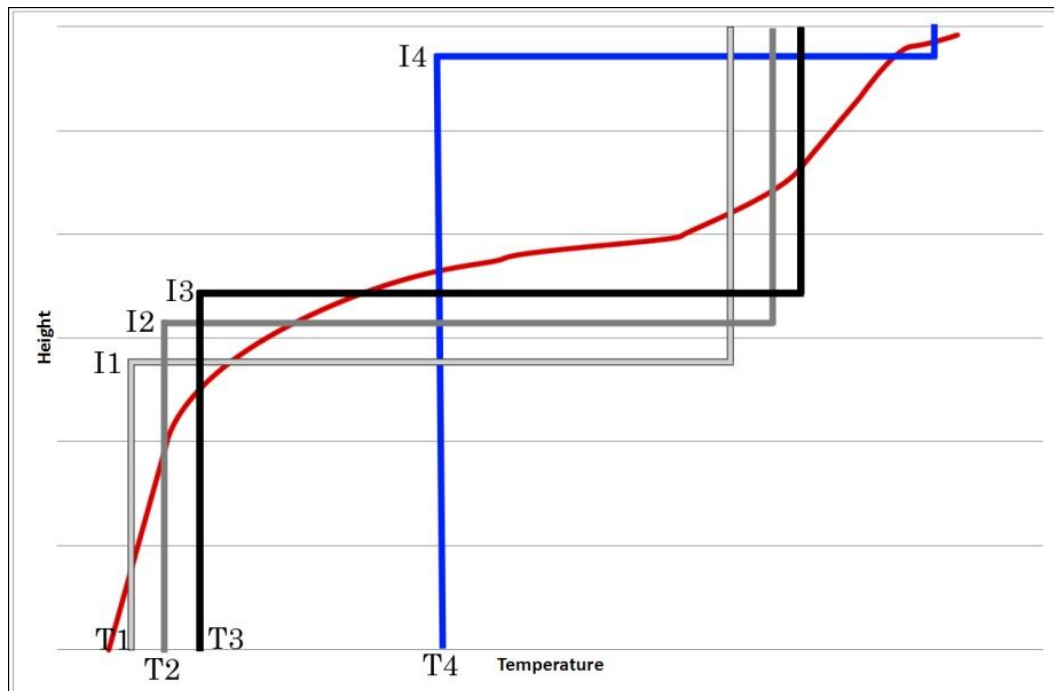
Figure 4-7. Relationship between layer height and temperatures.

4.5.4 Integral Relations Methods

The method presented below was implemented to address the discrepancy seen between the hybrid and CFD models towards the end of simulations. The method was developed independently during research by the author without prior knowledge of the details of a paper by He et al. [He1998] which discusses a method that is formulated slightly differently and relies on a different final condition.

The method takes the integral relations of Quintiere et al. [Quintiere1984] in equations 4.6.2 and 4.6.3 and attempts to solve them simultaneously, thereby obtaining values for layer height and upper and lower temperatures without first having to estimate one of these variables.

4.5.7 He et al. version [He1998]

He et al. [He1998] notice that for averages

$$x_{av1} = \frac{1}{(b-a)} \int_a^b x(y).\,dy \qquad (4.6.10)$$

and

$$x_{av2} = (b-a) / \int_a^b \frac{dy}{x(y)} \qquad (4.6.11)$$

then the ratio

$$\frac{x_{av1}}{x_{av2}} \geq 1 \qquad (4.6.12)$$

with unity realised when $x(y)$ is uniform over the interval (a, b). In this way the 'integral ratio' in (4.6.12) provides a measure of the uniformity of the distribution over a given region. Considering a layer height I, the above ratio can be found for the upper and lower layers over regions $(0, I)$ and (I, h) respectively, where h is again the height of the compartment. This results in upper ratio

$$r_u = \frac{1}{(h-I)^2} \int_I^h T(y) dy \int_I^h \frac{dy}{T(y)} \qquad (4.6.13)$$

and lower ratio

$$r_l = \frac{1}{I^2} \int_0^I T(y) dy \int_0^I \frac{dy}{T(y)} \qquad (4.6.14)$$

from which the 'ratio sum, $r_t = r_u + r_l$, is found. The layer interface height is then simply assumed to be located at the height at which the ratio sum is minimised.

4.5.8 Integral Ratio Version

The version of the integral ratio method used in the present work begins by splitting up (4.6.2) and (4.6.3) into four separate equations. In effect this goes further than the integral relations suggested by Quintiere et al. by implicitly equating the layer heights between the cell/probe data and two layer data

from the outset. By integrating either side of this layer height, the upper and lower layer temperatures can be separated giving

$$(h - I)T_u = \int_I^h T(y)dy \qquad (4.6.15)$$

$$IT_l = \int_0^I T(y)dy \qquad (4.6.16)$$

from the approximate enthalpy equivalency, and

$$\frac{(h - I)}{T_u} = \int_I^h \frac{dy}{T(y)} \qquad (4.6.17)$$

$$\frac{I}{T_l} = \int_0^I \frac{dy}{T(y)} \qquad (4.6.18)$$

from the mass equivalency.

Given any layer height I, there are therefore two ways to calculate each temperature depending on the equivalency used. It is apparent that both methods give different values for the temperature being calculated, and that the discrepancy becomes greater as a layer increases in depth (at the limit of 'no layer' the two temperatures agree). The ratio of these alternative temperatures are formed as

$$r_u = \frac{(h-l)^2}{\int_l^h T(y)dy \int_l^h \frac{dy}{T(y)}} \qquad (4.6.19)$$

and

$$r_l = \frac{l^2}{\int_0^l T(y)dy \int_0^l \frac{dy}{T(y)}} \qquad (4.6.20)$$

which are simply the reciprocals of those used by He et al. in (4.6.13) and (4.6.14), and are therefore always less than or equal to unity. Whereas He et al. then took the sum of these ratios and located the layer height at the point this sum was minimised, the present method again takes the ratio of these two values, $r_* = r_l/r_u$ and locates the layer at the point where r_* assumes unity. As the layer height increases from zero to h, r_u tends to one from below; similarly, as the layer decreases from h to zero, r_l tends to one from below. At the point where $r_* = 1$, the discrepancy between the temperature representations are equal for both upper and lower layers.

The generally monotonic nature of the ratios guarantees the existence of a minimum as sought by He et al., although it does not guarantee a unique minimum. In comparison, the value of unity sought by the present method is always unique for monotonic functions. Despite this, some severe and fairly unrealistic temperature profiles will prove troublesome for the present method. Both methods on occasion fail to find a minimum/unity, although the method of He at al. appears to suffer this fate much more regularly, and for some fairly benign temperature distributions; the present integral ratio method appears to be more robust in this regard, and is used in comparisons in later sections, see the summary in section 4.6.10.

4.5.9 Integral Relations Examples

 It must be noted that for many temperature distributions the layers reported by both methods are extremely close, if not in total agreement, but there is potential for large differences between the methods. Without further consideration of the problem of multiple minima, the figures on the next pages provide some examples of the two methods in use.

Figure 4-8a shows the layer reduction data obtained from the two methods when used on a convenient 'step' temperature profile and demonstrates that both methods are in exact agreement, finding the layer midway along the sloped section joining the uniform upper and lower sections. Figure 4-8b demonstrates the variation in the ratio values of the methods over the layer height. The ratio values have been transformed such that the integral ratio method locates the layer at the point its ratio equals zero, whereas the 'He et al. method' locates the layer at the maximum value reached by its ratio (≤ 2). The equivalence between the two approaches for this simple profile can be seen. (Note that due to the resolution of the numerics the hybrid ratio may appear not to reach zero since unity is found between plotted layer heights.)

Figures 4-9a and 4-9b demonstrate the same data but for a profile with a uniform upper and sloping lower. The methods once again agree closely with figure 4-9b demonstrating that the addition of variation in the lower affects the 'He et al.' ratio by causing peaks in this section, although a maxima is still clear; it appears the integral ratio value is unaffected. Figures 4-10a and 4.10b demonstrate the same for a sloping upper with the difference in reported layer heights more pronounced. It can be reasoned that the He et al. method provides a more accurate estimation of the layer since the large uniform lower section of the profile would suggest that the entirety of the sloping section is contained in the upper layer. This result is even more pronounced in figures 4-11a and 4-11b where the upper section of the profile experiences a step in temperature. It appears as though the He et al. method obtains a much more realistic layer height than the integral ratio method,

although from figure 4-11b it appears as though a potential problem may be arising in that a secondary peak has formed of a similar magnitude to the maxima.

In figures 4-12a and 4-12b a second step has been added to the upmost portion of the temperature profile. This seems to have caused the secondary peak seen in figure 4-12b to 'over take' the original peak, forming a new maxima that causes the layer height to be found by the He et al. method at an almost certainly incorrect position, close to the ceiling of the compartment. Again, figure 4-12b demonstrates that the integral ratio value remains fairly unaffected by these variations in the temperature profile. It is worth noting that the original peak in the He at al. ratio is actually at a position that would give an accurate value of layer height.

Figures 4-13a and 4-13b demonstrate an unrealistic 'saw-tooth' temperature profile. Figure 4-13b demonstrates that both ratios are varying in a highly irregular fashion yet both methods manage to find a value for the layer height. The two values are almost equal yet are probably incorrect due to their location near the ceiling of the compartment; it must be noted that the notion of a layer may have no validity for such a profile.

Figures 4-14a and 4-14b demonstrate a profile for which the integral ratio method fails to find a unique layer height, with the ratio equalling zero at five separate locations. The He et al. method does indeed find a unique layer, although again whether this is correct or whether the notion of a layer is even valid is doubtful; it is comforting how irregular the temperature profile must be to cause problems for the hybrid method.

The integral ratio method will always find an odd number of layers due to that fact that the zero corresponds to the intersection of two functions that begin such that $f_1(0) > f_2(0)$, and end with $f_2(h) > f_1(h)$, which is only possible with an odd number of crosses. In fact, for the vast majority of realistic temperature profiles, these two functions are monotonic, leading to

the singe intersection commonly seen; the presence of multiple intersections only becomes possible when these functions lose this property. For a true single intersection, f_1 will be decreasing and f_2 increasing at this point. Extending this condition to a multiple intersection case such as in figure 4-14b, the middle three intersections can be discounted, since they occur with either f_1 increasing, f_2 decreasing, or both. This leaves the two intersections at either end which interestingly are very similar to two peaks of the He et al. ratio. No genuine distinction can be made between these two intersections, although an argument can be made for selecting that which is located in the most uniform portion of the ratio, since irregularity is a requirement for the failure of the method. If this rule is followed then the integral ratio method actually locates the layer at a very similar position to the He et al. method.

Finally, figures 4-15a and 4-15b demonstrate a situation where the He et al. method fails to find a unique maxima. Unlike the temperature profile that the integral ratio method failed to find a unique zero for, this temperature profile could quite likely be experienced in reality since it monotonically increases over the height of the compartment. Figure 4-15b again demonstrates that the He et al. ratio experiences two peaks of equal amplitude, resulting in two possible locations of the layer. No distinction can be made between these two points since the plots are almost symmetrical, although the leftmost peak would give a fairly accurate layer height. The integral ratio method easily finds a unique zero in this situation.

(Figures 4-8a to 4-15b on following pages)
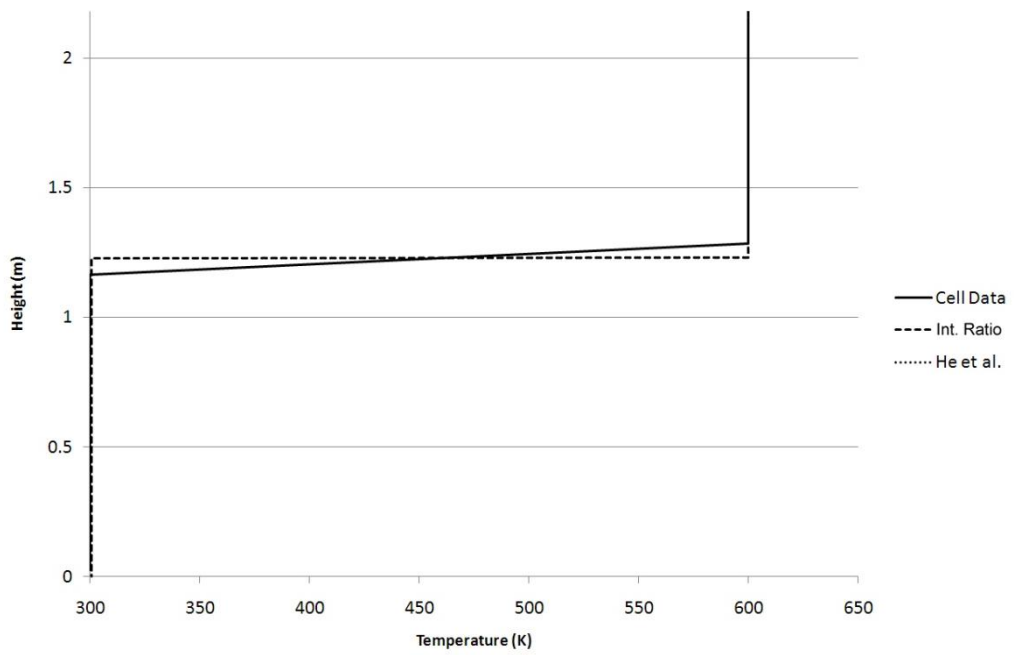
Figure 4-8a. Reduction data obtained from methods for 'step' temperature profile.
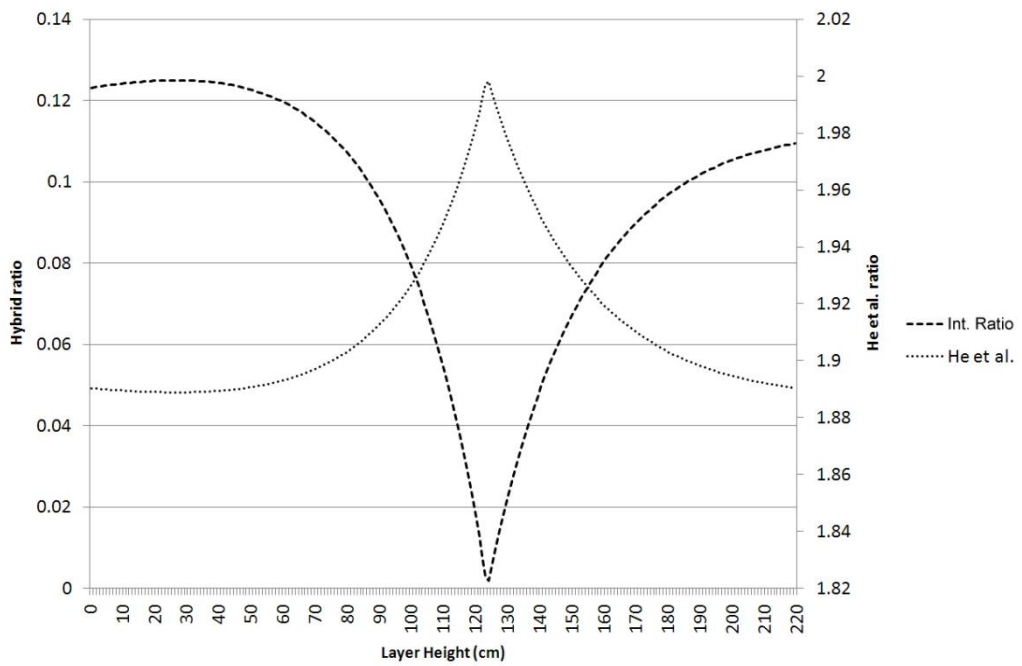
Figure 4-8b. Variation of ratio values over layer height for 'step' temperature profile.
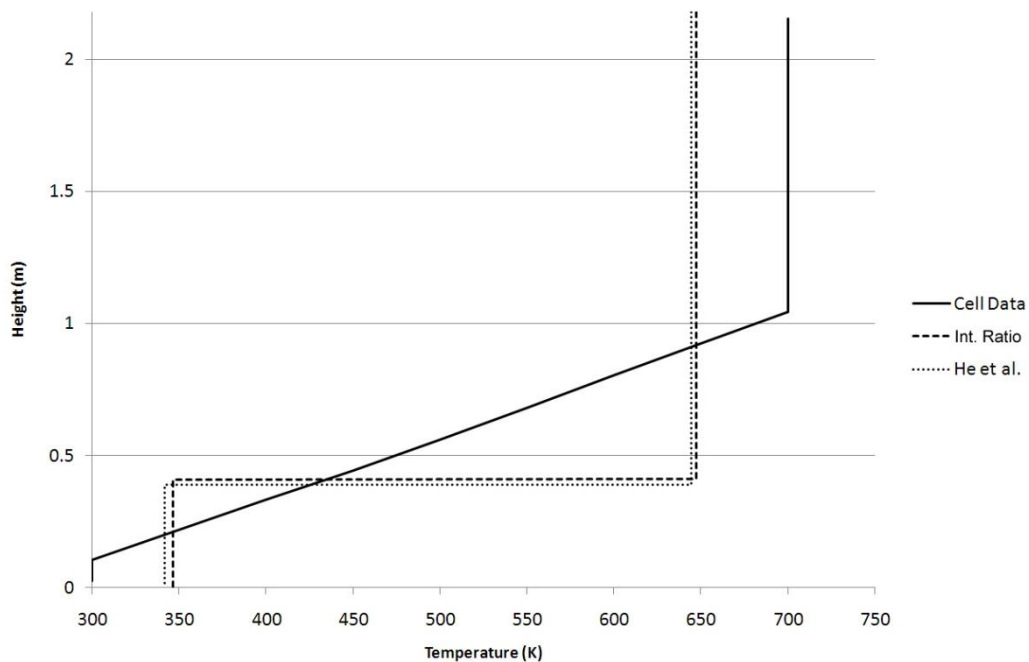
Figure 4-9a. Reduction data obtained from methods for uniform upper/sloping lower profile.
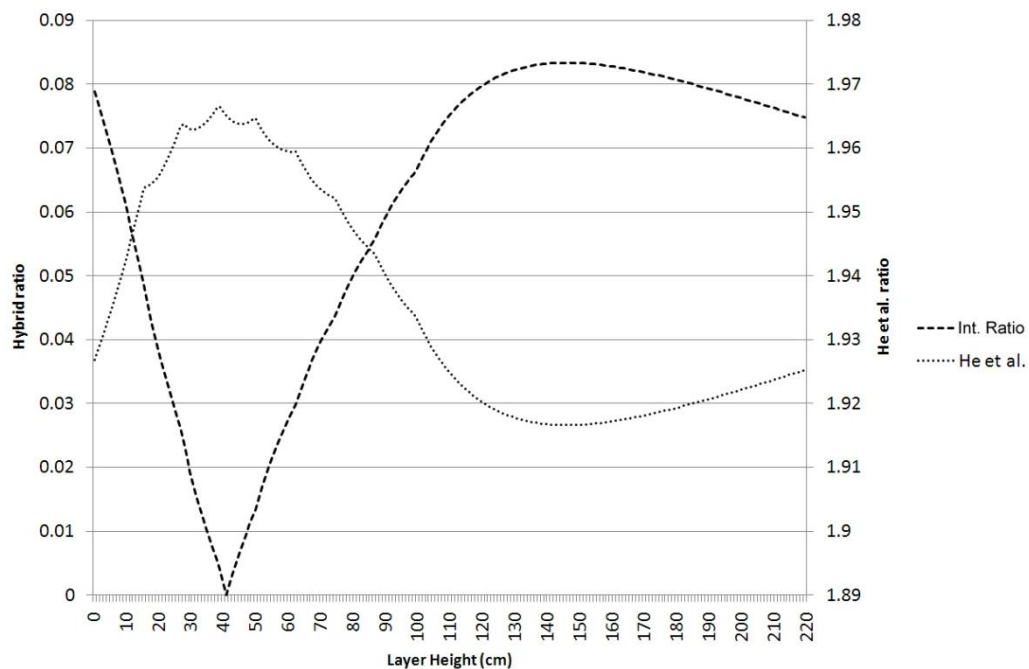
Figure 4-9b. Variation of ratio values over layer height for uniform upper/sloping lower profile.
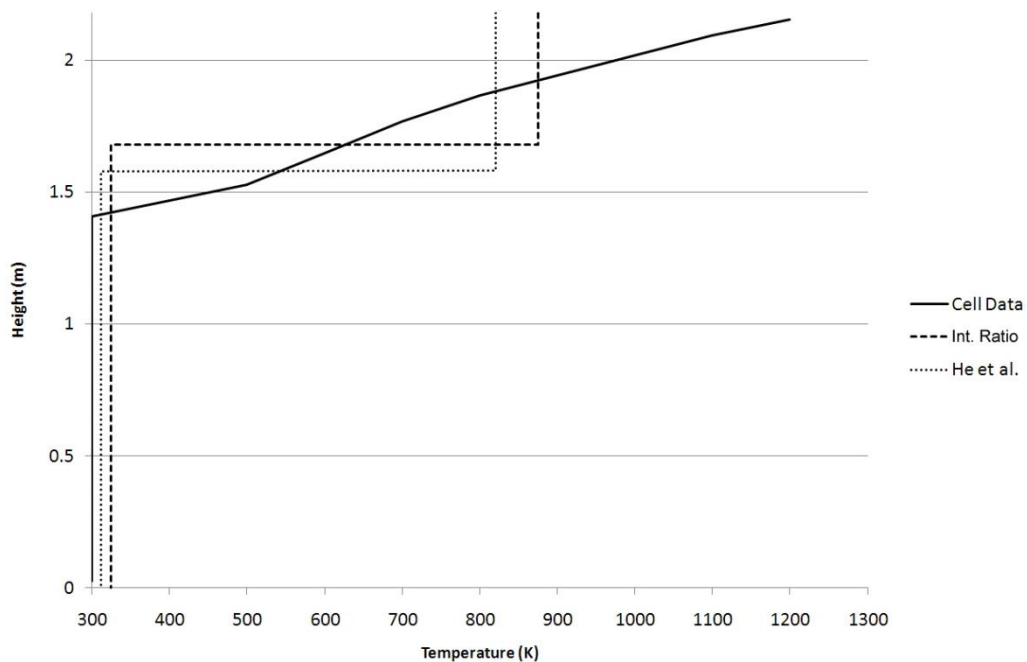
Figure 4-10a. Reduction data obtained from methods for sloping
upper/uniform lower profile.
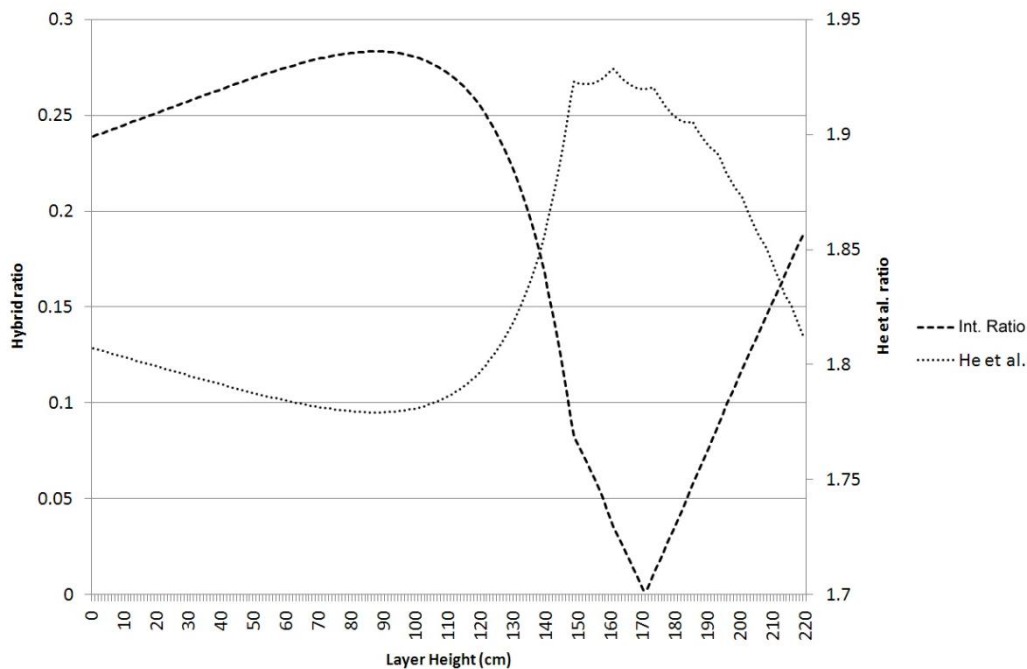
Figure 4-10b. Variation of ratio values over layer height for sloping
upper/uniform lower profile.
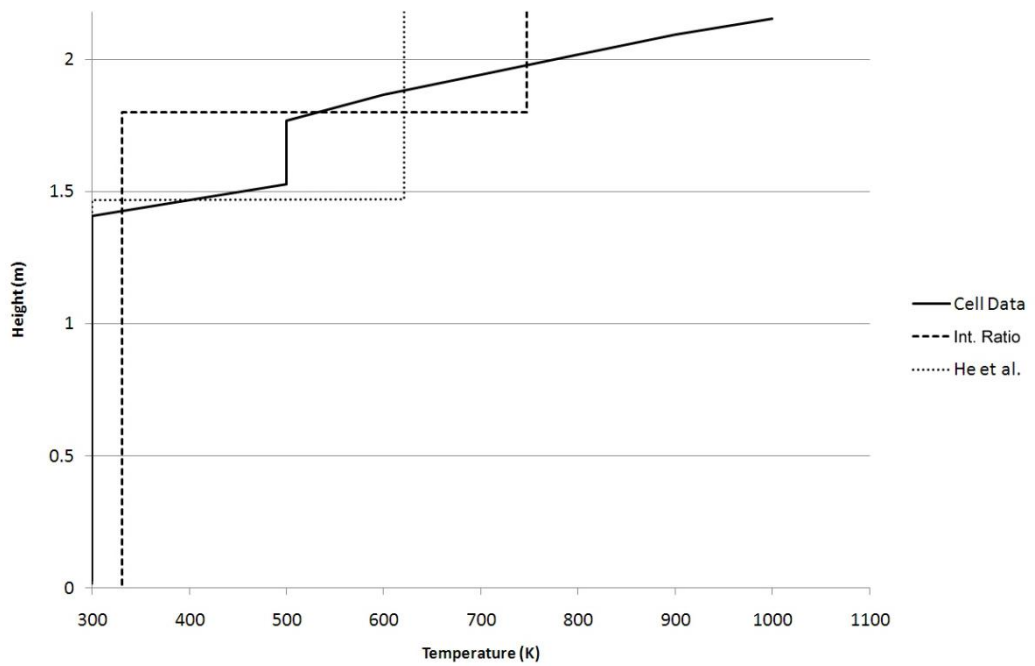
Figure 4-11a. Reduction data obtained from methods for step upper/uniform lower profile
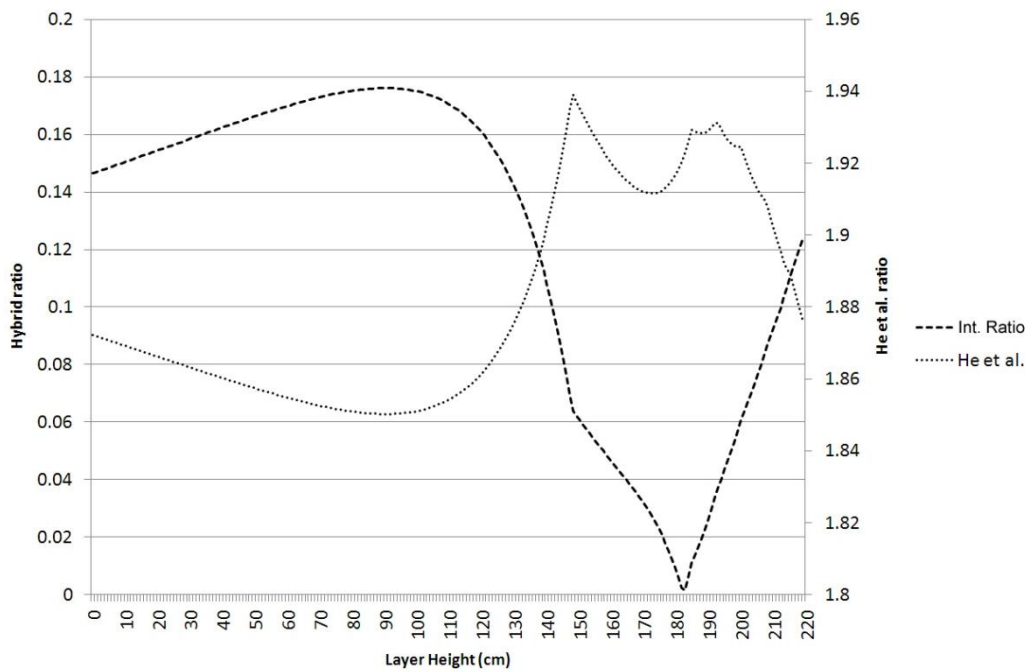
Figure 4-11b. Variation of ratio values over layer height for step upper/uniform lower profile.
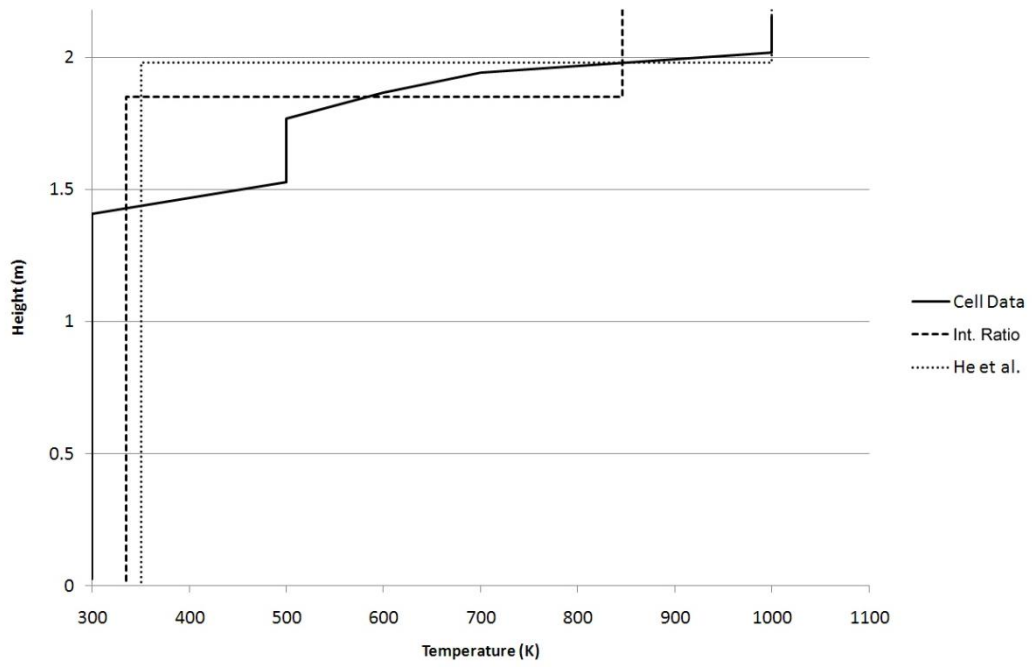
Figure 4-12a. Reduction data obtained from methods for stepping
upper/uniform lower profile.
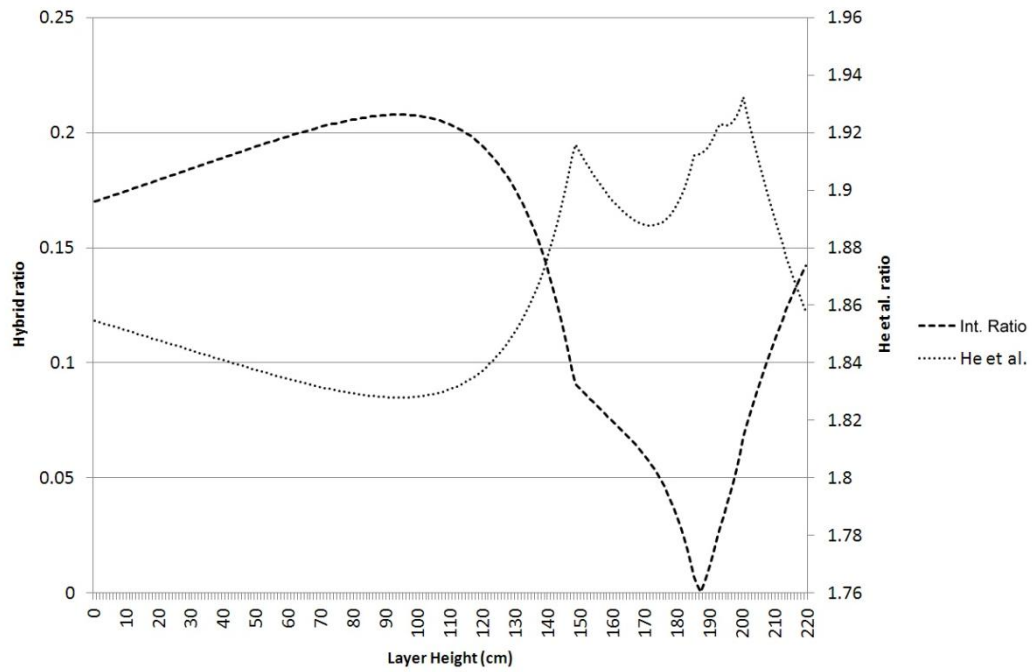
Figure 4-12b. Variation of ratio values over layer height for stepping
upper/uniform lower profile.
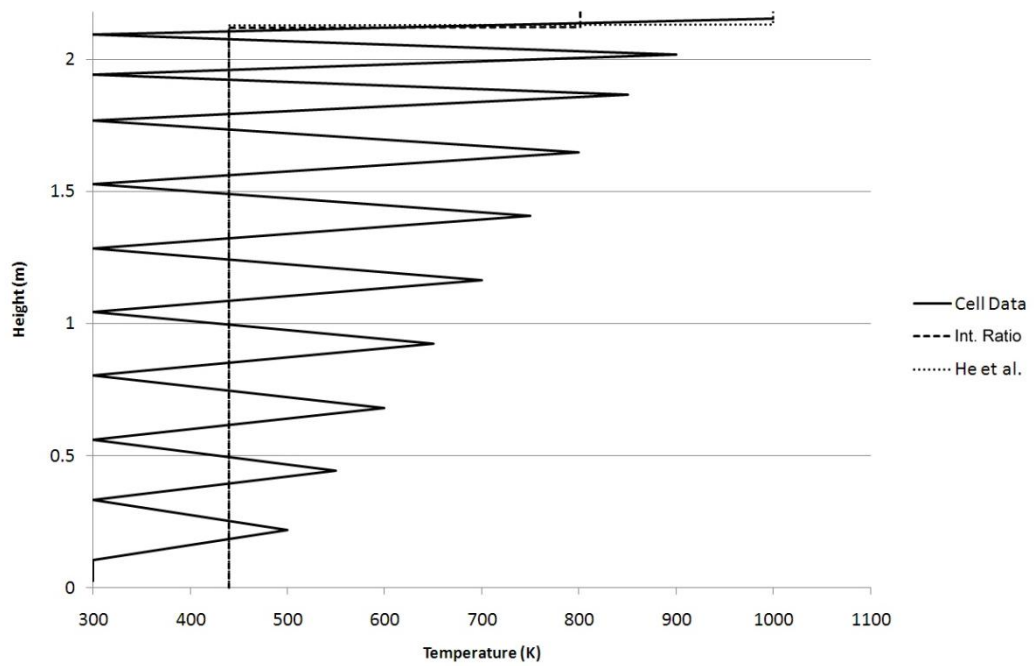
Figure 4-13a. Reduction data obtained from methods for varying sawtooth profile.
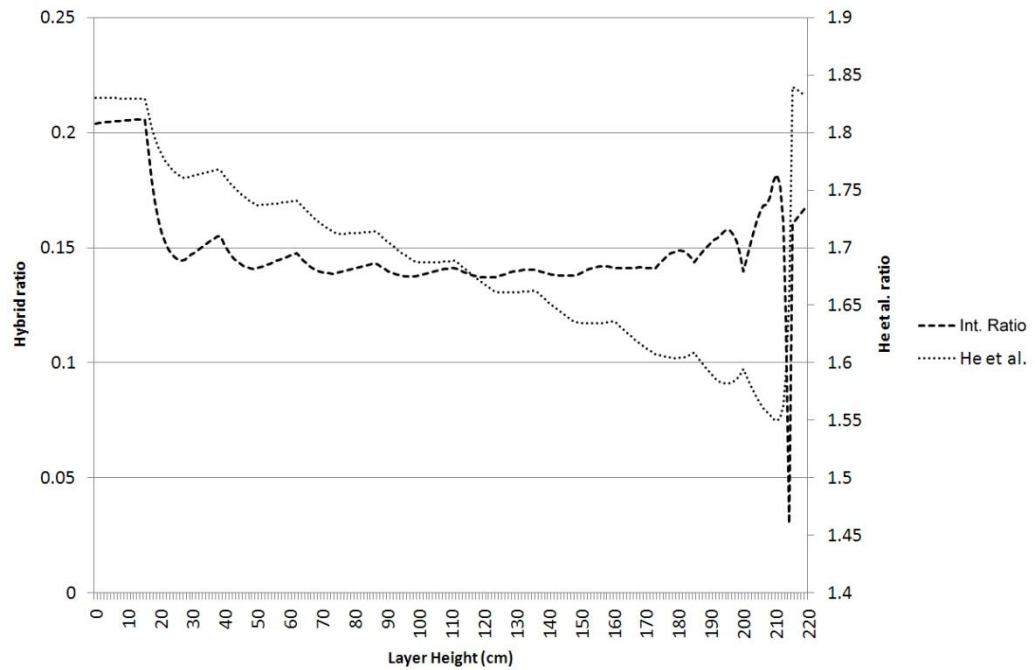
Figure 4-13b. Variation of ratio values over layer height for varying sawtooth profile.
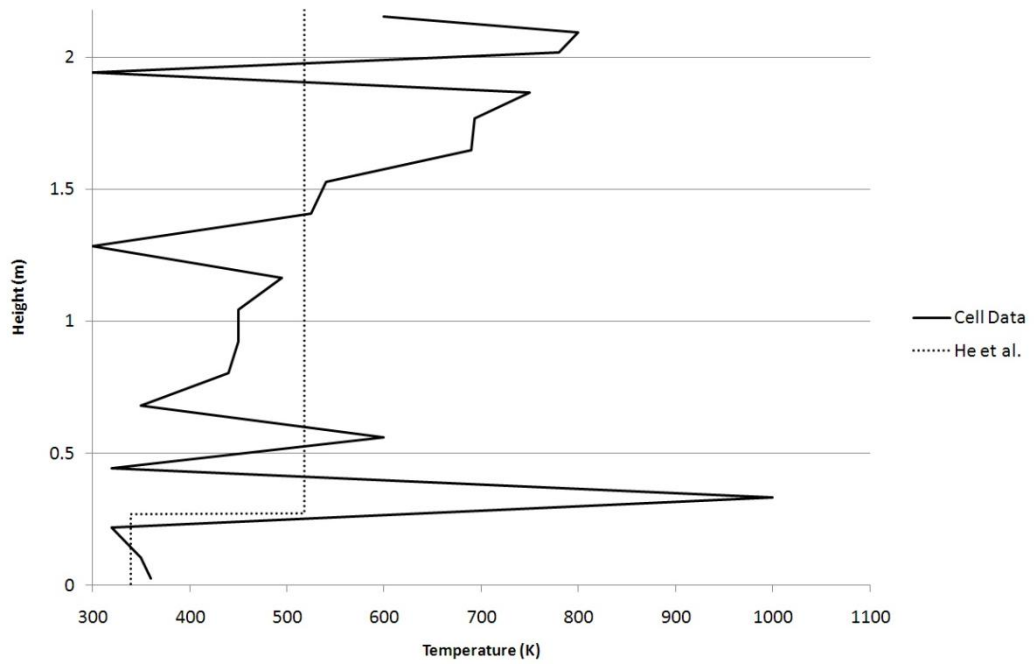
Figure 4-14a. Integral ratio method finding five minima for 'random' profile.
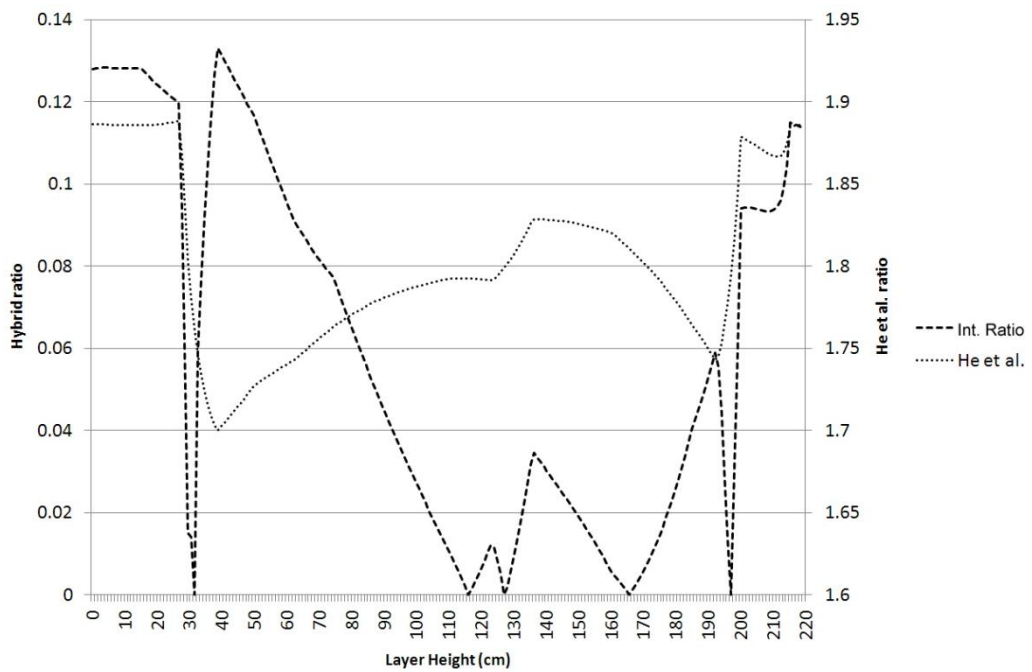
Figure 4-14b. Integral ratio method finding five minima for 'random' profile.
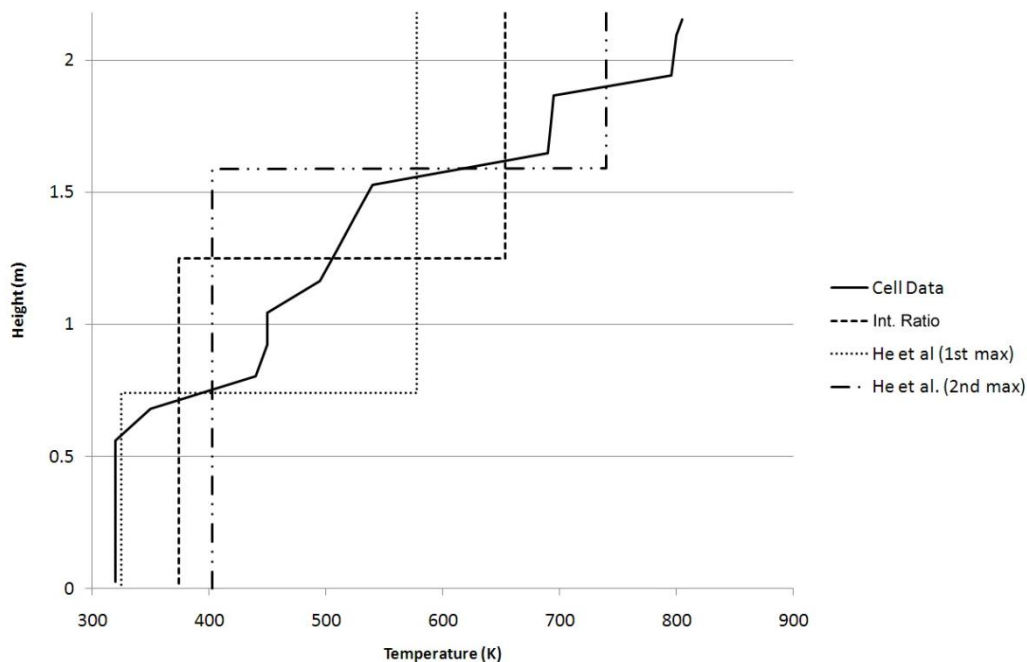
Figure 4-15a. He et al. method [He1998] finding two maxima for general profile.
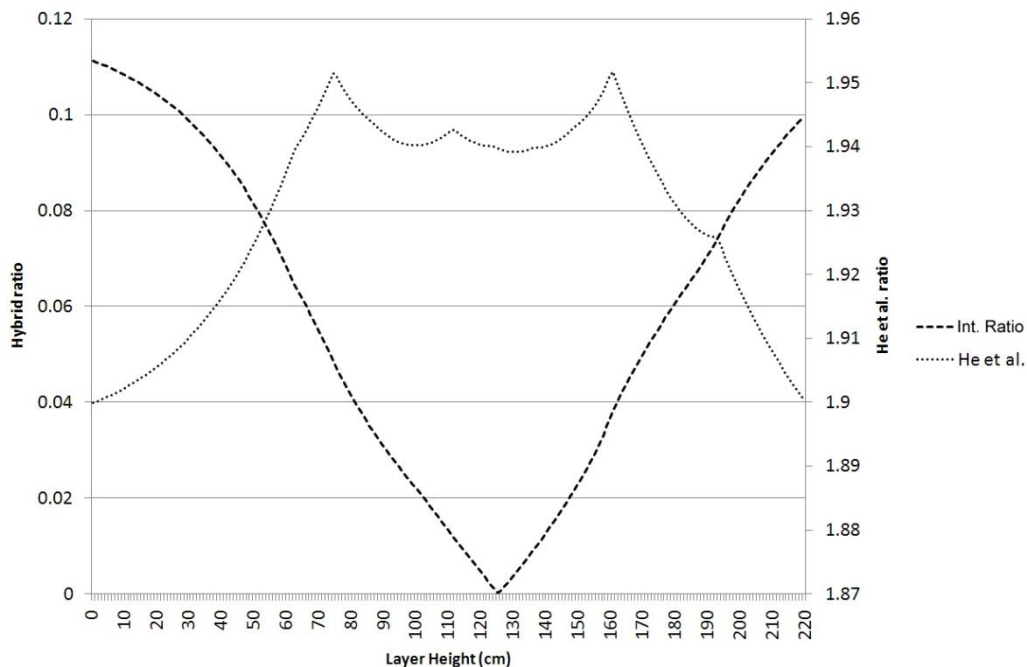
Figure 4-15b. He et al .method [He1998] finding two maxima for general profile.

4.5.10 Data Reduction Summary

The issues surrounding the reduction of high resolution cell/probe data to an equivalent two layer data set have been explored. The N% method [Cooper1982] and its validity are simply crippled by the huge amount of subjectivity required in its use. The greatest slope method [Emmons1989] can provide decent estimations of a likely layer height, especially for developed conditions in the latter stages of a simulation. Despite this its overly simple nature is easily foiled by quite gentle temperature profiles, and scientifically leaves a lot to be desired.

The integral ratio method first proposed by Quintiere et al. [Quintiere1984] appears to be more scientific in nature through its formulation over equivalency between species. By taking the temperature at the lowest point of the profile to be the corresponding lower layer temperature, the method actually performs fairly well at estimating layer height and temperatures for the early periods of a simulation, where the lower layer is yet to experience any significant variation. However, as simulations progress and the lower layer experiences change, the lower temperature assumption is invalidated and the method fails to provide accurate values.

Extension of the integral method, either by He at al. [He1998] or the integral ratio method, as presented in this chapter, seem to provide fairly accurate results of the layer height. Neither method is obviously better than the other, although the He et al. method seems to provide more accurate values for regular profiles and early conditions, whereas the integral ratio method seems more consistent in obtaining accurate values over a range of different situations, especially for the later stages of a simulation. Since the He et al. method aims to maximise uniformity it relates closely to the fundamental notion of layers and this is clearly responsible for it outperforming the integral ratio method under suitable conditions. Despite this it is not robust enough for use in general situations, yet there is certainly potential for the method to be developed further to address these issues (see chapter 8)

Despite their apparent basis on a scientific argument, these integral relation methods are similar to the other methods in that they are in truth little more than algorithms for curve fitting. The difference with the integral ration methods is that they remove the need for subjectivity, yet objective methods, while possibly more authoritative, do not guarantee more accurate results. The choice as to which method to use means that subjectivity is not entirely avoided.

For the comparisons in later sections, use will be made of two data reduction methods. The first method used will be the Quintiere et al. [Quintiere1984] method but with the estimation of the lower layer temperature assuming the value at the lowest point of the profile, see section 4.6.1. Estimating the lower temperature in this way causes the method to perform favourably in the initial stages of a simulation since the consequences of a relatively uniform lower layer are captured (lower layer height, cooler upper layer). The second method used will be the integral ratio method from section 4.6.8. Since this method attempts to balance the error between layers, it locates the layer at a point where the variation in the temperature profile is distributed between the layers more equally, and is therefore suited to the latter stages of a simulation when the lower layer will experience some variation. These methods are clearly expected to give different values due to their dependence on the stage of the simulation under consideration. It is reasonable to expect the hybrid results to be located close to the interval between these two values, possibly beginning in agreement with the first method before coming into closer agreement with the second as the simulation progresses.

These issues, while worthy of further consideration, are not of vital importance, since the reduction method is only required when validating the hybrid model by comparing the zone data to an independently run full CFD model. If the weaknesses inherent in these methods are kept in mind whilst performing these comparisons, the implications of using them will be minimised. It is imperative to remember that discrepancies between hybrid

and CFD models can and will be caused by errors and bias in the reduction methods in addition to the inaccuracies of the zone model.

A final implication of the reduction method concerns comparisons between the performance of the hybrid model versus increasing the coarseness of the mesh within a CFD simulation, performed in section 7.7.15. The most important measure of the mesh coarseness with regards to data reduction will be in the vertical direction, but as for reasons discussed in section 7.7.15 this will remain constant over the different comparisons. Increases in coarseness will therefore originate from a reduction in the number of cells in the horizontal directions, but this will have a small effect on the reduction method since these are summed and averaged in any case, meaning the errors within a reduction method will remain similar despite the mesh under consideration. This means that any discrepancy observed between the hybrid zone model and a 'fine' CFD mesh is likely to exist between the zone model and a 'coarse' CFD mesh. This will result in the coarse mesh room appearing to out perform the hybrid model simply by having its results subjected to the same biases as those of the fine mesh room.

4.6 Validating the Hybrid Model

The hybrid model consists of two fire modelling methodologies that, independently, have been extensively validated. The implication of this is that any errors or incorrect behaviour of the hybrid model will be attributable to the way the individual models are connected. Firstly and rather uninterestingly are human errors and bugs in the programming, these should be realised and addressed during development. The remaining issues will involve the theory behind the connection of the two models: the representation of one model within the other, the coupling of the solution procedure over the interface, and the conversion of data to respective forms.

For the conversion of data the primary concern is that of conservation, it must be ensured that transfers of species between models are performed accurately and consistently.

In regards to the coupling of the solution procedure, this is validated by the results obtained from the model, but it should be remembered that a procedure that obtains the correct solution is not necessarily optimum. An appreciable portion of the model development has been focussed on improving the performance of the solution procedure used.

The representation of the models within one another is addressed by both the pressure boundary in section 4.4.1 and the formation of zone model sources in section 4.4.3. While the remaining issues are generally by their very nature either right or wrong, this area is certainly open to subjectivity. Since any regime will necessary involve both simplifications and assumptions, no one regime can be deemed to be unequivocally correct. There are clearly many physically correct ways to formulate such a section of the model, but despite finding a regime that 'works' by providing sufficiently accurate results, this portion of the model is a clear candidate for future improvements and 'tweaks'. Other issues will manifest as obvious errors in the data, whereas the representation of the models and interface is likely to be the cause of more subtle deviations from agreement in the results.

4.6.1 Results Comparisons

The primary method of validating the hybrid model will be through comparisons with a full CFD simulation, comparing the results from the zone model component with those of a field model within an identical compartment. The reduction of CFD data to a form that allows comparison with zone model results is discussed at length in section 4.6.

The primary variables of interest are the layer height and temperatures, although extension of the model will mean that radiative flux, gas/toxic

species and smoke concentrations are also of importance. Layer densities are not of immediate concern since these are specified by the temperature and pressure through the state equation, and temperatures are clearly of more immediate use.

As discussed in section 4.6, the subjective and imperfect nature of the layer reduction methods mean that some discrepancy is to be expected between the CFD and zone model results during comparisons, and that a portion of any apparent error can certainly be attributed to these methods.

For two equally sized volumes of gas at different temperatures but similar pressures, the equation of state implies that their enthalpies are the same since

$$C_P mT = C_P \rho VT = C_P \frac{P}{RT}VT = C_P \frac{VP}{R}$$

and therefore the enthalpy is independent of the temperature if the pressure is specified. The implication of this is that for a compartment of given total enthalpy, the layers can assume any values of temperature and height and still satisfy this total, so long as the densities are allowed to vary as the equation of state requires.

Agreement between the CFD and zone layer heights and temperatures is certainly an indicator of the hybrid model performing correctly, yet the above means that this agreement alone is no guarantee of accuracy. For this reason two further comparisons are made between the models. The first is for compartment pressure, which ensures that the enthalpy is in agreement between the two models. The second is for total mass, and validates any agreement observed in the layer values by effectively 'fixing' the densities in the equation of state, meaning that the layer values satisfying the relationship above are unique.

5. CFAST / SMARTFIRE Hybrid Model

This chapter discusses the initial portion of work carried out in the development of the hybrid model, where the SMARTFIRE CFD model was combined with the CFAST zone model. The first section examines factors of the hybrid implementation that were unique to the use of CFAST, with the second section discussing some results of the work. These results from the first test case appeared in a paper by the author which was published in the Interflam 2007 conference proceedings [Burton2007] and is included as appendix 3; the results from the second case were presented in the poster section of the same conference.

5.1 Implementation Specifics

The vast majority of the CFAST specific implementation is similar to the FSEG-ZONE model, and is described in chapter 4. Discussed here are the specific details and issues encountered in attempting to couple SMARTFIRE with the existing CFAST zone model.

5.1.1 Mixed Compilation

The first issue encountered in attempting to couple SMARTFIRE with CFAST was that of mixed language compilation as SMARTFIRE is written in C++, and CFAST in FORTRAN. The majority of the work is performed automatically by the compilers, in this case using Microsoft Visual Studio 6 in

combination with Compaq Visual Fortran. Visual Studio 6 allows source files written in both C++ and FORTRAN to be included within the same project, these are then compiled by the respective compilers into the relevant objects, from which point the linking proceeds as usual.

To allow compilation to proceed, prototypes for the FORTRAN functions need to be declared, in this case as externals to be defined in another source file. To make successive declarations simpler and to improve the readability of the code, define directives were used as follows:

```
#define SUBROUTINE      extern "C" void    __stdcall
#define REAL_FUNCTION   extern "C" float   __stdcall
#define DOUBLE_FUNCTION extern "C" double  __stdcall
```

This allows simple declaration of fortran functions, allowing them to be called from the C++ code, for example

```
SUBROUTINE    CFAST_INI(CHARACTER CMDSTR)
REAL_FUNCTION COPY_TEMPERATURE(REAL* TEMPUP, REAL* TEMPLW)
```

The above informs the C++ compiler of the return value of these functions and that they exist although are declared elsewhere. The `__stdcall` token is the calling convention which informs the C++ compiler of the specifics of calling the external FORTRAN functions, such as stack management, argument order and name decoration, to allow the linker to take the correct actions.

There exist some differences between the languages in the way things are done by definition. For instance, in FORTRAN every function argument is passed by reference, meaning the actual variable in terms of address is passed, as opposed to creating a temporary and passing this to the function instead. Passing by reference is of course a requirement for some function calls where modifications are to be made to the arguments for use after the function has returned. C++ allows this in a simple manner, although it has to be explicitly declared that such a situation is intended. Instead C++ defaults

to passing arguments as dummy variables which are created on function entry and destroyed on exiting. Care must be taken when performing mixed compilation of these two languages to remember that every call of a FORTRAN function is in fact passing by reference, and therefore it must be ensured that modifications are not made to these values in the function body if indeed this was not the intent. Also by the nature of the FORTRAN function, the arguments passed by a calling C++ segment of code need to be in the form of pointers.

A further difference centres on the way arrays are implemented within the languages. In C++ an n dimensional array consists of elements indexed from 0 to $n-1$; in FORTRAN the indexing instead begins at 1 and reaches n. No method of indexing is inherently better than the other, with both being favourable under different circumstances. A further difference is the order of indexing used for multidimensional arrays where FORTRAN does this in the opposite order to C++ such that `Farray[k][j][i] = Carray[i][j][k]`. Here C++ is indexing the array in a row-first order with FORTRAN using column-first, again with no one way being more correct than the other. The row-first method does correspond more closely with the indexing commonly met in working with matrices and can therefore prove more intuitive to programmers exposed to such areas. Differences can exist where the contiguous nature of an array can make a difference depending on its order although such concerns may be of little significance when the majority of a program is written in an object orientated language such as C++. Both of the above array issues can be dealt with either by making the necessary considerations on a call by call basis, or more simply by creating a new object that can take care of all the necessary conversions and indexing in an automated fashion.

5.1.2 Calling CFAST

The CFAST code was modified to allow it to be callable from within SMARTFIRE as opposed to running as its own separate instance. This was

done by modifying the structure of the program, removing the FORTRAN 'PROGRAM' section (equivalent to a C++ 'main()') and creating several relevant 'SUBROUTINE' sections that could be called in a sequence and timing dictated by SMARTFIRE.

The sequence of CFAST is such that the program performs initialisation of the required data, then a single call of the solver routine, followed by program exit. The solver routine itself takes care of any specifics of the solution procedure, such as discontinuities and printouts requiring a certain partitioning of time, but for all intents and purposes the structure of this itself is also composed of a single call to the numerical solver DASSL [Brenan1989].

In this way the time-step in CFAST is not as defining a quantity as with SMARTFIRE. Here it is allowed to vary as the numerical solver sees fit, to ensure it remains favourable to the numerics involved. The solution routine is begun at the start time of the simulation and run to the end time, covering the total time in one sweep. As mentioned above, printouts and discontinuities may require the numerical solver to return command to the solution routine for specific actions, although this is an exception rather than the norm. In many respects the solver simply solves the entire simulation in one go, which is very different to the solution routine occurring in SMARTFIRE. In addition to this, the explicit solution routine in CFAST performs no iterations, instead stepping through time directly.

Due to these issues, the solver routine has been modified to allow this portion of the model to be called on a step by step basis, with the difference between the start and end times that are given to the numerical solver simply being the CFD time-step. Also, as SMARTFIRE iterates the sources provided to CFAST will change, therefore it is necessary to perform additional calls to the solver for the same segment of time. This results in a further requirement of storing the values used at the beginning of the first call of a time-step,

effectively allowing restarts of the solver from the same point for consecutive CFD iterations.

This is achieved by duplicating the solution vector within CFAST. On beginning the time-step a copy of the original solution vector is made and stored in a sweep vector. The numerical solver performs its calculations and updates the sweep vector, the values of which are past to the CFD model, to which control is returned. As the next iteration is begun, and the CFAST solver is re-entered, the sweep vector is reset to the values stored in the original solution vector and the numerical solver is called again. This repeats until the final iteration of the time step, at which point the original solution vector is passed instead to the numerical routine, resulting in this being updated for use in the next time step, for which the procedure is repeated.

5.1.3 Passing Variables

Zone values that are used on the hybrid interface, i.e. temperature and density of both layers, compartment pressure and layer height, are retrieved from the zone model by simple copy statements. The values are taken directly from the newly updated CFAST solution vector since the zone model is run at the very beginning of a SMARTFIRE iteration. It was also a requirement that the solution vector be transferred into a common block to allow access from outside of its original FORTRAN routine.

The variables passed to CFAST from SMARTFIRE are the source terms for mass and enthalpy for both layers. These sources are calculated as shown in section 4.4.3 and are copied into variables which are passed as arguments of the CFAST solver call. The CFAST routine HFLOW calculates inter-compartment fluxes of mass and enthalpy and stores them in corresponding variables for use in the solver. The hybrid source terms are simply summed on to these variables at the end of the HFLOW routine.

5.2 Results

5.2.1 Test case 1

Setup

The test case comprises three rooms in series; a middle fire room which is vented to two side rooms, these side rooms being further vented to the exterior. The case is symmetrical about the centre of the fire room, see figure 5-1; the line P in figure indicates the location where comparisons between the full field, hybrid, and zone models are made.
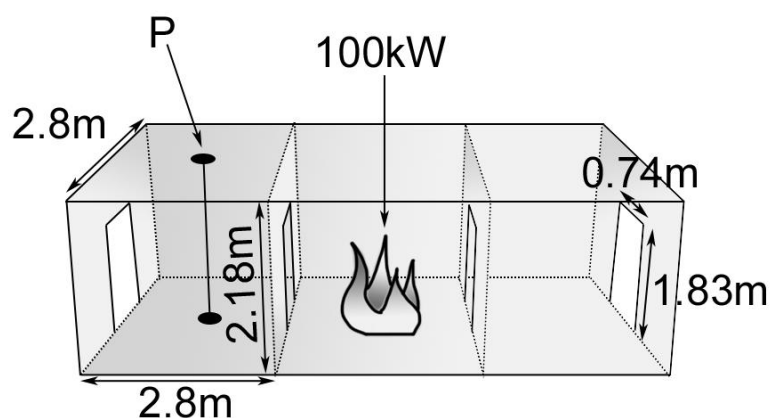
Figure 5-1. Test case configuration and data comparison location.

All rooms have equal dimensions: width 2.8m, depth 2.8m, and height 2.18m. Also all vents are doorways of height 1.83m and width 0.74m and centrally located on their respective walls. The vents/doorways are open for the entire duration of the simulation. The fire is modelled as a simple heat source of constant 100kW heat release rate, and is located centrally on the floor of the fire room. The simulation was run for 100 seconds using one second time steps, and was run in SMARTFIRE (full-field), CFAST (full-zone), and the hybrid model, where the right side room was replaced by a zone model; for the field and hybrid simulations 50 iterations were performed over each time step. The case was run full field to provide an upper bound to accuracy and computational time, and the hybrid model was expected to perform proportionally quicker than the full-field simulation. The case was run in

CFAST to provide an indicator of the computational resources required by the zone aspect of the hybrid model, and the Hybrid was expected to give more accurate results than the CFAST simulation. The cell budget was 9261 cells for each room; the total cell budget for the full field simulation was 33,957 cells (including extended regions), and the total cell budget for the Hybrid simulation was 21,609 cells (after removal of one side room and the respective extended region).

Results

The first comparisons are between the field section of the Hybrid model and the full field results. Depicted in Figure 5-2 is a 90°C iso-surface at the 10, 30 and 50 second times of the simulation, along with the velocity field. The full field simulation is shown on top, and the field section of the hybrid model is shown below.
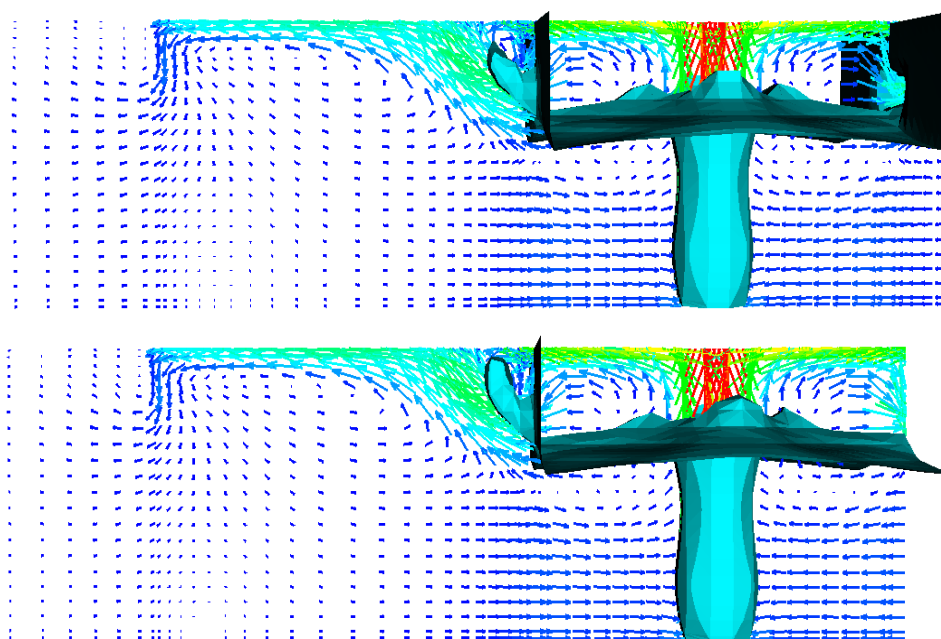
10 seconds

(Figure 5-2 continued on next page.)
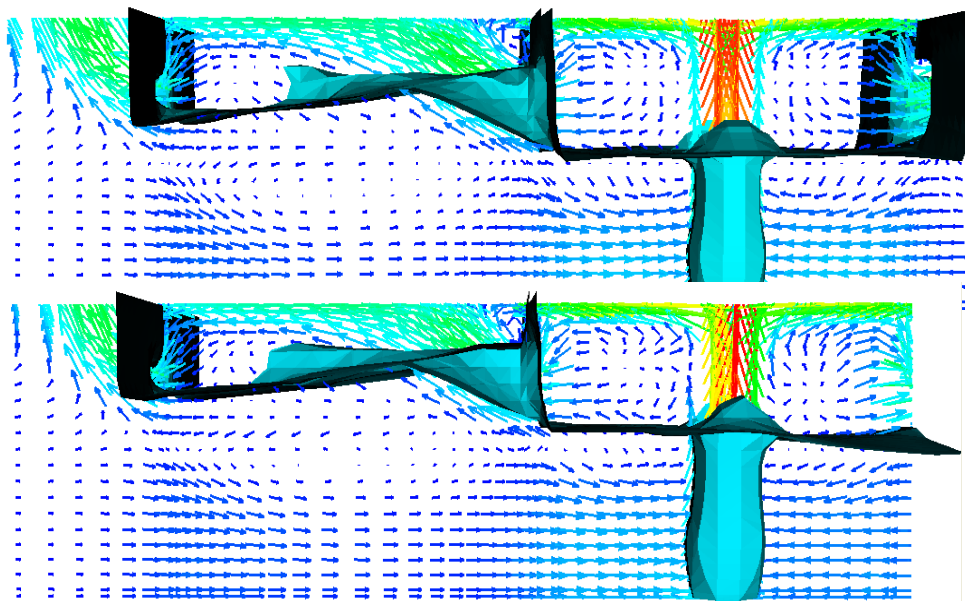
30 seconds
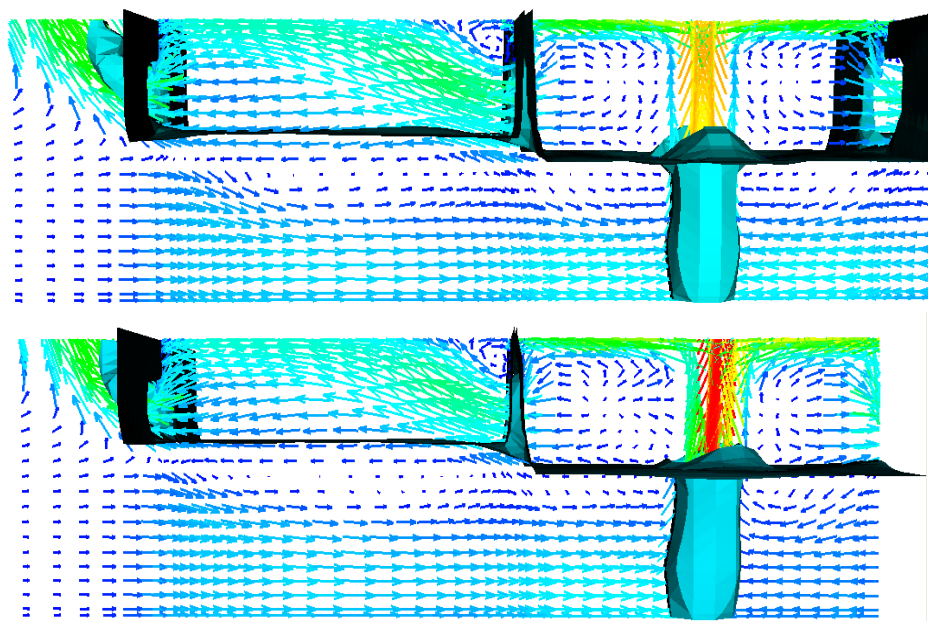
50 seconds

Figure 5-2. The 90°C iso-surface and velocity vectors in a vertical plane passing through the fire produced by the full-field (top) and hybrid (bottom) models for times 10, 30 and 50 seconds.

Depicted in Figure 5-3 are the vertical temperature distributions at location P over time. These comparisons highlight the effect that the implementation of the hybrid zone model has on the field results. As can be seen, there is good conformity between the two different models, with the temporal temperature values and velocity vectors being in excellent agreement. From the final comparison at 50s it can be seen that there is a slight plume lean in the hybrid model. This is to be expected due to the close proximity of the interface to the fire due to the reduction in data at the interface compared to the full field model.
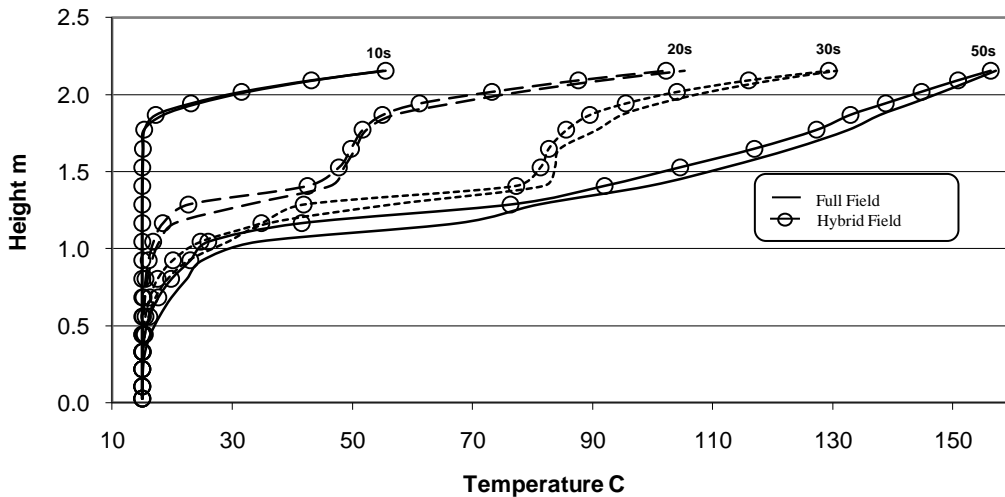
Figure 5-3. Vertical temperature distribution at location P for times 10s, 20s, 30s and 50s.

The next comparison illustrates the agreement between the zone section of the Hybrid model and the full field model. Presented in Table 5-1 are the upper and lower layer temperatures for SMARTFIRE, the Hybrid zone and CFAST, along with the percentage change over SMARTFIRE. To enable this comparison the data from the full field model was reduced to a two zone form equivalent to the zone model using the mass equivalency method (see section 3.3.9) Using these values for the full field, a comparison can now be made between the three different models. Looking at table 5-1, it can be seen that after an initial period, the Hybrid model agrees more closely with the full

field model than does CFAST. One assumption of the zone model is that the interface height is accurate to within a spatial error of approximately ten percent. Taking this into account, it can be seen that the hybrid model produces some very satisfactory results. The computational time for the full field model was approximately 3 hrs 33 mins while the computational time for the Hybrid model was approximately 2 hs 24 mins. This is a reduction of around a third, as is to be expected with the removal of a third of the solution domain.

Time	Model	Upper Layer Temp (C)	Change over SMARTFIRE	Lower Layer Temp (C)	Change over SMARTFIRE	Interface Height (m)	Change over SMARTFIRE
	SMARTFIRE	86.3	-	14.9	-	1.1	-
30s	Hybrid	106.4	23.29%	16.6	11.41%	1.4	21.62%
	CFAST	82.9	-3.94%	16.9	13.42%	1.3	16.22%
	SMARTFIRE	90.9	-	14.9	-	1.1	-
40s	Hybrid	108.4	19.25%	17.2	15.44%	1.3	20.56%
	CFAST	97.9	7.70%	18.9	26.85%	1.3	19.63%
	SMARTFIRE	108.0	-	14.9	-	1.1	-
60s	Hybrid	112.9	4.54%	18.3	22.82%	1.3	18.87%
	CFAST	120.0	11.11%	21.9	46.98%	1.3	24.53%
	SMARTFIRE	116.0	-	14.9	-	1.1	-
80s	Hybrid	114.1	-1.64%	18.4	23.49%	1.3	16.67%
	CFAST	131.0	12.93%	24.9	67.11%	1.4	25.00%
	SMARTFIRE	118.0	-	14.9	-	1.1	-
100s	Hybrid	115.4	-2.20%	18.1	21.48%	1.3	16.51%
	CFAST	137.0	16.10%	26.9	80.54%	1.4	24.77%

Table 5-1. Upper and lower layer temperatures, interface height and a percentage difference for the Hybrid and CFAST results over the full field (SMARTFIRE) at different times.

Conclusion

The above results demonstrate that a hybrid model can be a viable option when the computational resources demanded by a field model are too 'expensive'. It has been shown that the implementation of a zone model interface has a small effect on the final field results, even when the interface is situated in close proximity to the fire. It has also been shown that the

results reported by the Hybrid's zone are in good agreement with the SMARTFIRE (full field) results. The decrease in computational time required was equivalent to the percentage of CFD domain replaced by the zone model, which is in agreement with the methodology. As expected, the Hybrid model shows an improvement in computational time taken over the full field simulation, and also produces closer agreement to the full field model results than the full zone model. Future work is directed at implementing different aspects within the Hybrid frame, such as radiation, species flow, and turbulence. These will hopefully increase the accuracy of the method without significantly increasing the computational time required.

5.2.2 Test Case 2

The second test case is a simple extension of the first, where the zone domain now consists of multiple compartments. Since CFAST deals with this situation automatically, so long as its case files are modified accordingly, there is little extra work to be done as far as the hybrid implementation is concerned. Since the implementation both uses and modifies the array elements of the solver routine directly, the only extra concern of a multiple-room situation is ensuring these elements are mapped correctly, relating to the particular zone compartment containing the hybrid interface. Since the hybrid implementation affects this initial room alone, the results in further compartments are dictated by the validity and accuracy of the CFAST zone model itself, and are not such a direct test of the hybrid model. If the hybrid implementation is such that the first room is provided with the correct fluxes of both mass and enthalpy, then the remainder of the simulation will provide results of the level expected of CFAST.

Setup

The test case consists of a symmetrical floor plan with 2.5m high ceilings and two identical six compartment 'legs' coming off a main fire room (see figure 5-4). The legs consist of a corridor to which five rooms of differing size are

connected. The corridors are vented open at both ends with one end connected to the fire room and the other vented to the exterior, with all door soffits at 2m. The fire is modelled as a simple 150kW heat source, and solids are removed meaning no enthalpy is lost from the gases through conduction to the surfaces. The simulation was run for 150 seconds, with 50 iterations for each time-step.

Figure 5-4. Floorplan showing setup of test case 2.
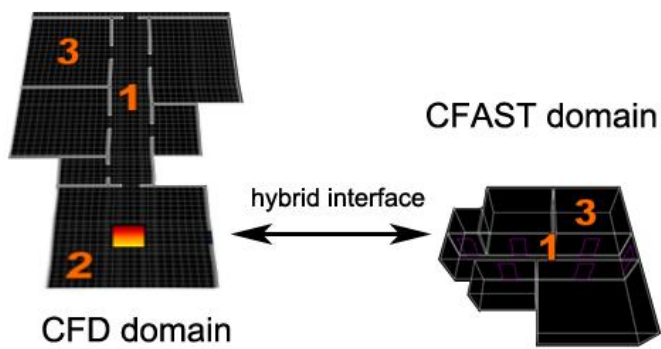
Figure 5-5. Replacement of the right leg of the domain with the CFAST zone model. Locations of comparisons are numbered.

For the hybrid simulation, the right hand 'leg' of the domain was removed to be modelled by CFAST, with the door linking the corridor to the fire room being replaced by the hybrid interface (figure 5-5 above).

Results

The first comparison is for the vertical temperature distribution at location '2' (see fig 5-5), between the full field simulation and the hybrid simulation and is shown in Fig 5-6 below.
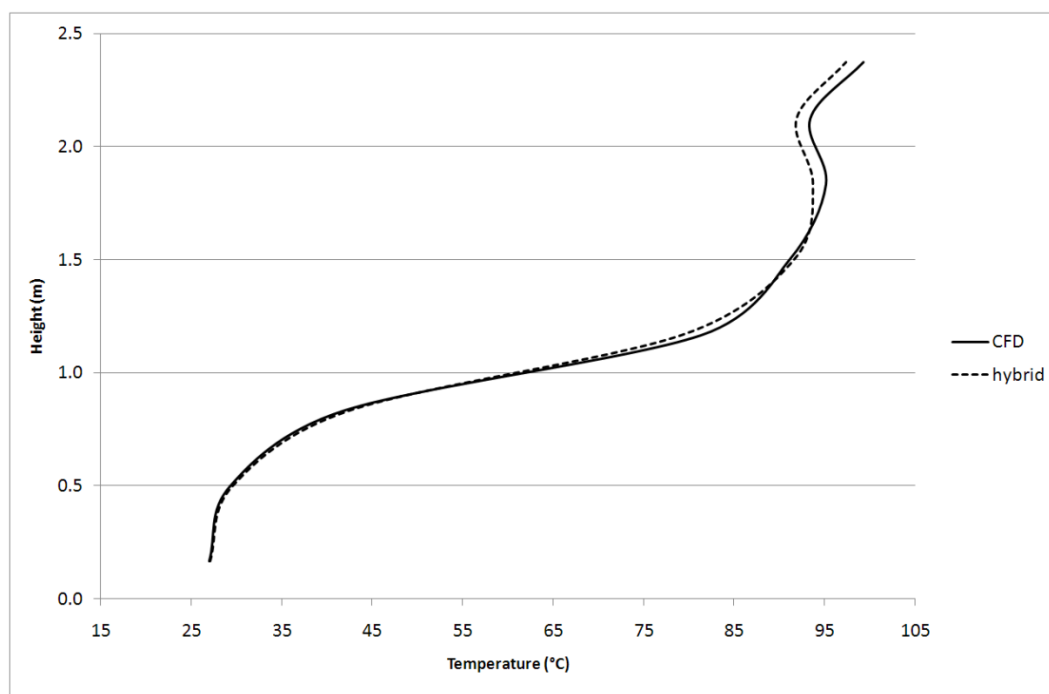
Figure 5-6. Plot of vertical temperature distribution at location '2'.

Here it can be seen that the two temperature distributions agree extremely well. Since this location is within the CFD domain of both simulations, it is a test of any detrimental effect that the inclusion of the zone model may have on the remainder of the domain. It can be seen that despite the close proximity of the hybrid interface to this location, and the size of the section of domain that has been removed, this effect is minimal. This can also be seen in figure 5-7 which is a cross sectional slice down the centre of the CFD

corridor (left leg) of both simulations, showing both temperature contours and velocity vectors. The CFD (top) and hybrid (bottom) results again compare well with slightly more variation seen in the velocities than the temperatures.
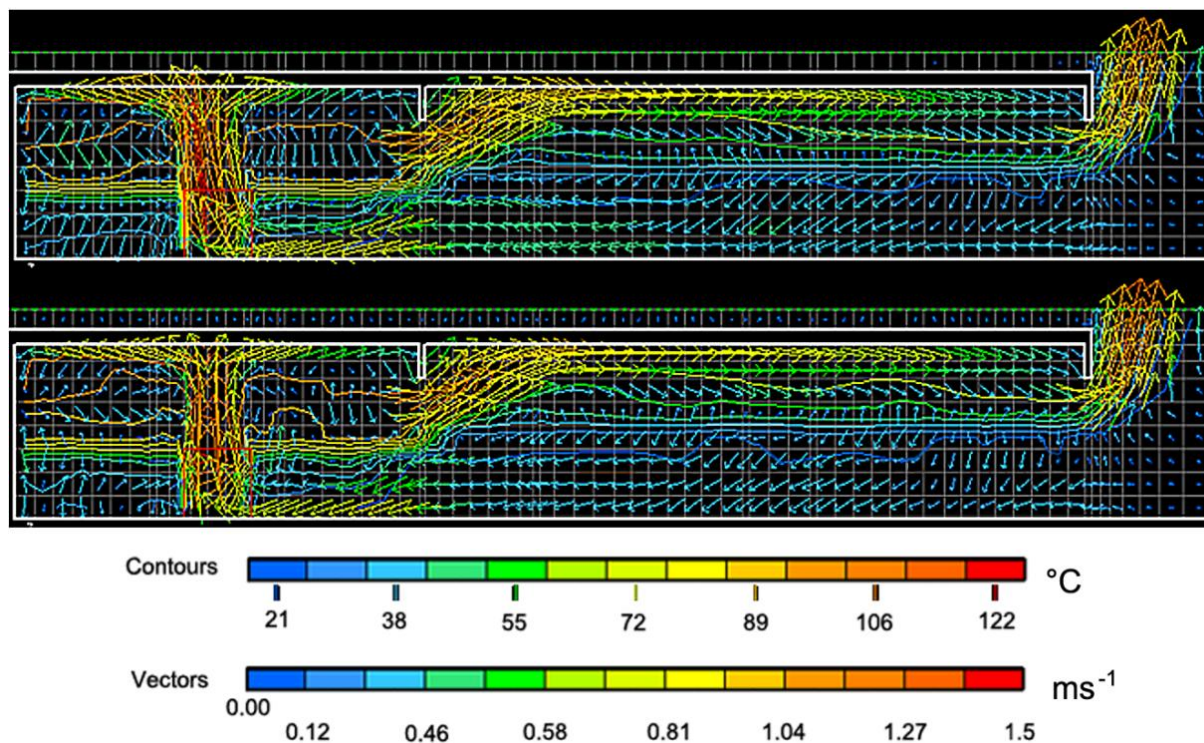
Figure 5-7. CFD (top) and hybrid (bottom) temperature contours and velocity vectors for the corridor section of the left leg.

The second set of comparisons are for sections of the domain that get replaced by the zone model; here the mass equivalency method (section 3.3.9) has again been used to reduce the CFD data down to a two layer equivalent. Figure 5-8 below shows plots of the temperature within the corridor section of the right leg.

Here the layer can be seen to be in reasonable agreement between the simulations, with the difference being slightly over ten percent. The lower layer temperature is slightly higher in the CFD simulation which is to be expected since opportunity exists here for heat transfer or mixing between layers, which is not possible in the zone model. The upper layer temperature

is higher in the zone model, although this may be explained by the thinner upper layer having less mass to spread any enthalpy over. Figure 5-9 shows a similar comparison, but for the room at location '3' (see figure 5-5).
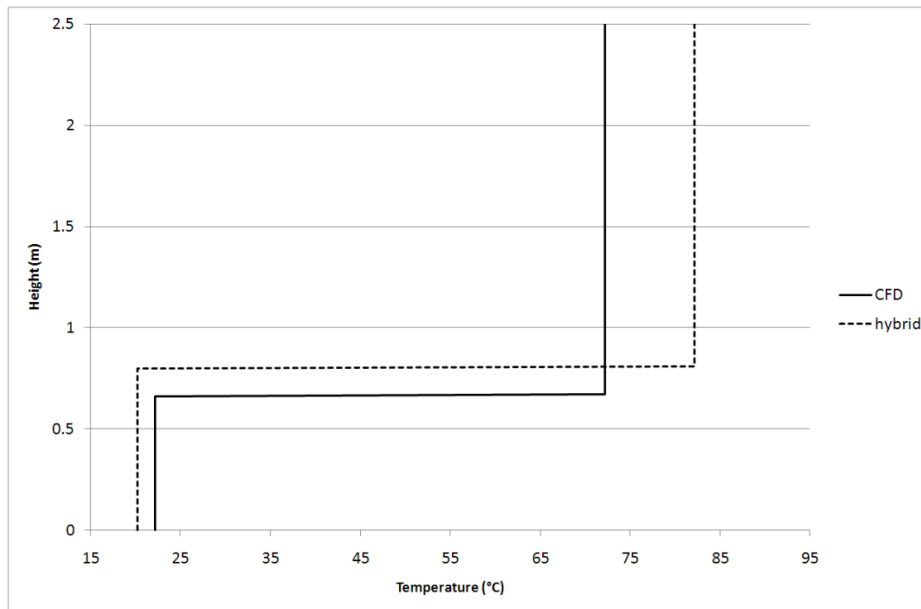
Figure 5-8. Vertical temperatures for the corridor section of the right leg.
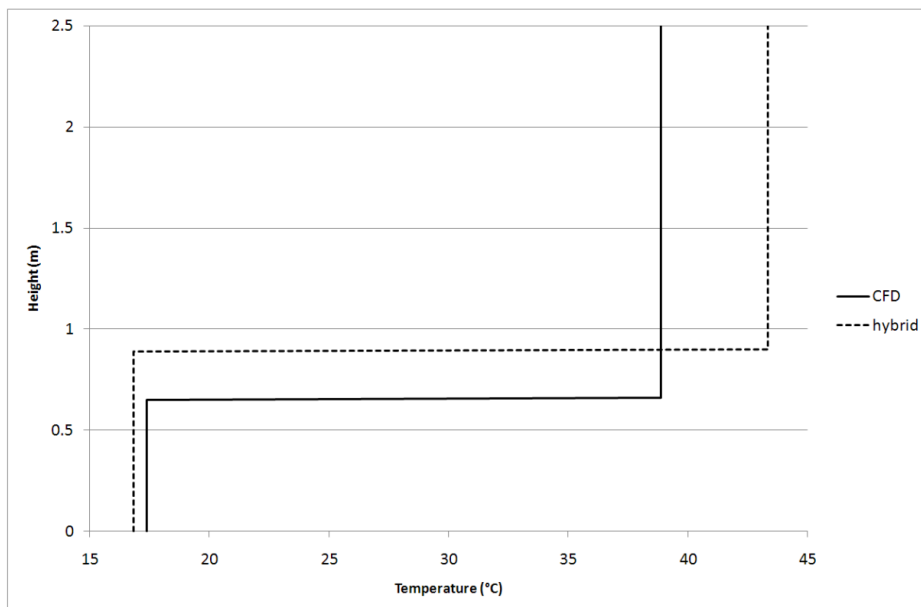
Figure 5-9. Vertical temperatures for the room at location '3' of the right leg.

Here the results agree less well than those for the corridor section in figure 5-8. The lower layer is again slightly hotter for the CFD simulation, which is likely to be due to a small amount of energy transfer as mentioned previously. The layers are not in such good agreement, with a difference significantly greater than the ten percent that is commonly expected from zone models. There is also an error of over ten percent in the upper layer temperatures, although it may again be possible to explain this with respect to the differences in layers. A further possible explanation for these differences in location '3' is that they are in a 'second-order' zone, in the sense they are separated from the CFD domain by another zone compartment. In this way the conditions they are exposed to are a further approximation since they come from a two layer zone model; this is in comparison to the corridor section, which is exposed to conditions at the boundary that are from the higher resolution CFD fire room.

The hybrid corridor upper layer is at a temperature corresponding to an average of the range reached in the upper layer of the CFD corridor. Rooms are not exposed to the section of upper layer that resides above their doors, therefore second order rooms connected to a hybrid corridor may very well be exposed to higher temperatures than their CFD counterparts since the averaging is for the entire layer and independent of any considerations of soffit height.

6. FSEG-ZONE / SMARTFIRE Hybrid Model

The problems in dealing with closed hybrid simulations centre around differences in model formulations and the necessity of different sized time-steps for explicit and implicit solution procedures. To remedy this, a custom zone model (FSEG-ZONE) was created which allowed total freedom over the solution procedure used. This not only allowed a common time-step to be used between models, but also allowed a solution procedure to be implemented that circumvented some of the issues of extreme sensitivity in the zone equations. This chapter discusses the formulation and implementation of the hybrid model linking SMARTFIRE with the custom zone model FSEG-ZONE.

6.1 Closed Case Formulation

The handling of the pressure boundary equation within the CFD model, along with the formation of the layer sources for use in the zone model are performed by the same method as presented in chapter 4. The differences in implementation centre on the calculation of zone variables which are now solved using a different formulation of the zone equations through the use of a custom bisection solver. The custom zone model replacing CFAST is self contained and its representation within the CFD domain remains identical to that of CFAST if the existing routines for obtaining boundary condition values are modified to make use of the custom zone variables instead.

The aim of the present method is simply to find the end of step zone pressure for use on the pressure boundary condition within the CFD model. The FSEG-ZONE solution is performed *between* the CFD iterations, with the solved value for pressure relying explicitly on the most recent CFD values reported in the cells on the boundary. Generally the solution of the zone

pressure varies along with the CFD variables over successive iterations, with these variations becoming smaller as convergence is reached.

The fundamental idea behind the formulation is that application of a specific zone-pressure at the boundary condition will result in the CFD model calculating a set of individual face fluxes across the interface, referred to herein as the CFD-velocities. In turn, a set of CFD-velocities summed over the interface and formed into zone layer source terms will result in a specific pressure change in the zone compartment. The solution desired is the value of pressure that equates these two situations such that the CFD-velocities and zone-pressure are consistent; i.e. when applied at the boundary the solved value of zone-pressure, P_Z^1, results in CFD-velocities that cause a change in zone-pressure over the time step, $P_Z^1 - P_Z^0$, sufficient to bring the previous value of pressure to this new solved value (see figure 6-1).
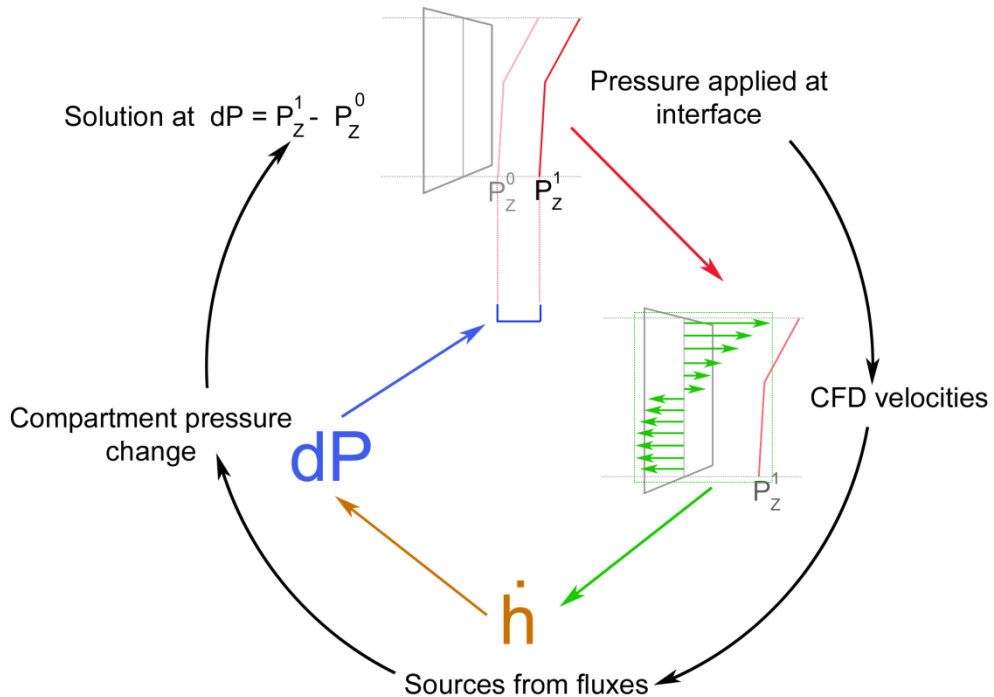
Figure 6-1. At the solution pressure the enthalpy flux and compartment pressure change are consistent .

During development of the FSEG-ZONE model various methods have been used to obtain the solution of the zone-pressure. The first method relied on a volume correction such that an error in interface fluxes resulted in a volume discrepancy at the current pressure. From the volume discrepancy a pressure correction term was constructed and used to update the pressure value. One issue with this method was that creating a pressure correction from a particular volume error was not a trivial matter since such a correction would need to take into account the dependency of the interface fluxes on the pressure variation. These dependencies are highly non-linear and are calculated by the CFD model, yet use of these values would render such a correction redundant since the requirement is to use it *between* CFD calculations. Another problem was the fact that there would be many orders of magnitude between the error and correction since a tiny change in pressure can cause a very significant volume error; since the calculation of one value explicitly relies on the other, rounding errors became a real problem in the corresponding calculations.

The volume correction method made the assumption that the current value of pressure was correct and that any error could be attributed to volume of the contained fluid. To counteract the problems above the formulation was modified such that the volume was assumed to be correct and that any error was contained in the pressure value. Since the volume at solution is naturally the compartment volume this value could be used throughout, effectively removing any consideration of the volume from the solution routine. In this way a calculation directly resulted in a pressure error which could then be used to update the pressure value and progress the solution.

Since the above method could easily be cast into a form of a zero or root finding problem it was naturally open to solution by numerous existing solvers. Use was made of the SNSQE solver, which is based on a modification of the Powell hybrid method [Powell1988], but again the highly non-linear and stiff nature of the zone equations meant that the solver was unable to solve the pressure to within any acceptable tolerance levels. The equation set

used by the zone model is neither particularly exotic nor difficult by general mathematical standards, simply the accuracy being sought by a method based on strict conservation of enthalpy and the magnitude differences involved meant that adequate tolerance was difficult to achieve.

Solution was occasionally attainable through extensive relaxation factors within the solver, but this caused prohibitive increases in the computational time required. Since the present FSEG-ZONE model is implemented on a single compartment basis, such that no two zone compartments directly affect one another, the formulation can be made in terms of a single dependent variable, the compartment pressure, and a bisection solver was implemented to make use of this fact. Given an interval within which a solution is known to lie, the bisection method is guaranteed to find this solution to a tolerance within the machine accuracy. Also, since the progression of the solution value is made in a controlled fashion by halving each successive interval, numerical stability is not an issue.

6.1.1 Bisection Solver

The solution method used is common to all bisection methods where an interval is successively made smaller by adjusting the end points in such a way that the true solution point is always contained in the interval. The initial interval is bounded by two extreme guesses of pressure such that the true solution can safely be assumed to exist between them, meaning that the residual error at these two points assumes different signs. The midpoint of these two initial guesses is then calculated and, depending on the sign of the residual, is assigned to one of the endpoints. This halves the size of the interval and ensures that the solution is still contained within. The procedure is then continued until the end points are less than a given tolerance (2ϵ) apart, the best guess at the true solution is then the midpoint of this final interval which will have an error less than half the tolerance, i.e. $|P_{actual} - P_{guess}| \leq \epsilon$.

As an alternative to the standard bisection solver, a Brent solution algorithm is also implemented [Brent1973]. The Brent method combines a bisection solver with both the secant and inverse quadratic interpolation methods. These additional methods tend to converge much quicker than the bisection method, yet are liable to experience difficulties with problematic equations. The Brent solver simply combines the methods to take advantage of these speedups, but reverts to the bisection method if the others experience convergence problems. As previously mentioned, the FSEG-ZONE equations have been problematic with regards to the stability of their solution, and during use of the Brent solver it has been apparent that little benefit is gained since the method generally reverts to the bisection solver regardless. Still, future model developments may improve this situation, and practically no overhead is experienced from including the option to use the other methods.

The key to performing this method is being able to accurately predict the effect that varying the zone pressure has on the CFD-velocities, since this solution procedure is performed without further calls to the CFD code. To do this a set of zone-velocities is introduced that can be varied through the zone solution in an attempt to predict what, if any, change will occur in the CFD-velocities once control passes back. At the beginning of each zone solution the CFD-velocities are copied into the zone-velocities, these are then used to form the fluxes for use in the zone equations. In this respect the CFD-velocities are not explicitly used, rather a corrected form of them; successive iterations between the models see these corrections tend to zero.

6.1.2 Velocity Correction

At the end of a CFD iteration the zone model is provided with newly calculated CFD-velocities, $v_{cfd,i}$. If it is assumed that these CFD velocities accurately represent the boundary pressure that was applied during that iteration, P^0, then any correction to velocity corresponding to a variation in pressure during this zone solution can be assumed to apply to these values.

At any point in the correction method the zone-velocities will consist of two components, the corresponding CFD-velocity and a pre-emptive velocity correction that is calculated from the difference between the new bisection pressure point (P^*) and the pressure applied over the last iteration (P^0), i.e.

$$v_{zone,i} = v_{cfd,i} + v' \qquad (6.1.1)$$

$$v' = f(P^* - P^0) \qquad (6.1.2)$$

where the value for this function or correction is a modified version of the pressure/velocity correction algorithm used within SMARTFIRE for internal cells (see section 3.3.7.2),

$$v' = -\frac{Ad(P^* - P^0)}{AP_{U_{vel}}} \qquad (6.1.3)$$

Now that it is possible to find the velocities at a given pressure point in the bisection method it is a simple matter of summing over these $v_{zone,i}$ to find the corresponding fluxes.

6.1.3 Zone Equations

The bisection method requires that for a particular pressure point, the zone equations must be evaluated directly without further iteration. This is generally performed in the order: compartment pressure, layer temperatures, layer densities and finally calculation of a volume error.

Flow variables and the calculation of the zone layer sources are performed in the same manner as in section 4.4.3 where variables are assigned depending on flow direction and layers assigned based on temperature and height. The mass and enthalpy sources are then used to evaluate the variables for layer i as follows (subscript 0 indicates 'old' values from the previous time step),

Volume

$$V_i = \frac{\left(m_{i,0} + \dot{m}_i \Delta t\right)}{\rho_i} \tag{6.1.4}$$

Temperature

$$T_i = \frac{T_{i,0} m_{i,0} + \dot{h}_i \Delta t \Big/ C_P}{m_{i,0} + \dot{m}_i \Delta t}$$

$$+ \quad \frac{1}{C_P \left(m_{i,0} + \dot{m}_i\right)} \cdot \frac{V_i}{V_{room}} \cdot (\gamma - 1) \cdot \left(\sum_i \dot{h}_i \, \Delta t\right) \tag{6.1.5}$$

Density

$$\rho_i = \frac{P_{ref} + P^*}{RT_i} \tag{6.1.6}$$

Pressure

$$P = P_0 + \frac{(\gamma - 1)}{V_{room}} \left(\sum_i \dot{h}_i\right) \tag{6.1.7}$$

Volume error

The volume error is a term that verifies that the calculations are being performed consistent to each other. For any given time-step, there will be a total room mass

$$m_{room} = m_u + m_l \qquad (6.1.8)$$

where the individual layer masses will be composed of the previous mass and any relevant flux

$$m_u = m_u^0 + \dot{m}_u \Delta t \quad , \quad m_l = m_l^0 + \dot{m}_l \Delta t \qquad (6.1.9)$$

The evaluation of the zone equations will provide a pressure P_{room} and layer temperatures T_u and T_l which result from enthalpy fluxes. The pressure and temperatures in turn directly imply densities ρ_u and ρ_l through the ideal gas equation. The layer volumes can then be calculated as

$$V_u = \frac{m_u}{\rho_u} \quad , \quad V_l = \frac{m_l}{\rho_l} \qquad (6.1.10)$$

with the total room volume then clearly being $V_{room} = V_u + V_l$. The difference between this calculated volume and the actual physically fixed room value is then the volume error.

Further development of the FSEG-ZONE model (see chapter 7) and future work to include additional phenomena will mean that the evaluation of the zone equations becomes more complicated. Additional terms will be required

in the zone equations and the particular order of evaluation also becomes a concern. The volume error becomes an important indicator that all these additions remain consistent to one another.

Another use of the volume error is for tracking any potential rounding error problems with regards to machine accuracy. Rounding errors are inherent to the nature of floating point arithmetic, with many simple decimal fractions not expressible as finite binaries. Increasing the precision of the data type used will reduce these errors but not entirely eliminate them. The precision afforded by the 'double' C++ data type is sufficient for the needs of the hybrid model, yet there is clearly potential for errors to compound as further calculations are performed, especially on running totals or for operations on numbers many magnitudes apart (such as enthalpy and mass). For this reason even the very first evaluation of the zone equations will result in a non-zero volume error, yet the key is to ensure that this value remains small for the duration of the simulation. Tracking the cumulative volume error from step to step is a useful way of ensuring that the compounding of rounding error is not invalidating conservation in any significant manner.

6.1.4 Modified Pressure Boundary Condition

The pressure boundary condition discussed in section 4.4.1 has four different components: a hydrostatic term, a SMARTFIRE normalisation term, a dynamic pressure drop term, and finally the zone floor pressure term; this final term is the predominant method of feedback for the zone compartment. Although the hydrostatic term varies for differing zone densities the actual pressure in the zone compartment is only represented in this floor pressure term, this term is therefore the most important with regards to coupling between the two models.

The methods for calculating vent flow in the CFAST zone model depend solely on the compartment pressures with a hydrostatic variation from this starting point. At the bottom of a vent between two rooms where the hydrostatic

contribution is zero, the pressure differential is simply the difference between the compartment pressures of the two rooms. Because of this, these values are also referred to as floor pressures and since the hydrostatic term manifests as a negative value these floor pressures are the highest value attained in the room. In this way the *average* pressure in a room will not correspond to these floor pressures, but to a lesser value somewhere midway up the hydrostatic distribution.

For the FSEG-ZONE model this discrepancy between the pressure at the bottom of the compartment and the actual total compartment pressure is taken into account. The value of pressure calculated in the zone model is the total room pressure and not the floor pressure, therefore using this calculated value on the pressure boundary is incorrect. A method is required to obtain the actual floor pressure from the room average and corresponding pressure distribution, allowing the pressure boundary to be handled in a more consistent manner, this is discussed below.

Average pressure

In a CFD cell, the pressure assumes a uniform value corresponding to the mass and energy within. For a 'room' of cells, the total pressure will again correspond to the total mass and energy in the room, from the ideal gas equation

$$P = \rho RT \qquad (6.1.11)$$

multiplying by the room volume gives

$$VP = mRT \qquad (6.1.12)$$

or

$$\frac{C_P V P}{R} = C_P m T \tag{6.1.13}$$

where the right hand side is the room enthalpy. This is equal to the sum of the individual enthalpies in all the cells composing the room, therefore

$$\frac{C_P V P}{R} = \sum C_P m_i T_i = C_P \sum V_i \rho_i T_i \tag{6.1.14}$$

$$V P = \sum V_i \rho_i R T_i = \sum V_i P_i \tag{6.1.15}$$

but since the room volume is again just the sum of the individual cell volumes

$$P = \frac{\sum V_i P_i}{\sum V_i} \tag{6.1.16}$$

Therefore the room pressure is the volumised average of the individual cell pressures. Extending this idea to the zone compartment pressure,

$$P_Z = \frac{\sum V_j P_j}{\sum V_j} \tag{6.1.17}$$

but since there is no variation in the horizontal directions the volumes can be split up into the product of the compartment floor area and the vertical displacement

$$P_Z = \frac{\sum Ah_j P_j}{\sum Ah_j} = \frac{\sum h_j P_j}{\sum h_j} \qquad (6.1.18)$$

Therefore the zone compartment pressure can be calculated by taking the average of the pressure distribution over the height of the room. Having no cells the zone pressure varies continuously over the height of the room, therefore the sums become integrals giving

$$P_Z = \frac{\int_b^t P(h)dh}{\int_b^t dh} \qquad (6.1.19)$$

where $P(h)$ is the pressure at height h, given by

$$P(h) = -g\rho_l h - 2g\rho_{ref} h + P_{ref}\left(e^{\frac{g\rho_{ref} h}{P_{ref}}} - 1\right) + P_{floor} \qquad (6.1.20)$$

when h is below the layer height I, or

$$P(h) = -g\big(\rho_l I + \rho_u(h-I)\big) - 2g\rho_{ref}\,h \qquad (6.1.21)$$

$$+ P_{ref}\left(e^{\frac{g\rho_{ref\,h}}{P_{ref}}} - 1\right) + P_{floor}$$

when h is above the layer. Equations 6.1.20 and 6.1.21 are simply the original pressure boundary evaluations from section 4.4.1 with the zone term now explicitly referring to the real floor pressure as opposed to the compartment pressure. The pressure drop term is also absent since this does not contribute to the zone pressure; it is a term representing phenomena in the CFD domain and is simply 'lumped' with the zone pressure for convenience. Equation 6.1.19 is then integrated using (6.1.20) and (6.1.21) and rearranged for the floor pressure to give

$$
\begin{aligned}
P_{floor} &= P_Z - \frac{1}{r}\Bigg[\frac{(r^2 - I^2)g\rho_u}{2} + \frac{I^2 g\rho_l}{2} \\
&\qquad + Ig(I-r)(\rho_u - \rho_l) - \rho_{ref}\,gr^2 \\
&\qquad + \frac{P_{ref}^2}{\rho_{ref}\,g}\left(e^{\left[\frac{\rho_{ref}\,gr}{P_{ref}}\right]} - 1\right)\Bigg]
\end{aligned}
\qquad (6.1.22)
$$

where r is the room height $(t-b)$. Once the compartment pressure P_Z has been found from the zone equations, P_{floor} can then be found for use on the boundary.

6.1.5 Bisect Difference

The evaluation for the bisection method depends on the difference between the current bisection pressure point and the pressure realized from the respective fluxes

$$\Delta P_{bisec\,t} = P^* - (P^0 + dP_{bisect})\qquad(6.1.23)$$

As mentioned in section 6.1.1, the bisection is begun with left and right values of P^* between which the actual solution definitely exists; i.e. $\Delta P_{bisect\,,left} \ll 0$ and $\Delta P_{bisect\,,right} \gg 0$. The midpoint of these two is then taken, the zone equations are calculated with corresponding ΔP found, and this point then replaces one of the end points such that $\Delta P_{left} < 0 < \Delta P_{right}$. In this way each bisect halves the interval under consideration, maintaining the solution within, and steps progressively towards the solution pressure point for which there is total agreement between all equations. Once this point is reached within a given tolerance, the zone equations are evaluated for a final time and the values are returned to the CFD model for use on the boundary condition.

6.2 Convergence

Due to the formulation and implementation of the closed hybrid model, conservation is tightly adhered to within the zone compartment(s). This side of the model is derived entirely from the fundamental concept of conservation, through the first law of thermodynamics, and over elementary relationships, such as the equation of state and those for density and internal energy]. The hybrid zone model equations are ordinary differential equations derived solely from this basis and no approximations are used in the process. In this way, these equations are entirely consistent with one another; conservation is realised through variation of any variable having the precise effect on the

remaining variables. The basic inputs provided to the zone model are fluxes of mass and enthalpy, with the inclusion of species (i.e. smoke, combustion, toxic products) and radiation handling extending these inputs to fluxes of these variables, which are fundamentally also of the enthalpy/mass variety. These source terms are used as the starting point for a complete evaluation of the zone equations in a specific order that ensures that each variable is consistently updated at the correct moment, in line with the particular fluxes having been considered to that point. Despite all fluxes acting simultaneously, the path independent nature of energy conservation makes it possible to structure the order of the equations in a way that simplifies the procedure, while ensuring the final result remains consistent. In this way the zone portion of the hybrid model attains conservation up to the numerical accuracy of the machine/data types used.

The main consideration for conservation therefore lies with the calculation and provision of these flux source terms to the hybrid zone model. As mentioned in section 6.1, the extremely stiff nature of the zone equations necessitates a specific solution procedure when dealing with a 'closed' hybrid compartment, where a complete solution of the zone model is required for each CFD iteration. These solved values within the zone model are not necessarily correct with regards to the actual solution to be reached at the end of the present time-step, these will naturally change with the evolving conditions in the CFD domain, but are instead accurate with regards to the present state of the CFD solution. The CFD solution reacts not only to a changing hybrid boundary condition, but also to changes within its own domain, such is the implicit nature of its equations; the zone model on the other hand is almost explicit in its formulation given that it is effectively allowed to perform any number of its own iterations (bisect method) for the single one performed by the CFD model. In this way, the CFD model converges to a solution over the iterations while the zone model in effect provides an accurate solution at each. Consequently, the error exists within the variables on the CFD side of the interface, most significantly with the velocities reported at the faces along the interface (the densities and

temperatures also clearly play a part although are less sensitive to the changes in pressure).

These velocities are considered by both models: the CFD model solves them accurately through its own PDEs, predominantly the momentum equation, whereas the zone model considers them in light of its comparatively crude velocity correction. The velocities provided by the CFD model are to be considered the more accurate of the two in the sense that the zone velocity correction cannot hope to capture the true dynamics open to consideration by the CFD equations, but until the CFD error is effectively zero the zone velocities must be used to calculate the fluxes to be passed across the interface. This is for the reason that despite their possibly dubious accuracy, these velocities guarantee the net fluxes required to satisfy the zone model equations, and it is paramount this is the situation to ensure numerical stability.

This procedure is more accurate than it may at first seem as the zone velocities find their basis in the values calculated by the CFD model; at the beginning of each zone solution, the zone velocities use the current CFD interface velocities as a starting point on which to perform the velocity corrections. The correction is similar to that used for internal cells during the velocity correction step of the SIMPLE procedure in SMARTFIRE, but only considers the direction normal to the interface. The zone velocity correction obtains an estimate of the *next iteration* CFD velocities for the given pressure change being returned to the boundary. This change in CFD velocities, from the present to the next iteration, is clearly non-linear due to its dependence on numerous factors; the zone correction is *linear,* but at convergence it provides an accurate approximation as the pressure changes are very small. This is an area where the hybrid model adds additional time to the computational procedure as there is a discrepancy between the two velocities until the residuals become small enough such that a linear approximation of the velocity correction is valid.

Once this stage is reached, the small pressure differences from one iteration to the next result in a uniform 'step' for the entire interface velocity profile in the opposite direction to the change in pressure gradient. At this point both the CFD and hybrid velocities appear very similar; the profiles are in exceptional agreement, but remain a very slight distance apart as residuals are never entirely eliminated. The extremely stiff nature of the zone pressure equation and the necessity of continuing to use the zone velocities for construction of sources can now be demonstrated through an example.

Consider a room of volume $V\ m^3$ with a door of area $A\ m^2$; also, corresponding to the 'step' between profiles mentioned above, consider a constant error of $\varepsilon\ ms^{-1}$ between all the velocities at the doorway; considering the flux through the doorway, this results in a volume error of

$$\varepsilon A\ m^3 s^{-1}$$

Assuming a temperature T Kelvin and density ρ throughout, this volume error corresponds to an enthalpy error of

$$C_P T \rho \varepsilon A\ J\ s^{-1}$$

which in turn will result in a pressure error of

$$\frac{(\gamma - 1)}{V} h\ =\ \frac{\left(\frac{C_P}{C_V} - 1\right)}{V} C_P T \rho \varepsilon A\ =\ R\gamma \left[\frac{T\rho A}{V}\right] \varepsilon\ Pa\ s^{-1}$$

Assuming a similar sized room to that used in later test cases ($2.18m$ x $2.8m$ x $2.8m$) with a door $1.83m$ high and $0.74m$ wide, and a relatively cool temperature throughout of $400K$ ($\rho \sim 0.89$ at atmospheric) gives

$$(283.28)(1.37) \left[\frac{(400)(0.89)(1.35)}{(17.09)}\right] \varepsilon\ \cong 1\ E^5\ \varepsilon\ Pa\ s^{-1}$$

This implies that to calculate the zone pressure to within a fairly loose tolerance of $0.1\,Pa$, would require calculating the velocities to within an error of $\varepsilon = 1\,E^{-5}\,ms^{-1}$, velocities correct to within one hundredth of a millimetre per second.

The reason for the order of magnitude between the respective tolerances in the different variables is the presence of enthalpy in the pressure equation. The mass flux is simply related to the velocity through both the interface area (generally less than $3m^2$) and the density ($1.2413\,kg\,m^{-3}$ at ambient). Enthalpy on the other hand is calculated from the mass flux multiplied by a factor of $C_P T$, which for the coolest of air under consideration is approximately $3E^5$. This poses the questions of which variables to consider when checking residuals during solution, and what tolerances to use when doing so.

Since the enthalpy flux is in practice almost proportional to the mass flux, having similar tolerances for both effectively renders the mass flux tolerance redundant as its residual is always many orders of magnitude below that of enthalpy. Taking into account that $1kg$ of ambient air has an energy content of approximately $0.3\,MJ$, it is tempting to consider the enthalpy in terms of mega Joules when calculating residuals. Making this change can affect the numerical stability of a scheme but adds nothing to its final accuracy as the effect is equivalent to simply increasing the tolerance of enthalpy by a factor of $1E^6$. Considering that asking similar tolerances of mass and enthalpy is superfluous, that assigning different tolerances can be either equivalent or arbitrary, and that both variables are approximately proportional to each other, the hybrid model considers only the mass flux at the interface when checking residuals. This choice was made for two reasons: firstly the mass flux is of the same order of magnitude as the remaining interface variables; secondly, SMARTFIRE uses a float representation for its variables which is limited to just over seven significant figures. Since the specific enthalpy is considered, i.e. on a per unit mass basis, it attains a minimum value of around $3E^5$ at ambient conditions. This means that changes around 0.01 and smaller are essentially lost, meaning the variable itself is not accurate

enough for residual calculation. The use of larger containers for the numerical data can address this final point, but the preceding issues remain.

6.3 Test Cases

6.3.1 Test Case

The first test case is the 'closed' counterpart of the case in section 5.2.1 which used the CFAST zone model. Here the zone compartment's external vent is removed, with the sole remaining vent being the hybrid interface which is connected to the CFD domain.

Case Setup

The case consists of three equal sized rooms, each 2.8m long, 2.8m wide and 2.18m high. All vents are 0.74m wide and 1.83m tall and are open for the duration of the simulation; the walls between rooms are 10cm thick. The rooms are connected in series although the right most room is only connected to the middle room; the left most room is additionally connected to the exterior (see figure 6-2).
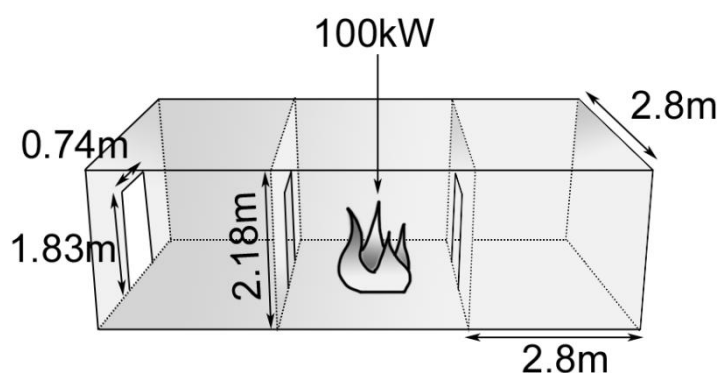
Figure 6-2. Setup for first test case.

The fire is modelled as a constant 100kW heat source and is centrally placed in the middle room. In the hybrid simulation, the rightmost room is to be

removed from the CFD domain and replaced by the FSEG-ZONE model. The cases are run for 300 seconds (5 minutes) using 1 second time-steps, with 100 sweeps used for each. Ambient temperature is assumed to be 288.15K and all surfaces are adiabatic (non-conducting). The cell-budget for the CFD simulation is 31,311 and for the FSEG-ZONE simulation is 22,932.

Results

The first comparison is for the variation in total compartment pressure and mass over the length of the simulation in the right-most room, this is shown in figure 6-3. Here it can be seen that the values between the CFD and FSEG-ZONE models for pressure agree exceptionally well up to the one minute mark of the simulation; from this point a slight discrepancy develops which is maintained for the remainder of the simulation, although the values do remain in very good agreement. The mass values begin to deviate around 45 seconds, although again they remain in close agreement and in fact begin to get closer towards the end of the simulation.
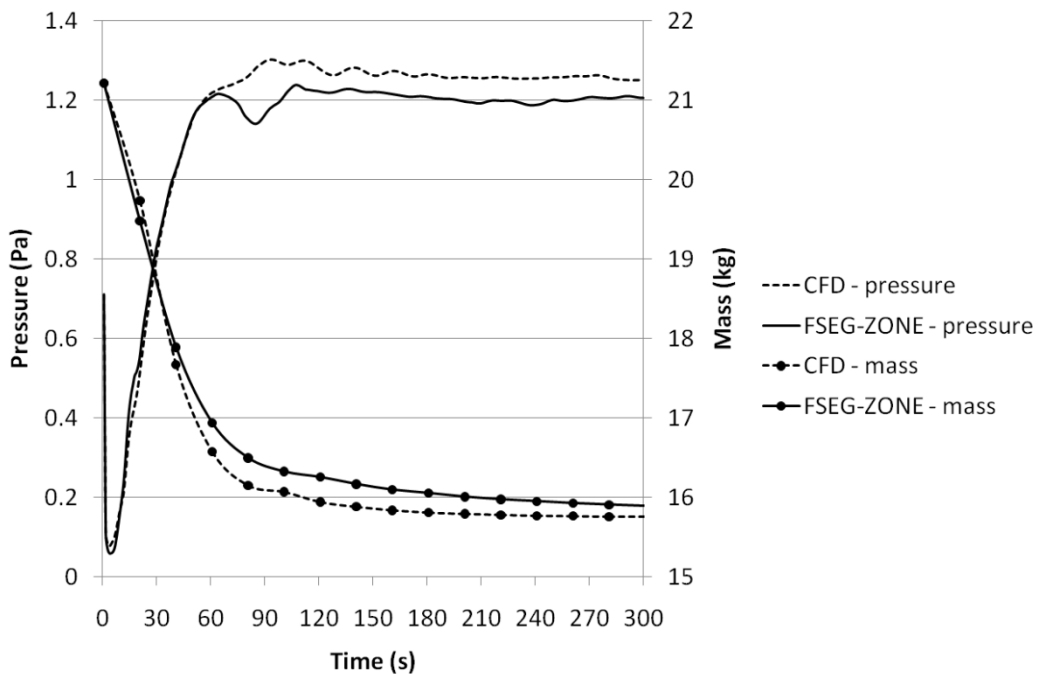
Figure 6-3. Pressure comparison between CFD and FSEG-ZONE.

As discussed in section 4.7, the differences seen in figure 6-3 are likely to be caused by the absence of variation in the layers of the FSEG-ZONE model. Since the pressure (and density) distributions are fundamentally different between the models, a discrepancy is to be expected since at the limit of accuracy the FSEG-ZONE model will still be a 'best fit' of the CFD data. The close agreement at the start is related to the small variation observed in the starting conditions, but as the simulation progresses the variation increases and therefore the discrepancy also. The results coming into better agreement towards the end of the simulation may be due to the more uniform nature of a situation approaching steady state, but it should still be remembered that such conditions will still present variation in the vertical direction.

The next set of comparisons is for both the upper and lower layer temperatures and is shown in figures 6-4 and 6-5; both the Quintiere method and the integral ratio method of layer reduction are used. There is exceptional agreement between the FSEG-ZONE results and the Quintiere layer reduction until the 180 second mark, but after this point the FSEG-ZONE results tend toward those of the integral ratio method, as expected. The Quintiere method assumes an ambient lower layer, suited to the initial period of a simulation, whereas the integral ratio method situates the layer at a height that assumes some lower layer heating, corresponding to the later periods of a simulation; this has been discussed at length in section 4.6. It is encouraging to note that the two reduction methods appear to act as bounds for the FSEG-ZONE data.

From figure 6-5 it can be seen that the FSEG-ZONE lower layer temperature agrees fairly well with both the reduction methods. The FSEG-ZONE seems to experience a delay of approximately 60 seconds before heating up whereas both CFD temperatures do so immediately. This can be attributed to the fact that there is no mixing between layers in the FSEG-ZONE model, meaning any increase in temperature needs to come from a corresponding flow of hotter gas from the CFD domain; this in turn requires development of

conditions within the neighbouring CFD compartment, hence the delay in time.

This is one of the obvious weaknesses of the FSEG-ZONE model at present, although the agreement is still commendable considering the small range of temperatures concerned (<50°C). It is interesting to note that the discrepancy seen between results over the duration of the simulation has already been gained during this initial 60 second period, after which all three results experience very similar variations. This would suggest that addressing the initial period more accurately in the FSEG-ZONE model would result in very close agreement between the two models.
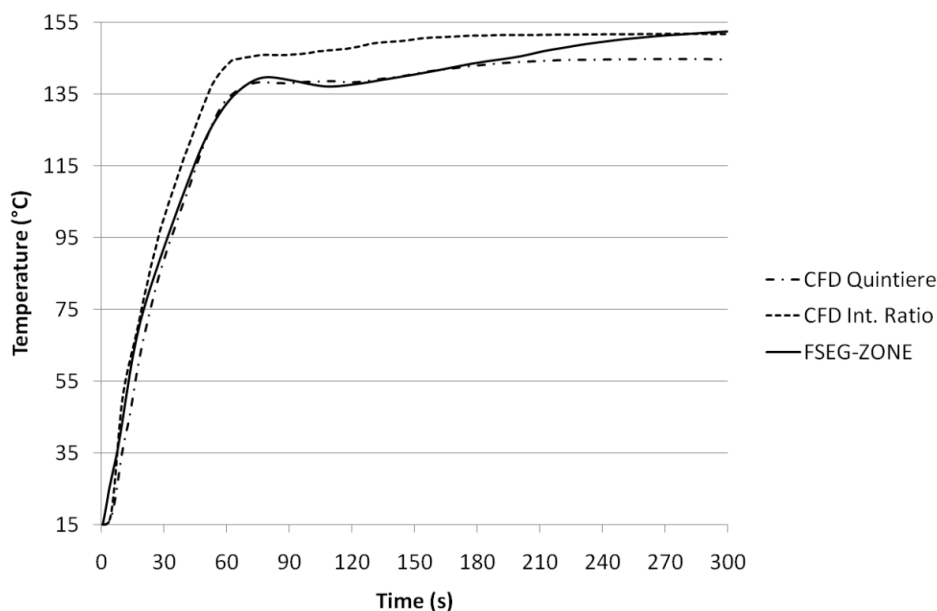
Figure 6-4. Upper layer temperature comparison between CFD and FSEG-ZONE.

Figure 6-6 shows the development of the layer height between the CFD reduction methods and FSEG-ZONE simulations and again demonstrates good agreement between the two models. The FSEG-ZONE layer spends the first 30 seconds of the simulation in close agreement with the Quintiere

method, then tending towards the integral ratio method as the simulation progresses.
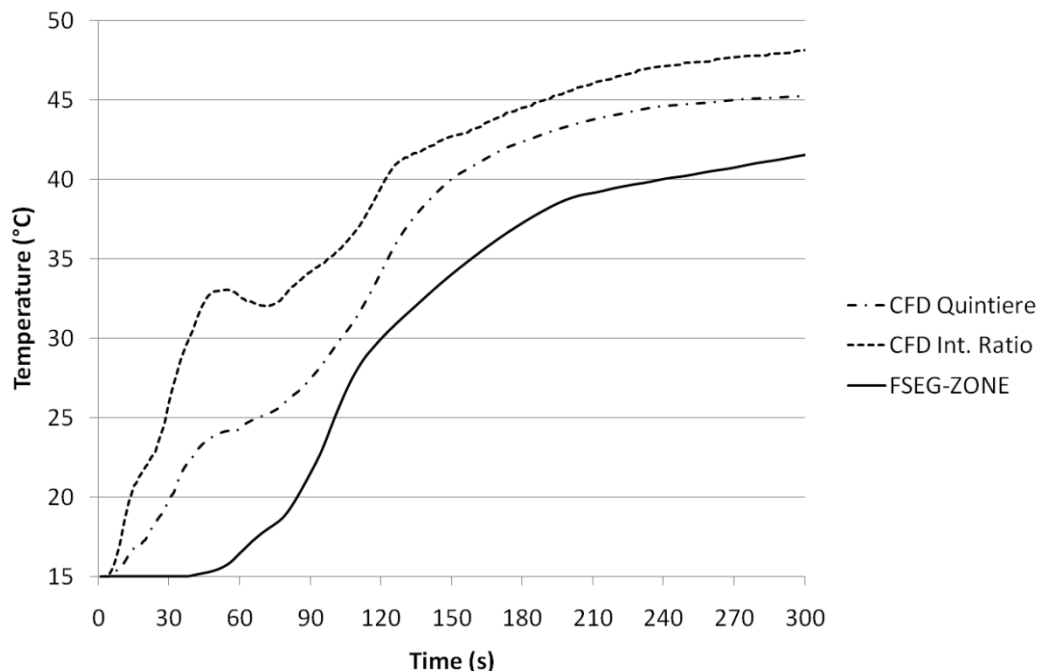
Figure 6-5. Lower layer temperature comparison between CFD and FSEG-ZONE.

There is exceptional agreement between these two values for the last minute of the simulation. The variation seen in the CFD layers during the first 10 seconds of results is caused by both layer reduction methods experiencing trouble in finding a definite layer in a temperature profile with very little variation. Again, the two reduction methods appear to act as bounds for the FSEG-ZONE layer which is always well within the accepted 10% error of the zone model [Steckler1982], [Quintiere1984], [Jones2009].

The above comparisons have all been made for the compartment being replaced by the zone model. Figures 6-7 and 6-8 below show comparisons for both temperature and velocity in the portion of domain that remains modelled by the field model in both CFD and FSEG-ZONE simulations. The

close agreement seen demonstrates that inclusion of the hybrid interface does not detrimentally affect the remainder of the domain.
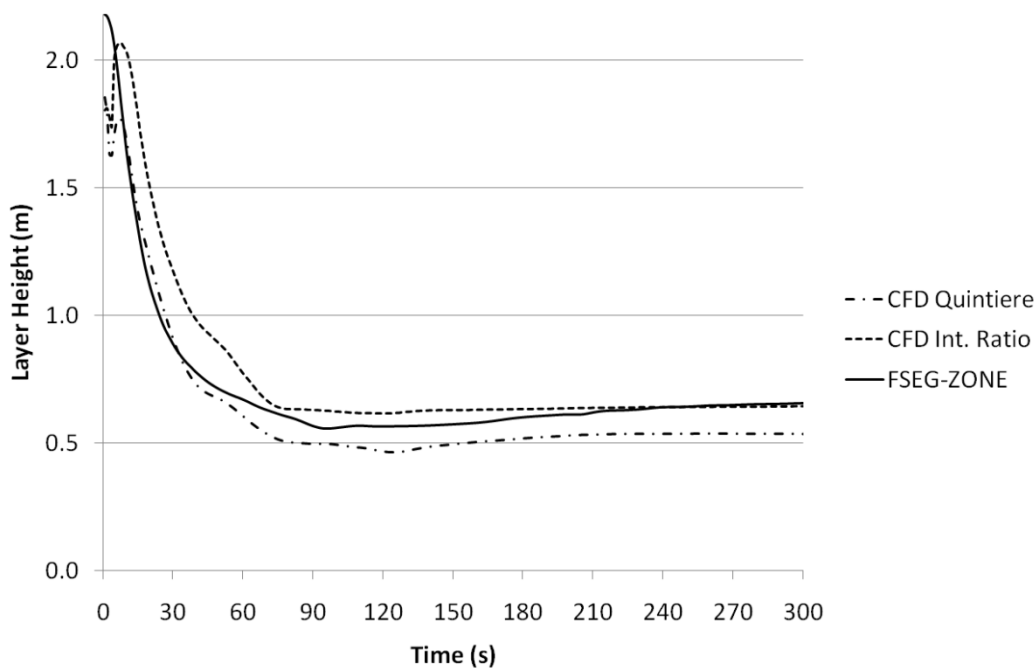
Figure 6-6. Layer development between CFD and FSEG-ZONE.

The full CFD simulation took 11h 14m 29s to complete; the FSEG-ZONE simulation took 7h 04m 06s to complete, resulting in a reduction in computational time of just over 37%; this is compared to a 26% reduction in the number of cells. The apparent 'over-unity' or super-linear efficiency may be attributed to the fact that removal of cells not only reduces the size of the system matrix, but also reduces the number of components of residuals such as total mass error. The strict conditions enforced over the hybrid interface net fluxes by the stiff zone equations may mean that intra-iteration convergence is made slightly easier to attain in the FSEG-ZONE simulation. It is certainly possible that the relatively simple nature of the present test case results in this effect being so pronounced in the final timings.
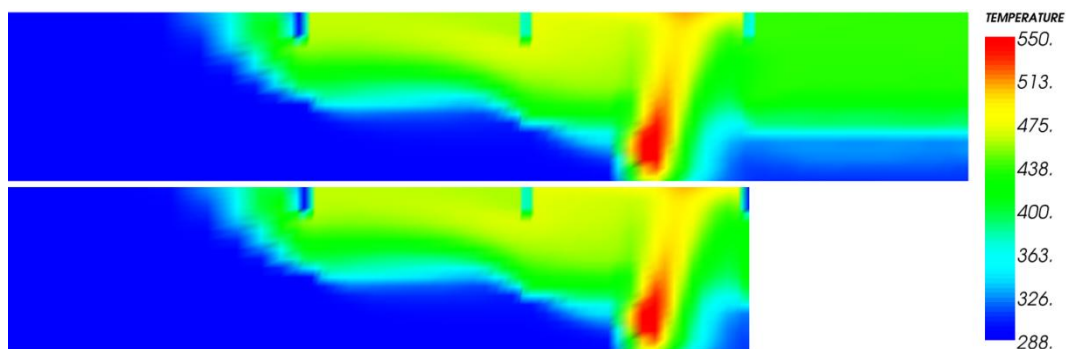
Figure 6-7. Temperature (K) cut-plane for full CFD (top) and FSEG-ZONE (bottom).
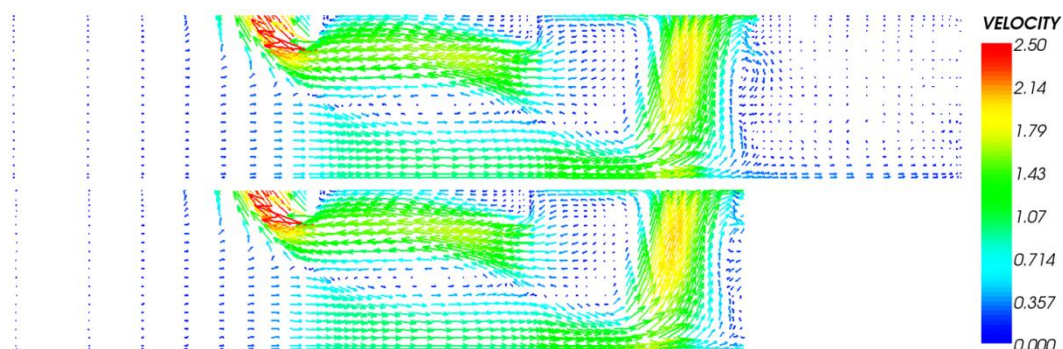
Figure 6-8. Velocity vector cut-plane (m/s) for full CFD (top) and FSEG-ZONE (bottom).

Further possible causes could be due to hardware configuration where for example cache effects, which are commonly experienced in parallel computing, will cause subtle differences in the accessing of data within the processor caches. Such effects are also observed in serial systems since even single processors are likely to include as optimisations various internal parallelisms. These effects are certainly not obvious and pose interesting questions for the potential optimisation of the SMARTFIRE CFD model.

6.3.2 Test Case – Wall and outlet alternatives

The second test case centres on the expected bounds of performance of the hybrid model as discussed in section 4.2. This case explores the effect on the remainder of the domain of replacing a compartment with the FSEG-ZONE model, compared to simply removing the room through the use of a wall patch or an outlet. Any hybrid model certainly needs to perform better than these two alternatives and the case presents a good opportunity for both the verification of the FSEG-ZONE implementation, and, since SMARTFIRE is separately validated, the validity of the FSEG-ZONE model itself.

Case Setup

The setup is identical to that in section 6.3.1 and figure 6-2 above, the results of which are used for comparisons below for the CFD and FSEG-ZONE simulations. The first additional simulation results from removal of the right most room from the CFD domain and simple closure of the vent by the placement of a wall patch, although the door frame remains (10cm depth); the second simulation uses an outlet patch at the same position. Since the rightmost room is removed for both the outlet and wall patch simulations, results do not exist at this location. The results below are all obtained through use of the layer reduction method on the leftmost room (field modelled in all cases) of the domain and since the reduction is employed in all four cases it is sufficient to assume a single method, here use is made of the Quintiere reduction (see section 4.6.2).

Results

Figure 6-9 below shows the compartment pressure for the four alternative approaches. It can be seen that the FSEG-ZONE model is in much better agreement with the full CFD results than either the outlet or wall patch alternatives, capturing both the magnitude and development of the pressure. As expected, the outlet's opportunity for pressure release results in a much lower overall pressure.
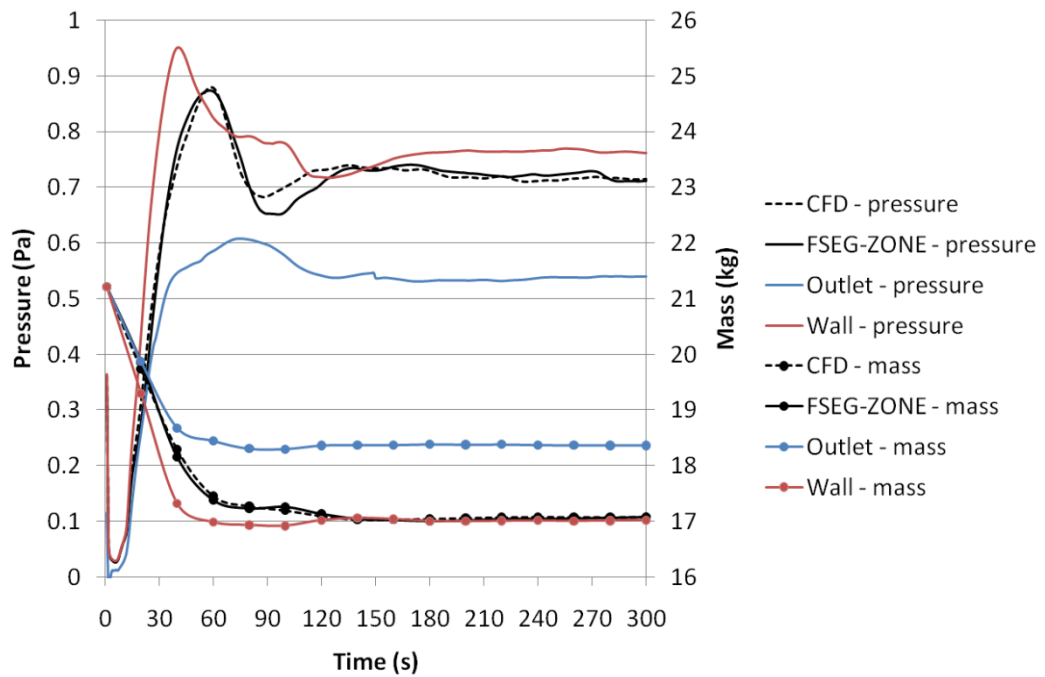
Figure 6-9. Pressure plot for the four alternative approaches.
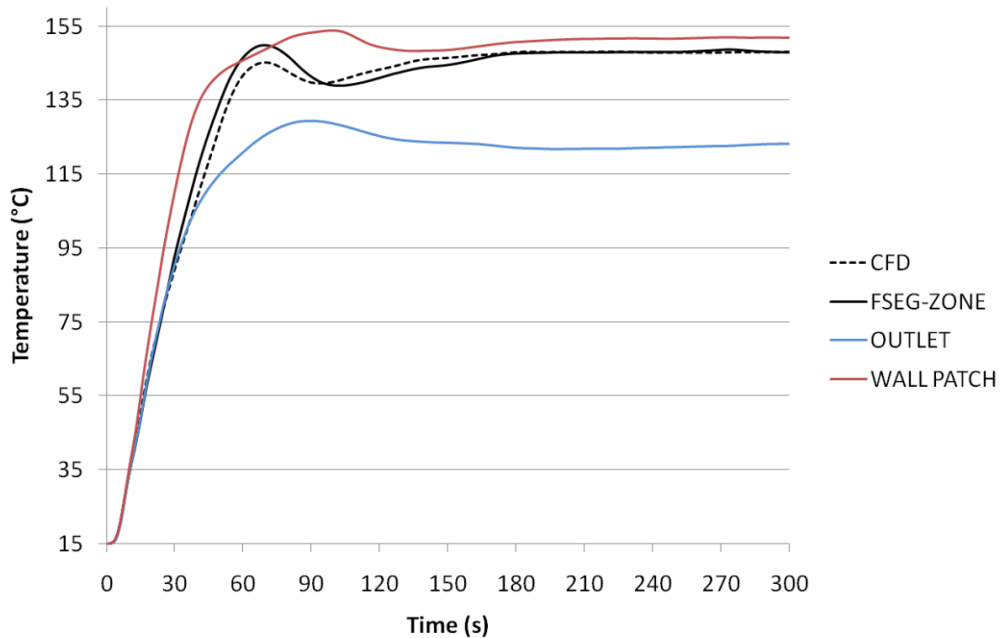
Figure 6-10. Upper layer temperatures (°C) for alternative approaches.
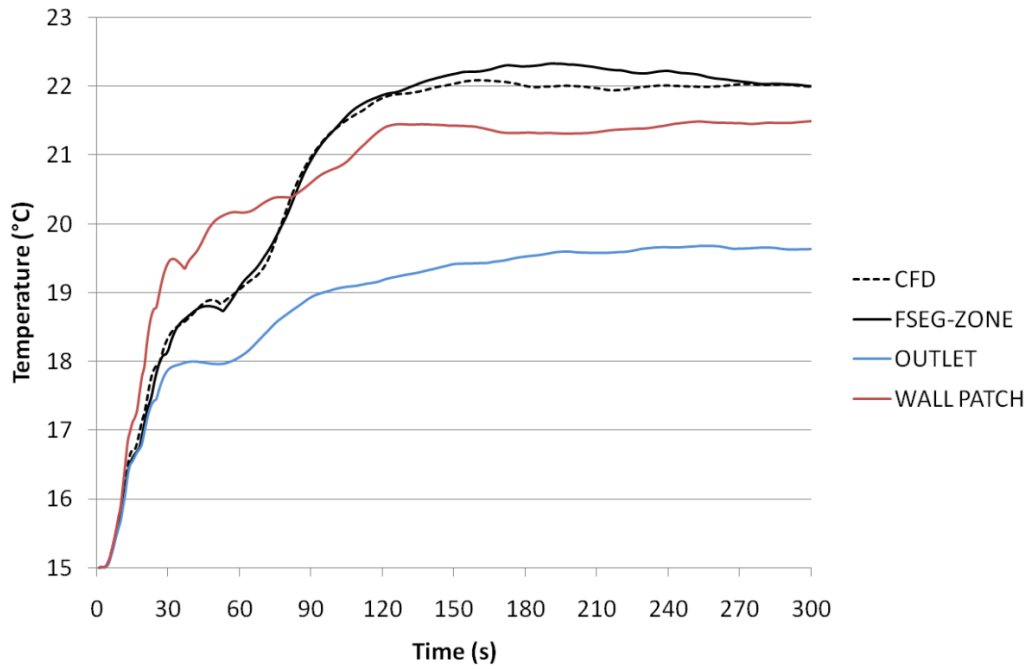
Figure 6-11. Lower layer temperatures (°C) for alternative approaches.

The upper layer temperatures are shown in figure 6-10 with the FSEG-ZONE model again in much better agreement with the full CFD results. Exceptional agreement can be seen throughout the simulation with final steady-state temperatures agreeing particularly well. Figure 6-11 shows the lower layer temperatures with the FSEG-ZONE model again providing significantly better results than either the outlet or wall patch alternatives.

The final comparison can be seen in figure 6-12 which plots the layer development for the four alternative approaches. Again the FSEG-ZONE model out-performs the outlet and wall patch alternatives with excellent agreement throughout the duration of the simulation. It is worth noting that although the wall patch simulation has the layer initially descending quicker then both the CFD and FSEG-ZONE simulations, it still comes into almost exact agreement with both towards the end of the simulation. This demonstrates that once a steady state has been reached, the removed compartment ceases to provide opportunity for pressure release and begins to behave similarly to the wall patch. As discussed in section 4.1, the room

ceases to behave as a sink and therefore the general dynamics of the simulation become similar as seen in the comparisons of pressure and layer height. Despite this the room still provides opportunity for enthalpy redistribution and this non-trivial behaviour can be seen in the lower layer temperature comparison in figure 6-11.
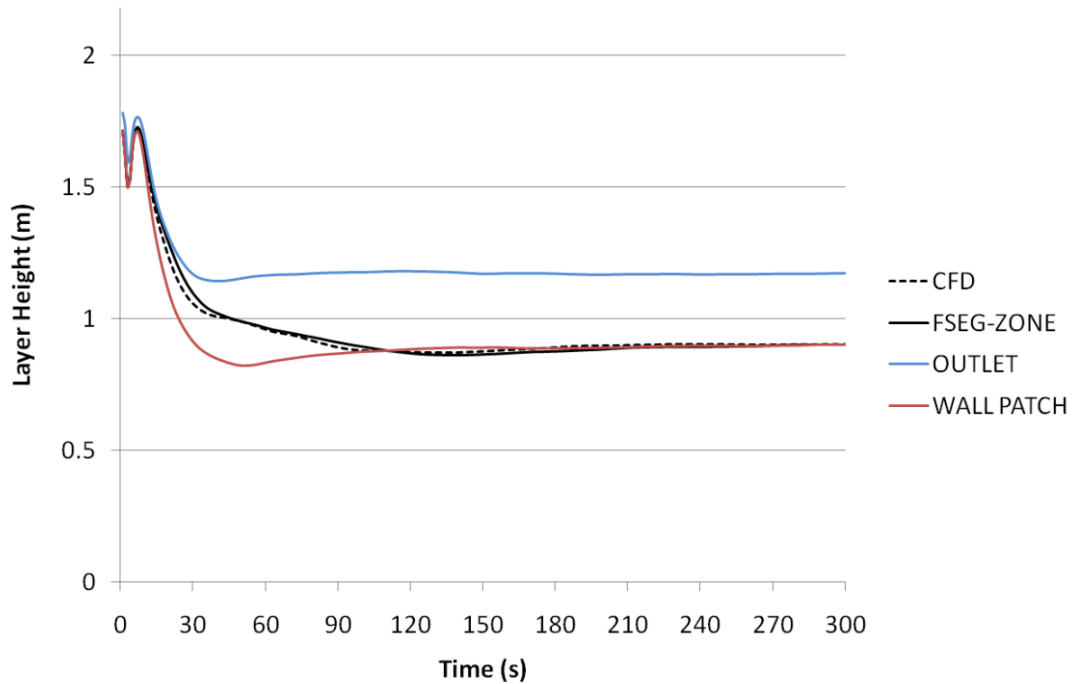
Figure 6-12. Layer height for the four alternative approaches.

The above case demonstrated that the FSEG-ZONE model consistently outperforms the alternatives of using either an outlet or a wall patch with regards to the remainder of the domain. In addition to this the FSEG-ZONE model is simultaneously providing results for the removed compartment which is impossible to perform for the other two methods; these results were discussed in section 6.3.1. The cell budgets for the outlet and wall patch alternatives were equal to those used in the FSEG-ZONE simulation and therefore all three cases result in a 26% reduction in the number of cells. The outlet simulation took 7h 04m 04s and the wall patch simulation took 7h 03m 42s; both these times again correspond to savings of ~37%, an over unity efficiency relative to the domain being replaced. As discussed in 6.3.1, this is

probably due to improvements in intra-iteration convergence rates, but despite the source of these improvements it is clear that this is contained by SMARTFIRE and is not a side effect of the use of the FSEG-ZONE model. Suffice to say, the FSEG-ZONE model cannot be expected to provide computational savings greater than the use of the outlet or wall patch alternatives, yet the model is clearly performing favourably by coming so close to these timings (2s longer than the outlet simulation and 24s longer than the wall patch).

6.3.3 Test case – Effect of varying volume

This test case extends the ideas presented in section 6.3.2 above to demonstrate the effect of room size as a model parameter. This is discussed in section 4.2 where it was stated that since the hybrid model is bounded in accuracy by the outlet and wall patch alternatives, and since these alternatives correspond to the two extremes of room size (zero and infinity), it follows that the room size locates the 'true' results between these bounds. The results below affirm the validity of the FSEG-ZONE model in capturing the effect of varying the room size.

Case Setup

The case setup is similar to section 6.3.1, figure 6-2, with the exception that the rightmost room which is replaced by the zone model is now allowed to vary in size (volume). The height remains constant at 2.18m but the widths take one of nine values: 2.8m, 4.4m, 5.5m, 6.5m, 7.3m, 8.1m, 8.8m and 9.4m. The values are chosen such that the volume is increasing in an approximately linear fashion from room to room, with square floor area.

Results

The first set of results are for the rightmost room whose volume is the varying parameter, these are shown in figures 6-13 to 6-16. From these

results it can be seen that varying the room size has the expected effect on the results witnessed in the zone room. This can most clearly be seen in the layer temperatures and height in figures 6-14, 6-15 and 6-16, where there are clear trends for increasing room size. There are nuances such as the 'bounce' seen in the 2.8m room in figure 6-16 which suggests that the actual effect of room size is slightly more complicated than anticipated; this 'bounce' is also apparent in the 4.4m plot towards the end of the simulation suggesting it is a common feature that takes longer to occur with increasing room volume. A similar 'bounce' and delay, although less clear, can be seen in upper layer temperature in figure 6-14. These temporal trends are expected since different sized rooms will attain steady state at different rates.
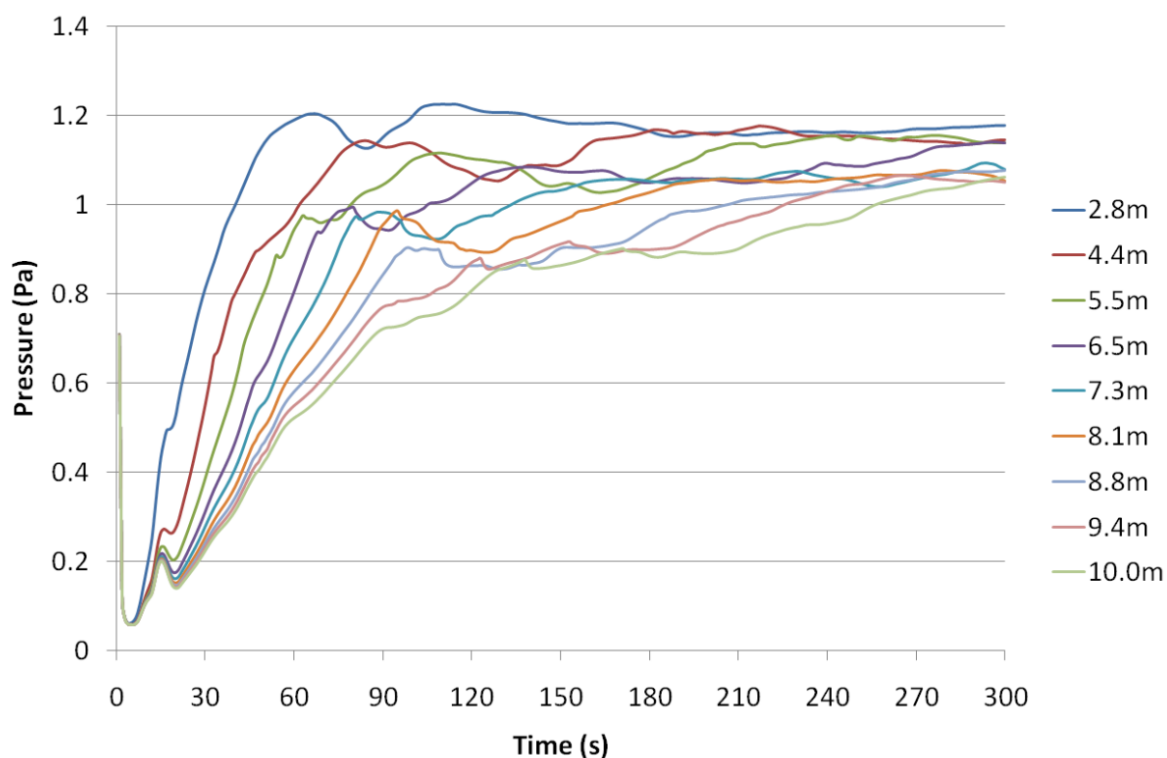
Figure 6-13. Pressure in zone room for different room sizes.
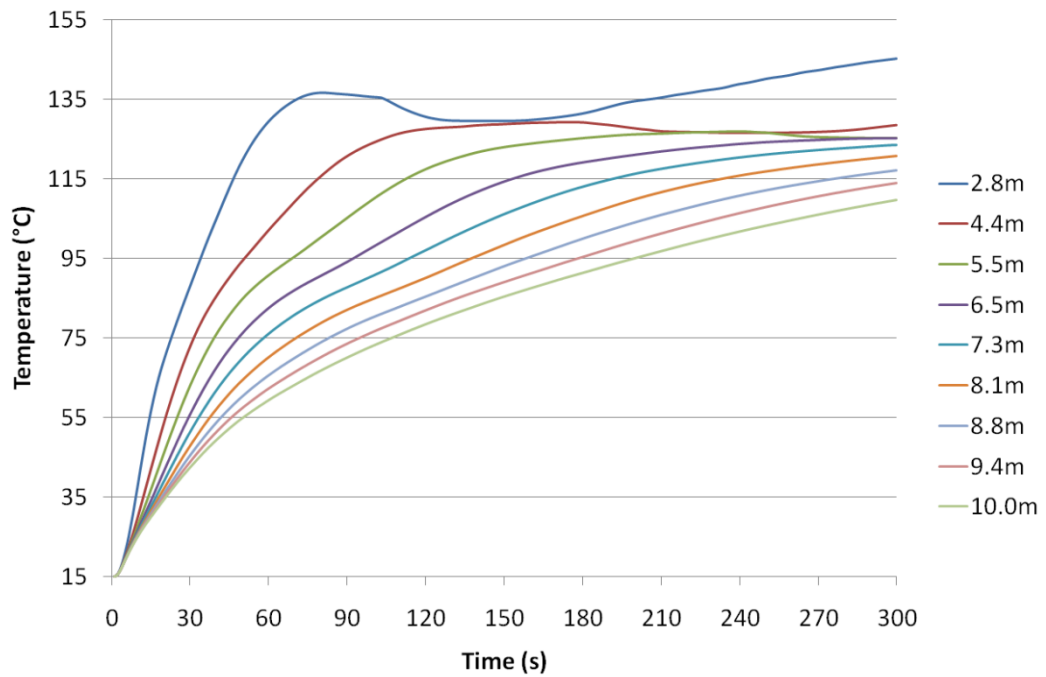
Figure 6-14. Upper layer temperature in zone room for different room sizes.
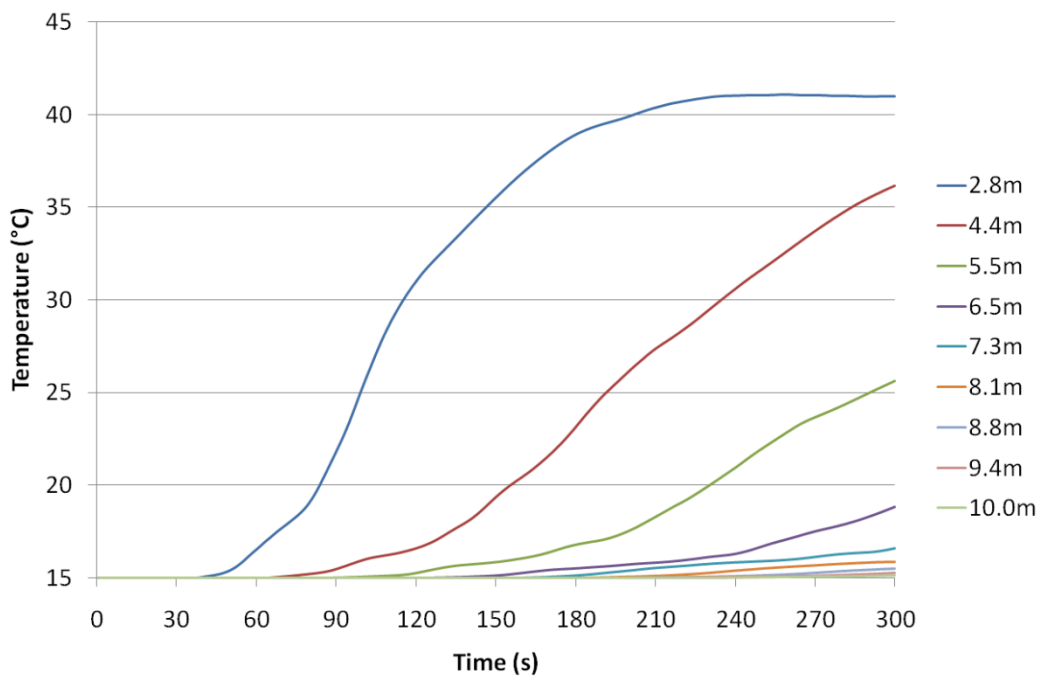
Figure 6-15. Lower layer temperature in zone room for different room sizes.
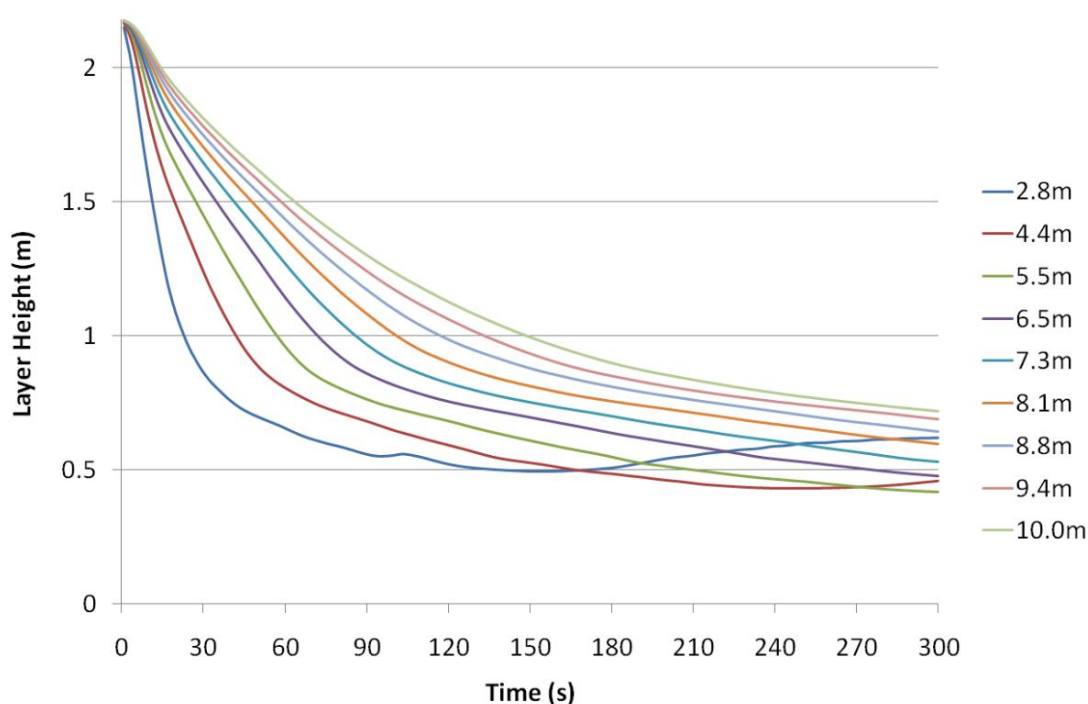
Figure 6-16. Layer Height in zone room for different room sizes.

The pressure as shown in figure 6-13 also demonstrates trends though not as clearly as those discussed above. Initially (< 60s) the room size has a clear affect on the results with a larger room corresponding to a slower development and lower overall pressure. Again, the 'bounce' is seen in the various plots occurring at larger delays for larger sizes, but the combination of these nuances means that a clear trend is not easy to see in the later stages of the simulations. This alludes to the highly non-linear nature of the models and the close interdependency between variables. This is more clearly seen in figures 6-17 to 6-20 below which make the same comparisons but for the leftmost room which remains modelled by the CFD model. Here the results for the outlet and wall patch alternatives from section 6.3.2 are included out of interest.
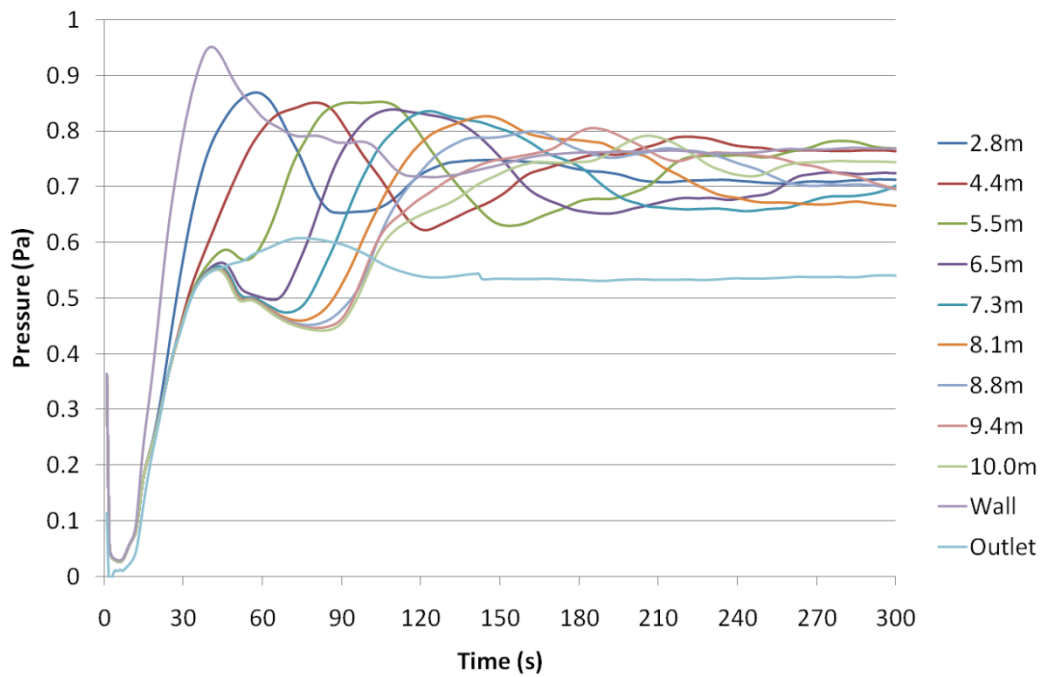
Figure 6-17. Pressure in CFD room for different zone room sizes.
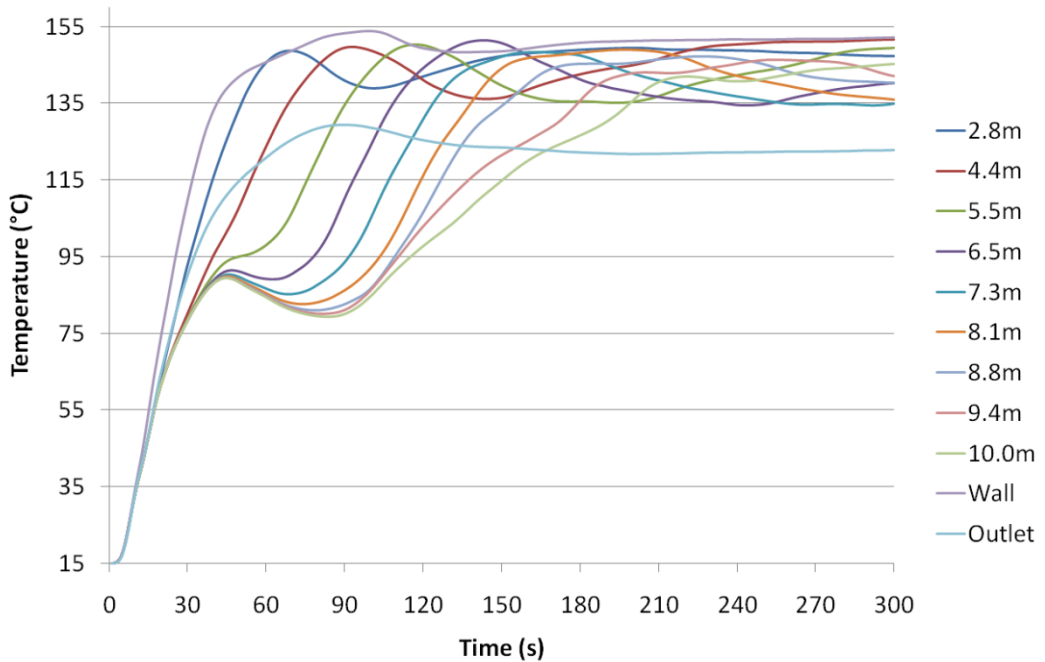
Figure 6-18. Upper layer temperature in CFD room for different zone room sizes.

Again, trends are evident in these results such as those seen in the plot for layer height in figure 6-20. Here it can be seen that increasing zone room size causes the layer in the CFD room to develop at a slower rate, yet all layers tend towards the same value at steady state which is to be expected. It is also evident from this plot that the varying room sizes are bounded by the outlet and wall patch results, and that the ordering is in line with the wall corresponding to a zero size (results closer to 2.8m plot) and the outlet corresponding to an infinite size (results closer to 10m plot).
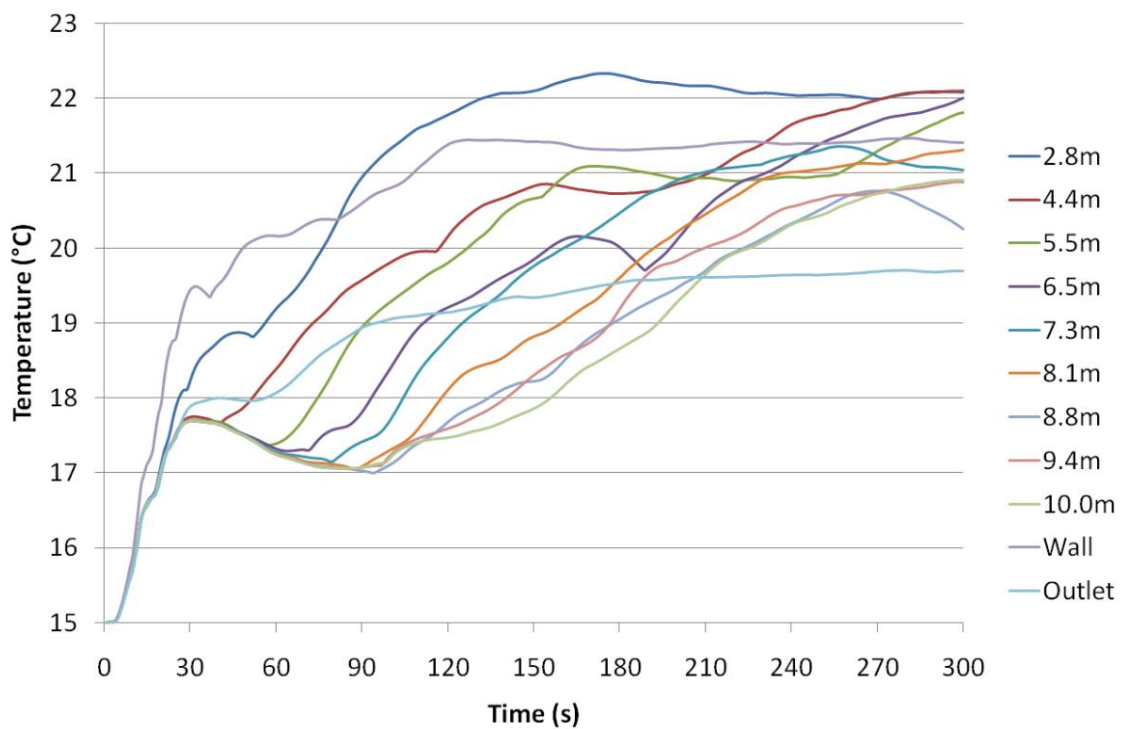
Figure 6-19. Lower layer temperature in CFD room for different zone room sizes.

The trends are also present in figure 6-17 for pressure and figures 6-18 and 6-19 for layer temperatures, yet again the non-linear nature of the variables means that this is not so apparent. This complicated interplay between variables is seen in the pressure plot in figure 6-17 where it seems that plots 6.5m and larger actually lie outside the bounds dictated by the outlet plot between 30 and 90 seconds. Such intricacies re-affirm the need to use a

suitable field model counterpart with the hybrid model that will allow these dynamics to be captured. Clearly, despite some agreement from the 'wall-patch' in the latter stages of the simulation, these alternatives for the zone model are simply not valid for use in a transient simulation. The relationship between room size and layer height seen in figures 6-16 and 6-20 suggest that at least a two layer zone model is required since the layer height appears to be characteristic of the developing dynamics, a second layer allows variation in the hydrostatic pressure that is simply not possible with a single layer.
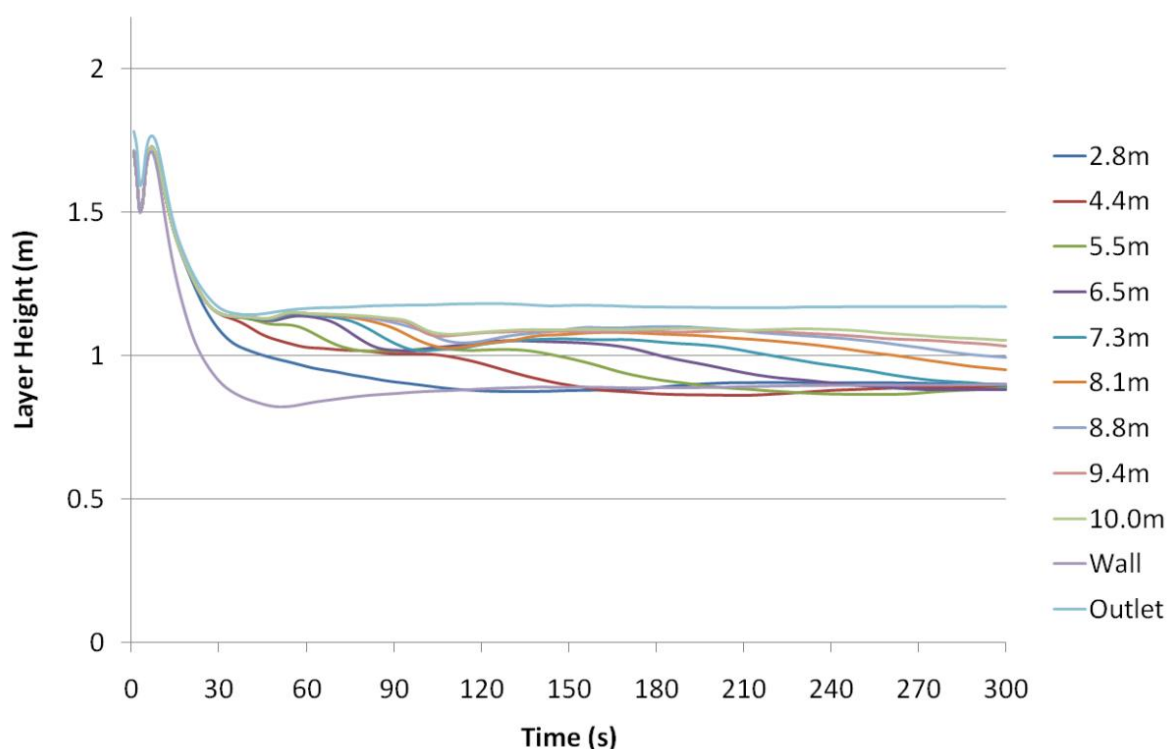
Figure 6-20. Layer height in CFD room for different zone room sizes.

6.3.4 Test Case – Heat source removed at 120s

The fourth test case is similar to the first test case presented above but here the heat source is terminated at the 120 second mark. With the heat source removed, any developed hot layer should now cool and shrink as the domain returns to ambient conditions, testing the ability of the FSEG-ZONE model to

capture such phenomenon. Preliminary results from this test case appeared in a paper by the author which was published in the IAFSS 2011 symposium proceedings [Burton2011] and is included as appendix 4.

Case Setup

The case is identical to that in section 6.3.1 above with the exception that the heat source is now switched off at 120 seconds.

Results

The first comparison in figure 6-21 is for both the compartment pressure and mass in the rightmost room, the room being removed for simulation by the zone model. Here the results are identical to those in section 6.3.1 until the heat source is removed at 120 seconds. At this point it can be seen that the FSEG-ZONE model captures the resulting drop in pressure, along with the increase in mass, extremely well. The downward spike seen in pressure is likely to be an artefact of the numerics attempting to deal with the removal of an enthalpy source.

Figure 6-22 shows a comparison of the upper layer temperature reported by the two reduction methods and the FSEG-ZONE model, with the results again identical to those in section 6.3.1 for the first 120 seconds. Once the heat source is removed all three values proceed to cool at comparatively similar rates, although the Quintiere method experiences a sudden drop between 120 and 150 seconds.
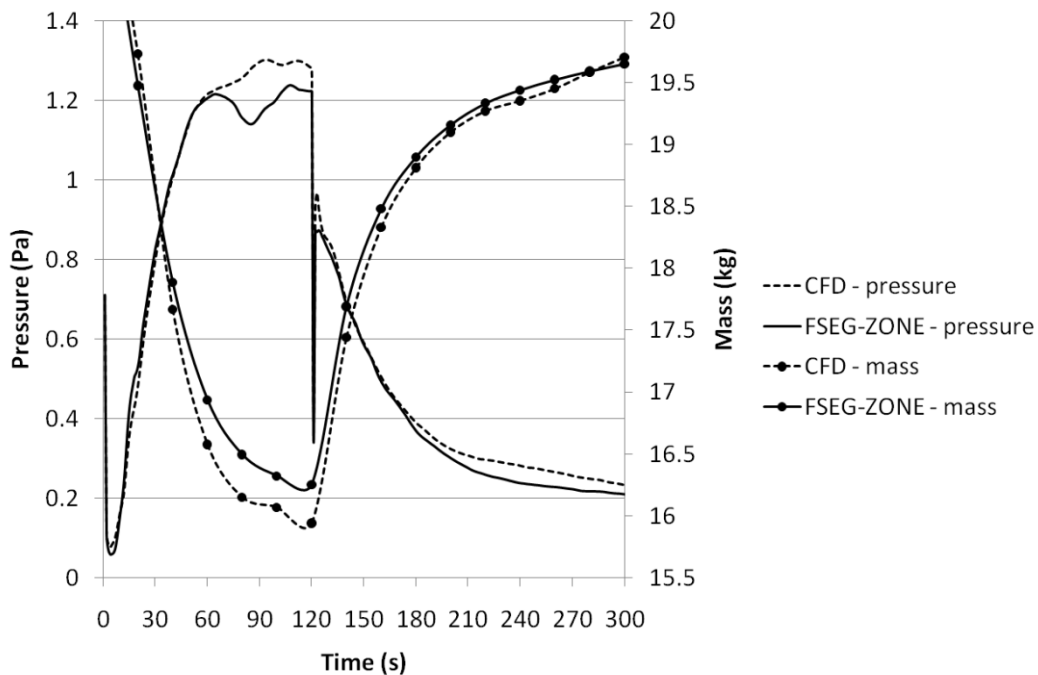
Figure 6-21. Pressure plot with heat source removed at 120 seconds.
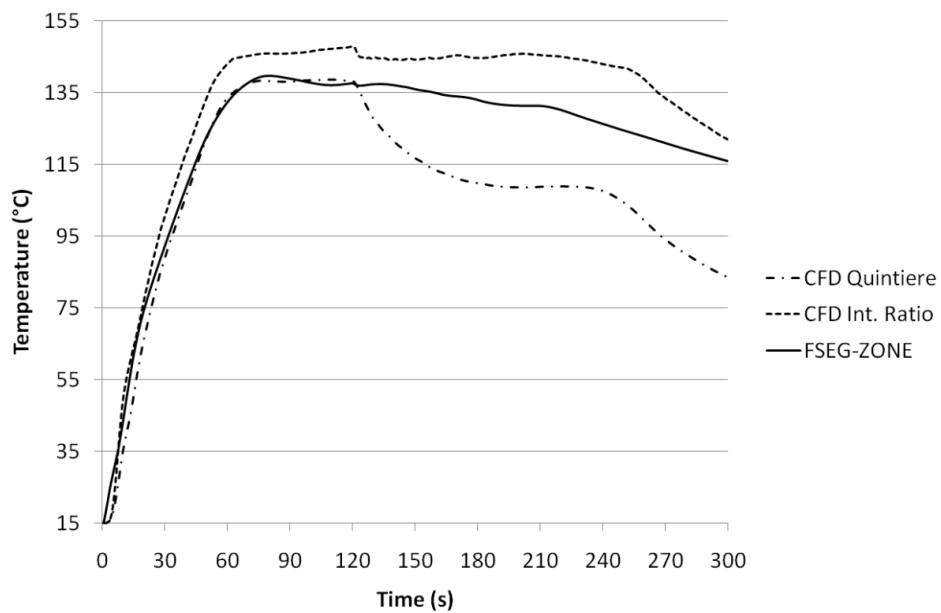
Figure 6-22. Upper layer temperature with heat source removed at 120 seconds.

One explanation for this sudden drop, and the corresponding variation between reduction methods, is as follows. The Quintiere method locates a layer height corresponding to an ambient lower layer, the value for which is taken to be the lowest observed in the compartment; the integral ratio method on the other hand is not limited by such an assumption. The ambient air being drawn in from the exterior to the left of the geometry does not experience the heating and corresponding buoyant forces once the heat source is removed, but instead enters the right most room. Due to this, the lower cells of the right room will experience an immediately lower temperature, in turn affecting the Quintiere reduction calculation and resulting in a significantly lower layer height. For a short period after the heat source is removed there can in effect be three 'layers' in the right most room: the previous hot layer, previous cool layer, and a new ambient layer since the cool layer is likely to have experienced an amount of heating. Since the Quintiere method is based on a lower layer assumption and only considers two layers, it is clear that the above situation can lead to the drop in layer height observed.

For the lower layer temperature, comparisons can be seen in figure 6-23. The FSEG-ZONE temperature again experiences the delay in heating observed in 6.3.1, but in comparison to the previous test case the value is located between the reduction methods towards the end of the simulation. It is tempting to conclude that the FSEG-ZONE model is performing better in this test case, yet this is unlikely since the cause of the underestimation seen in 6.3.1, namely the absence of mixing between layers, has not been addressed. The likely cause of the favourable location of the FSEG-ZONE value is simply the underestimation of the lower layer temperature by the Quintiere method caused by the issues discussed in the previous paragraph. As in the first test case, the discrepancy between the results is largely introduced during the initial 60 seconds, after which the variations are similar; addressing this initial period more accurately in the FSEG-ZONE model would result in very

close agreement between the models. Regardless, the FSEG-ZONE model performs well despite the inherent weakness.
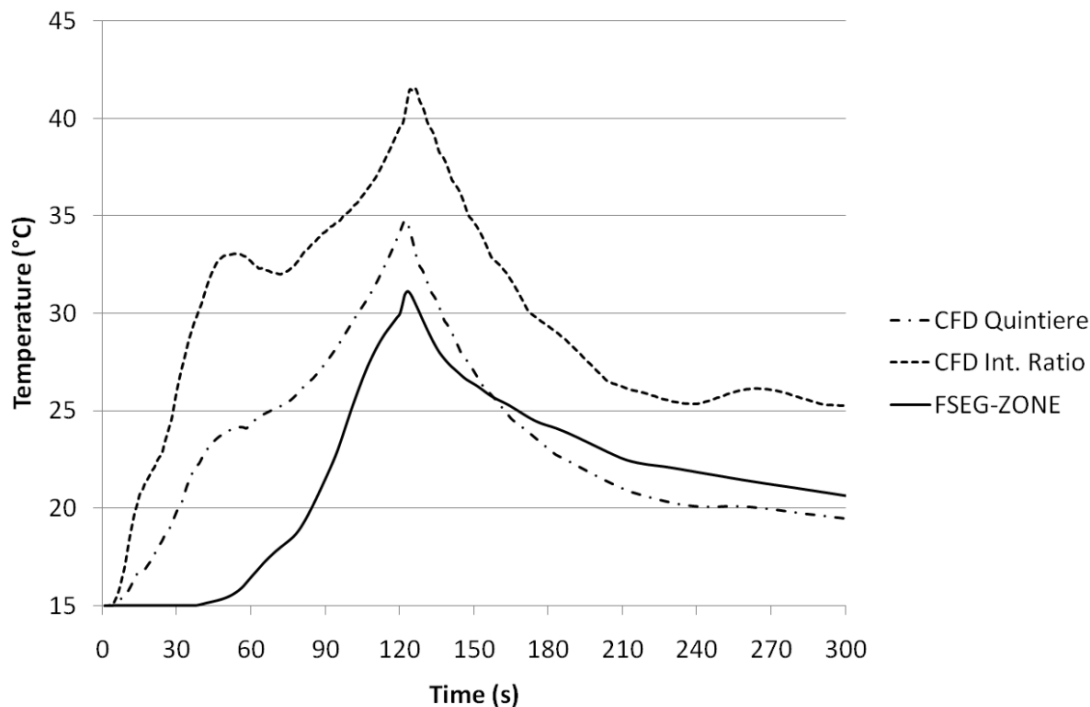
Figure 6-23. Lower layer temperature with heat source removed at 120 seconds.

Figure 6-24 shows the layer height development for the two models. In comparison to the results in section 6.3.1 the removal of the heat source appears to result in a situation which serves to increase the discrepancy between the two reduction methods; the subsequent venting and cooling of the domain clearly introduces new dynamics. The FSEG-ZONE model performs favourably, again in close agreement with the Quintiere method at the beginning of the simulation and tending towards the integral ratio method as it progresses. Good agreement is seen in the rate of accent of the layer in comparison to the integral ratio method.
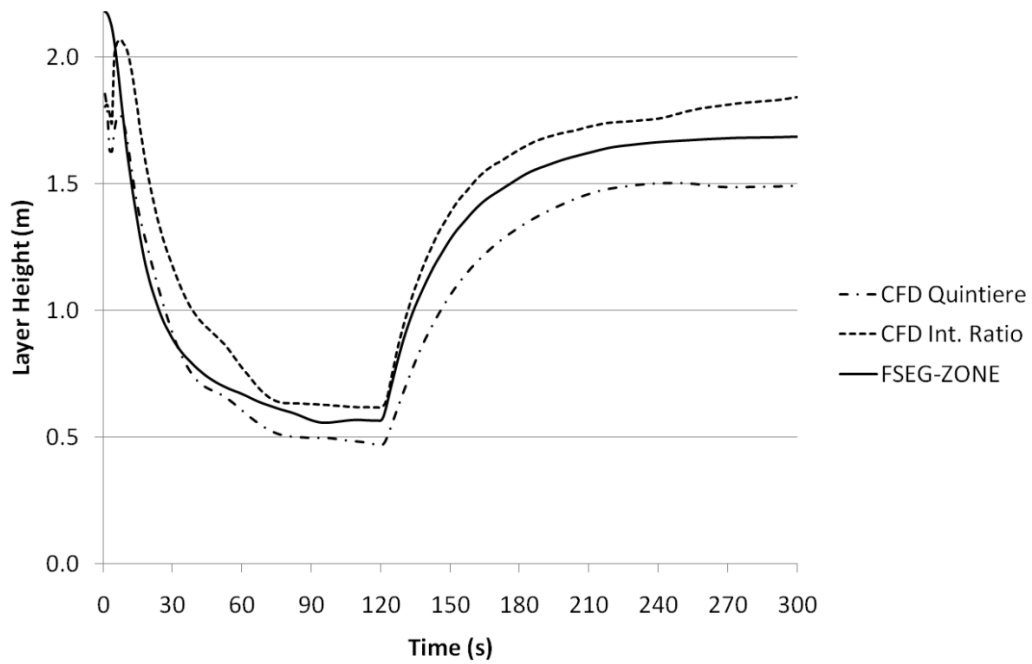
Figure 6-24. Layer height development with heat source removed at 120 seconds.

It is worth noting that the FSEG-ZONE results come from the actual zone equations whereas the layer reduction methods are simply numerical operations; this does not eliminate blame entirely from the FSEG-ZONE model but it is certainly a possibility, as seen with the Quintiere method, that both reductions can contain errors, as opposed to assuming the CFD results to be perfectly accurate and assigning all error to the zone results. In fact, due to the nature of the two reductions being considered, it can be argued that the 'correct' layer is likely to be located somewhere between these methods, and the positioning of the FSEG-ZONE value is indeed quite encouraging. It is also interesting to note that the best apparent performance of the FSEG-ZONE model is seen in the pressure and mass results in figure 6-21, where the layer reductions are not used.

Finally, figure 6-25 compares the temperatures in the remainder of the domain at the end of the simulation (300 seconds); again, excellent agreement is seen between the CFD and FSEG-ZONE simulations. The cell budget

remains as in section 6.3.1 with the CFD simulation taking 11h 19m 51s and the FSEG-ZONE simulation taking 7h 04m 04s; this again results in a reduction in computational time of ~37% as seen in the previous cases.
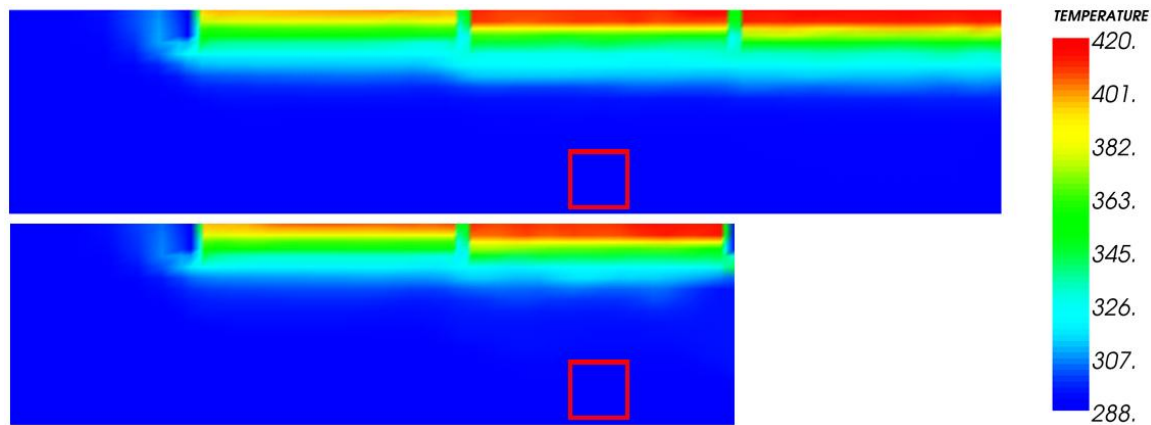
Figure 6-25. Cut-plane of temperature (K) for CFD (top) and FSEG-ZONE (bottom) at 300 seconds.

7. Extending the FSEG-ZONE model

The FSEG-ZONE implementation discussed in chapter 6 provided favourable results in the test cases considered, yet the model itself lacks some very important features that are required of a fire model. This chapter looks at the extension of the FSEG-ZONE model to include phenomena vital to any model of thermal fluid flow, such as conduction and radiation, along with phenomena of specific interest to fire simulations, such as combustion, smoke and species transport. These developments clearly increase the usefulness and field of applicability of a hybrid fire model, yet they also introduce opportunity for additional errors as further assumptions are made in attempting to model more complex phenomena.

The computational requirements of the hybrid model are in comparison to those of the adjoining CFD model, whereas those of dedicated zone models have no counterpart. A per step CPU time of say 50ms as opposed to 25ms means a huge 100% increase in the computational requirements (time) of a zone model, but for the hybrid model the extra amount would be insignificant to the number of seconds or minutes taken by the CFD model. This gives opportunity for the FSEG-ZONE model to be developed without timing efficiencies being the principal concern. In this way the hybrid model can, amongst other things, be developed to have less abstractions, and can be made in a modular fashion such that different sections of the model are in isolation to each other. This allows future developments to be made in a simpler fashion, with the overall code being much easier to understand and therefore maintain.

The previous work performed on hybrid field/zone fire models as discussed in chapter 2 made use of severely limited zone models that were capable of considering mass and enthalpy transport solely by the convection between segments of the domain; it is clear that these models, whilst important as interim solutions, can not be expected to give physically accurate results. It is therefore extremely important that any hybrid field/zone model is capable of addressing these additional phenomena if it is to improve the fidelity of high-speed CFD simulations.

7.1 Multiple hybrid instances

The hybrid model can be used to replace as large a section of the field domain as required so long as the dimensions of compartments remain suitable for a two-zone representation, but its real power is realized when using it to replace numerous separate unconnected rooms that surround a CFD modelled section, e.g. zone modelled cabins along a CFD modelled corridor, or zone modelled prison cells surrounding a CFD modelled common area. As a consequence of having differing open and closed formulations, handling multiple instances is also performed in different manners and is described below.

The FSEG-ZONE implementation is encapsulated entirely within a C++ class that gets created as the SMARTFIRE CFD Engine encounters the declaration of a hybrid boundary condition within the case specification file. The class contains all the variables, arrays and parameters required for the calculations and solution procedure, and provides public member functions for retrieval of these values for use on the CFD boundary conditions. The bisection solver is designed to solve a single pressure variable over multiple interfaces each connecting a single zone compartment to the CFD domain, it is not capable, at present, of solving a configuration of inter connected zone compartments connected to the CFD domain by a single interface (see section chapter 8 on further work).

The present method allows for consideration of numerous zone compartments so long as each is in isolation such that none have any direct requirements on the results of the others, at least within the bisection solution routine. To deal with multiple zone instances a separate class is created for each zone compartment that is to be created. Each class is created as before when the specification file is read, but these classes are then inserted into a single vector representing the entire hybrid replacement. By providing each hybrid boundary condition with a pointer to its corresponding vector element, the zone variables can be retrieved by calling the same member functions as before. Handling the hybrid implementation as an object in this way by completely encapsulating it ensures the abstraction that makes improving and maintaining the code a simpler matter. Any future development on the hybrid model can be implemented by simply modifying internal components of the class without altering the existing SMARTFIRE code. Multiple instances are demonstrated in test cases 7.7.13 and 7.7.14 in section 7.7 on radiation.
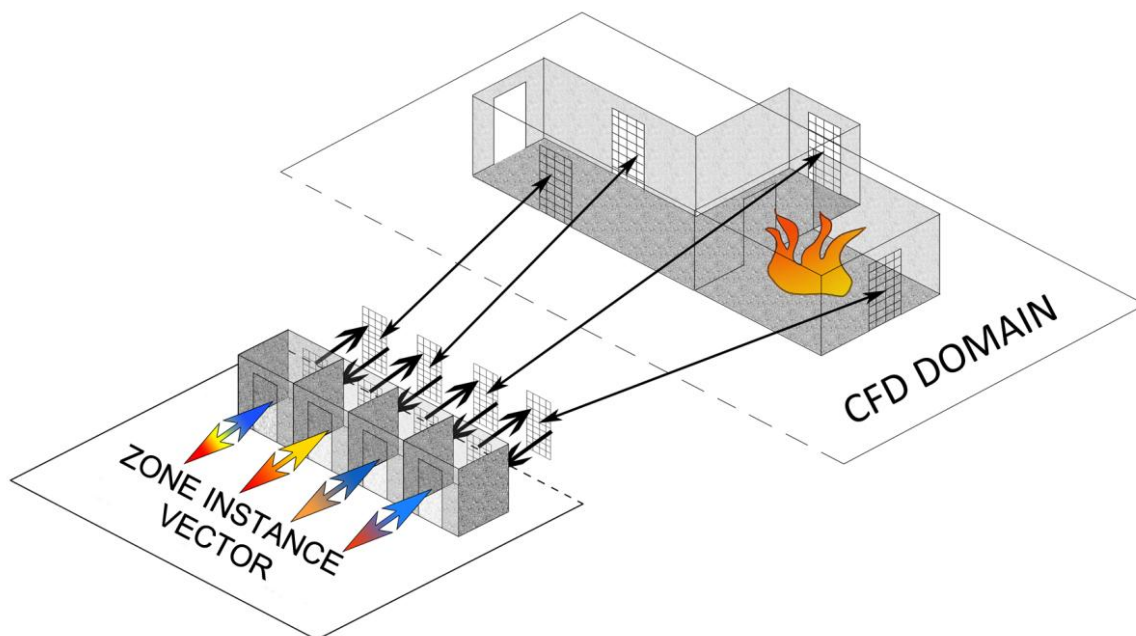
Figure 7-1 - Multiple zone instances are stored as a vector of class objects

7.2 Multiple Hybrid Interfaces to a Single Zone

The idea of the closed zone room, as modelled by the FSEG-ZONE model, requires that the zone compartment has no vent of its own, rather that any vent is a hybrid interface connecting it to the CFD domain. This requirement places no limit on the number of hybrid interfaces a zone compartment may have, allowing the zone domain to act as a connecting region between separated CFD compartments. The idea behind using the CFD model in a hybrid simulation is to ensure the accuracy of results in a particular section of the domain, yet allowing flow to 'pass-through' a zone compartment can possibly be detrimental to this requirement of accuracy. The option to model geometries in this way is an interesting possibility, yet its use in a genuine simulation would require careful consideration by the user over whether such a representation can be made whilst maintaining the validity of results in the further CFD sections.

The option to have multiple instances is implemented by creating a new face patch within SMARTFIRE. The first hybrid interface is created as usual and becomes the 'master' instance; further interfaces are created using the new face patch and derive the required values for calculations from the master instance. Also, the vectors of CFD cells and faces for each interface are adjoined to the master interface vectors allowing calculations such as the bisection solver evaluation to be performed in the same manner as for a single interface compartment.

Previous results from the test case below appeared in a paper by the author which was published in the IAFSS 2011 symposium proceedings [Burton2011] and is included as appendix 4. The present results have been obtained from a revised version of the FSEG-ZONE model.

7.2.1 Test case – CFD/ZONE/CFD

This test case takes the same three room setup used in previous cases but replaces the middle room with the FSEG-ZONE model, leaving the remaining left and right rooms to be modelled by the CFD model. The first room in the series contains a 62.9kW heat source, and is vented only to the middle zone room. The middle zone room connects the CFD rooms, with the third room additionally being vented to the exterior, see figure 7-2. The case was run for 300 seconds, with the heat source removed at 120 seconds; the time-step size used was 1 second. The CFD case used 31,311 cells, while the FSEG-ZONE case used 23,814, resulting in a saving of 24%.
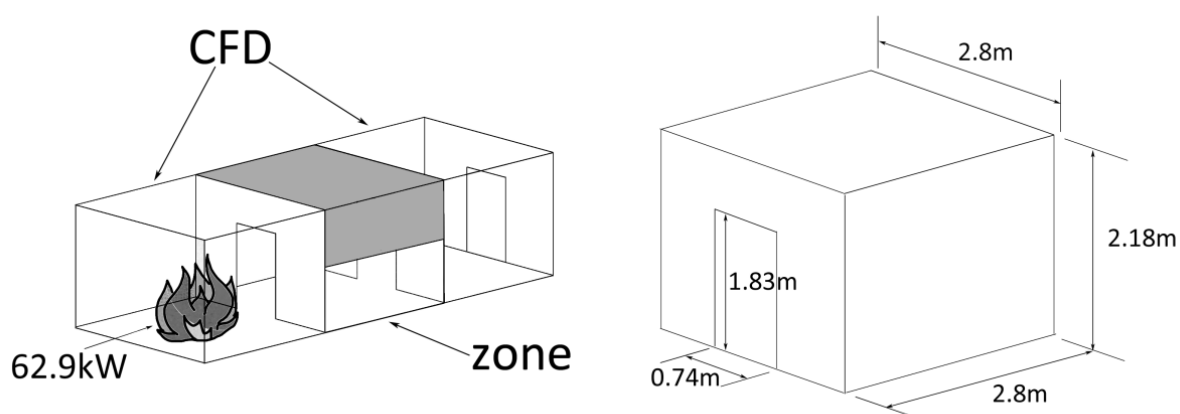
Figure 7-2. Setup for test case.

The first set of results concern the portion of the domain that remains modelled by the CFD model in both simulations. Figures 7-3a and 7-3b below show a cut-plane of temperature along the length of the domain for times 15, 30, 60, 120, 180 and 300 seconds; the temperature scale is the same for each and the legend is displayed at the bottom of the figure. The CFD results are presented at the top of each time, with the FSEG-ZONE results below this. Data from the zone compartment showing both layer height and temperatures has been imposed on the centre room for the FSEG-ZONE results.
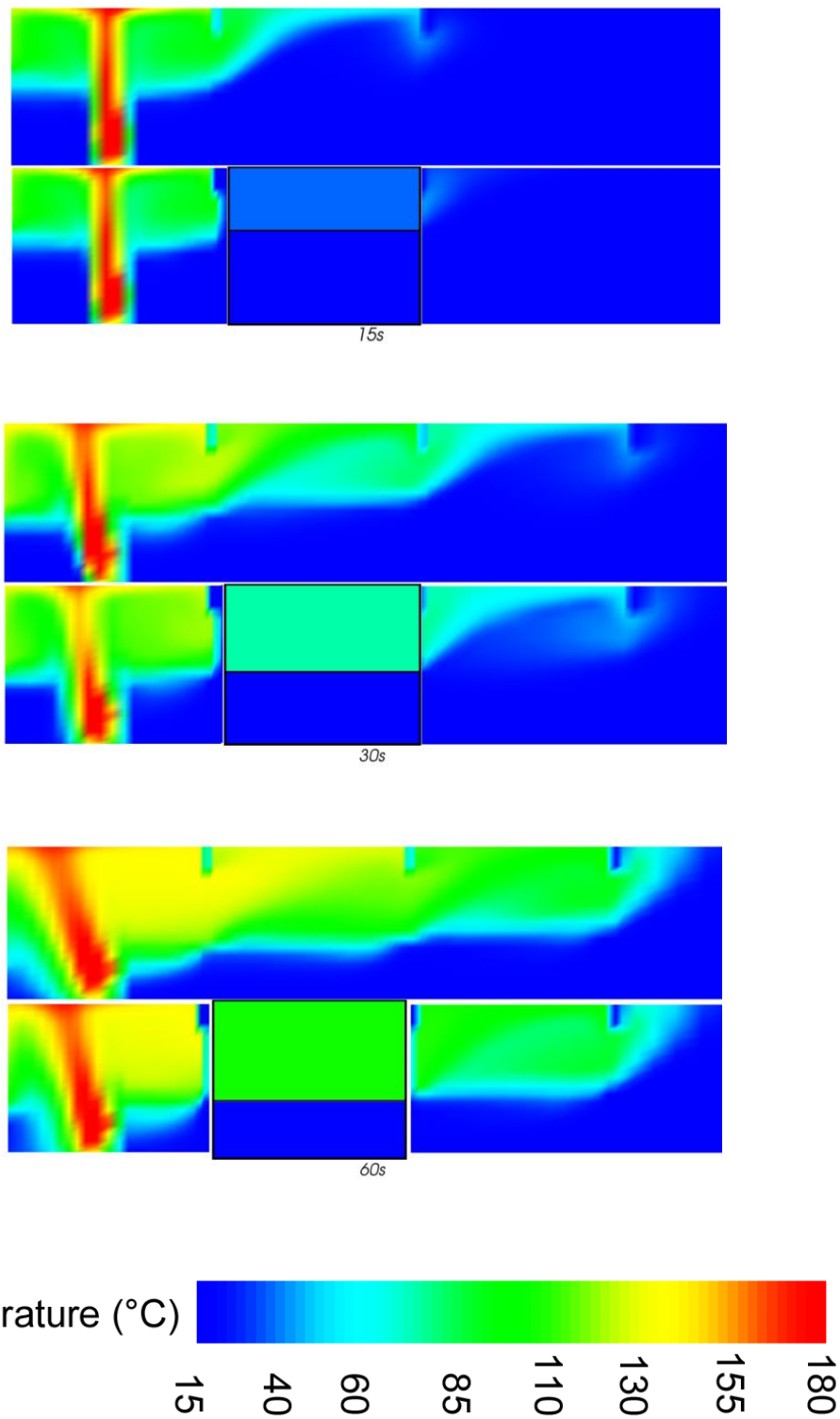
Figure 7-3a. Temperature (°C) cut-plane at time 15, 30 and 60 seconds. CFD (top) is compared with FSEG-ZONE (bottom) with zone data imposed on central room.
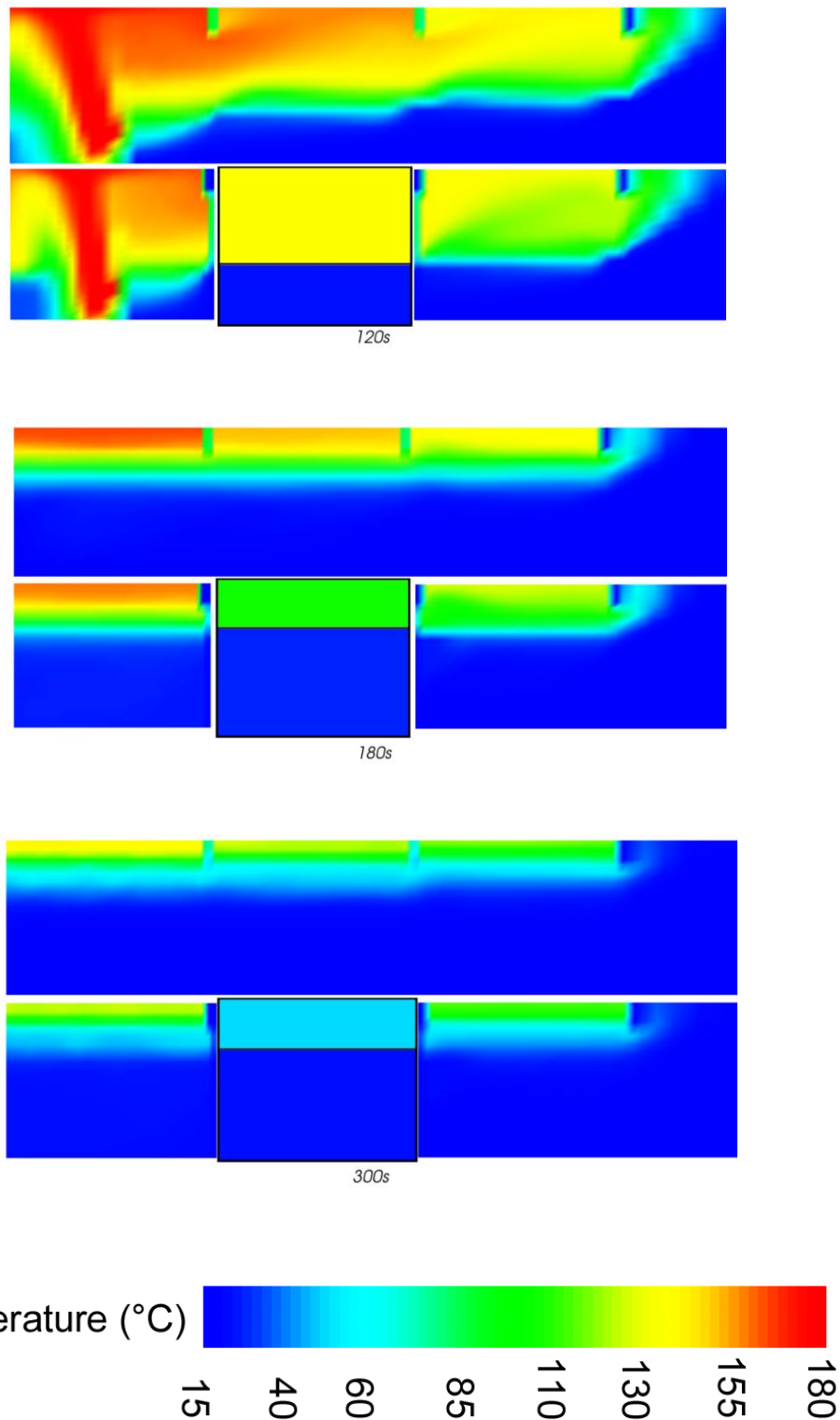
Figure 7-3b. Temperature (°C) cut-plane at time 120, 180 and 300 seconds. CFD (top) is compared with FSEG-ZONE (bottom) with zone data imposed on central room.

It can be seen that the FSEG-ZONE results agree closely with those of the full CFD simulation, with both the values for temperature and the general development of the layer and subsequent spill into the third room captured well. It seems that the FSEG-ZONE model slightly underestimates the temperatures once the heat source has been removed. One possibility for this discrepancy is that the zone upper layer has a single uniform temperature which means that every flux leaving this layer does so at the same temperature. For the CFD model fluxes leaving the central room can do so at a range of temperatures since there is no 'layer' as such. This in combination with the linear pressure distribution imposed on the boundary conditions may explain the slightly cooler temperatures seen.

Since the zone model neglects momentum and any horizontal variation the conditions at each interface are equal, meaning any inflow from the left room is instantly distributed throughout the layer. In comparison, flow must traverse the central room in the CFD simulation, therefore a delay will be apparent in flow re-emerging into the right room. This effect, although slight, can be seen in the 30 seconds comparison where the FSEG-ZONE results display a higher rate of flow into the right room. This is another potential reason for the cooler temperatures since the central room in the FSEG-ZONE model experiences outflow sooner, leading to higher net outflow.

Figures 7-4 to 7-7 below show the results from the central room over the length of the simulation. Figure 7-4 shows the development of the compartment pressure between the CFD and FSEG-ZONE models with good agreement between both the values and trend.
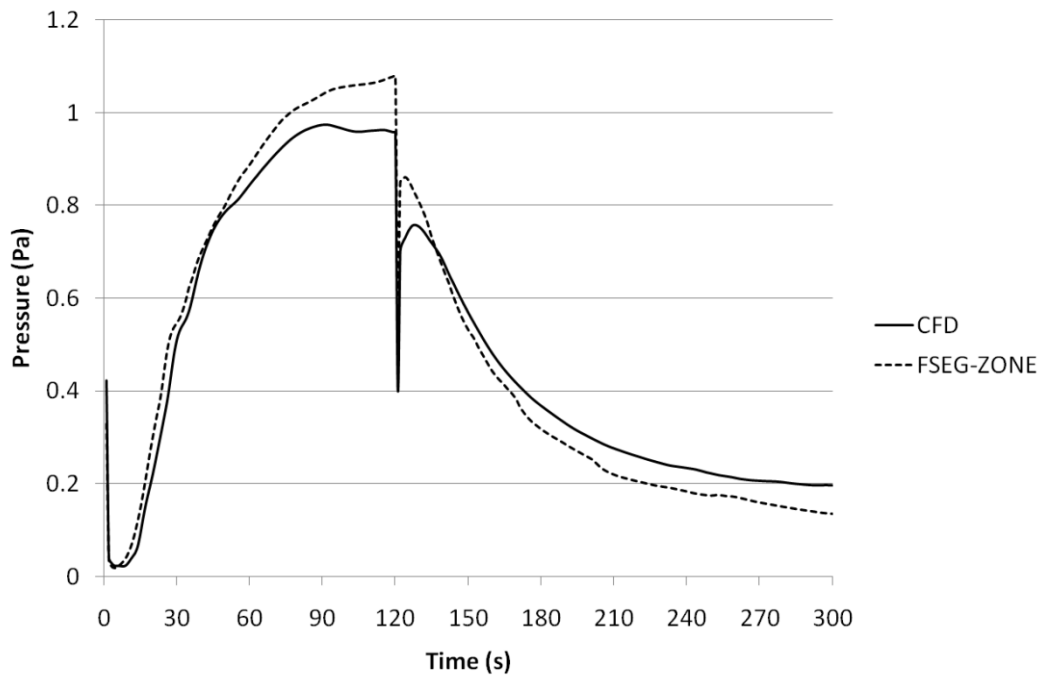
Figure 7-4. Pressure development comparisson.
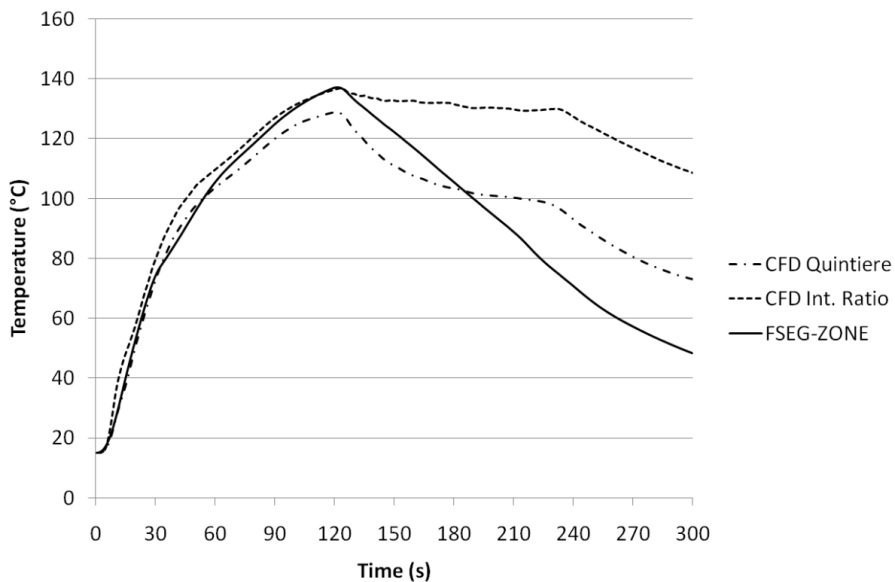
Figure 7-5. Upper layer temperature comparison.

Figure 7-5 shows the upper layer temperature for the two models. The FSEG-ZONE model again agrees closely with the Quintiere method for the initial period of the simulation, but tends towards the integral ratio method earlier than in the case in section 6.3.4. The cause of this is not immediately clear although it clearly has basis in the presence of the second doorway of the centre room.

One explanation is that the presence of the second doorway ensures that the upper layer does not get the same opportunity to develop, since the hot gases are vented to the rightmost room. In the CFD simulation the effect of the vent soffit is to ensure that the comparatively cooler portions of the upper layer are vented, increasing the overall temperature of the shrinking upper layer. In the FSEG-ZONE simulation the venting of the upper layer results in a lower mass over which to distribute the enthalpy of incoming flow, again resulting in a higher overall temperature. These higher upper layer temperatures increase the likelihood that incoming gas from the left most fire room finds itself at a temperature between the upper and lower layers, meaning that both layers receive various portions of it. The result of this is that the lower layer experiences some heating, resulting in the integral ratio method, with its assumption of developed lower layer, being more suited to this case as compared to the Quintiere method.

After the heat source is removed the upper layer of the FSEG-ZONE model clearly cools at a faster rate than either the CFD reduction methods. A likely explanation for this is that since the upper layer is uniform in the FSEG-ZONE model, the gas vented to the right room is at the same temperature despite the soffit, whereas in the CFD simulation the soffit, as discussed above, results in the cooler portion of the upper layer being removed. The effect of this is to reduce the rate of cooling of the CFD model, resulting in the FSEG-ZONE model appearing to cool quicker. In addition, the absence of momentum in the FSEG-ZONE model means that hot gases entering from the left fire room do not have to traverse the middle room before being

available for venting to the right room, in contradiction to the lag that would be witnessed in both the CFD model and reality.

The lower layer temperatures are shown in figure 7-6, where the range of temperatures is relatively small (15°-29°C).. The usual delay in the FSEG-ZONE model can again be seen although the value is located between the layer reduction methods for the second half of the simulation. Once again the location of the lower layer temperature of the FSEG-ZONE model between the reductions is likely to be an effect of the underestimation made by the Quintiere method.

Figure 7-7 shows the comparison of layer height between the models. Again the FSEG-ZONE results agree closely with the Quintiere method for the first 30 seconds of the simulation, and then come into agreement with the integral ratio method. In the first test case in 6.3.1, the heat source was active for the duration of the simulation, and the FSEG-ZONE model ended in close agreement with the integral ratio method, affirming its validity in a well mixed situation. In the test case in section 6.3.4, the heat source was removed, and the resulting venting and drawing in of ambient air resulted in the FSEG-ZONE model reporting a final layer between the two reduction methods. In the present case the FSEG-ZONE model ends in close agreement with the Quintiere method which is likely to be the more suitable method since the removal of the heat source and the second doorway encourage the development of an ambient lower layer. Using the two reduction methods alone it is not apparent which one should be considered more correct; it is remarkable that the FSEG-ZONE model appears to validate the choice of reduction method, not just by remaining within the bounds set, but by achieving the level of agreement seen in the last 60 seconds of figure 7-7.

The CFD simulation took 11 hours 12 minutes and 19 seconds to run; the hybrid simulation took 7 hours 21 minutes and 47 seconds to run. The saving in computational time is just over 35%, compared to a cell saving of 24%, again displaying a 'super-linear' speedup as observed in previous cases.
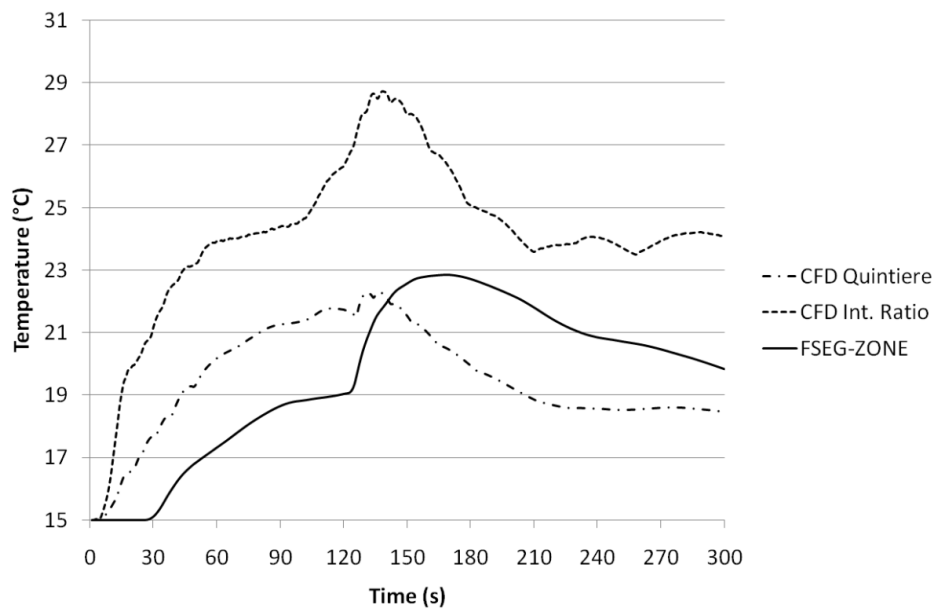
Figure 7-6. Lower layer temperature comparison.
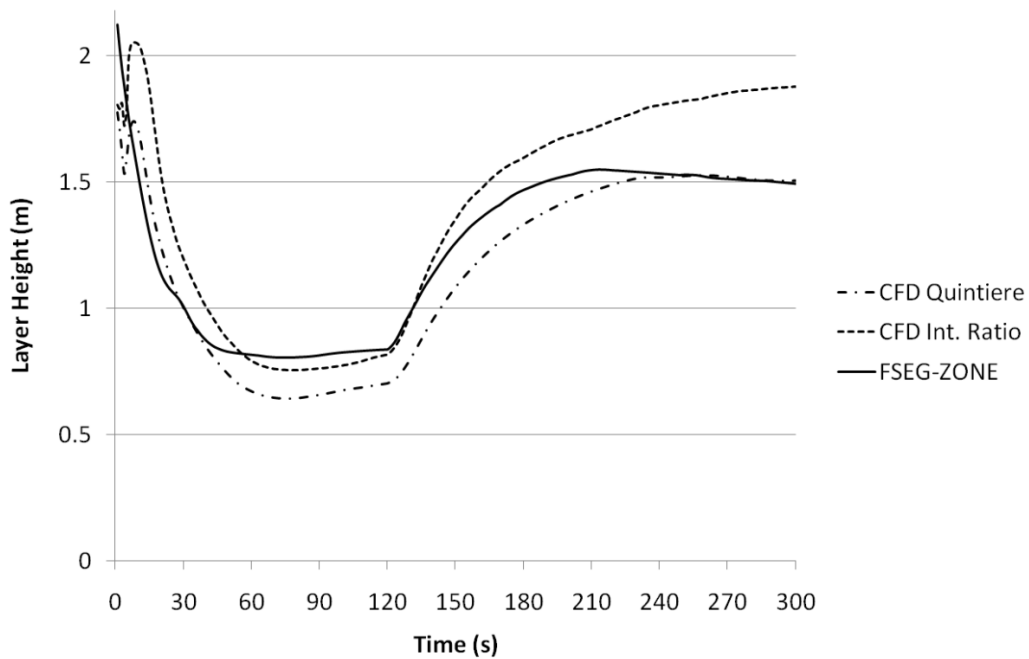
Figure 7-7. Layer height development comparison.

The above results demonstrate that despite the opportunity for error to be greater when multiple hybrid interfaces reside on a single zone compartment the agreement between the models is still good. The main difference is seen in the upper layer temperature and originates from the fact that the upper layer now experiences outflow as well as inflow for the duration of the simulation; along with the uniform temperature assumption this can certainly cause a discrepancy in temperatures. Since the zone model is in effect 'driving' the field model at the rightmost interface there is an opportunity for greater error. The uniform layers of the zone model affect the enthalpy fluxes directly, but possibly more important is the effect it has on the pressure boundary condition by enforcing a piece-wise linear distribution as opposed to the more continuously varying pressure of the field model. Despite this the method still provides valid results, yet the additional potential for error must be kept in mind during its use. Larger zone compartments will certainly reduce the accuracy of the method therefore whether or not the particular geometry is suited to this treatment is an important consideration. The discrepancies seen in this test case demonstrates that compartments with highly directional momentum driven flows may not be suitable for replacement with the zone model.

7.3 Species Transport

The transport of species such as smoke, toxic gases and combustion by-products is of particular interest in the simulation of fires. It is often stated that these consideration often present a much greater danger to occupants of buildings than those due solely to heat or even structural integrity. The formulation of a CFD model naturally lends itself to the consideration of transport of additional species through the general fluid variable discussed in section 3.2.

Species are considered within SMARTFIRE by their mass fractions, the proportion of mass within a cell that is due to the species in question. This allows simple calculation of the flux of a species across a face simply by

taking the product of the total mass flux with the corresponding mass fraction. As with the fundamental fluxes across a hybrid interface, those of other species are simply found by summing over the relevant faces. The mass of individual species in a zone layer is constantly tracked, allowing the mass fraction to be calculated and applied on the boundary condition for return flow to the CFD domain.

It should be noted, that while in reality the presence of various species in a volume of air will affect such quantities as the density and specific heat of the mixture, these variations will, in general, be much smaller than those caused by the range of temperatures being considered and their inclusion would introduce a great number of complications. Good results have been observed from neglecting the inclusion of these variations and at present SMARTFIRE assumes that species have no effect on these particular fluid properties (although the treatment of smoke allows it to affect densities). If future developments of SMARTFIRE address this issue the extension of the zone model to include such factors would be considerably easier than doing so for the CFD model due to the uniform nature within the layers.

An exception to this is the transport of smoke which, due to being the suspension of soot particles, is modelled as such and can have a significant effect on the density of the fluid. This is discussed further in section 7.6.

Since species transport is a key requirement for the consideration of combustion and smoke transport, the relevant test case is presented later in section 7.7.12.

7.4 Surfaces

For the zone model implementation discussed up until this point, absolute location of compartment components such as doors/vents, ceilings/floors and walls, along with their spatial proximity to one another, are not a required consideration for a zone calculation since these quantities make no

appearance in the zone equations. Other zone models (e.g. CFAST) explicitly state that certain assumptions are placed on these locations, such as centrally placed fire sources and doors located centrally on their respective wall. Certainly, floor location of a fire source can make a complex difference to the dynamics involved in a compartment fire and these effects would need addressing in the various equations used to model fire characteristics such as heat release rate, incomplete burning of fuel and plume size & entrainment; by the very nature of zone models these modifications would almost certainly find a basis in empirical relations of some kind.

Due to the nature of the Hybrid model implementation, consideration of sources is limited to interface fluxes between the CFD and zone domains, meaning that sections of algorithm common to other zone models are absent; this has allowed the zone formulation, up until this point, to be made without use of these terms. Some considerations, such as fire sources, are unnecessary; others, such as door placement, have been rendered unnecessary (through for instance the 1-D treatment of only using velocities normal to the interface).

Despite this there are developments that now need to be made to the hybrid model, specifically inclusions of radiation and conduction phenomena, which require a treatment based on the location and proximity of the surfaces that characterise the compartment. Until now the surfaces have simply defined the volume under question, but now their spatial relation with respect to layers and each other is required.

Consideration of the handling of heat transfer between the layers and their neighbouring surfaces requires knowledge of which surfaces are adjacent to each layer, along with their area, temperature and other parameters, such as specific heat and conduction. Radiation requires the data available for conduction as well as separation distances, angles and specific radiation parameters, such as absorptance and emissivity.

The modelling of surfaces in other zone models can be made in an abstract fashion; CFAST considers a fire compartment to be made of four surfaces: ceiling, floor, walls in contact with upper layer and walls in contact with lower layer; remaining compartments are made of just two surfaces: upper layer walls and lower layer walls, where the ceiling and floor have been incorporated into the relevant set.

In the FSEG-ZONE model, all physical surfaces of a compartment have model counterparts, with vertical walls having individual upper and lower versions. For a four wall compartment with no door this would result in ten model surfaces; one ceiling, one floor, four upper walls and four lower walls. When a wall contains a door, the number of surfaces are increased such that the section of wall from the door soffit upwards, the door itself, and the sections either side of the door are individually modelled (see figure 7-10). For the usual four-wall compartment with a single door this results in sixteen surfaces.

Within the code each surface is created as an instance of a surface class which are stored in a vector belonging to the respective hybrid object. Surfaces are assumed to be uniform, except with regard to temperature gradient normal to surface. Each surface object has members representing physical quantities such as height, width, length, depth, thickness and area, along with material properties of density, specific heat and conductivity. In addition each surface has a number of vectors storing temperatures, along with some extra variables storing previous step values. All the relevant quantities can revert to the equivalent SMARTFIRE default values, or can be set separately by the user.

Since these surfaces are composed of upper and lower counterparts, their dimensions will naturally vary as the layer descends during a simulation. This is taken account of on a per sweep basis where in addition to dimensions, the enthalpy is also considered to ensure conservation.

7.4.1 Surface Conduction

The rate at which heat flows through a wall material is dependent on its conductivity, with higher values giving a quicker spread of heat. For materials with high conductivity (such as copper, with $k = 401\ Wm^{-1}K^{-1}$), significant temperature gradients may never develop as the heat flows easily from regions of high temperature to low. If compartment walls were made of such materials, it may be an acceptable assumption to assume a uniform temperature throughout, that any flux into the surface is instantly distributed throughout the thickness of the wall. Walls of compartments serve many purposes, such as shelter, insulation or separation of areas (in which case sound insulation is a preferable quality), and for the vast majority of situations low thermal conductivity will be an extremely desirable quality.

This means that the assumption of uniform temperature will not be valid. The nature of the zone model means that allowing variation of temperature over the surface of a wall is not practical, since all parts of a surface are basically receiving the same 'flux'. However, modelling of temperature gradients normal to the surface is possible since in this situation different sections of the surface are experiencing different fluxes, e.g. the exposed surface may be making contact with a hot gas, whereas the back (or outside) of the wall may be at ambient conditions, or possibly totally insulated (zero flux). Such variations are important to consider since they can greatly affect the dynamics of a simulation. For instance, the exposed surface of a wall of very low conductivity might heat up to the same temperature as the contacting gas, meaning heat transfer between them becomes zero; in contrast the exposed surface of a high conductivity wall may lose any appreciable gain in heat rapidly to the surrounding material, meaning the temperature never increases. In this case heat transfer from the hot gas remains at a maximum throughout the simulation and the surface ends up taking substantially more enthalpy from the layer than is correct.

Conduction through the surfaces is performed through use of the finite difference method (see below), with the surface itself being split up into ten slices of differing thickness, referred to herein as 'cells' in keeping with the terminology of CFD models. The thickness of each cell can be chosen such that the volumes are biased towards the exposed surface of the wall. This may be done because during fire situations, where the contacting gas is generally hotter than the surface, the gradient of temperature will be steepest in this section. The increased resolution in this area of rapid change affords favourable numerical qualities and more accurate capture of physical results by reducing one of the drawbacks of the finite difference approach, attempting to represent the variation between cells by a linear profile.

The particular choice of scaling the cell thicknesses has not been optimised (certainly some distributions will perform better than others) but has been implemented such that extra resolution can be added simply in the future. The first and thinnest slice is situated at the exposed surface with each successive slice doubling in thickness, up to slice ten which is 2^9 times thicker than the first. Since $1 + 2 + 2^2 + \cdots + 2^9 = 1023$,

$$\left[\frac{dx}{1023} + \frac{2dx}{1023} + \frac{2^2 dx}{1023} + \cdots + \frac{2^9 dx}{1023} \right] = dx$$

so for total wall thickness dx the individual slice thicknesses are given by the ten terms in brackets. Despite this capability for varying cell thicknesses to be used, it was not implemented for the remaining test cases since the purpose of these is to compare the FSEG-ZONE model to results from SMARTFIRE.

SMARTFIRE uses a different solid partitioning that is based on fixed values, as opposed to scaling with the solid thickness. The FSEG-ZONE partition tends to achieve finer slices at the surface exposed to the fluid, although the accuracy gained over the SMARTFIRE method is not necessarily significant;

in additions finer slices can potentially cause numerical issues. For the test cases a partitioning equivalent to the SMARTFIRE method has been implemented in the FSEG-ZONE method.

Formulation of the conduction method begins with the unsteady 1-D heat conduction partial differential equation,

$$\frac{\partial T}{\partial t} = \frac{\partial}{\partial x}\left(\alpha \frac{\partial T}{\partial x}\right) \tag{7.4.1}$$

where α is the thermal diffusivity, or the ratio of conductivity to the volumetric heat capacity, alternatively

$$\rho c \frac{\partial T}{\partial t} = \frac{\partial}{\partial x}\left(k \frac{\partial T}{\partial x}\right) \tag{7.4.2}$$

with specific heat ρ, conductivity k and displacement in the direction of cell thickness x. This is integrated over both x and the time-step giving

$$\rho c \int_{i-1}^{i+1} \int_{t}^{t+\Delta t} \frac{\partial T}{\partial t} \, dt \, dx = \int_{t}^{t+\Delta t} \int_{i-1}^{i+1} \frac{\partial}{\partial x}\left(k \frac{\partial T}{\partial x}\right) dx dt \tag{7.4.3}$$

where the integrations are taken in such an order as to simplify matters; $i+1$ and $i-1$ represent the cells either side of the cell under consideration, i. Temperature is taken at the centre of the cell although the conduction k may need to be taken at the interface between two cells and may therefore require averaging of some kind. Since T is constant along the thickness of a cell,

$$\rho c \int_{i-1}^{i+1} \int_{t}^{t+\Delta t} \frac{\partial T}{\partial t} \, dt \, dx = \rho c \left[T \right]_{t}^{t+\Delta t} \int_{i-1}^{i+1} dx$$

$$= \rho c \left(T_i^{\Delta t} - T_i^0 \right) \Delta x_i \qquad (7.4.4)$$

Also,

$$\int_{t}^{t+\Delta t} \int_{i-1}^{i+1} \frac{\partial}{\partial x} \left(k \frac{\partial T}{\partial x} \right) dx \, dt = \int_{t}^{t+\Delta t} \left[k \frac{\partial T}{\partial x} \right]_{i-1}^{i+1} dt$$

$$= \int_{t}^{t+\Delta t} \left[k_{i+1,i} \frac{(T_{i+1} - T_i)}{\frac{1}{2}(\Delta x_{i+1} + \Delta x_i)} \right.$$

$$\left. - k_{i,i-1} \frac{(T_i - T_{i-1})}{\frac{1}{2}(\Delta x_i + \Delta x_{i-1})} \right] dt \qquad (7.4.5)$$

From this point the formulation can differ depending on the assumptions made over variation in T over the timestep. In line with the remainder of the model, which is implicit, it is assumed here that the value of temperature reached at time $t + \Delta t$ has applied for the entirety of the step, ΔT,

$$\int_{t}^{t+\Delta t} T_i(t) \, dt = T_i^{\Delta t} \int_{t}^{t+\Delta t} dt = T_i \Delta t \qquad (7.4.6)$$

meaning the entirety of (7.4.5) can be moved outside of the integral; the superscript $t + \Delta t$ has also been dropped with T now referring to the next temperature and T^0 referring to the old value. Equation 7.4.3 finally becomes

$$\rho c(T_i - T_i^0)\Delta x_i = k_{i+1,i} \frac{(T_{i+1} - T_i)}{\frac{1}{2}(\Delta x_{i+1} + \Delta x_i)} \Delta t$$

$$- k_{i,i-1} \frac{(T_i - T_{i-1})}{\frac{1}{2}(\Delta x_i + \Delta x_{i-1})} \Delta t \qquad (7.4.7)$$

where grouping of terms gives (7.4.7) in the usual finite difference discretisation form of

$$a_i T_i = a_{i+1} T_{i+1} + a_{i-1} T_{i-1} + a_i^0 T_i^0 + S_i \qquad (7.4.8)$$

with

$$a_{i+1} = \frac{2k_{i+1,i}}{\Delta x_{i+1} + \Delta x_i} \qquad (7.4.9)$$

$$a_{i-1} = \frac{2k_{i,i-1}}{\Delta x_i + \Delta x_{i-1}} \qquad (7.4.10)$$

$$a_i^0 = \frac{\rho c \Delta x_i}{\Delta t} \qquad (7.4.11)$$

$$a_i = a_{i+1} + a_{i-1} + a_i^0 \qquad (7.4.12)$$

Since (7.4.2) is the one-dimensional heat transfer equation, y and z are absent from the formulation. The equation is also valid for three dimensional

solids so long as there is no cross-sectional variation because the gradients are on a per unit area basis (adiabatic boundaries in these directions are a necessity for zero variation). If it is necessary to quote a source in total terms as opposed to per unit area then the area can be explicitly included in equation 7.4.2 leading to equivalent representations for the coefficients as

$$a_{i+1} = \frac{2\Delta y \Delta z k_{i+1,i}}{\Delta x_{i+1} + \Delta x_i} \qquad (7.4.9\text{a})$$

$$a_{i-1} = \frac{2\Delta y \Delta z k_{i,i-1}}{\Delta x_i + \Delta x_{i-1}} \qquad (7.4.10\text{a})$$

$$a_i^0 = \frac{\rho c \Delta x_i \Delta y \Delta z}{\Delta t} \qquad (7.4.11\text{a})$$

$$a_i = a_{i+1} + a_{i-1} + a_i^0 \qquad (7.4.12\text{a})$$

For a cell i at the exposed surface, there is no neighbour volume but instead a flux from or to the contacting gas layer. For such a situation, the respective coefficient becomes zero, i.e. $a_{i-1} = 0$, and the flux enters the source term, $S_i = \dot{h}$. At present for simulations it is assumed that the volume on the other end of the surface, the outside of the wall, is insulated from the surroundings, meaning the corresponding coefficient once again becomes zero but the source term also remains zero. Despite this the capability has been included such that both a fixed value beyond this last volume *or* a flux term can also be modelled. This will allow simple extension of the hybrid model to allow features such as heat loss to the external domain or heat transfer between walls of the zone and CFD models if the correct fluxes are provided.

Until this point the conductivity has kept its subscript denoting its dependence on location. This is now dropped as it is assumed that conductivity remains constant throughout the surface, but it is worth noting that the present implementation would allow an easy extension of the model to include composite 'sandwich' materials, as long the conductivity is calculated correctly at the interfaces between volumes.

The system is solved iteratively: by beginning with the vector of temperatures from the previous step a vector of present temperatures is found, this is continued until the difference between the old and present vectors is such that the required gain/loss in enthalpy is equal to the flux at the exposed surface, to within a given tolerance.

The equations are evaluated in order, starting from the exposed surface and progressing towards the outside edge. This is done since for the present implementation the variation will be experienced at the exposed end and therefore this method allows this to propagate through the solution quicker. From (7.4.8a) to (7.4.12a) above the equation for temperature in this first cell is given by

$$\left(\frac{\Delta y \Delta z k}{\Delta x_1} + \rho c \frac{\Delta y \Delta z \Delta x_1}{\Delta t}\right) T_1^{n+1} = \dot{h} + \frac{\Delta y \Delta z k}{\Delta x_1} T_2^{n+1} + \rho c \frac{\Delta y \Delta z \Delta x_1}{\Delta t} T_1^n \qquad (7.4.13)$$

where $\dot{h}$ is the flux entering the exposed surface; rearranging gives

$$\rho c \frac{\Delta y \Delta z \Delta x_1}{\Delta t} \left(T_1^{n+1} - T_1^n \right) = \dot{h} + \frac{\Delta y \Delta z k}{\Delta x_1} \left(T_2^{n+1} - T_1^{n+1} \right) \qquad (7.4.11)$$

where it can be seen that the left hand side is simply the change in enthalpy of the cell and the right hand side are the energy fluxes at the two edges.

Obviously the flux $\dot{h}$ into this cell remains constant regardless of the cell thickness Δx_1 since it is acting on the surface, yet the conduction term on the right does depend on this value. Dividing through by the Δx term on the left hand side means that the effect of $\dot{h}$ on the temperature scales with $(\Delta x)^{-1}$ yet the effect of the conduction term scales with $(\Delta x)^{-2}$, so although the energy flux into the cell is having a greater effect as the mass of the cell decreases there is potential for the conduction term to swamp this effect.

In an explicit formulation the time '$n+1$' terms on the right hand side are instead evaluated at 'n' and the above problem is prevented since the magnitude of the conduction term does not increase with T_1^{n+1}. This can instead lead to a stability issue since the scaling of the $\dot{h}$ term is now not being counteracted by the conduction term, and this is where the requirement of a stability criterion for explicit formulations is apparent where the maximum time-step is dictated by the size of Δx.

Since the present method is implicit, with the intent of maintaining full freedom over the time-step size, the conduction term on the right of (7.4.14) is evaluated at '$n+1$', yet due to the nature of the equation evaluations T_2^{n+1} is in essence a step behind at the point of calculation of T_1^{n+1}. The issue with this is that as Δx gets smaller, the actual difference between T_1 and T_2 gets less as these points get closer together, but the delay in evaluating T_2 means that this effect is lost. Looking again at (7.4.14) it can be seen that if $T_2^{n+1} - T_1^{n+1}$ was allowed to tend towards zero with Δx then the conduction term would scale in line with $\dot{h}$ and the problem would be averted. This hints that the use of a more advanced solver as opposed to simply stepping through the volumes could prevent any such problems and this is an avenue for further work, see chapter 8.

The above problem manifests itself as sluggishness in convergence as T_1^{n+1} is slowly allowed to increase whilst maintaining $T_2^{n+1} - T_1^{n+1}$ close to zero. Contrary to the stability issues of an explicit scheme, the above method is guaranteed to provide an accurate solution so long as it is afforded the

required time for convergence; one caveat of this is that for sufficiently small Δx the small increases in T_i^{n+1} can actually be lost to the numerical accuracy of the floating point representation and the solution never progresses. The convergence tolerance is set in line with the remainder of the model tolerances yet can be adjusted by the user.

Validity of conduction method

The conduction method above was compared to a solution obtained from a high res (1000 element) MATLAB numerical solution (R2009a, The MathWorks Inc., 2000). Here values for surface quantities such as density and specific heat were chosen in line with the default wall material used in SMARTFIRE. At $x = 0m$ the solid experiences a convective flux $h(T_g - T_{x=0})$ where the gas temperature is taken to be $400K$ and the convective coefficient is $h = 5$. The opposite end of the solid at $x = 0.2m$ is held fixed at $288.15K$.

Figure 7-8 below demonstrates that the conduction method used in the FSEG-ZONE model provides results that agree well with those from MATLAB when the number of cells used is 100. The figure also demonstrates the negative effects of using too coarse a mesh (too few cells); this is most obvious in the plot for 4 cells where the method clearly underestimates the temperatures. This is due to the increased resistance to temperature change provided by the larger mass involved for a larger cell. Calculations show that the average temperature can be captured well, i.e. the first value from a 4 cell simulation agrees well with the average value from the first 25 cells of a hundred cell simulation; although due to the non-linearity involved this quality can neither be assumed nor made use of in any rigorous fashion.

A further test of the validity of the conduction method is demonstrated in figure 7-9; here the 'steady state' conditions are calculated both through the FSEG-ZONE model and through direct calculation. Here for simplicity the conduction is taken as unity, specific values for density and specific heat are

unnecessary since the steady state solution is independent of these quantities (although these quantities dictate the rate at which steady state is achieved).
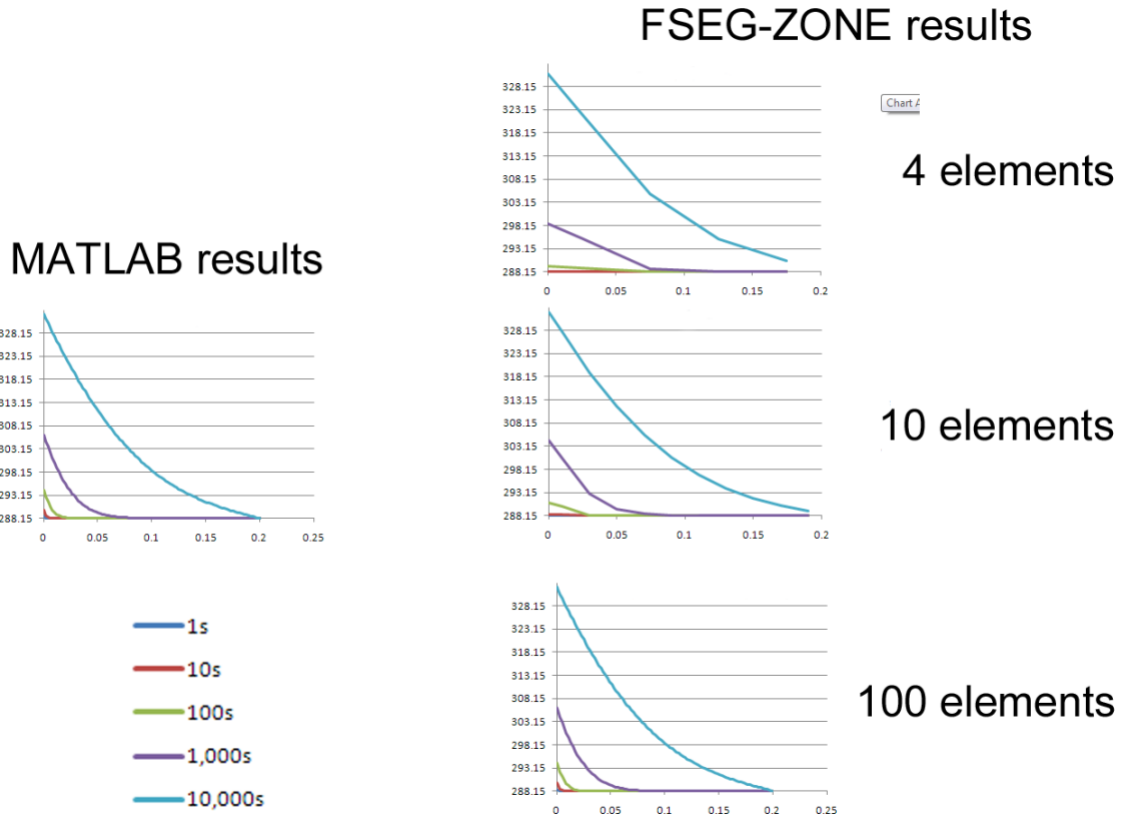
Figure 7-8. Plots showing temperature (K) variation through a 0.2m thick solid at times 1, 10, 100, 1,000 and 10,000 seconds. MATLAB results (left) are compared against the FSEG-ZONE conduction method (right) using 4, 10 and 100 elements.

At steady state the temperature gradient through the solid is constant and must be equal to the convective enthalpy flux at $x = 0$, giving

$$\frac{T_s - 288.15}{0.2} = 5(400 - T_s)$$

where T_s is the surface temperature at $x = 0$. Rearranging gives

$$T_s = \frac{2000 + {288.15}/{0.2}}{5 + {1}/{0.2}} = 344.075K$$

Figure 7-9 shows the steady state temperature provided by the FSEG-ZONE model, with the surface temperature being reported as $344.0755K$, $0.005K$ over the true solution.
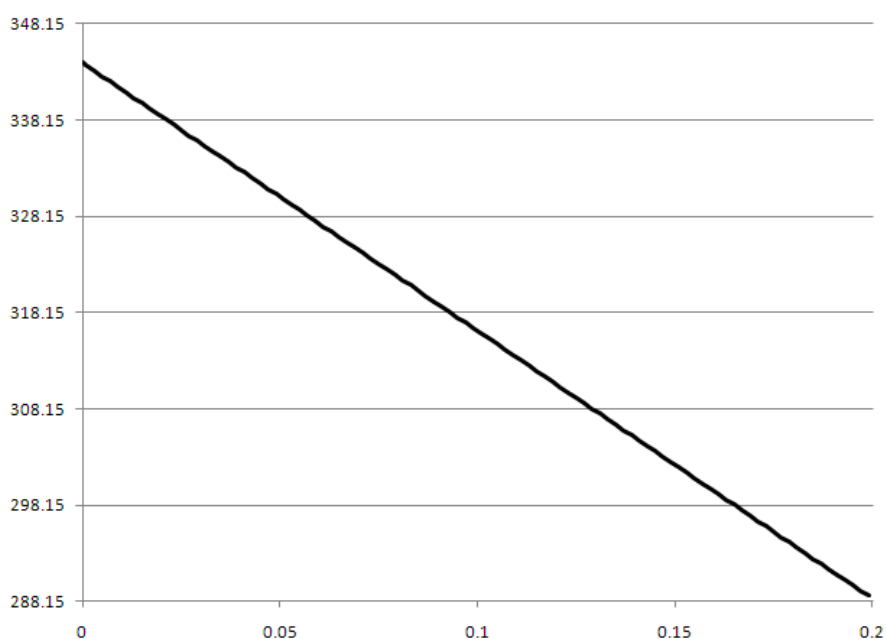
Figure 7-9. Steady-state temperature variation through the solid obtained from the FSEG-ZONE model.

7.4.2 Convective Heat Transfer

The conduction method in section 7.4.1 addresses heat transfer within a solid with ends either held at a fixed temperature, insulated or exposed to a given flux of energy. The most likely source of such a flux in a fire situation will be from the convective heat transfer occurring at the interface between a gas and surface at different temperatures. Such a flux is commonly assumed to be

proportional to this temperature differential, with the constant of proportionality being the convective heat transfer coefficient h, in essence representing the efficiency with which this difference gives rise to a transfer of energy. The convective transfer coefficient will depends on numerous factors such as the type of fluid under consideration, the temperature of the fluid, properties of the flow i.e. whether a turbulent regime is developed and characteristics of the surface. Since many of these attributes are neglected by the uniform layer assumption of a zone model, the methods used to evaluate the convective transfer coefficient will naturally depend somewhat on empirical relationships.

The method used within the FSEG-ZONE model is derived from [Atreya1992]. A version of this is used in the CFAST zone model, which also makes some approximations to remove a significant proportion of the calculations involved. Since the computational time is not such a limiting factor in the hybrid model the full calculations of the method have been retained, along with the calculation of fluid properties from a table of values allowing their variation with temperature to be modelled.

The fluid under consideration is assumed to be air and the properties required for a calculation of the convective transfer coefficient are the kinematic viscosity v, the thermal conductivity k, the thermal diffusivity α and the Prandtl number Pr. The table of values used is presented in [Atreya1992], a section of which is reproduced below as table 7-1. The table considers variation in the specific heat of air as its temperature changes, in contradiction with the remainder of the FSEG-ZONE model. This inconsistency will not have a detrimental effect since these values are used to calculate h only and conservation is certainly not affected in any way. Still, for this reason the values of α and Pr, which are in fact ratios of the other known quantities, are still taken from the table as opposed to directly calculating them. The table assumes the air to be at atmospheric pressure, therefore the affect of a change in compartment pressure is not addressed by

this method. Also, any effect from species or smoke concentration is not considered.

T	ν 1.E-06	k 1.E-03	α 1.E-06	Pr
K	m²/s	W/mK	m²/s	
100	2.000	9.34	2.54	0.786
150	4.426	13.8	5.84	0.758
200	7.59	18.1	10.3	0.737
250	11.44	22.3	15.9	0.720
300	15.89	26.3	22.5	0.707
350	20.92	30.0	29.9	0.700
400	26.41	33.8	38.3	0.690
450	32.39	37.3	47.2	0.686
500	38.79	40.7	56.7	0.684
550	45.57	43.9	66.7	0.683
600	52.69	46.9	76.9	0.685
650	60.21	49.7	87.3	0.690
700	68.10	52.4	98	0.695
750	76.37	54.9	109	0.702
800	84.93	57.3	120	0.709
850	93.8	59.6	131	0.716
900	102.9	62.0	143	0.720
950	112.2	64.3	155	0.723
1000	121.9	66.7	168	0.726
1100	141.8	71.5	195	0.728
1200	162.9	76.3	224	0.728
1300	185.1	82	238	0.719
1400	213	91	303	0.703
1500	240	100	350	0.685
1600	268	106	390	0.688
1700	298	113	435	0.685
1800	329	120	482	0.683
1900	362	128	534	0.677
2000	396	137	489	0.672
2100	431	147	646	0.667
2200	468	160	714	0.655
2300	506	175	783	0.647
2400	547	196	869	0.630
2500	589	222	960	0.613
3000	841	486	1570	0.536

Table 7-1. Required thermophysical properties of air for the convective coefficient calculation; reproduced from [Atreya1992].

The air properties are first found by using the film temperature $T_f = (T_s + T_g)/2$, where T_s is the surface temperature and T_g is the temperature of the contacting gas layer. With these the Rayleigh number over length can be calculated as

$$Ra_l = \frac{g\beta(T_s - T_g)L^3}{\nu\alpha}$$

(7.4.12)

where g is gravity, β is the thermal expansion coefficient $(1/T_f)$ and the length L depends on the orientation of the surface; for vertical walls the length is given by the height of the surface, for horizontal ceilings and floors the value is given by a character length defined as the ratio of the area of the surface to its perimeter (A/P).

From the Rayleigh number, the Nusselt number over length can then be calculated for vertical surfaces as [Atreya1992] [Incropera2006]

$$Nu_L = \left[0.825 + \frac{0.387Ra_L^{1/6}}{[1 + (0.492/Pr)^{9/16}]^{8/27}}\right]^2$$

(7.4.13)

and for horizontal surfaces as

$$Nu_L = 0.54Ra_L^{1/4} \qquad for \ 10^5 \leq Ra_L \leq 10^7$$

(7.4.13)

$$Nu_L = 0.15Ra_L^{1/3} \qquad for \ 10^7 \leq Ra_L \leq 10^{10}$$

(7.4.14)

Finally the convective coefficient is calculated as

$$h = \frac{Nu_L k}{L} \qquad (7.4.15)$$

allowing the corresponding flux per unit area into the given surface to be calculated from

$$\dot{q} = h\left(T_g - T_s\right) \qquad (7.4.16)$$

This flux can then be used at the corresponding end of the solid and the conduction calculated as per section 7.4.1.

7.4.3 Surfaces and Layer Changes

Because every surface apart from the ceiling and floor has upper and lower counterparts, a change in layer height will change the vertical dimension of these sections. A wall without a door will comprise of an upper and lower section, and a change in layer will result in one of these sections getting bigger by the amount of the change, the other getting smaller by the same amount. Walls with doors experience the same changes although there are situations where further consideration is required. For instance, for a layer that was previously above a door soffit, an upper and lower section existed for the horizontal surface above the door. If the layer now descends below the door, the sections change such that the lower section is exhausted and the surface becomes exclusively upper. In this situation the sections do not grow/shrink by an amount equal to the layer change, but are limited to the dimensions of the original surface; layer movement below the soffit has no further effect on this surface. A similar situation is true for the surfaces that

begin at floor level, with layer movement across the door soffit again requiring consideration.

Since the upper and lower parts of a surface are generally at different temperatures, a moving layer also necessitates consideration of a change in enthalpy as say an upper section 'consumes' part of a lower section. For sections decreasing in size this is not an issue, e.g. cutting a section of metal bar results in two pieces at the same temperature. For increasing sections the difference is that the new enlarged section will contain a part of the reduced section, and since these sections are assumed to be at uniform temperatures an averaging of the new enthalpy over the new volume of the surface is required. The inclusion of conduction and the existence of a temperature gradient through the surface complicates matters somewhat, but if each cell is considered separately the same averaging can be performed on an individual basis, resulting in a modified surface that maintains a temperature variation. Figure 7-10 below provides an example of the surfaces and their numbering for a single door compartment.
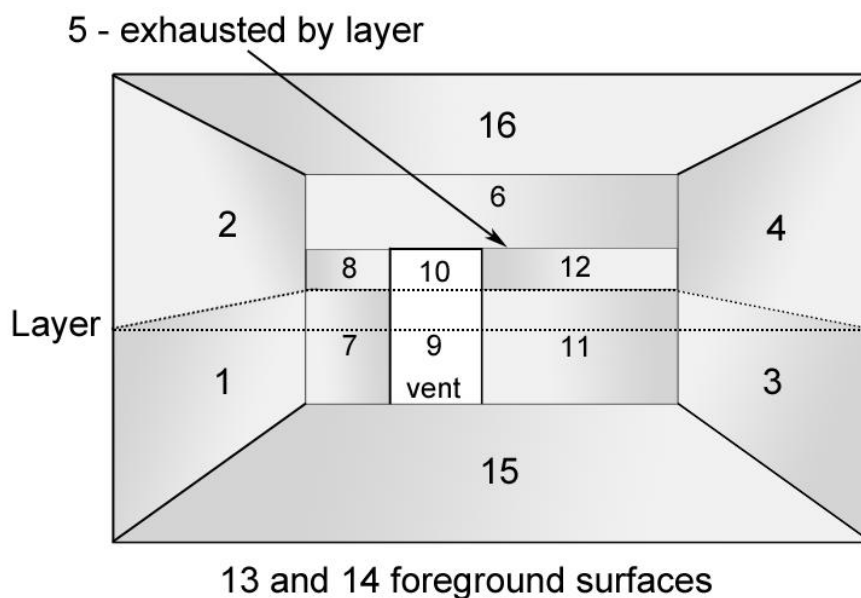
Figure 7-10. Example surface numbering for a compartment with a single vent.

7.4.4 Test Case – Surface heat transfer

The following test case corresponds to that in section 6.3.4 which had the heat source removed after two minutes to model the resulting cooling of the domain. Here the surfaces which were previously adiabatic are now modelled as conducting surfaces through use of the method discussed in this section. The convective heat transfer at the interface between surface and gas is modelled as discussed in section 7.4.2.

The surfaces are assumed to be made of a material with the following properties: conductivity $0.69\ W/Km$, specific heat $840\ J/Kkg$ and density $1600\ kg/m^3$. The surfaces are $20\ cm$ thick and begin at an ambient temperature of $288.15\ K$.

Results

The first plot in figure 7-11 shows the development of compartment pressure and mass for both the CFD and FSEG-ZONE models. Again, very good agreement is apparent with the FSEG-ZONE model capturing both the general trend and values seen in the full CFD model, although the FSEG-ZONE model consistently underestimates the temperature and over estimates the mass. A maximum error of approximately $0.17Pa$ can be seen at 90 seconds, although after the heat source is removed the FSEG-ZONE pressure remains within $0.07Pa$ of the CFD solution.
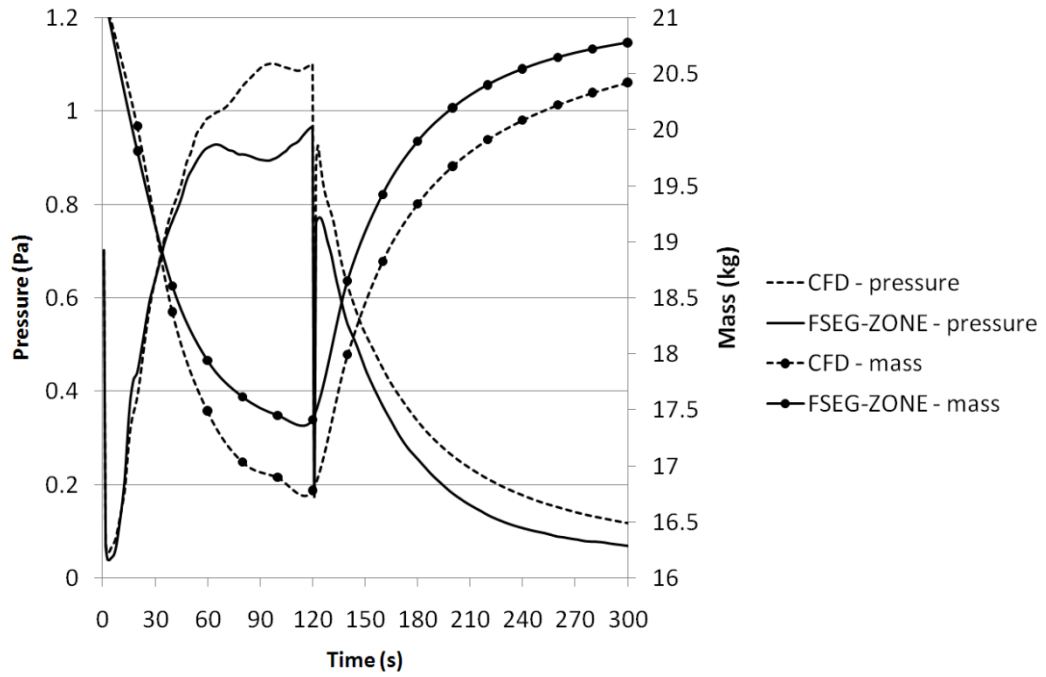
Figure 7-11. Comparison of pressure with surface conduction enabled.
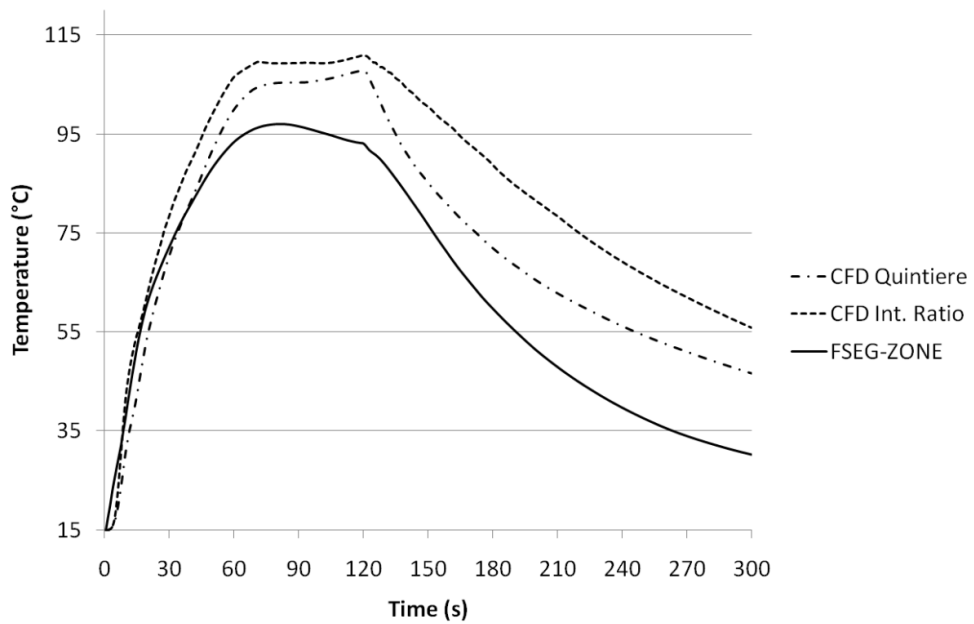
Figure 7-12a. Upper layer temperatures with surface heat transfer enabled.
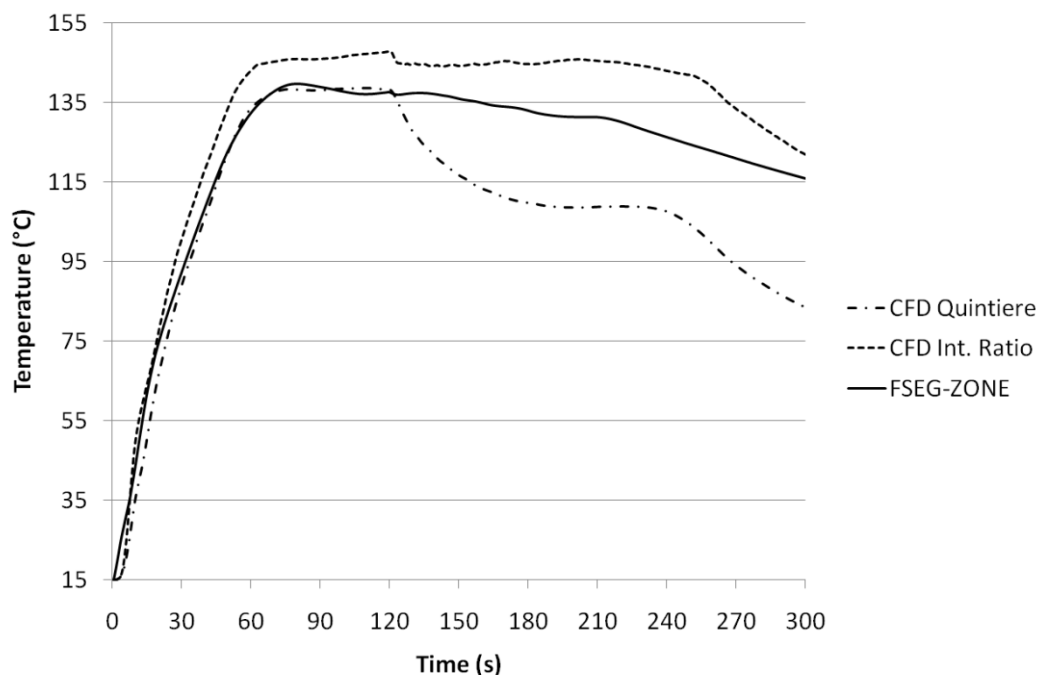
Figure 7-12b. Upper layer temperatures with surface heat transfer disabled.

The upper layer temperature comparisons can be seen in figure 7-12a above. Again the general trend is captured well, with the FSEG-ZONE model heating up at the same rate as the CFD model during the first 45 seconds of the simulation. After this point, it is apparent that the inclusion of heat transfer to the surfaces of the compartment causes the FSEG-ZONE model to cool significantly quicker than the CFD model. The equivalent results sans surface heat transfer were presented in figure 6-22, but since the preceding test cases may have confused matters this is reproduced above for convenience as figure 7-12b.

It is apparent that the enabling of surface heat transfer has a significant effect in both models, yet takes considerably more energy from the upper layer of the FSEG-ZONE model. It is tempting to assume that such an effect can be fully explained by the uniform temperature in a zone layer. Since the heat transfer relationship is fundamentally linear (if the convective coefficient is assumed to be independent of temperature), variation in the gas temperature along the wall surface is not sufficient to explain the difference.

On the other hand, temperature variation *within* the gas volume will have an effect on the total energy transfer; the most obvious occurrence of this situation is the cooling experienced by near-wall gas, leaving relatively hotter temperatures in the centre of the gas volume. This cooler gas 'boundary' between layer and wall will result in less energy being removed from the CFD, giving higher temperatures. Although this cooler near-wall gas was witnessed in the CFD simulations, the magnitudes involved were not sufficient to fully explain the discrepancies observed between models.

On investigating the issue further it became apparent that the different methods used by the two models to calculate the heat transfer coefficient actually provide significantly different values. Both methods are empirical in nature, but the CFD model has the opportunity to take velocity magnitudes into account. It is not clear which calculation is more accurate, yet the CFD model has been observed to regularly provide values for the convective coefficient that are 3-7 times smaller than those provided by the zone model. This is a fundamental difference between the models at present and should be kept in mind.

Figure 7-13 on the next page compares the lower layer temperatures between models and is similar to previous test cases where the inability of the FSEG-ZONE model to consider mixing between layers results in a delay in the heating of the layer. Again, the variations experienced by all three values are very similar after the initial 60 seconds and if this period was addressed more accurately in the FSEG-ZONE model it would likely result in very close agreement between the models.

Finally, figure 7-14 on the next page again demonstrates how the FSEG-ZONE value seems to be bounded by the two reduction methods and demonstrates some very favourable agreement throughout the simulation.

The time taken by the CFD model was 11 hours 17 minutes and 23 seconds, whereas the hybrid model took 7 hours 1 minute and 37 seconds, a saving of

37% resulting from a cell saving of 24%. It is worth noting that activating surface convection/conduction had a negligible effect on the simulation times of both models.
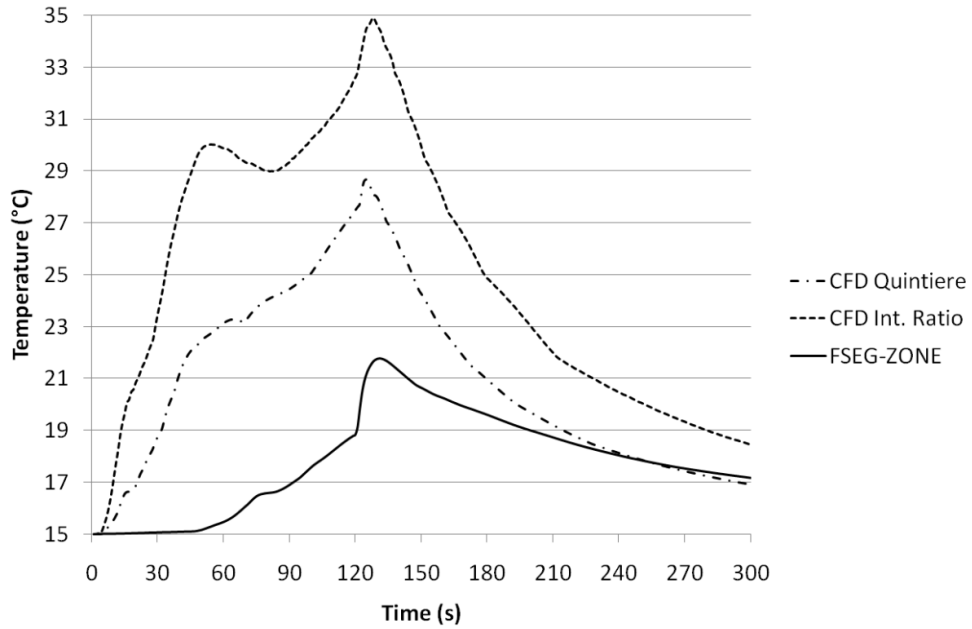
Figure 7-13. Lower layer temperatures with surface conduction enabled.
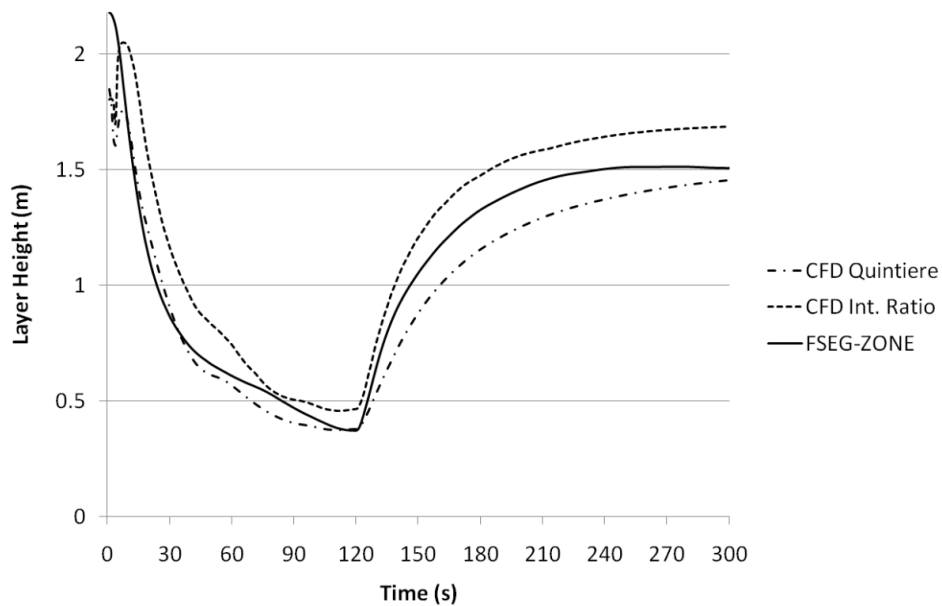
Figure 7-14. Layer height development with surface conduction enabled.

7.5 Combustion

The process of combustion is an important consideration in the simulation of fires. Its inclusion can greatly affect the dynamics of a simulation, both in the sense that it allows a more accurate treatment of temperature and product concentrations, and can also act as a limiting factor on enthalpy release, such as when conditions are unfavourable for complete combustion. Consideration of combustion within the hybrid model means increased accuracy for the simulation as the fluid being passed from zone to CFD is now different to fluid that simply comes from the external conditions (i.e. if the room was replaced by an outlet). SMARTFIRE employs the Simple Chemical Reacting System (SCRS) scheme [Versteeg2007], this is discussed below with regards to implementation within the FSEG-ZONE model.

Consideration of combustion centres on the combustion equation,

$$fuel + oxidant \rightarrow products$$

or, in a stoichiometric sense,

$$1kg\ fuel + \ s_{ox}\ kg\ oxidant \ \rightarrow (\ 1 + \ s_{ox}\ )kg\ products$$
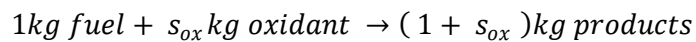
For alkane fuels, the oxidant tends to be oxygen, with the products then being water and carbon dioxide, i.e.

$$C_n H_{2n+2} \ + \ O_2 \ \rightarrow \ H_2O \ + CO_2$$

or in the correct ratios,

$$C_n H_{2n+2} \ + \ \frac{(3n+1)}{2}O_2 \ \rightarrow \ (n+1)H_2O \ + nCO_2$$
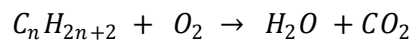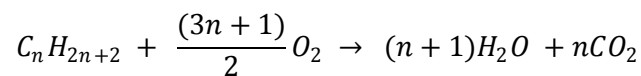
The stoichiometric amounts of the elements and compounds in the above equation will clearly depend on the choice of fuel; SMARTFIRE allows the user to arbitrarily set these amounts permitting different fuels to be modelled, but defaults to the values representing methane, i.e.

$$CH_4 \; + \; 2O_2 \; \rightarrow \; 2H_2O \; + \; CO_2$$

From the above equation, a mole of methane requires two moles of oxygen for complete combustion, resulting in two moles of water along with a mole of carbon dioxide. Since the mass of a single mole of methane is $12 + 4(1) = 16 \; grams$, and that of two moles of oxygen is $2.2(16) = 64 \; grams$, then each kg of methane will require $\frac{64}{16} = 4 \; kg$ of oxygen for complete combustion. More generally, one unit mass of fuel will require s_{ox} units of oxidant, where

$$s_{ox} = S_{ox} \; \frac{M_{ox}}{M_f} \qquad\qquad (7.5.1)$$

where M_{ox} and M_f are the molecular weights of the oxidant and fuel respectively, and S_{ox} is the molar stoichiometric ratio of oxidant to fuel in the combustion equation (the coefficient of the oxidant if the equation is normalized to a single unit of fuel).

The supplies of both fuel and oxidant may not consist entirely of the components under consideration, e.g. if the oxidant itself is assumed to be air then only a proportion of this will be the actual oxygen used in the combustion process (e.g. air is commonly quoted as containing 23% oxygen by mass). As calculations are performed within SMARTFIRE on the mass fractions of fuel and oxidant, these proportions of actual fuel and oxidant within the fuel and oxidant 'streams' need to be taken into consideration. In general, one unit mass of impure fuel (containing a proportion w_f' of actual

pure fuel by mass) will require s_{ox} units of oxidant (containing a proportion $w_{ox}^{'}$ of oxidizing agent by mass), where

$$s_{ox} = \frac{w_f^{'}}{w_{ox}^{'}} \left(S_{ox} \frac{M_{ox}}{M_f} \right)$$

(7.5.2)

If it is assumed that combustion takes place instantaneously then masses of both fuel and oxidant cannot exist simultaneously within the same cell. If the reactants were previously in the stoichiometric ratio above, then neither will be present after combustion; conversely, if this ratio is exceeded in either direction, then an amount of one of the reactants will be left over post combustion. The assumption of instantaneous combustion and the limits it places on valid values for the reactants means that when there is a positive mass of fuel, knowledge of the mass of oxidant becomes redundant, since it is identically zero; conversely, consideration of fuel becomes unnecessary when there is oxidant mass. Because of this quality, it is possible to fully describe the behavior of these two quantities by a single variable, called the mixture fraction.

As the process of combustion reduces the amount of reactants, the highest concentration of these will be attained in their respective streams. The mixture fraction f_m is formed such that within a cell,

$$f_m = \frac{\left(s_{ox} w_f - w_{ox} \right)_{cell} - \left(s_{ox} w_f - w_{ox} \right)_{ox}}{\left(s_{ox} w_f - w_{ox} \right)_{f} - \left(s_{ox} w_f - w_{ox} \right)_{ox}}$$

(7.5.3)

with the subscripts outside the parentheses indicating the location at which the difference inside is to be evaluated, either within the fuel or oxidant

streams, or within the cell in question. Since no fuel exists in the oxidant stream, and vice-versa, the above definition can be simplified as

$$f_m = \frac{\left(s_{ox} w_f - w_{ox}\right)_{cell} - (-w_{ox})_{ox}}{\left(s_{ox} w_f\right)_f - (-w_{ox})_{ox}} \qquad (7.5.4)$$

and since the mass fractions of reactant sources are being considered, which are clearly unity at the steams, this further reduces to,

$$f_m = \frac{\left(s_{ox} w_f - w_{ox}\right)_{cell} + 1}{s_{ox} + 1} \qquad (7.5.5)$$

The mixture fraction is a representation of the mass fraction of fuel or oxidant present at a location, and is scaled to vary linearly from 0 to 1 as it moves from oxidant to fuel stream. This variable is solved for within SMARTFIRE since and actual mass fractions of fuel and oxidant are recovered from this variable when needed. The mixture fraction at a location at which the reactants were previously in the correct ratio (where both w_f and w_{ox} are now zero, is given by

$$f_m^s = \frac{1}{s_{ox} + 1} \qquad (7.5.6)$$

Since the mixture fraction has been scaled to vary from 0 to 1, this value is obtained at the surface between fuel and oxidant and can be used to ascertain either fuel or oxidant mass fractions, depending on whether the actual mixture fraction is greater or less than this ratio.

Consideration of combustion handling within the hybrid model generally consists of simply tracking masses of fuel, oxidant and products that may cross the interface into the zone model. The initial conditions and masses within the zone rooms must be consistent with those of the CFD model in this respect, i.e. the mass fractions of both fuel and products are zero, while that of oxidant is unity (recall that the oxidant mass fraction is with respect to the 'impure' oxidant, air, where the proportion of oxygen has already been taken into account). The main occurrence over the hybrid interface will be the transport of products into the zone room, effectively diluting the oxidant content of the layers, which in turn can get passed back into the CFD domain. The zone model must calculate the value of the mixture fraction from these components for use on the boundary condition, since the CFD model solves their transport using this variable.

In extreme conditions, for instance where a fuel jet makes contact with the hybrid interface, fuel mass may enter the zone room. Masses of fuel and oxidant cannot simply coexist in a layer, and consideration of their combustion and the resultant enthalpy and product release is required. Since the layers in a zone model are assumed to be completely mixed, any fuel entering a zone layer over a time step is assumed to instantaneously combust, removing the fuel from the layer along with a corresponding amount of oxidant, whilst adding some product mass along with a portion of energy. The energy released by the fuel as it combusts is termed its 'heat of reaction', ΔH_r, with the value used in the hybrid model being on a per unit mass basis. Therefore, for a mass of fuel m_F that accumulates in a layer over a timestep, the resulting release in energy will be

$$h_{CMB} = m_F \Delta H_r \ joules \qquad (7.5.7)$$

It is possible that a significant amount of fuel can enter a layer, such that there is insufficient oxidant for its complete combustion. In this situation the

portion of fuel that combusts is limited by the present mass of oxidant m_{OX} such that the heat released is

$$h_{CMB} = \frac{m_{OX}}{s_{OX}} \Delta H_r \qquad (7.5.8)$$

Once this situation has occurred the layer will consist solely of fuel and product, any future influx of oxidant to the layer will result in a corresponding combustion.

The energy term h_{CMB} is simply combined with the remaining energy sources of the model for use in the pressure and temperature equations during the solution routine.

7.6 Smoke Transport

The transport and concentration levels of smoke are vital factors for consideration in a fire simulation. Smoke is often the element of a fire that poses the most danger for evacuees, both in its extremely nocuous nature and its ability to substantially reduce visibility. It is also closely linked to the radiative qualities of a gas, affecting both the absorption and emission of such volumes. Smoke is a dense material, and although the actual spatial presence of smoke in a gas volume may be very small, it can still add significant mass, increasing its density and subtly modifying the flow. Due to its density it also contains significant internal energy, and can act as a source or sink of heat for the surrounding gas.

These effects are concerned with the concentration of smoke, both at a certain point or location and along a path, either of evacuation or line of sight. The variable solved within SMARTFIRE is the smoke mass fraction w_s, where

$$w_s = \frac{m_s}{m}$$

(7.6.1)

with mass of smoke m_s and total mass m, here on a cell basis. The smoke mass flux across a particular CFD face on the hybrid interface can then be calculated simply by taking the total mass flux across this face, $\rho A v$, and multiplying it by the mass fraction, giving

$$\dot{m}_s = w_s \rho A v$$

(7.6.2)

with the mass flux of remaining species, e.g. air, clearly given by

$$\dot{m}_{other} = (1 - w_s)\rho A v$$

(7.6.3)

Due to the assumption of 'super-fast thermal equilibrium', smoke is assumed to have the same temperature as the gas it is suspended in. The smoke is also assumed to have the same specific heat or enthalpy per unit mass, allowing enthalpy fluxes to be calculated as before. Smoke is assumed to move together with the gases it is contained in, and so the previous rules for assigning flow to/from the zone layers also remain valid. Smoke within SMARTFIRE has a constant density which defaults to $1800 kgm^{-3}$ but can be modified by the user if so required.

Through summation of the above fluxes for each time step, the proportion of smoke and other species that make up the total mass in a zone layer is known at any point in the simulation. These proportions for each layer can then be used as the value for smoke mass fraction applied at the interface boundary

condition for return flow to the CFD domain, with the smoke mass fraction in layer i, $w_{s,i}$, given by

$$w_{s,i} = \frac{m_{s,i}}{m_i} \tag{7.6.4}$$

Density

For calculation of the total density for layer i, ρ_i, volume fractions are now required as opposed to mass fractions,

$$\rho_i = \varphi_s \rho_s + (1 - \varphi_s)\rho_g \tag{7.6.5}$$

where φ_s is the smoke volume fraction and ρ_s and ρ_g are the densities of the smoke and remaining gases respectively; the density of the gas remains calculated by the ideal gas equation as before but is affected by the modifications to pressure and temperature discussed below. Noting that

$$w_s \rho_i V_i = \varphi_s V_i \rho_s \tag{7.6.6}$$

with both sides equalling the total mass of smoke in a layer, the smoke volume fraction can also be given by

$$\varphi_s = w_s \frac{\rho_i}{\rho_s} \tag{7.6.7}$$

substitution of this into the above equation for layer density gives

$$\rho_i = \frac{\rho_g}{1 \; + \; w_s (\rho_g/\rho_s - 1)} \qquad (7.6.8)$$

This completes the treatment of smoke transport with regards to the interface itself, but further consideration is required for the effects that including smoke has on the zone model equations.

As the zone equations are in turn based on the ideal gas equation, treatment of smoke as a gas would be possible, but to remain consistent the density of the smoke would have to be allowed to vary with the temperature. Since this is in contradiction with the assumption of constant density made by the CFD model, smoke is treated as a solid within the zone domain of the hybrid model. Essentially, as the zone equations for pressure and temperature are applicable only to gas volumes, the addition of smoke mass to a layer corresponds to compressing the existing gas volume to ensure the total volume remains constant; note that the density remains calculated over the total volume. The work done on a layer in compressing it results in direct changes in the calculation of both the pressure and temperature; density is indirectly affected through both the temperature of the gas (i.e. not smoke) and the compartment pressure as a whole. It should be noted that the discussion below considers solely the net addition of smoke, but that removal is addressed similarly by the same equation simply by reversing its sign.

It is convenient to think of the addition of a volume of gas and smoke to a compartment layer as occurring in three steps,

1. Addition of the volume of smoke, in effect compressing the existing compartment volume.

2. Addition of the volume of gas, consisting of the addition of mass, enthalpy and a compression factor.

3. Finally, transfer of enthalpy to/from the smoke volume to ensure the gas and smoke within a layer are at equal temperature, satisfying the assumption of 'super-fast thermal equilibrium'.

Compression

Obtaining a new volume V_{new} through compression by reducing an original volume V_{old} by a factor α, where

$$\alpha = 1 - \frac{V_{new}}{V_{old}} \tag{7.6.9}$$

is equivalent in terms of work done to beginning with the smaller volume V_{new} and adding sufficient enthalpy to equate both final states; the amount of enthalpy required is clearly the surplus in V_{old} over V_{new}, or αh_{old}. The corresponding pressure increase can then be calculated using the usual equation, i.e.

$$\Delta P_V = \frac{(\gamma - 1)}{V_{new}} (\alpha h_{old}) = \frac{(\gamma - 1)}{(1 - \alpha)V_{old}} (\alpha h_{old})$$

$$= \frac{\alpha}{(1 - \alpha)} \frac{(\gamma - 1)}{V} h \tag{7.6.10}$$

where the *old* subscript has been dropped from the final equality since these values are known at the time of the calculation.

The compression of a layer also results in a corresponding change in temperature, this is given by

$$\Delta T \;=\; \frac{1}{c_P \mathrm{m}}(\gamma - 1)(\alpha h) \tag{7.6.11}$$

Step 1 – smoke compression

First the change in pressure due to the compression is calculated,

$$\Delta P_V \;=\; \left(\frac{\alpha}{1 - \alpha}\right) \cdot \left(\frac{\gamma - 1}{V_0}\right) h_0 \tag{7.6.12}$$

where the h without subscript i is the total volume of both layers and the subscript 0 indicates that these values are the starting values, obtained from the last step. The temperature of both layers after compression is then calculated,

$$T_i \;=\; T_{i,0} \;+\; \left(\frac{1}{c_P m_{i,0}}\right) \cdot \left(\frac{V_{i,0}}{V_0}\right) \cdot (\gamma - 1) \cdot \alpha h_0 \tag{7.6.13}$$

followed by the calculation of density,

$$\rho_i = \frac{P + \Delta P_V}{RT_i} \tag{7.6.14}$$

which contains the change in pressure due to compression, ΔP_V. These variables now represent the state of the compartment and layers after the compression by the smoke volume.

Step 2 – standard gas treatment

Now the usual addition/subtraction of mass and enthalpy corresponding to the gas flux is performed. This is performed in a similar way to the case without smoke. The pressure change due to addition of enthalpy remains unchanged, but now the total change in pressure, required for the calculation of the remaining variables, must include the change observed from compression in the previous step, i.e.

$$
\begin{aligned}
\Delta P \;=\;& \Delta P_h \;+\; \Delta P_V \\
=\;& \frac{(\gamma - 1)}{V_1} \sum_i \dot{h}_i \;+\; \frac{\alpha}{(1 - \alpha)} . \frac{(\gamma - 1)}{V_0} . h_0
\end{aligned}
$$

(7.6.15)

Notice that the two components are making use of different values for the volume, V_0 and V_1, where the subscript 1 corresponds to the value of the variable obtained after completion of the first compression step; in this case the volume of gas for consideration has been changed by the addition of a volume of smoke to the compartment. Calculation of temperature is then performed through

$$T_i = \frac{T_{i,1} m_{i,1} + \dot{h}_i \big/ c_P}{m_{i,1} + \dot{m}_i}$$

$$+ \quad \frac{1}{c_P (m_{i,1} + \dot{m}_i)} \cdot \frac{V_{i,1}}{V_1} \cdot (\gamma - 1) \cdot \left(\sum_i \dot{h}_i \right)$$

(7.6.16)

again noting the use of subscripts; although the mass used in this step has not been affected by the compression step it continues to have the subscript for consistency. Density is then calculated through

$$\rho_i = \frac{(P + \Delta P)}{R T_i}$$

(7.6.17)

Step 3 – Thermal equilibrium of smoke volume

Until this point the smoke has simply had the affect of compression on the compartment. It is now required to address the issue of the thermal equilibrium of the smoke and its containing layer, where a certain amount of enthalpy must be transferred between the volumes so that both have equal temperature at the end of the process. If smoke is present in only a single layer, this value, h^* is found as follows.

At thermal equilibrium

$$T_{layer,equilib} = T_{smoke,equilib}$$

(7.6.18)

$$T_{layer\,,old} \;+\; \Delta T_{layer}\,(h^*) \;=\; T_{smoke\,,old} \;+\; \Delta T_{smoke}\,(h^*) \qquad (7.6.19)$$

$$T_{i,2} + \frac{h^*}{c_P m_{i,2}} + \frac{V_{i,2}}{V_2}(\gamma - 1)\frac{h^*}{c_P m_{i,2}} \;=\; T_{s,0} - \frac{h^*}{c_P m_{s,0}} \qquad (7.6.20)$$

rearranging for h^* gives

$$h^* \;=\; \frac{m_{i,2}\,m_s\,c_P\,(T_{s,0} - T_{i,2})}{\left[1 + \dfrac{V_{i,2}}{V_2}(\gamma - 1)\right]m_s \;+\; m_{i,2}} \qquad (7.6.21)$$

If smoke is present in both layers then the calculation is much more complex. Clearly, it's now necessary to find both h_u^* and h_l^* to represent the transfers of enthalpy required from both smoke volumes to their respective layers. Furthermore, the total transfer for the compartment as a whole, $h_u^* + h_l^*$, causes work to be done on both gas volumes, resulting in each transfer intimately affecting the other, therefore ensuing in a convoluted relationship between these values. The requirements of thermal equilibrium in both layers provide two simultaneous equations in two unknowns (h_u^* and h_l^*),

$$T_u + \frac{h_u^*}{c_P m_u} + \frac{V_u}{V}(\gamma - 1)\frac{(h_u^* + h_l^*)}{c_P m_u} \;=\; T_{s,u} - \frac{h_u^*}{c_P m_{s,u}} \qquad (7.6.22)$$

$$T_l + \frac{h_l^*}{c_P m_l} + \frac{V_l}{V}(\gamma - 1)\frac{(h_u^* + h_l^*)}{c_P m_l} \;=\; T_{s,l} - \frac{h_l^*}{c_P m_{s,l}} \qquad (7.6.23)$$

where the order subscripts have been dropped for sake of clarity. Considerable algebra results in

$$h_u^* = \frac{(T_{s,u} - T_u) - \theta_l^{-1}(T_{s,l} - T_l)}{\theta_u - \theta_l^{-1}\omega_u \omega_l} \tag{7.6.24}$$

$$h_l^* = \frac{(T_{s,l} - T_l) - \omega_l h_u^*}{\theta_l} \tag{7.6.25}$$

where

$$\omega_i = \frac{V_i}{V}.\frac{(\gamma - 1)}{m_i} \quad , \quad i = u, l \tag{7.6.26}$$

and

$$\theta_i = \frac{1}{C_P m_i} + \omega_i + \frac{1}{C_P m_{s,i}} \quad , \quad i = u, l \tag{7.6.27}$$

Once these required transfers are found they are used in a further application of the pressure, temperature and density equations.

If a layer has an existing volume of smoke before the addition under consideration here, then thermal equilibrium between these smoke volumes must be performed before performing the transfer calculations above. For an existing volume of smoke with enthalpy $C_P m_{s,old} T_{s,old}$ being augmented by a new amount $C_P m_{s,add} T_{s,add}$, the equilibrium temperature is found simply by

$$T_s = \frac{m_{s,old}\, T_{s,old} + m_{s,add}\, T_{s,add}}{m_{s,old} + m_{s,add}} \qquad (7.6.28)$$

as the smoke layer requires no consideration of compression due to the assumption of it being a solid.

7.7 Radiation

Radiation is an extremely important form of heat transfer to consider, the fourth power relationship with temperature means it can make up a large proportion of the heat given off by fire sources, along with providing significant opportunities for cooling and/or heating of the different components of the domain. Radiation differs from the mechanisms of convection and conduction in that it requires no intermediate matter for the transfer of heat. In fact, consideration of radiation becomes simpler if no matter exists between the entities that transfer is taking place between, i.e. if these are separated by a vacuum. Clearly, this exceptional situation is not to be expected in the overwhelming majority of fire situations, still, assumptions can be made over the 'transparency' of gas volumes which allows treatment of radiation similar to that over a vacuous separation to serve as a starting point for a zone radiation model; this can later be extended to more accurately represent the reality of the situation.

Assuming that the gas is totally transparent such that radiation passes through it totally unhindered, i.e. it neither absorbs or scatters, nor emits radiation of its own, the initial consideration can concentrate solely on the direct transfer of radiation between surfaces of the compartment. Assuming an initial state where the surfaces are at ambient temperature, the inclusion of radiation transfer between these surfaces should have no effect but simply provide a solution of heat transfer between them that maintains all the surfaces at this ambient temperature. Since surfaces even at the relatively

cool ambient conditions are still emitting a non negligible amount of heat, ensuring that the radiation handling preserves this temperature serves as a good initial test of its validity.

An in-depth treatment of radiation needs to take into account the fact that these various qualities of the materials and bodies, such as absorption, reflection and emission actually vary substantially across the wavelength spectrum. Surfaces for which these values remain constant over all wavelengths are referred to as greybodies, attesting to their 'averaged' nature, and are purely theoretical entities that do not exist in nature but can serve as good approximations to some materials. Since the temperatures involved in fires are relatively cool with regards to those witnessed in wider branches of physics, attention can be focussed around the section of the electromagnetic spectrum containing infrared and the lower portion of visible light. Being concerned exclusively with this narrow band means that the assumption that surfaces are indeed grey bodies can prove to be a valid simplification whilst greatly reducing the work required by a treatment of radiation.

7.7.1 Emissivity

All bodies at temperatures above absolute zero emit thermal radiation which has as its basis the excited states of electrons within the material. A body's ability to emit radiation is referred to as its emissivity and this can depend on several properties, such as material, thickness or surface texture, but with the most dominant factor by far being the temperature. The hotter a body gets the larger the amount of radiation emitted, in fact the radiated energy increases extremely quickly with increasing temperature, being approximately proportional to its fourth power (the constant of proportionality in general varies with temperature). The Stefan-Boltzmann law quantifies this relationship for a body that is emitting the maximum amount for a given temperature, where this radiant flux is given the value

$$j = \sigma T^4 \qquad\qquad (7.7.1)$$

where $\sigma \approx 5.6704\,E^{-8}$ is the Stefan-Boltzman constant and T is the temperature of the body. Such 'perfect' emitters do not exist in a nature and so the emmisivity of the body is a measure of the proportion of this available radiant energy it is capable of emitting, i.e.

$$j = \varepsilon\sigma T^4 \qquad\qquad (7.7.2)$$

where an emissivity of $\varepsilon = 0.5$ for example would mean that the body is emitting only half of the theoretical maximum. A 'perfect' emitter, in the sense of one that is radiating the maximum amount for its temperature ($\varepsilon = 1$), is referred to as a black body (this is because its absorptivity is also unity and the distribution of the radiation then emitted favours the lower end of the wavelength spectrum; at commonly experienced temperatures visible light is completely absorbed and re-emitted as infrared, hence appearing black).

7.7.2 Absorptivity and Reflection

Closely related to an object's emissivity is its absorptivity, which is its ability to absorb incoming radiation incident upon it. Radiation that fails to be absorbed does not simply cease to exist, but must be returned back into the environment through reflection. The reflection can maintain directionality such as with a mirror, but more commonly diffuses the radiation with the exact performance possibly being a complex function of angles and wavelength. The surfaces herein are assumed to be such diffuse entities, with both the emitted and reflected radiation propagating in all direction equally from every point on the surface, independent of both angle and wavelength.

Since incident radiation is either absorbed or reflected,

$$\alpha + \rho = 1 \tag{7.7.3}$$

where α is the absorptivity and ρ the reflectivity. Clearly, absorption and emission serve to work in opposite directions with the former increasing the internal energy of the body, and the latter decreasing it. In a state of thermal equilibrium, these two factors must balance to maintain the constant temperature (momentarily disregarding other forms of energy transfer). Assume a body exists in a vacuum contained and surrounded by a blackbody surface which in turn is insulated such that it forms a sealed system, with both body and bounding surface at equal temperatures. The only source of heat transfer in this situation will be radiation with the blackbody emitting at a rate of $E_b = \varepsilon\sigma T^4$ and the enclosed body emitting $\varepsilon\sigma T^4 = \varepsilon E_b$, both in $Js^{-1}m^{-2}$; further assume a configuration such that both surface areas are $1m^2$ in size. Since this is a closed system and the body and surface are at the same temperature, the second law of thermodynamics requires that no change in temperature occurs. Since the blackbody performs no reflection the only energy reaching the enclosed body is that which is being emitted by the blackbody, with an amount αE_b being absorbed (the remaining portion, ρE_b is then reflected back to the black body and is entirely absorbed meaning no further consideration is required). For the enclosed body to remain at a constant temperature, the energy leaving the surface must equal that being absorbed by it,

$$\varepsilon E_b = \alpha E_b \tag{7.7.4}$$

or,

$$\varepsilon = \alpha \qquad (7.7.5)$$

A similar argument can be made for the blackbody which absorbs the entirety of the radiative energy reaching it; this is made up of both the energy emitted by the enclosed body along with the reflected portion of the blackbody radiation it failed to absorb. Again, steady temperature requires

$$E_b = \varepsilon E_b + \rho E_b \qquad (7.7.6)$$

$$\Rightarrow \varepsilon = 1 - \rho = \alpha \qquad (7.7.7)$$

The above heuristic derivation corresponds to a simplified version of Kirchoff's Law, which makes the same conclusion yet considers both ranges of wavelengths and angles of emission.

7.7.3 Transfer of Energy

Since radiation is electromagnetic, it can be assumed to act solely in a straight line for any terrestrial problems. Radiation emitting from a point on one surface will travel along the same path until it reaches a second surface, at which point it will either be reflected or absorbed, or a combination of the two (addition of a medium between the two surfaces also introduces the possibility of scattering or refraction, or absorption of its own). Since the surfaces are assumed to be both grey bodies and diffuse, the angle of incidence is important only for the initial journey since any reflection spreads this energy out over all angles. This allows a treatment to be based solely on

the angles and distances between pairs of surfaces only, as opposed to having to compute and store 'second-order' measurements between successive surfaces.

For any single point, the energy is radiated out equally in all directions, and so any solid angles of equal size with regard to a sphere centred on the point receive the same energy. If the total energy radiating from a point is known, finding the amount reaching a given surface is then simply a matter of finding the proportion of the corresponding solid angle to the total sphere. In simple terms, this proportion corresponds to just how much of the total 'view' from the point the surface takes up. For instance, for a point radiating a total of E joules per second evenly in all directions, the amount reaching a surface j that has solid angle of Ω_j steradians with regard to the sphere is given by

$$I_j = \frac{\Omega_j}{4\pi} E \qquad\qquad (7.7.8)$$

since a sphere contains 4π steradians in total. The fact that a solid angle is taken with regard to the sphere centred on the point is important since the orientation of a surface dictates just how much of the field of view it inhabits. Any rotation of a flat surface away from the normal to the viewpoint clearly decreases its solid angle and apparent size. Working with solid angles means that this orientation is automatically taken into account since a surface angled away from the normal direction shares the same solid angle as its projected area onto the sphere, with this projected area being by definition the very 'view' from the point. Using solid angles also means distance is not an explicitly required consideration (when the separating medium is totally transparent) as this distance is again taken into account through the projected area in figure 7-15, corresponding to the intuitive notion of objects appearing smaller as they move further away.
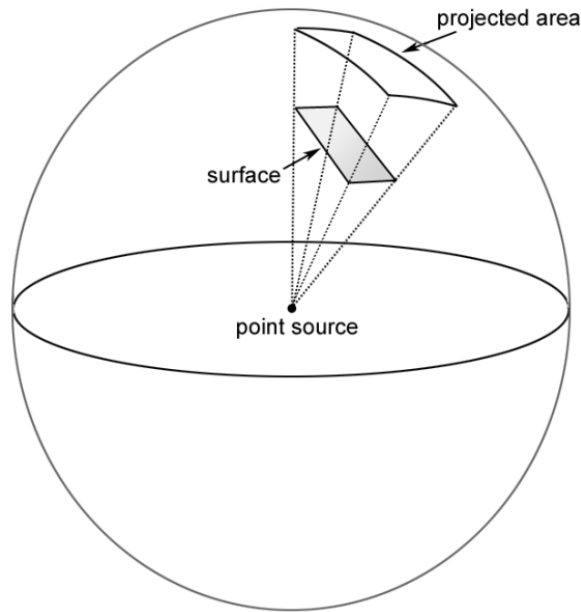
Figure 7-15. Surface and projected area onto a sphere centred on a point source.

Equation 7.7.8 above then is sufficient for considering transfer of radiation from one point to another (an infinitesimal point will clearly receive no energy) or to a surface, with the assumptions made at present. Since the surfaces both reflect and emit their own radiation, further consideration is required for anything further than the trivial case of a system of point sources.

The idea of a projected area and solid angle with regards to a point can be extended to consider transfer between two surfaces. Again, the surface will be emitting a known amount $A_i E_i$ (since the emission is per unit surface area) and this will be spread out uniformly across its area. The difficulty at this point is that the second surface, at which the radiation is arriving, will appear different when seen from different points on the first surface. In general, for any pair of points the second surface will have a different solid angle and projected area. The calculation of a *view factor* $F_{i,j}$ is required, which, similarly to a solid angle, accounts for the proportion of the 'view' from

surface i that is taken up by the surface j, and this must take account of this variation over the emitting surface.

7.7.4 View Factors

Heuristically, the idea for the calculation of a view factor is to take the solid angle views used earlier but to then integrate these over every point on the surface i, providing in a sense an average view from each point

$$A_i F_{i,j} = \iint \frac{\Omega_i(x, y)}{2\pi} dx dy \qquad (7.7.9)$$

where the integral is taken over A_i, the area of surface i, and the division is by 2π because the consideration is now for a flat surface which can only emit outwards, such that every solid angle is with regards to a hemisphere as opposed to the full sphere of a single point. The above derivation is heuristic because the actual integration is performed not over the points, but over differential areas of each surface. These differential areas are the infinitesimal sections of each surface as an area is brought smaller and smaller towards zero. This differential view factor, from one differential area to another is given by

$$dF_{i,j} = \frac{\cos \theta_i \cos \theta_j}{\pi \|S_{i,j}\|^2} dA_j \qquad (7.7.10)$$

where θ_i and θ_j are the angles between the line $S_{i,j}$, which connects the 'centres' of the differential areas, and the respective surface normals. Calculation of the actual view factor for two finite areas will then require a double integration of this term with respect to both areas, such that

$$A_i F_{i,j} \; = \; \iint \frac{\cos \theta_i \cos \theta_j}{\pi \|S_{i,j}\|^2} \, dA_j \, dA_i \qquad\qquad (7.7.11)$$

Notice that switching round i and j has no effect on the integral on the right hand side, giving

$$A_i F_{i,j} \; = \; A_j F_{j,i} \qquad\qquad (7.7.12)$$

This is referred to as the reciprocity relation, and comes in very handy when calculating view factors. At the very least it halves the number of calculations required since the areas are generally given, and the second factor is found simply by multiplying the first by the ratio of these two areas.

For all but the most trivial of setups the view factor integral proves extremely difficult to evaluate. Fortunately, the relatively simple geometry of the zone compartment means that every possible configuration can be described by one of four standard view factors, for which the solutions already exist. Since the compartments are rectangular surfaces exist solely in the coordinate planes, therefore any two surfaces not in the same plane will be on planes either parallel or perpendicular to each other. The first two view factorscorrespond to surfaces on parallel planes: one for surfaces equal in size and opposite each other; the other is for surfaces of different area and those that do not face each other. The remaining view factors are for perpendicular surface areas: the first for surfaces that meet each other at the intersection of their planes and have the same length at this common edge; the second for all other perpendicular surfaces.

7.7.5 View Factor Configurations

Shown in figures 7-16 to 7-19 below are the four configurations of view factor used in the FSEG-ZONE model. The formulas for the calculation of these factors are discussed in Appendix 1.

Equal, directly opposed surfaces
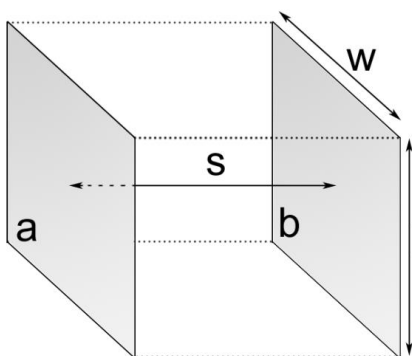
Figure 7-16. Equal, directly opposed surfaces

Arbitrary parallel surfaces
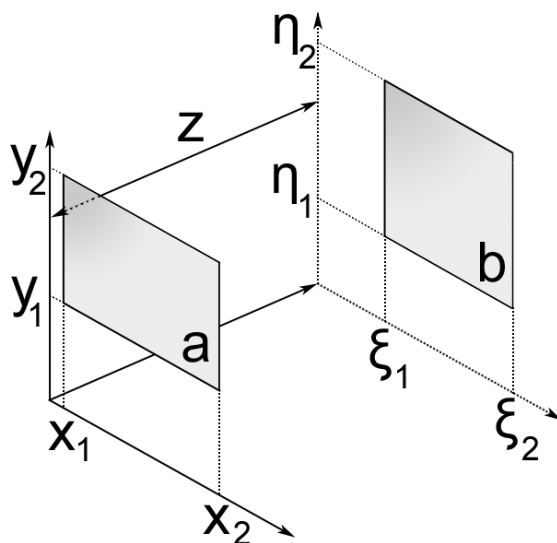
Figure 7-17. Arbitrary parallel surfaces.

Perpendicular surfaces with a common edge
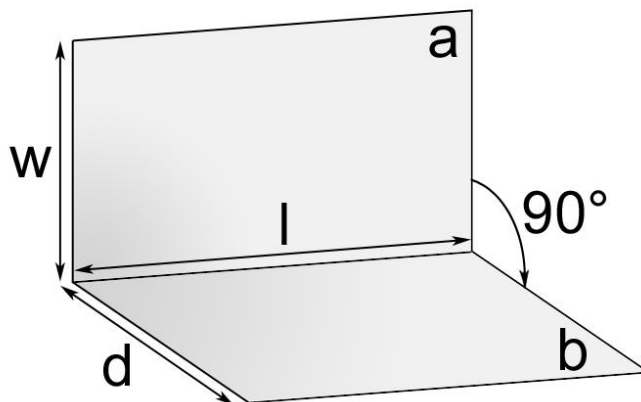
Figure 7-18. Perpendicular surfaces with common edge

Arbitrary perpendicular surfaces
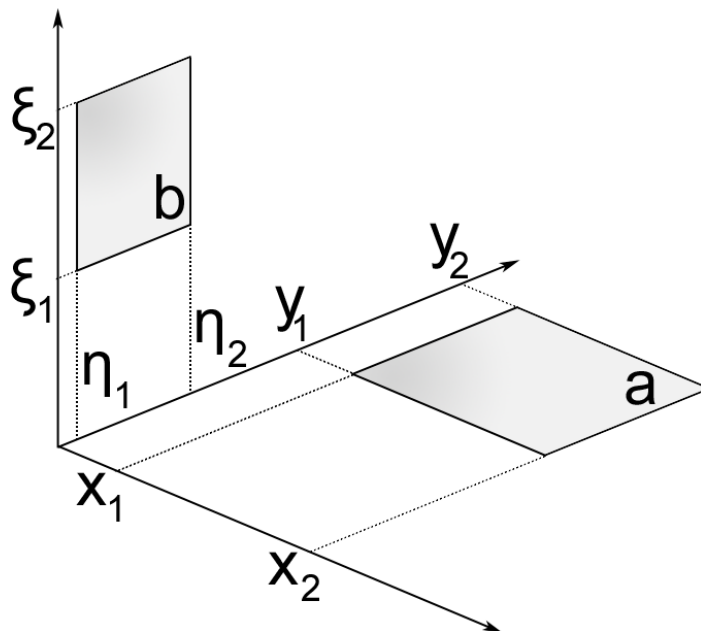
Figure 7-19. Arbitrary perpendicular surfaces.

7.7.6 Radiosity Equations

Using these view factors it is possible to calculate the proportion of energy that reaches any surface. Since the surfaces emit uniformly in all directions the proportion of the total emitted energy from surface i, reaching another surface j, is simply the view factor $F_{i,j}$. The next complication arises because the total radiosity of a surface is not composed solely of the emitted radiation, but also of the incident radiation from other surfaces that it reflects back,

$$A_i J_i = A_i E_i + \rho I_i \qquad (7.7.13)$$

where J_i is the total energy radiated from surface i per unit surface area and I_i is the total energy incident on surface i. Rearranging equation 7.7.13 for the incident energy gives

$$\rho I_i = A_i J_i - A_i E_i \qquad (7.7.14)$$

$$(1 - \alpha) I_i = A_i (J_i - E_i) \qquad (7.7.15)$$

$$I_i = \frac{A_i (J_i - E_i)}{(1 - \varepsilon)} \qquad (7.7.16)$$

This incident energy is the sum of all the radiated energies of the other surfaces that happens to land on surface i, which is naturally defined in terms of the view factors,

$$I_i = \sum F_{j,i} A_j J_j \tag{7.7.17}$$

Equation 7.7.16 gives the incident energy in terms of the radiosity for the same surface whereas equation 7.7.17 gives it in terms of the radiosity of all the other surfaces. Equating these representations and using the reciprocity relationship gives

$$\frac{A_i(J_i - E_i)}{(1 - \varepsilon)} = \sum F_{i,j} A_i J_j \tag{7.7.18}$$

or when rearranged,

$$\frac{A_i}{(1 - \varepsilon)} J_i - A_i \sum F_{i,j} J_j = \frac{A_i}{(1 - \varepsilon)} E_i \tag{7.7.19}$$

Equation 7.7.19 written for all n surfaces will result in a set of n similtaneous equations in n unknowns, namely the surface radiosities; the known values are just the surface emissivities, areas, view factors and temperatures, with this final value included through the emitted energy ($E_i = \varepsilon \sigma T_i^4$).

Writing this system in matrix form,

$$
\begin{bmatrix}
A_1/(1-\varepsilon) & -A_1F_{1,2} & \cdots & & -A_1F_{1,n} \\
-A_2F_{2,1} & A_2/(1-\varepsilon) & & & \vdots \\
\vdots & & \ddots & & \\
& & & & -A_{n-1}F_{n-1,n} \\
-A_nF_{n,1} & & \cdots & -A_nF_{n,n-1} & A_n/(1-\varepsilon)
\end{bmatrix}
\cdot
\begin{bmatrix}
J_1 \\ \vdots \\ \vdots \\ \vdots \\ \vdots \\ \vdots \\ J_n
\end{bmatrix}
=
\begin{bmatrix}
\varepsilon\sigma T_1^4 \\ \vdots \\ \vdots \\ \vdots \\ \vdots \\ \vdots \\ \varepsilon\sigma T_n^4
\end{bmatrix}
$$

where the emissivities ε can also vary between the surfaces but the index has been left out for sake of clarity.

Since $0 \le \varepsilon, F_{i,j} \le 1$ and $\sum_j F_{i,j} = 1$, the above matrix is always diagonally dominant; in fact it is strictly diagonally dominant apart from the unusual situation when $\varepsilon = 0$, corresponding to a perfectly reflective surface that absorbs no radiative energy. This means that the above matrix is always non-singular, and that this solution is attainable through a simple application of Gaussian elimination.

There are two assumptions that make this system a valid representation of the present situation. Firstly, the temperature of each surface is assumed to be constant over the length of the time-step; this quasi steady state allows the emitted energy to be a constant in the equations, where in reality this will change as the temperature depends on the absorbed energy from other surfaces. This assumption is fairly conservative since the formulation of the remainder of the model is fully implicit so final values are assumed to have applied for the duration of the step. In addition the surfaces are generally assumed to be made of a very dense material ($\sim 1600 \; kg \; m^{-3}$) making the actual changes in temperature over a time step very small. The second assumption is that the radiation has an infinite velocity, which allows all the reflections, re-reflections and so on, to be considered to land everywhere all at once, with the first emitting of energy. Again, this assumption is conservative since radiation being electromagnetic has velocity $c \approx 3E^8 \; m \; s^{-1}$, which is as

good as infinite considering the dimensions of rooms and the time steps being used. Also, the surfaces have default emissivity/absorptivity of around 0.8 which means that the energies contained in the consecutive reflections reduce by 80% each time, becoming negligible after only a small number.

7.7.7 Solving the Radiosity Equations

The method used to solve the system of radiosity equations is a simple Gaussian elimination, or LU decomposition. More advanced methods of solution are available, but the relatively small dimension of the matrix and its diagonal dominance means that an LU decomposition method is both simple to apply and computationally efficient. A solution routine was programmed especially for the hybrid model to allow greater control over the procedure.

It is worth noting that the implementation of the surfaces within the hybrid model, such that some surfaces are in effect turned 'off' for various layer heights, means that the radiosity matrix can at times have empty rows and columns. The symmetrical nature of the matrix ensures that an equal number of rows and their corresponding columns are identically zero and can simply be removed, reducing it to a smaller matrix that is once again 'full', diagonally dominant and open to simple solution. Once this solution is found, the solution vector can be expanded back to the full order through reinserting the zero elements, meaning the remainder of the hybrid model can use this full solution without having to be aware of any transformations.

LU Decomposition

The idea behind an LU decomposition is to decompose a matrix A into the product of upper and lower triangular matrices L and U, such that $A = LU$. The solution of a system can then be found as follows,

$$A\bar{x} = \bar{b} \tag{7.7.20}$$

$$LU\bar{x} = \bar{b} \tag{7.7.21}$$

letting $\bar{y} = U\bar{x}$,

$$L\bar{y} = \bar{b} \tag{7.7.22}$$

since L is a triangular matrix the above is easily solved for $\bar{y}$; similarly for

$$U\bar{x} = \bar{y} \tag{7.7.23}$$

which, with $\bar{y}$ from above, is easily solved for $\bar{x}$ giving the final solution. See Appendix 2 for a practical example of LU Decomposition.

The difference between using back substitution from equation 7.7.22 and carrying on with the full LU decomposition is that the back substitution method requires that the operations used to obtain the matrix U from matrix A also be applied to the solution vector $\bar{b}$. With the LU decomposition method, matrices U and L are found without any regard for vector $\bar{b}$, which is only used from equation 7.7.22 onwards. This difference is seen more clearly in the practical example given in Appendix 2.

The majority of work to be performed in solving the original problem is in the initial elimination stage (decomposition) which obtains U and L, the actual substitutions themselves require much less computational effort. For

instance, for a compartment with 16 surfaces the elimination stage requires 1,480 multiplications and 1,360 additions; the backward substitution stage with a triangular matrix requires just 136 multiplications and 120 additions.

Since the backward substitution method requires these operations to be performed on $\bar{b}$, if this solution vector changes the elimination procedure has to be performed again; this is in comparison to the LU decomposition, which once found is valid for all $\bar{b}$. The effort in coding both methods is roughly equivalent, the differences being that row operations are stored in L as opposed to being performed on $\bar{b}$, and there is an extra substitution stage for L, although this is simpler than general due to the upper diagonal of L being the same as the identity matrix. Looking at the radiosity matrix equation, matrix A depends solely on the areas and emissivities of the surfaces, whereas $\bar{b}$ depends on the temperatures. The details will be case specific, but for any consecutive calculations involving constant areas but varying temperatures, use of the LU decomposition will significantly speed up the procedure. On the other hand, the L matrix solution step proves to be a small penalty when simple back substitution would have sufficed. It should also be noted that additions to the radiation model, both those discussed later and in future developments, can cause additional terms to appear in the solution vector, meaning the LU decomposition has further opportunity to improve the solution procedure than on temperature variation alone.

Using The Radiosity

Solution of the system of equations above provided the values of radiosity for each of the surfaces. The radiosity is the total energy radiated per unit surface area, and includes both the emitted energy and that which the surface is reflecting. Using these values along with the view factors, the total radiation reaching a surface i is simply

$$I_i = \sum F_{j,i} A_j J_j \qquad (7.7.24)$$

This means that the net energy exchange at the surface is

$$\dot{Q}_i = I_i - A_i J_i$$

$$= \sum F_{j,i} A_j J_j - A_i J_i \qquad (7.7.25)$$

or using the reciprocity relation and the fact that $\sum F_{i,j} = 1$,

$$\dot{Q}_i = A_i \sum F_{i,j} J_j - A_i \sum F_{i,j} J_i \qquad (7.7.26)$$

$$= A_i \sum F_{i,j} (J_j - J_j)$$

Through the use of the radiosities, the net energy gain or loss at a surface is therefore expressible simply in terms of the radiative difference with all other surfaces, without having to reconsider the absorptivities or reflectivities. Each $\dot{Q}_i$ is then treated as any other source or sink of energy and applied to the surfaces total enthalpy, concluding the basic treatment of radiation with a totally transparent medium.

7.7.8 Absorbing Medium

The medium in a fire situation generally begins as ambient air, for which the assumption of zero absorptivity, or total transparency, can be a first

approximation. As the situation develops this air becomes increasingly hotter and laden with both various gas species and smoke (soot particles), such that this assumption is no longer valid. It is now necessary to consider both the absorptivity and emissivity of such fluids which must be treated as volumes as opposed to the solid surfaces discussed previously. Since these values will vary substantially for differing conditions, the uniform layer assumption of the zone model simplifies the treatment considerably, since these values can be taken to be constant throughout a given layer.

Transmittance

Assuming that the absorptivity for a layer is known, then the amount of radiation absorbed from a ray directed through it is dependent on the distance travelled through the gas. The absorptivity may remain constant, but the actual amount of energy liable to being absorbed over a section of path is continuously decreasing as the path through the gas is traversed, resulting in an exponential relationship between the path length and the total energy absorbed. The proportion of energy that remains after travelling a distance l through the absorbing medium is termed the transmittance, τ_l, and is given by

$$\tau_l = e^{-\alpha l} \qquad (7.7.27)$$

such that the proportion of energy that is not transmitted, $1 - \tau_l$, is the amount absorbed over this path,

$$\alpha_l = 1 - e^{-\alpha l} \qquad (7.7.28)$$

Absorptivity

In general α and α_l are different; the first is an intensive quantity of the medium quoted per unit length, whereas the second is extensive and depends on the path travelled through the volume by the rays of radiation. It remains true that $0 \le \alpha_l \le 1$ since these bounds correspond to total and zero absorption, and values outside of this range correspond to creation of energy, either absorbing or transmitting more radiative energy than initially exists. For these values to be attainable the bounds on the intensive layer absorptivity must change such that $0 \le \alpha \le \infty$, allowing $\alpha_l = 1$ in a finite distance l. Technically the value of unity will never be attained but the upper bound allows this value to be approached as closely as required in a limiting sense. The formulation allows the medium to become essentially 'opaque' for given paths travelled through it over a certain length, but the fact that $\alpha_l = 1$ in the limit only means that no special consideration is required for such an occurrence since conservation is adhered to.

There are three methods for calculating the absorptivity of the layers within the hybrid model. Two of these are equivalent to SMARTFIRE's treatment, which correspond to whether smoke production is enabled; the third method is identical to that used within CFAST [Jones2009] and is based on concentrations of carbon dioxide and water.

The first method discussed is that used by SMARTFIRE when smoke production is disabled. In this situation, smoke can still be considered through the use of a 'light extinction coefficient' variable which is dependent on the density and mixture fraction (see section 7.5) of the gas volume under consideration. Through this relationship, the concentration of smoke can still be considered without having to introduce a new solved variable for the transport of smoke, although clearly this amounts to a significant simplification. In this situation, the absorptivity of the gas is calculated from a linear piece wise variation with temperature. These values are modifiable by the user with the intent of capturing different relationships between gas

absorptivity and temperature, but default to set values. If smoke production is turned off then the hybrid model defaults to using the same method.

If smoke production is enabled, SMARTFIRE uses the actual concentration of smoke within a cell to calculate the gas absorptivity coefficient as $\alpha_{gas} = K_s \varphi_s T$, where $K_s \approx 1{,}200$ is the smoke absorbtion coefficient, φ_s is the smoke volume fraction and T is temperature [Ewer2008]. In situations where the calculated absorption coefficient is less than a pre-set ambient absorption coefficient (e.g. before smoke reaches sufficient concentrations) the absorption is set to this ambient amount. If smoke production is enabled, the hybrid model defaults to using the exact same method for the calculation of layer absorption.

The final method available to the hybrid model for calculating layer absorption is a modified version of the smoke concentration method above, and extends the consideration to include concentrations of both carbon dioxide and water. For the thermal radiation commonly experienced in fire situations, these species are by far the predominant source of absorption [Incropera2006] such that remaining species (i.e. carbon monoxide, oxygen, nitrogen) can be ignored. This method is used by CFAST and finds it basis in [Tien2002] with tables providing the values of relationships between absorption and partial pressures of the two species along with temperature found in [Edwards1985]. The data is tabulated for base 10 logarithms of these values with $log_{10}\alpha_{CO2}$ and $log_{10}\alpha_{H2O}$ defined as a surfaces, varying over $log_{10}T$ on one axis and $log_{10}(P_{CO2}l)$ or $log_{10}(P_{H2O}l)$ on the other, where P is the partial pressure of the corresponding species and l is the length of the path travelled through the gas. Since these species absorptivities already include the path length, the final relationship is given in terms of the transmittance as

$$\tau = e^{-K_s \varphi_s Tl}(1 - \alpha_{H2O} - 0.5\alpha_{CO2}) \qquad (7.7.29)$$

Here SMARTFIRE's smoke concentration calculation, seen in the exponential, is augmented by the species absorptivities, with that of carbon dioxide reduced by half due to address band overlap, where both species absorb a similar wavelength of the thermal radiation. This method is not defaulted to by the hybrid model and must be specifically enabled by the user.

Using layer absorption/transmittance

Once calculated the values α_l and τ_l can be used to modify the preceding treatment of radiation by varying the amounts of radiation reaching a particular surface, taking into account that the medium is absorbing a proportion of this energy. Since the energy now reaching a surface is the transmitted portion of the ray, the system matrix can be modified,

$$
\begin{bmatrix}
A_1/(1-\varepsilon) & -A_1 F_{1,2}\tau_u\tau_l & \cdots & & -A_1 F_{1,n}\tau_u\tau_l \\
-A_2 F_{2,1}\tau_u\tau_l & A_2/(1-\varepsilon) & & & \vdots \\
\vdots & & \ddots & & \\
& & & & -A_{n-1}F_{n-1,n}\tau_u\tau_l \\
-A_n F_{n,1}\tau_u\tau_l & & \cdots & -A_n F_{n,n-1}\tau_u\tau_l & A_n/(1-\varepsilon)
\end{bmatrix}
$$

where τ_u and τ_l are with regard to the portion of the paths travelled through the upper and lower layer respectively. Since the surfaces are changing dimensions with a varying layer, these distances travelled through the layers are also changing. The average distance travelled between any two surfaces is assumed to be the line between their mid-points, although this simplification does tend to underestimate the path lengths (more obviously for parallel surfaces); a more approximate average calculated from the integral of this length over all possible paths would be desirable although is not considered in this work. These distances are split into upper and lower layer portions which are stored in separate matrices. From these values, matrices for upper and lower layer transmittances can be calculated at the beginning of each iteration which allows the system matrix to be modified accordingly.

The transmittance matrices are also used to account for the corresponding absorption that occurs by allowing the simple formation of source terms for the layers. For example, an entry $-A_i F_{i,j} \tau_u \tau_l$ means that the original energy being emitted, $A_i F_{i,j}$, has experienced absorption along its path through the layers, with a portion $\tau_u \tau_l$ now reaching the incident surface. The remaining amount experiences absorption by the layers, but the exact amounts depend on the direction of the ray. For radiation traversing the upper layer first, the energy absorbed will be $A_i F_{i,j}(1 - \tau_u)$, this means the energy reaching the lower layer will be reduced, such that the amount absorbed by it will now be $A_i F_{i,j} \tau_u (1 - \tau_l)$. Correspondingly for a ray that traverses the lower layer before the upper layer, the lower absorbed amount is $A_i F_{i,j}(1 - \tau_l)$ and the upper is $A_i F_{i,j} \tau_l (1 - \tau_u)$. These terms are calculated directly from the transmittance matrices and applied simply as enthalpy source terms within the layers.

Layer emissivity

The final consideration for an absorbing medium is the fact that such a volume will also emit its own radiation. This too will vary for differing paths and orientations, but to avoid further complications these volume sources are to be modelled as surface emitters of radiation. Treatment as an actual volume source would require the calculation of further paths and distances than are already considered, such that further assumptions could prove dubious/inconsistent with those already made up to this stage. Also, the uniform assumption of the layers means that a volumetric treatment may make model calculations more accurate but may introduce further errors when compared to the non-uniform layers of reality. In addition, further assumptions can begin to introduce artefacts that serve to increase directionality, when the reality of energy transfer is that it serves to reduce variations. For these reasons the emitting medium in this context is considered as a solid volume, a rectangular cuboid that radiates equally in all directions from every point on its surface. This serves to distribute energy

equally in all directions, and avoids the possibility that previous assumptions that have had to be made on surfaces and paths are not compounded.

The surfaces of the layers are therefore treated in a similar fashion to the wall surfaces. Five of the faces of the cuboid will be in direct contact with wall surfaces, such that the emitted energy is transferred immediately without further layer absorption. The sixth face corresponds to the surface between the layers and provides a final opportunity for layer absorption as this energy must traverses the other layer towards the remaining surfaces. All these energies are then reflected/absorbed as previously discussed and become extra terms in the source vector of the matrix equation,

$$
\begin{bmatrix}
\varepsilon\sigma T_1^4 + R_{u,1} + R_{l,1} \\
\vdots \\
\\
\\
\\
\\
\\
\varepsilon\sigma T_n^4 + R_{u,n} + R_{l,n}
\end{bmatrix}
$$

where for instance $R_{u,i}$ would be the energy incident on the ith surface from the emitting upper layer and can take one of two forms,

$$
R_{u,i} = A_i \varepsilon_u \sigma T_u^4 \tag{7.7.30}
$$

if surface i is an upper surface in contact with the layer, or

$$
R_{u,i} = A_u F_{lay,i} \tau_l \varepsilon_u \sigma T_u^4 \tag{7.7.31}
$$

if the surface is a lower surface and the energy must first travel through the lower layer; in this case A_u is the area of the layer and $F_{lay,i}$ is the view factor from the layer to the surface, calculated in the same way as the surface view factors.

Calculating the layer emissivity

The layer emissivity is calculated through the use of an argument similar to that used in section 7.7.2, where both medium and black body surfaces are assumed to be in thermal equilibrium. An energy balance is then formed for a chosen surface, with the correct value for emissivity corresponding to zero net gain/loss in energy.

First for the upper layer emissivity and forming an energy balance for surface U, since a black body the energy emitted will be $A_U E_b$ and the surface will absorb all radiation incident upon it. At thermal equilibrium these two values must be equal giving,

$$A_U E_b = A_1 F_{1,U} E_b \tau_{1,u} + A_2 F_{2,U} E_b \tau_{2,u}$$

$$+A_3 F_{3,U} E_b \tau_{3,l} \tau_{3,u} + A_4 F_{4,U} E_b \tau_{4,l} \tau_{4,u} + A_L F_{L,U} E_b \tau_{L,l} \tau_{L,u}$$

$$+A_U \varepsilon_u E_b + A_U \varepsilon_l E_b F_{lay,U} \tau_{lay,u} \qquad (7.7.32)$$

where the first set of terms are energy received from the other upper surfaces, the second set is that received from the lower surfaces, and the last two terms are energy received from both direct contact with the upper layer and from the lower layer after travelling through the upper layer. Using the reciprocity relation for the view factors and grouping terms,

$$A_U E_b = A_U E_b \sum_{surf} F_{U,i} \tau_{i,u} \tau_{i,l} + A_U \varepsilon_u E_b$$
$$+ A_U \varepsilon_l E_b F_{lay,U} \tau_{lay,u}$$

(7.7.33)

dividing through by $A_U E_b$ and rearranging,

$$\varepsilon_u = 1 - \sum_{surf} F_{U,i} \tau_{i,u} \tau_{i,l} - F_{lay,U} \tau_{lay,u} \varepsilon_l$$

(7.7.34)

A similar argument for surface L gives,

$$\varepsilon_l = 1 - \sum_{surf} F_{L,i} \tau_{i,u} \tau_{i,l} - F_{lay,L} \tau_{lay,l} \varepsilon_u$$

(7.7.35)

Substituting 7.7.35 into 7.7.34 and rearranging gives

$$\varepsilon_u = \frac{1 - \sum F_{U,i} \tau_{i,u} \tau_{i,l} - F_{lay,U} \tau_{lay,u}(1 - \sum F_{L,i} \tau_{i,u} \tau_{i,l})}{1 - F_{lay,U} \tau_{lay,u} F_{lay,L} \tau_{lay,l}}$$

(7.7.36)

When calculating the layer emissivities ε_u is found first, allowing ε_l to be calculated from equation 7.7.35.

The above method ensures that the layer absorptions and emissivities are as close as possible to being consistent with the fact that net transfer of heat is zero in a state of thermal equilibrium. Discrepancies will still exist with

regards to the previous assumptions of paths between surfaces, since lower and upper surfaces will differ in this regard. Also, energy transfer between CFD and zone domains is not considered for the above calculations of emissivity, although at ambient conditions these differences will be negligible. The above method was introduced because the previous formulation relying on the 'characteristic length' of the layer volume resulted in emissivities that caused non-negligible heating up of the layers while the environment was still at ambient conditions. These differences become insignificant once fire heated fluid enters the zone compartment, yet are very apparent in the initial stages of a simulation. It is believed that this method derived from a physical energy balance is more appropriate to the present situation since it is specific to the actual path directions and lengths used, as opposed to the generalised method based on characteristic lengths.

7.7.9 Radiation at the interface

To complete the treatment of radiation in the hybrid model, consideration is required for transfer in both directions across the hybrid interface. Here an assumption of scattering at the interface allows the treatment to remain uncomplicated.

For radiation travelling from zone to CFD, the CFD faces on the interface are given values of radiosity corresponding to the total energy reaching the interface surfaces from within the zone compartment. Here the assumption of scattering allows the energy to simply be summed without concern for its angle of incidence, allowing treatment within the CFD model similar to that of a wall where energy is emitted/reflected equally in all directions. This loss of energy is accounted for within the hybrid model as these interface surfaces have no entries in the system matrix; they are not solved for and any energy incident on them is lost from the zone domain.

For radiation travelling from CFD to zone, the radiosities of the hybrid surfaces forming the interface are given values corresponding to the total

energy reaching the interface from the CFD domain. Here the assumption of scattering allows the interface surfaces to be treated in the same manner as the wall surfaces. Again, these radiosities are absent from the system matrix, but this time they appear as modifications to the source vector where a typical entry from the radiosity matrix A becomes

$$\varepsilon \sigma T_i^4 + R_{u,i} + R_{l,i} + R_{int\,,i} \qquad (7.7.37)$$

with $R_{int\,,i}$ the radiation from the interface reaching surface i, given by the usual areas, view factors and transmittances.

Use of the accurate multi-ray model within SMARTFIRE may allow modelling of reflection phenomena such as compartment shapes and dimensions favouring certain exit angles over others. Applying the zone radiation without the scattering could result in similar dependency over exit angles, but the validity would be extremely questionable considering that the assumptions made on paths and diffuse surfaces means that the zone directionality does not maintain the same level of detail as the CFD domain affords. Here the averaging effect of scattering prevents unrealistic situations. In any case, angular directionality is essentially lost with the first reflection off a diffuse surface even for the highest number of rays used, with any artefact of direction depending simply on which surface performed this initial reflection.

Use of the six flux radiation model within SMARTFIRE means that only the flux normal to the zone compartment is a consideration, i.e. only the flux in the positive direction of the x-axis for a hybrid boundary patch on a high-x plane. To apply this radiation to the zone compartment directly would result in a small area the size of the interface on the opposite wall receiving all the energy; use of scattering here prevents this unrealistic heating up of this surface.

Considering the above, the assumption of scattering at the interface is not so much a simplification as a required conversion for the different forms of the two models. It serves to reduce some erroneous situations at the expense of some accuracy in the multi-ray model which may not be attainable in the first place.

7.7.10 Radiative flux

The radiative flux is a measure of interest to the fire engineer since it has importance in life tenability calculations where it can directly cause great injury or fatality. It can be compared directly since its treatment in the FSEG-ZONE model through numerous surfaces and calculated view factors is performed in an accurate way. The spatial dimensions of the rooms and location of the doors and surfaces are considered in the calculations and for the radiative flux it is now valid to ask questions based on location, as opposed to the averaged uniform nature of the remainder of the zone model. Despite this, the remaining variables do play a large part in the calculations of the radiosity and therefore this effect is not totally avoidable. Also there are some simplifying assumptions made in the radiation method, notably the radiation at an interface in section 7.7.9 and the calculation of distances between surfaces in section 7.7.8, which again will serve to reduce the accuracy of the method despite its basis on an accurate representation of the compartment.

SMARTFIRE allows the definition of zones which in turn allow the calculation of various averaged quantities over such a region. In some respects this reduces the CFD data to a data set akin to a zone model, yet the 'layer height' is a fixed value that is determined during case setup. Use is made of such data for export to the evacuation software EXODUS (also developed by FSEG at the University of Greenwich) with the fixed layer height corresponding to the average head height of an evacuee. Despite this SMARTFIRE 'zone' data having little interest to the present method, the value of radiative flux reported does indeed have a use since this is

independent of the fixed layer. The radiative flux is calculated at a point at the centre of the *floor* of the compartment, and considers energy received from the remainder of the domain.

A related measure is made in FSEG-ZONE by defining a further surface, $1\,cm$ by $1\,cm$, at the centre of the compartment floor. The radiative flux is then calculated by dividing the irradiation of this surface by the area; the relatively small area of $0.0001\,m^2$ allows this to be a valid approximation to the flux at a point.

7.7.11 Test Case – Radiation flux comparison

This test case again uses the setup common to previous test cases which considered three identical rooms located in series. As in section 7.4.4 the heat source is removed at 120 seconds to allow opportunity for the subsequent cooling of the domain to be captured. The 24 ray radiation model is enabled in SMARTFIRE, and the radiation implementation discussed in the above section is enabled in the FSEG-ZONE model.

For the first simulation the surface temperatures in both the SMF and FSEG-ZONE compartments are fixed at ambient, meaning that any energy transfer between surface and contacting fluid has no effect on the temperature of the solid. This fixed surface temperature assumption allows the radiative qualities of the fluid itself to be analysed in isolation from the surface radiosities. For this reason, and since the variation is minimal, the remaining variables are not addressed here for the sake of clarity (the test case in the next section will make the full set of comparisons for a radiation enabled simulation). The comparison of radiative flux for fixed surface temperatures is shown in figure 7.20 below.

For the second simulation, the surfaces in the models are allowed to vary in temperature. The corresponding radiative fluxes are shown in figure 7-21 below.
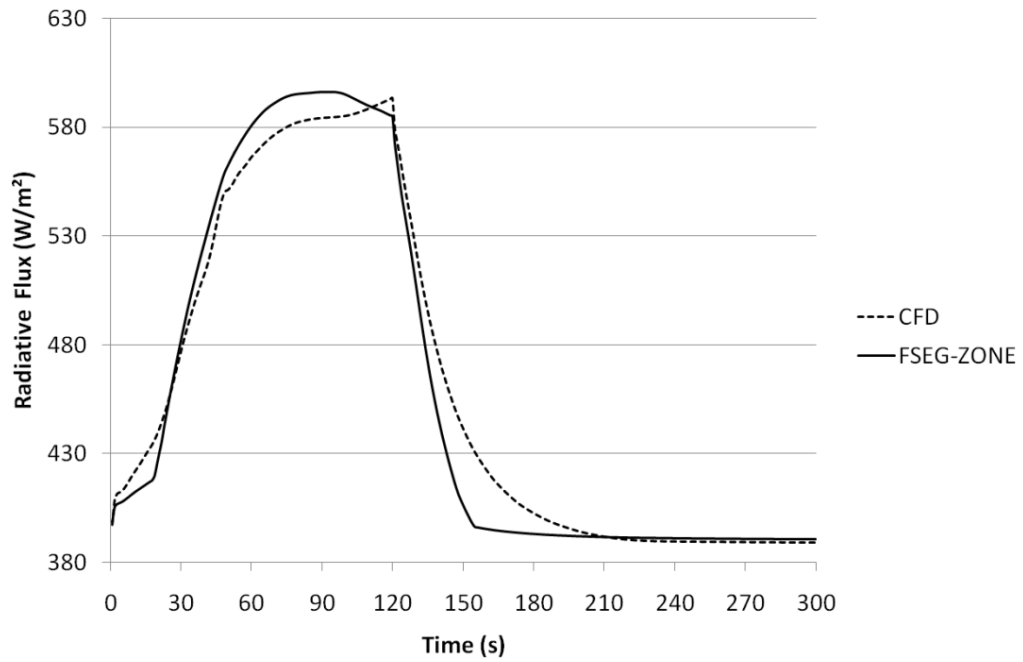
Figure 7-20. Comparison of radiative flux with fixed surface temperatures.
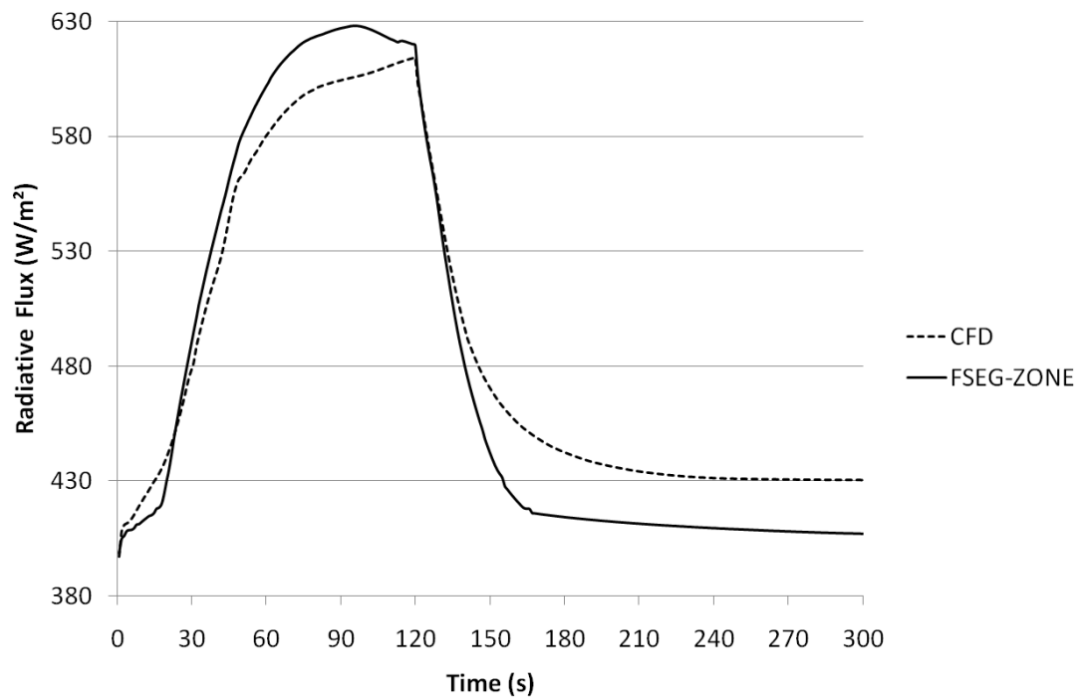
Figure 7-21. Comparison of radiative flux with normal (varying) surface temperatures.

In figure 7-20, despite reaching the maximum value slightly earlier and then returning to ambient a little quicker, the FSEG-ZONE model provides an extremely accurate representation of the flux reported by SMARTFIRE. It should be noted that the dependence of radiosity on the fourth power of temperature would serve to exaggerate any errors, considering the uniform nature of the zone model this result is very favourable. The fact that this simulation had fixed surface temperatures means that the variations in radiative flux observed are solely dependent on the gas layers, this serves to validate the treatment of radiation from an absorbing medium discussed in section 7.7.8.

In figure 7-21, agreement is still very favourable considering the nature of the FSEG-ZONE model, although it reaches a maximum value approximately $20 \, W/m^2$ greater than SMARTFIRE. The most obvious difference can be seen in the second half of the simulation where the two models appear to settle on different values. Since the previous case demonstrated such good agreement in this region, it is fair to assume that the differences seen are caused by surface temperature alone.

A likely explanation is the nature with which the surfaces get modified by a changing layer height within the FSEG-ZONE model. As the layer descends, previously ambient lower surfaces are engulfed and become part of the upper surface. As the layer ascends after the heat source is removed, previously hot upper surfaces once again become part of the corresponding lower surface. As this happens, the enthalpy contained in the surface sections changing from upper to lower is redistributed throughout the lower surface. As opposed to reality where a surface remains hot for a period after emerging from the upper layer, the surfaces in the FSEG-ZONE model tend to cool immediately once they are no longer exposed to the hot gas.

With fixed surface temperatures the CFD simulation took 10 hours 26 minutes and 20 seconds to run; the hybrid simulation took 6 hours 47 minutes and 37 seconds to run; resulting in a 35% saving in computational time for a 24% saving in number of cells.

With varying surface temperatures the CFD simulation took 11 hours 40 minutes and 38 seconds; the hybrid simulation took 7 hours 34 minutes and 56 seconds; also a saving in computational time of 35% for a cell number saving of 24%.

7.7.12 Test Case - Multiroom

This test case considers several instances of the radiation enabled FSEG-ZONE model in the same domain. This is likely to be the common usage of the FSEG-ZONE model, in replacing several smaller or less important sections of the domain. Since the saving in runtime has been seen to be equivalent to the section of domain replaced, multiple instances promise to deliver the greatest savings. Figure 7-22 below demonstrates the case setup.
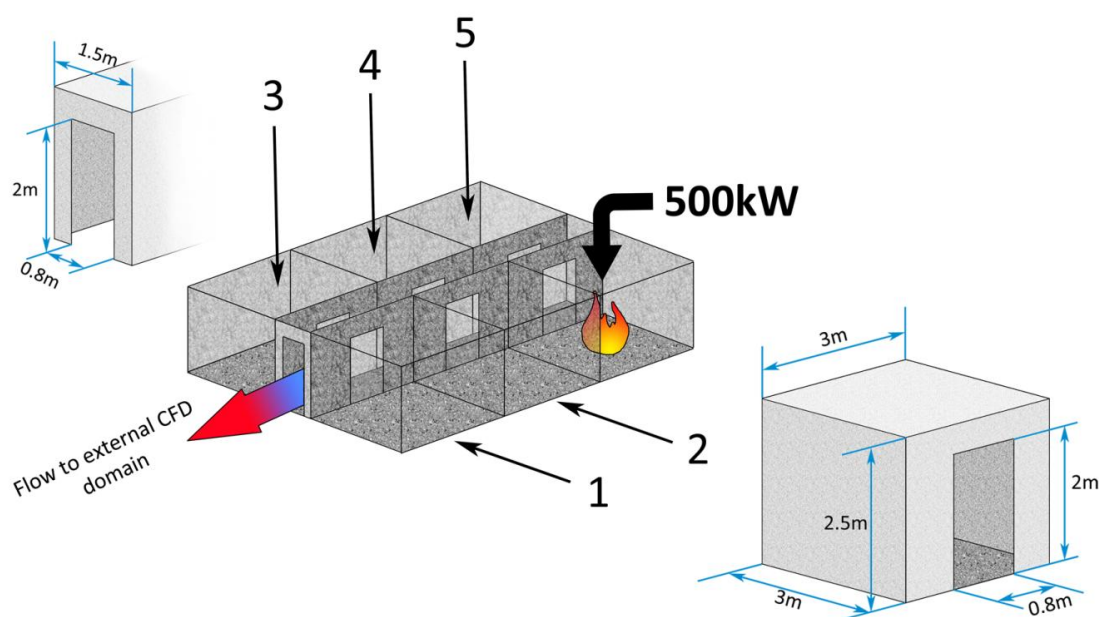
Figure 7-22. Multiroom setup for test case 7.7.13.

The case consists of six identical rooms, each $3m$ by $3m$ by $2.5m$ high, all venting to a common corridor through doors $0.8m$ wide and $2m$ high. The corridor is $1.5m$ wide and is vented at one end to the exterior thorugh a similar door. A fire is situated in a room at the closed end of the corridor and is modelled as a $500kW$ heat source. The fire is active for the duration of the simulation which is run for 300 seconds over 1 second time-steps, each consisting of 200 iterations. The 24 ray radiation modelled is used in the field model domain and as an optimisation is solved once every 10 iterations. All surfaces are $0.1m$ thick and made of default material with conduction $0.69\,W/mK$, density $1600kg/m^3$ and specific heat $840\,J/kgK$. The fire is modelled as a methane fuel source of 0.0125 kg/s, with a smoke to fuel ratio of 0.015. Species release rates are calculated using the default values for SMARTFIRE's equivalency ratio. The CFD simulation uses 77,418 cells while the hybrid simulation uses 35,466 cells, a saving of just over 54%.

Results

For sake of clarity, results are only shown for rooms 1, 4 and 5; rooms 2 and 3 express similar trends and agreements. Since room 5 is directly opposite the fire room the largest variation in temperatures and therefore difficulty for the FSEG-ZONE model is to be expected here.

Figures 7-23 through 7-31 on the following pages show the comparisons for compartment pressure, upper and lower layer temperatures, layer height, radiative flux and species mass fractions. The model considers smoke, oxidant, fuel, product, hydrochloric acid, carbon monoxide, carbon dioxide and oxygen, resulting in a great deal of data to consider. For the sake of clarity not all the species are discussed here. Smoke is unique in its treatment as a solid in the FSEG-ZONE model, and therefore results are included here. The three species of oxidant, fuel and product are derived from the mixture fractions, therefore it suffices to include the results of one, in this case the

product mass fractions. Similarly, the remaining species are based on the combustion equivalency ratio, and again it is acceptable to consider just one value, in this case the carbon monoxide mass fractions.

The results demonstrate the same trends observed in previous test cases, therefore these are only briefly discussed here. The FSEG-ZONE model again slightly underestimates the pressure and over estimates the mass, due to the linear nature of the zone pressure distribution. The temperatures again display good agreement with similar trends, although the issue with heat transfer to surfaces again causes more energy to be removed from the FSEG-ZONE model, resulting in lower temperatures. The layer height is once again captured exceptionally well by the FSEG-ZONE model, and it remains between the values reported by the CFD reduction methods. Similarly, quite excellent agreement is seen in the radiative flux, considering the nature of the zone model. One thing that is apparent from the consideration of a multi-room case is that larger discrepancies are seen in rooms that are exposed to the greatest amount of variation in interface variables. This is clearly seen in the figures below where the FSEG-ZONE model consistently performs comparatively worse in room 5.

Also of interest is that despite room 1 being located further from the fire than room 4 it attains higher pressures, temperatures and radiative flux. Such an occurrence is certainly not obvious, although one explanation may be that the doorway soffit at the open end of the corridor serves to promote an accumulation of hot gases in this area; it is encouraging to observe the FSEG-ZONE model also capturing this effect.

The mass fractions all display similar trends and are in excellent agreement. Apart from slightly lower values seen in room 4, the species values reported by the FSEG-ZONE model are consistently within the interval dictated by the CFD reduction methods.

The CFD simulation took 96 hours 14 minutes and 54 seconds to run; the hybrid simulation took 39 hours 14 minutes and 40 seconds to run. This is a saving in computational time of 59%, compared to a reduction in cells of 54%.
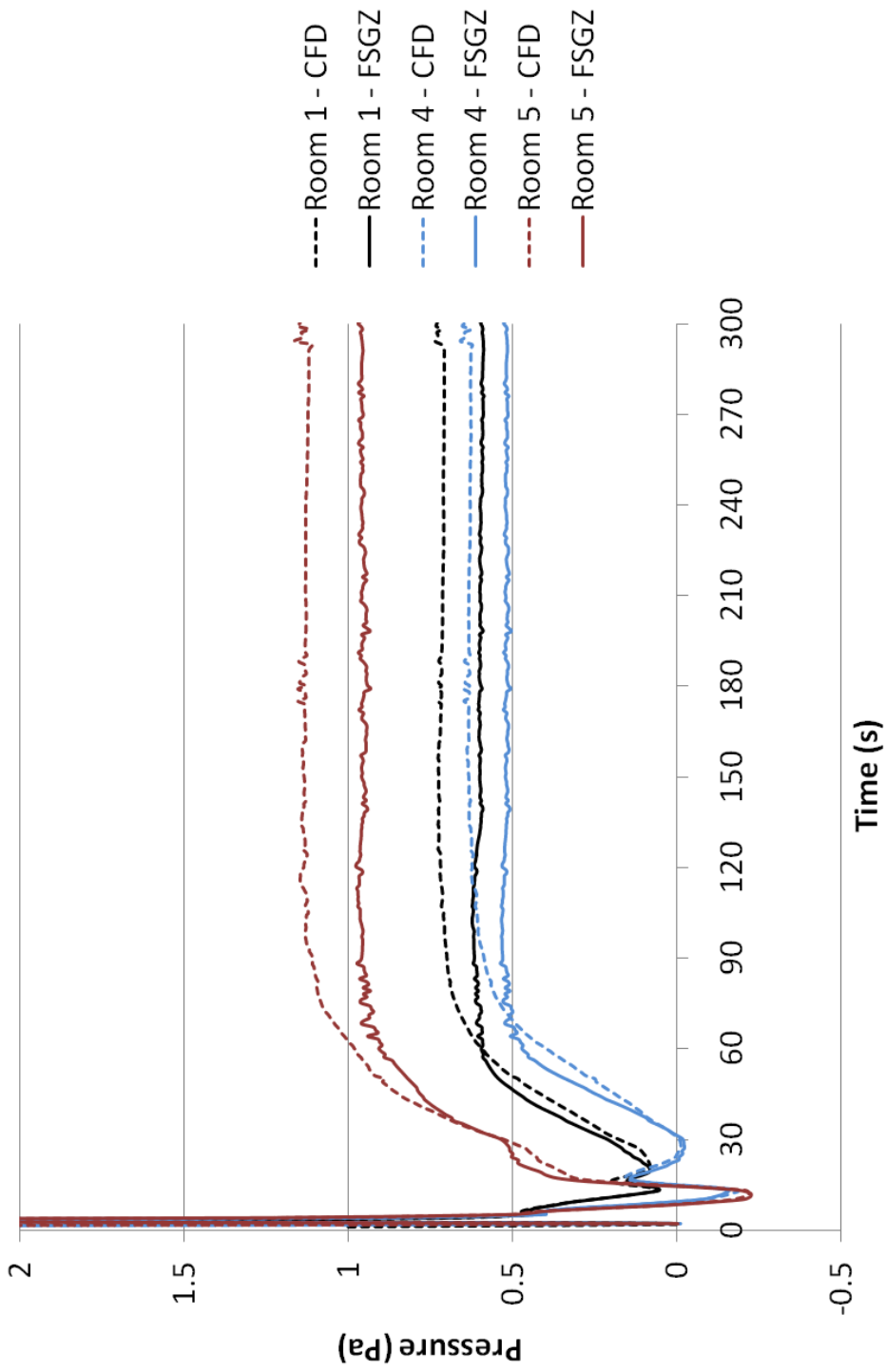
Figure 7-23. Compartment pressure comparisons.
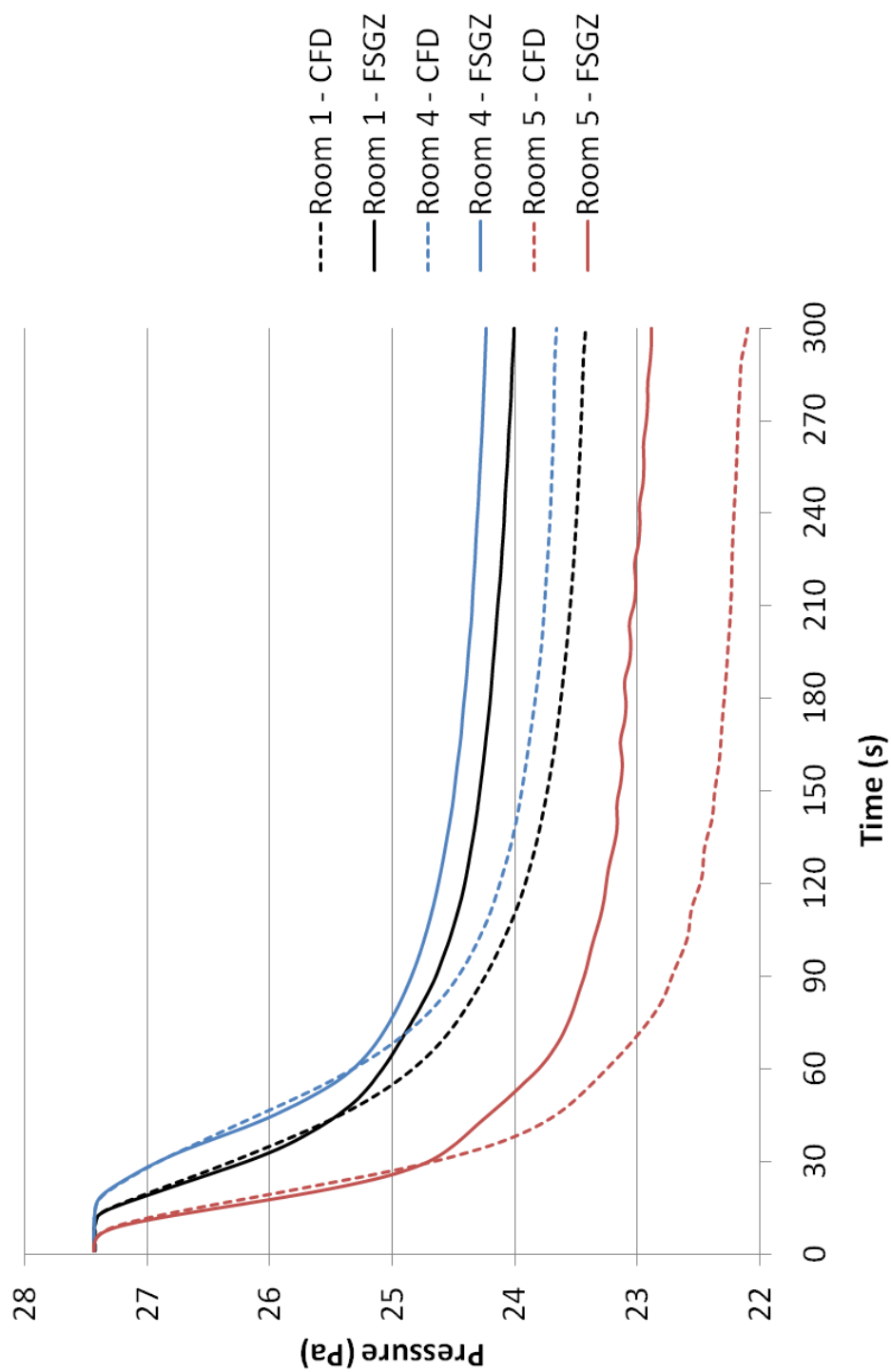
Figure 7-24. Compartment mass comparisons.
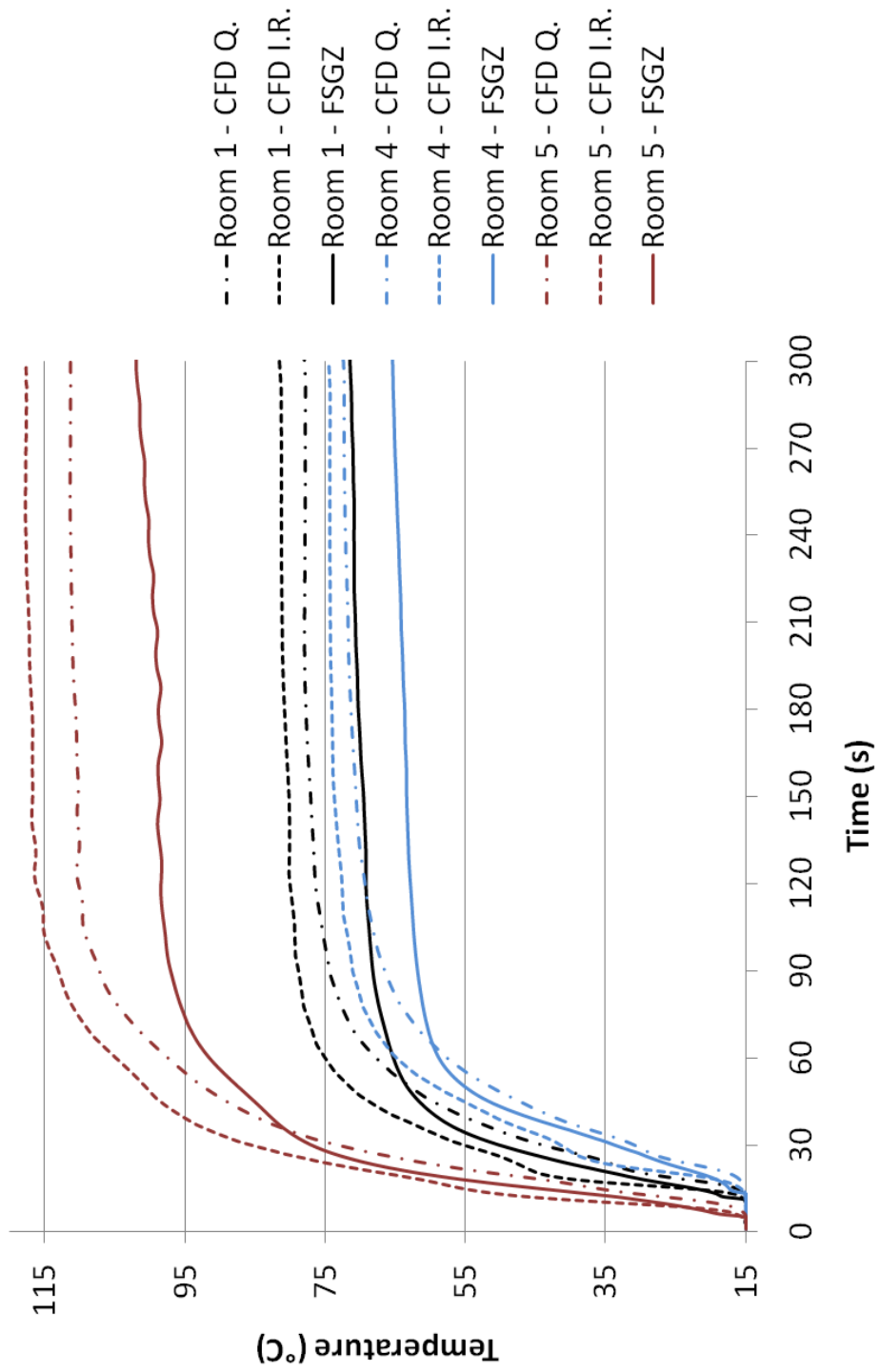
Figure 7-25. Upper layer temperature comparisons.
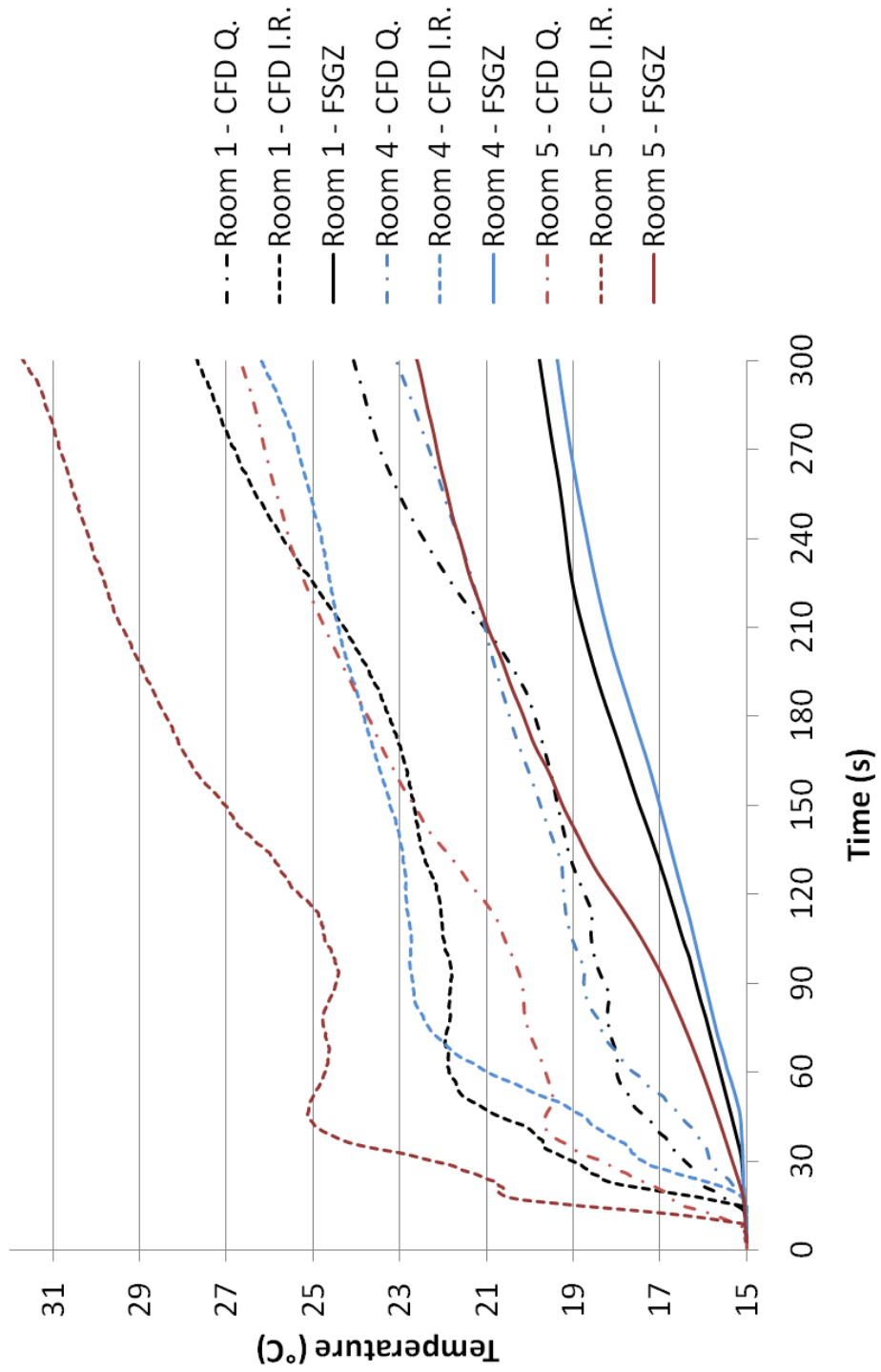
Figure 7-26. Lower layer temperature comparisons.
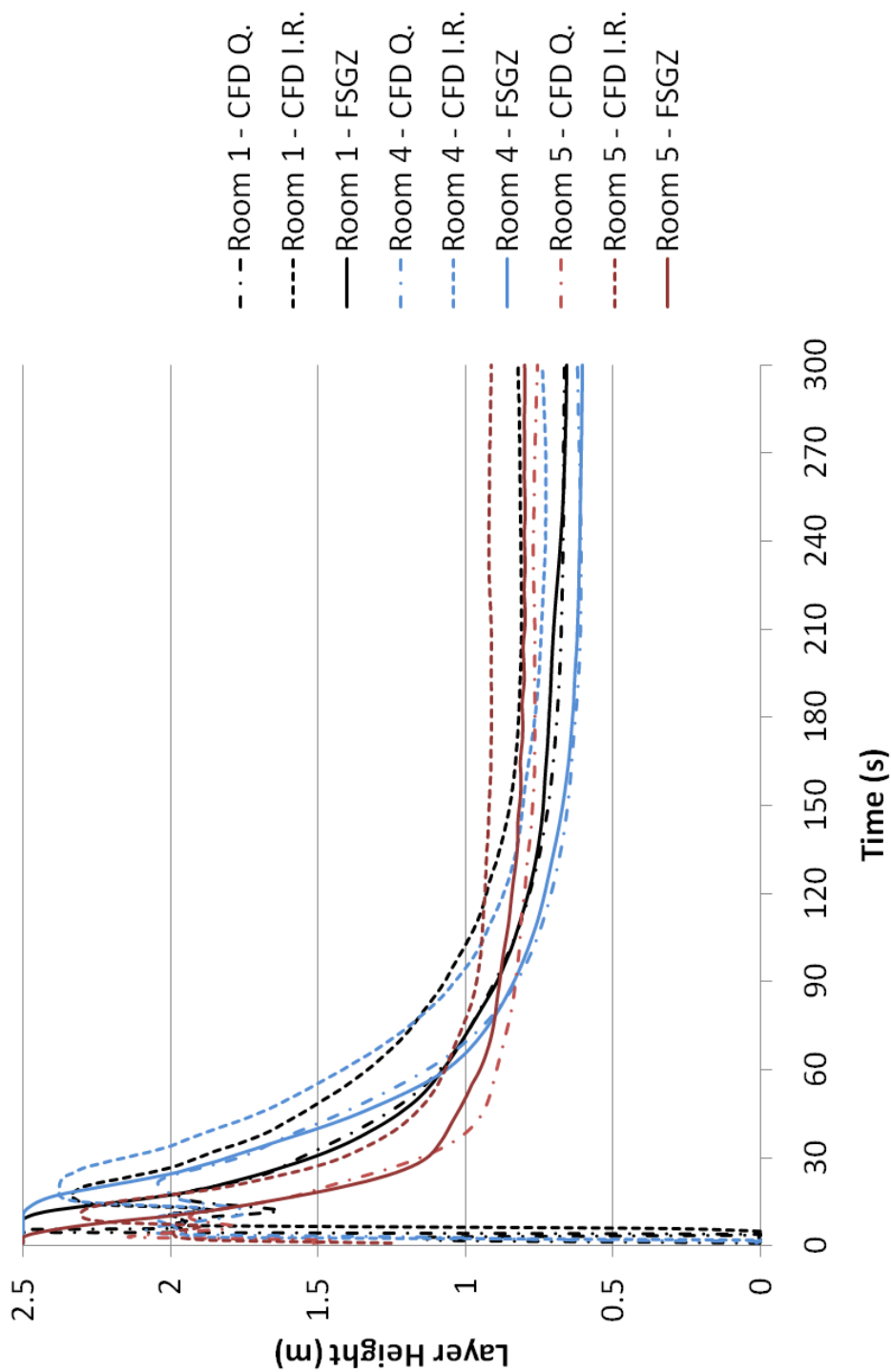
Figure 7-27. Layer height comparisons.
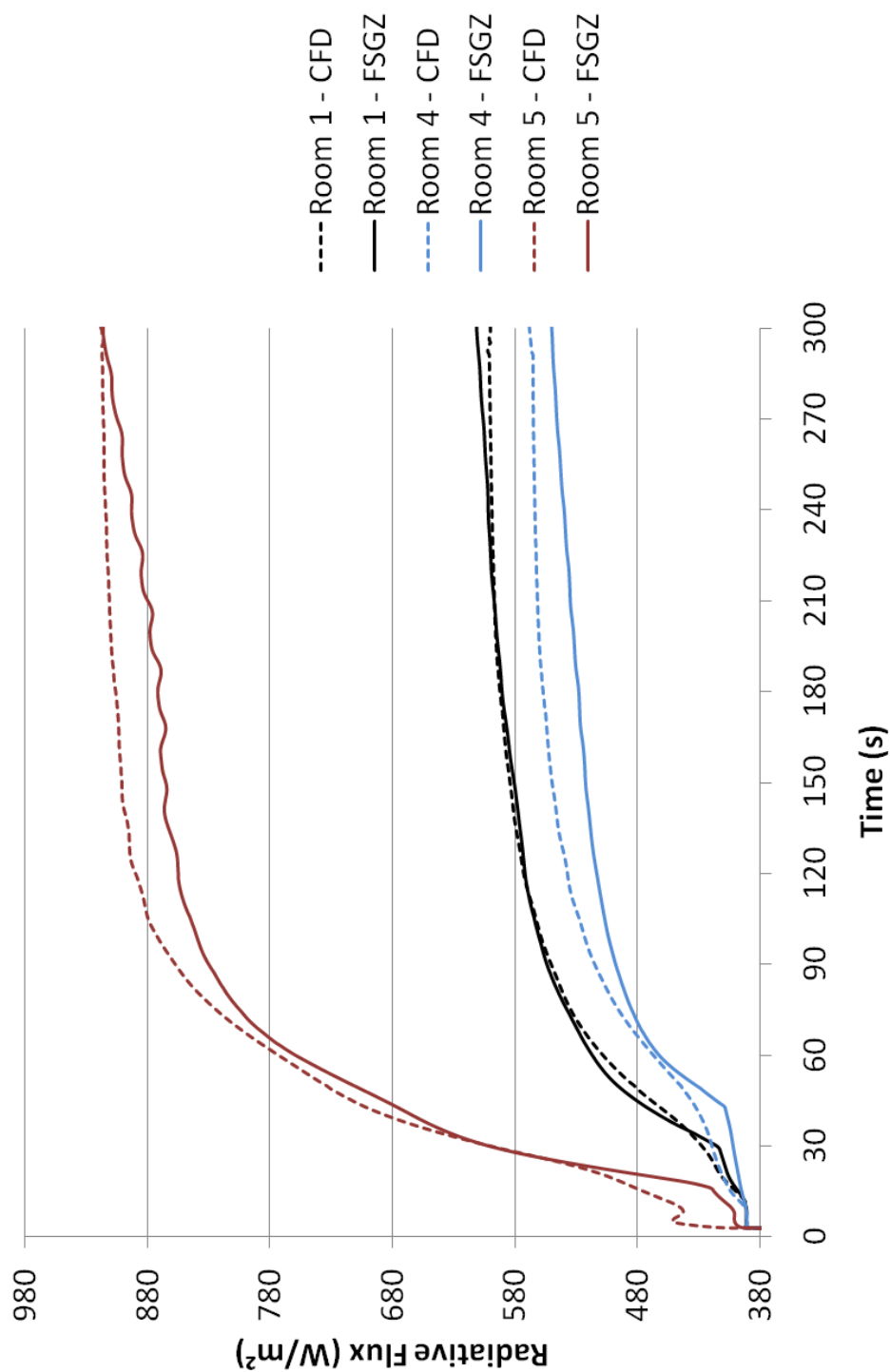
Figure 7-28. Radiative Flux Comparisons.
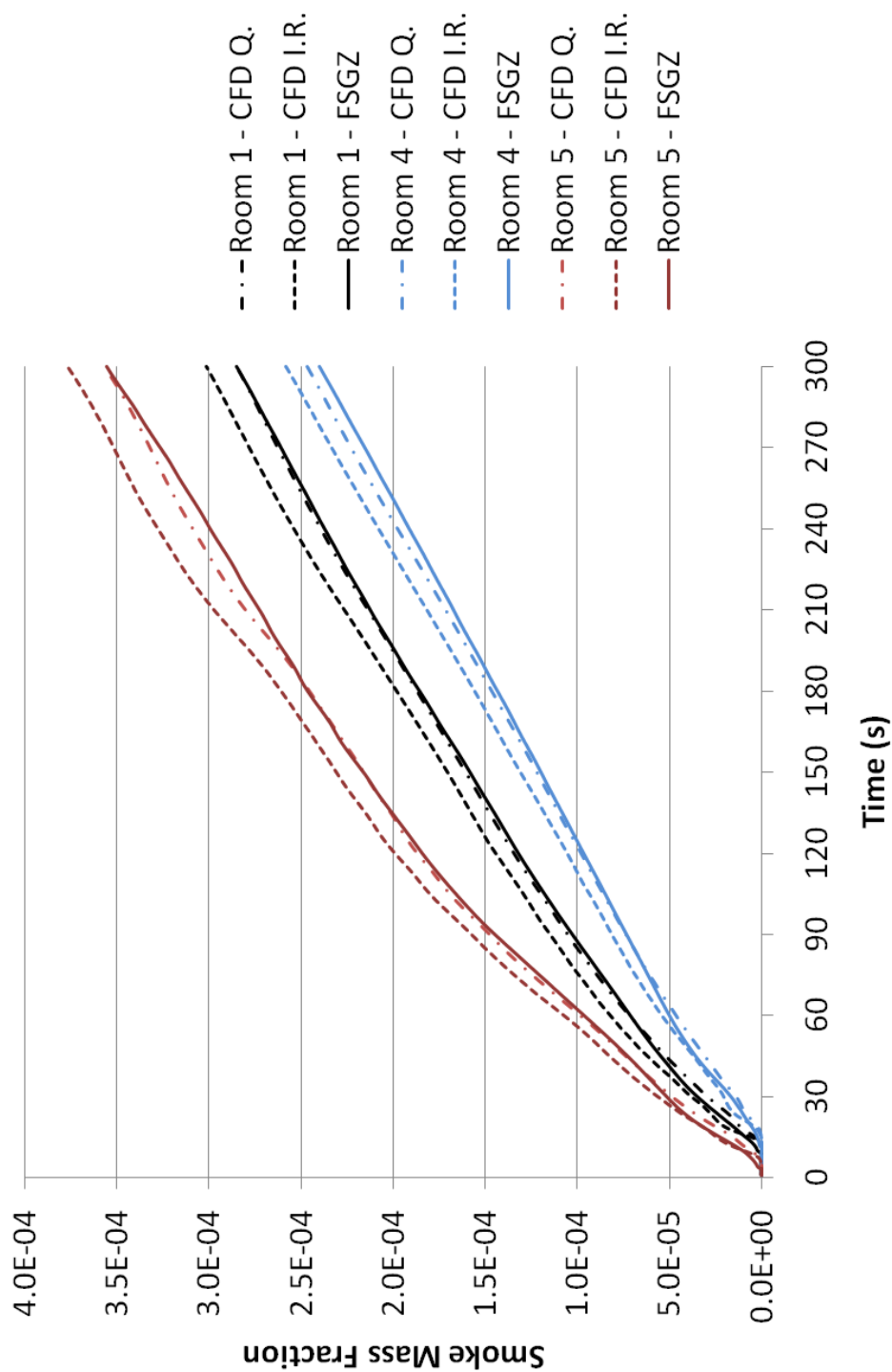
Figure 7-29. Smoke mass fraction comparisons.
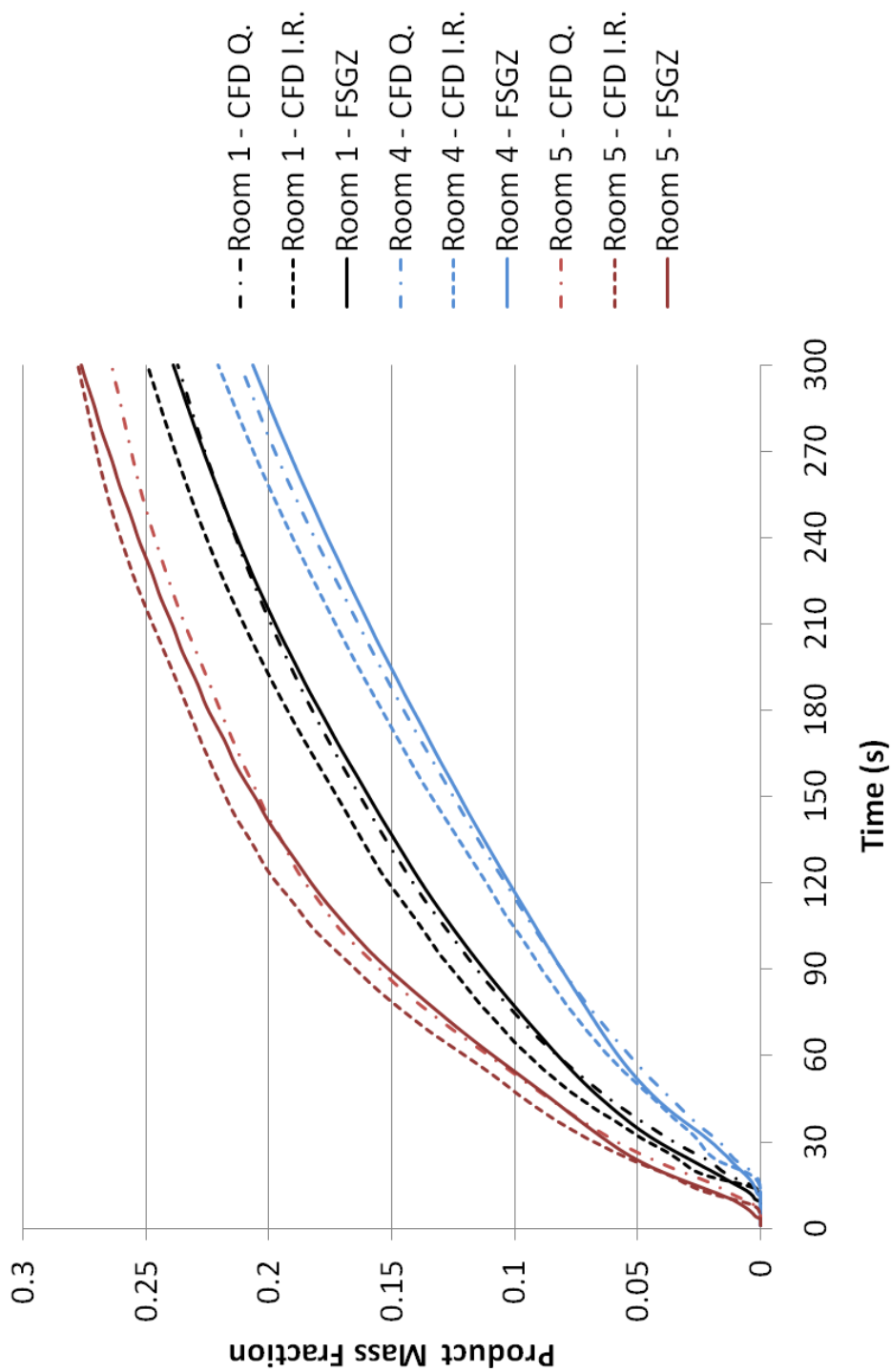
Figure 7-30. Product mass fraction comparisons.

Legend:
- Room 1 - CFD Q.
- Room 1 - CFD I.R.
- Room 1 - FSGZ
- Room 4 - CFD Q.
- Room 4 - CFD I.R.
- Room 4 - FSGZ
- Room 5 - CFD Q.
- Room 5 - CFD I.R.
- Room 5 - FSGZ
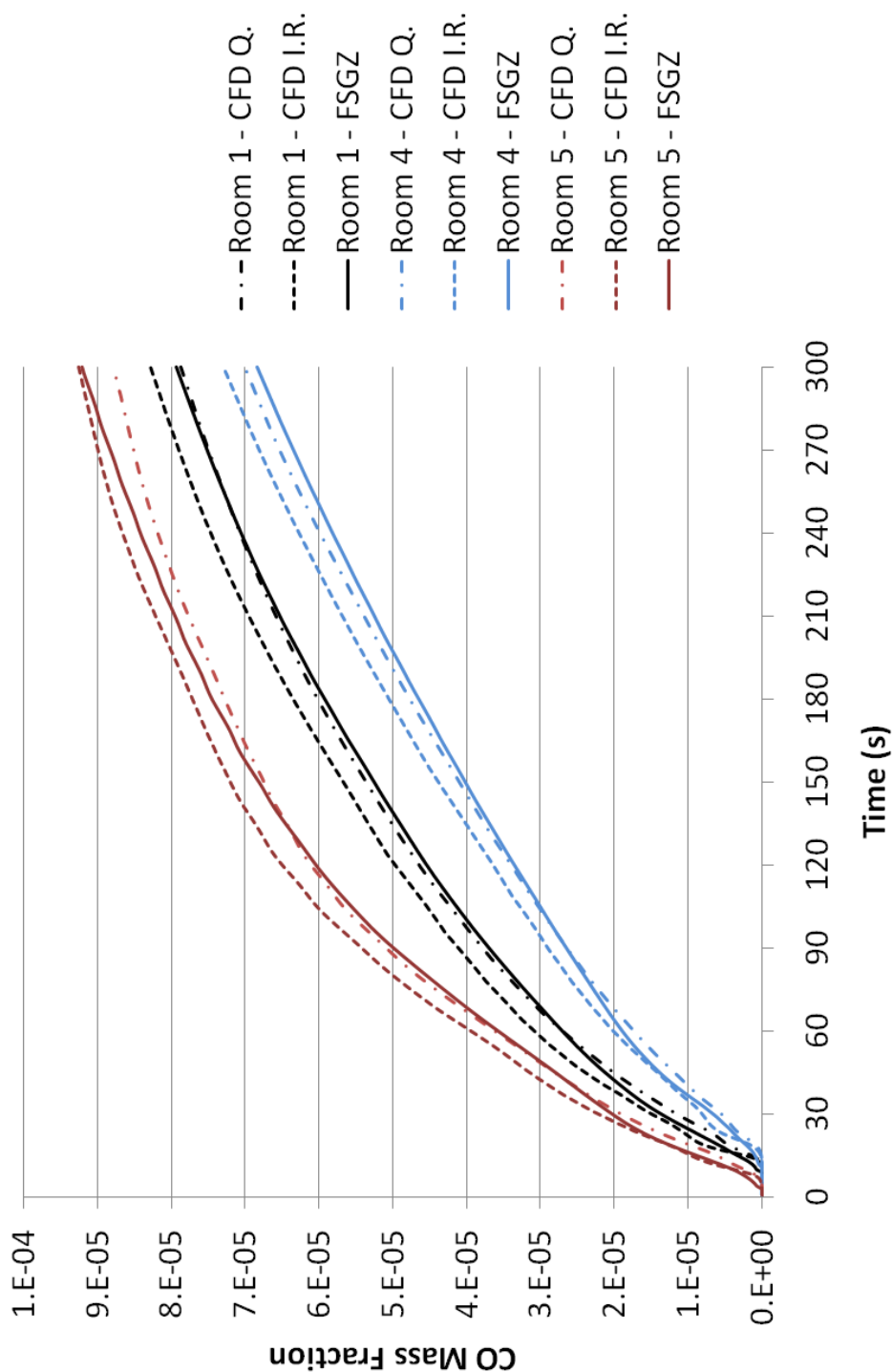
Figure 7-31. Carbon Monoxide mass fraction comparisons

7.7.13 Test case – Ship

The case presented here is simply an example of a possible practical use for the hybrid model, it appears in the WP2.2 report for the EU framework 7

project FIREPROOF; the FSEG-ZONE model discussed in this paper forms part of the integrated fire model developed for this project.

It must be noted that the long corridors being replaced by the FSEG-ZONE model in this case are actually not suitable for treatment by a zone model; the large rooms will experience a great deal of spatial variation that zone models simply cannot capture. Despite this the case demonstrates the use of the FSEG-ZONE model in an interesting geometry and demonstrates that the results obtained are comparable to those provided by the layer reduction method. Since this method acts on the actual CFD data for these rooms it appears that the FSEG-ZONE model can provide satisfactory results, regardless of the nature of the corridors, if a two layer data set is deemed suitable.

Figures 7-32a and 7-32b show the floor plan of the geometry and a 3-D visualisation of the domain. The ceiling height is 2.1m and the floor plan is repeated for the five floors comprising the geometry.
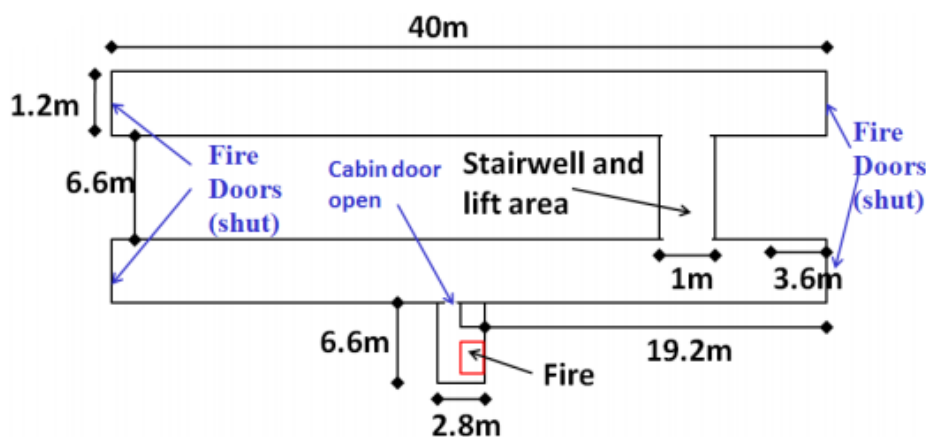
Figure 7-32a. Floor plan of the ship geometry.
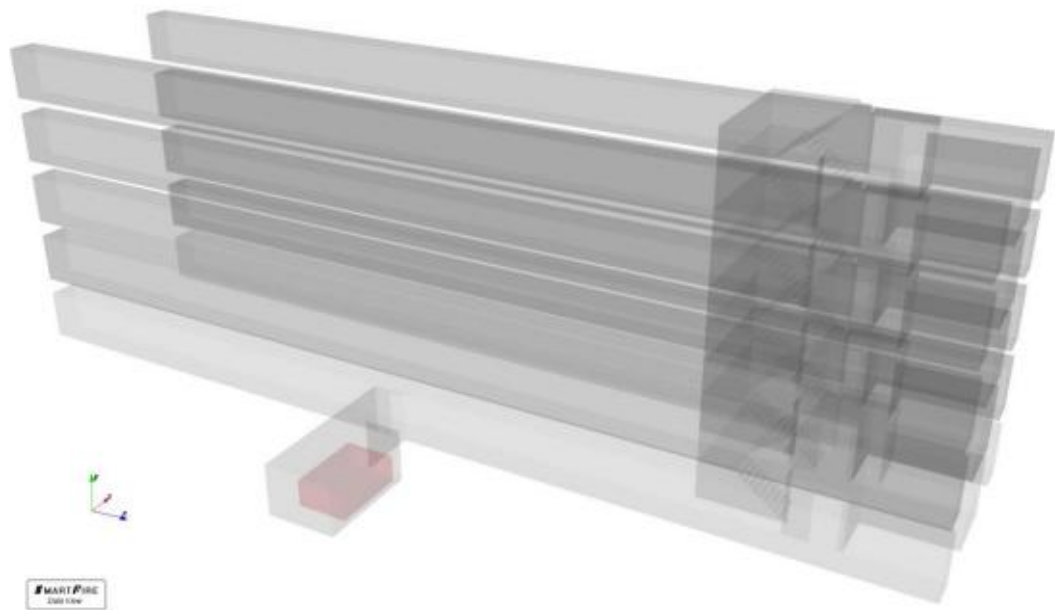
Figure 7-32b. Visualisation of the ship geometry.

The stairwell is the only connection between the floors and the dimensions and visualisation is shown in figures 7-33a and 7-33b below.
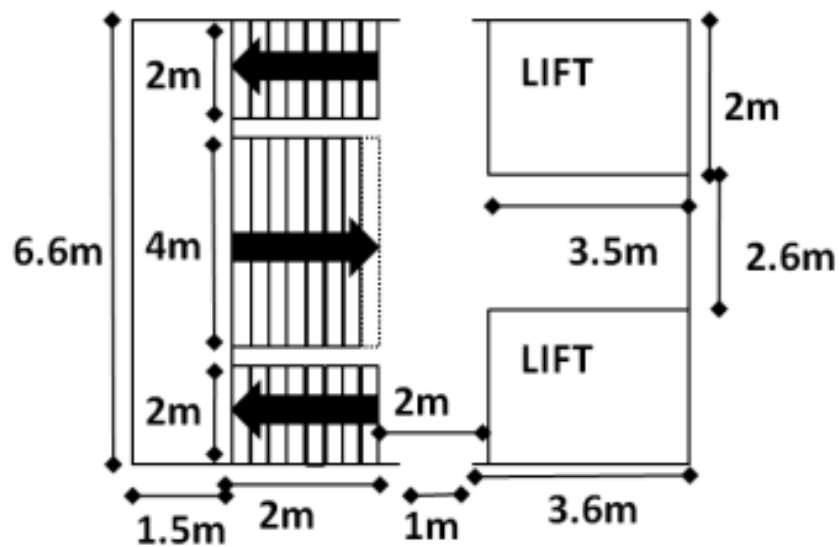
Figure 7-33a. Floor plan of the stairwell section.
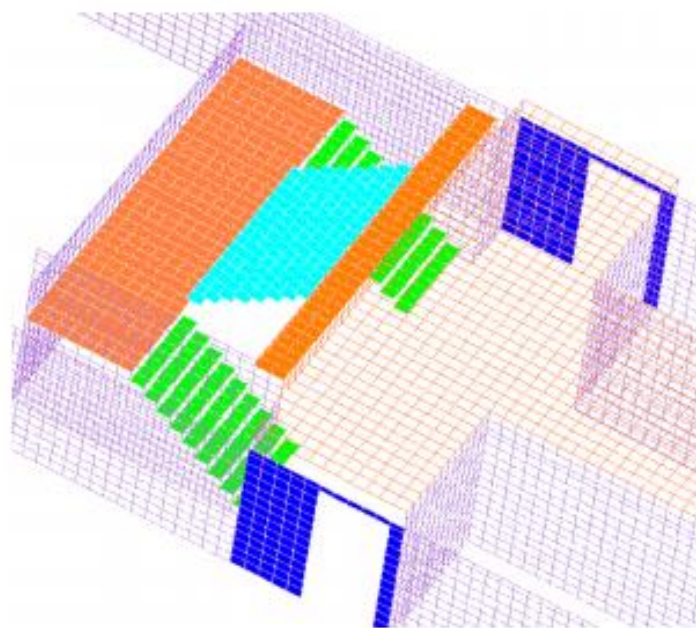
Figure 7-33b. Visualisation of the stairwell section.

The fire is situated in a cabin on the bottom floor and has been assigned a heat release rate based on an experimental measurement [Arvidson2008] of a mock up of a ship cabin and modified due to ventilation characteristics of the geometry used; the development of this is shown in figure 7-34.

In the hybrid simulation the FSEG-ZONE model is used to replace the nine corridor sections leaving the geometry shown in figure 7-35 to be simulated by the field model.

The simulation is run for a total time of 10 minutes over 1 second time-steps consisting of 200 iterations each. The CFD simulation uses 93,045 cells whereas the hybrid simulation uses 43,905 cells, resulting in a saving of almost 53%.
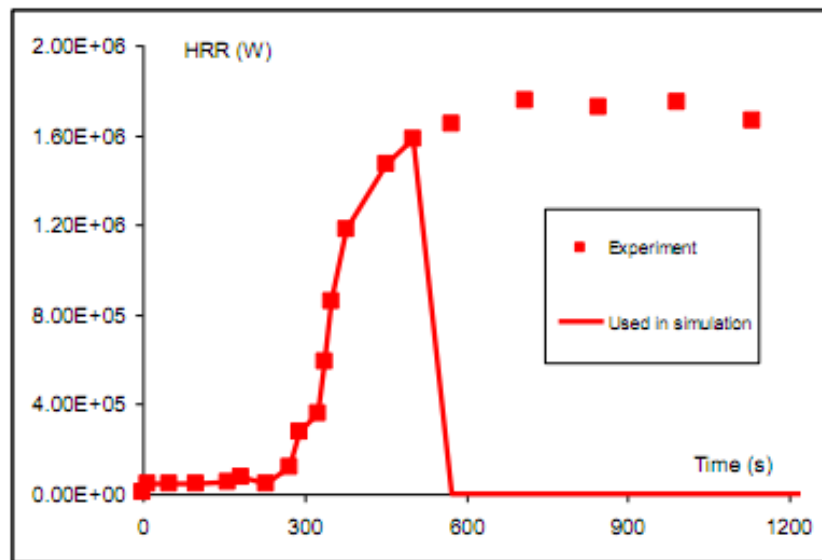
Figure 7-34. Heat release rate used in simulation.
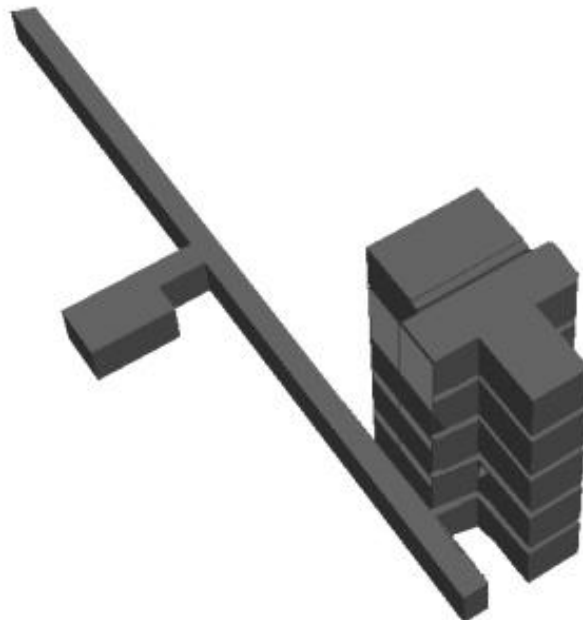
Figure 7-35. CFD domain after replacement of corridors with FSEG-ZONE model.
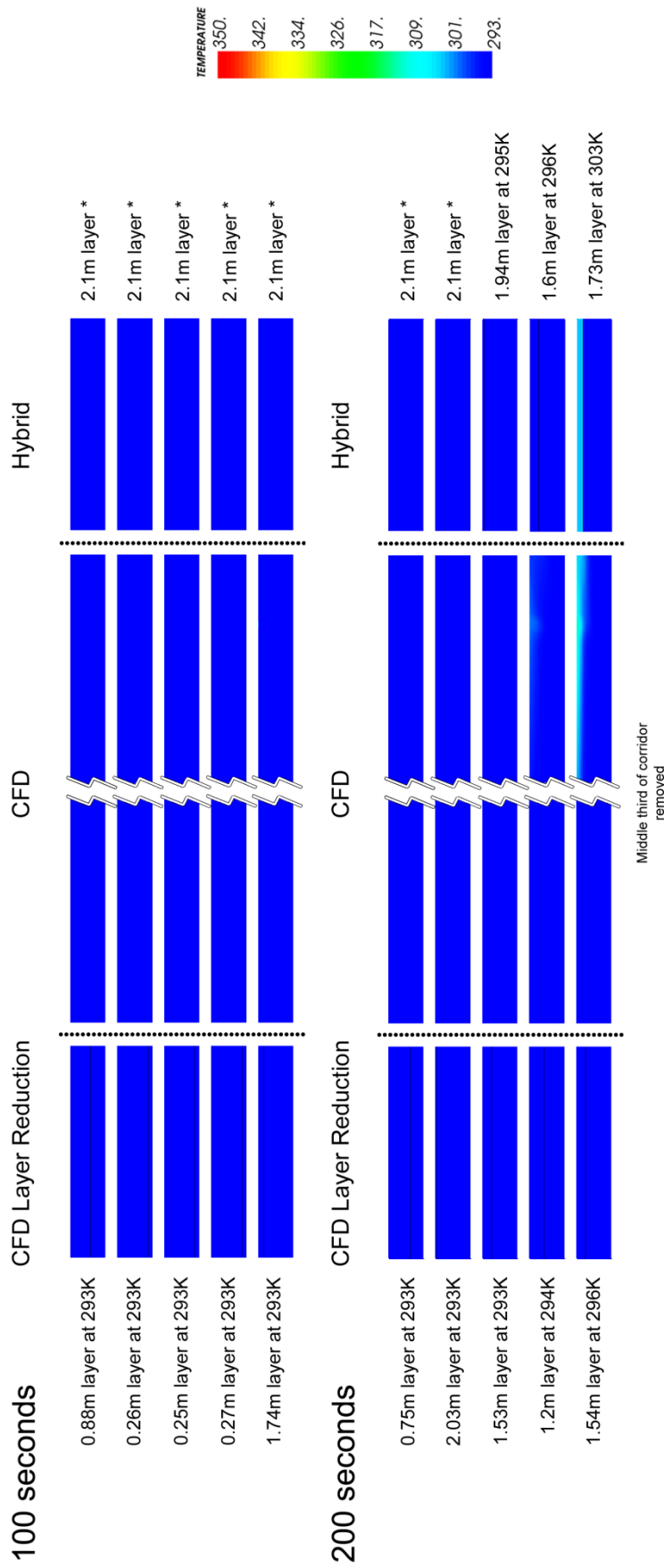
Figure 7-36. Temperature comparisons at 100 and 200 seconds.
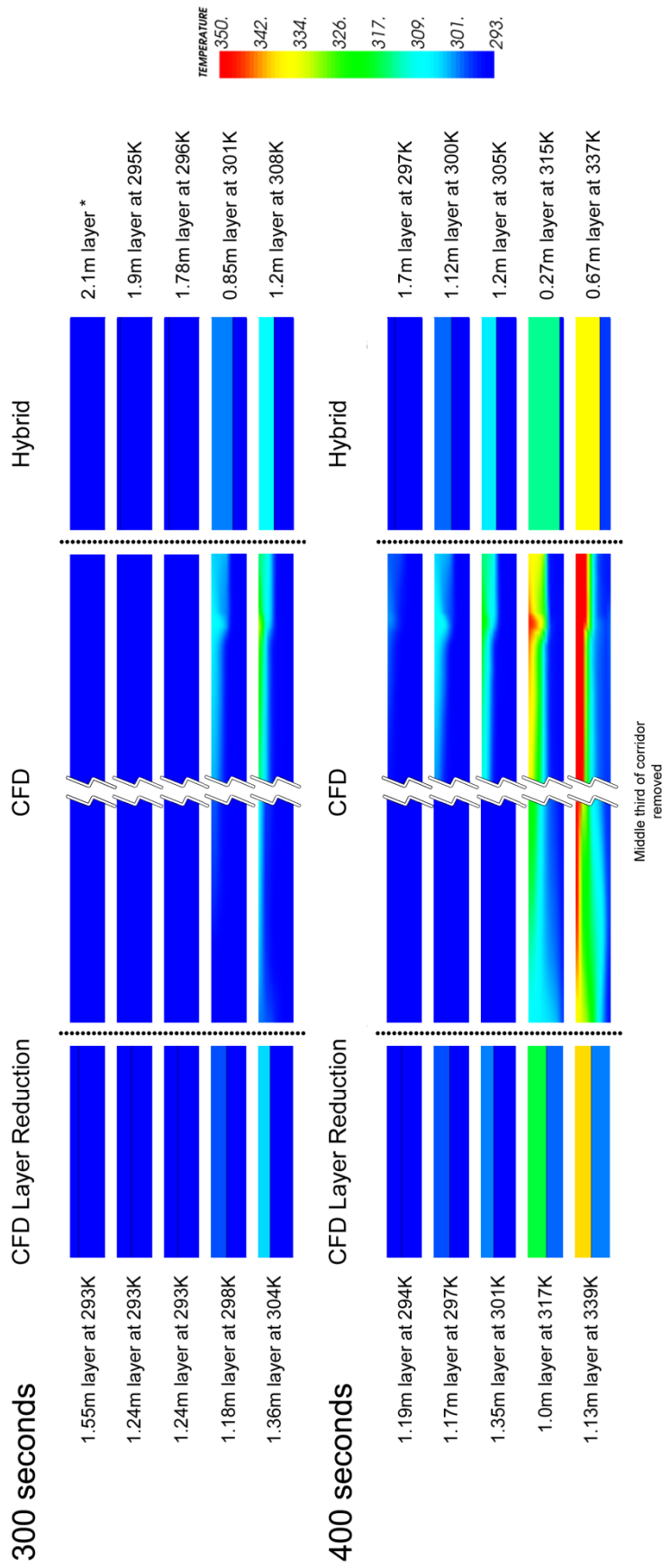
Figure 7-37. Temperature comparisons at 300 and 400 seconds.
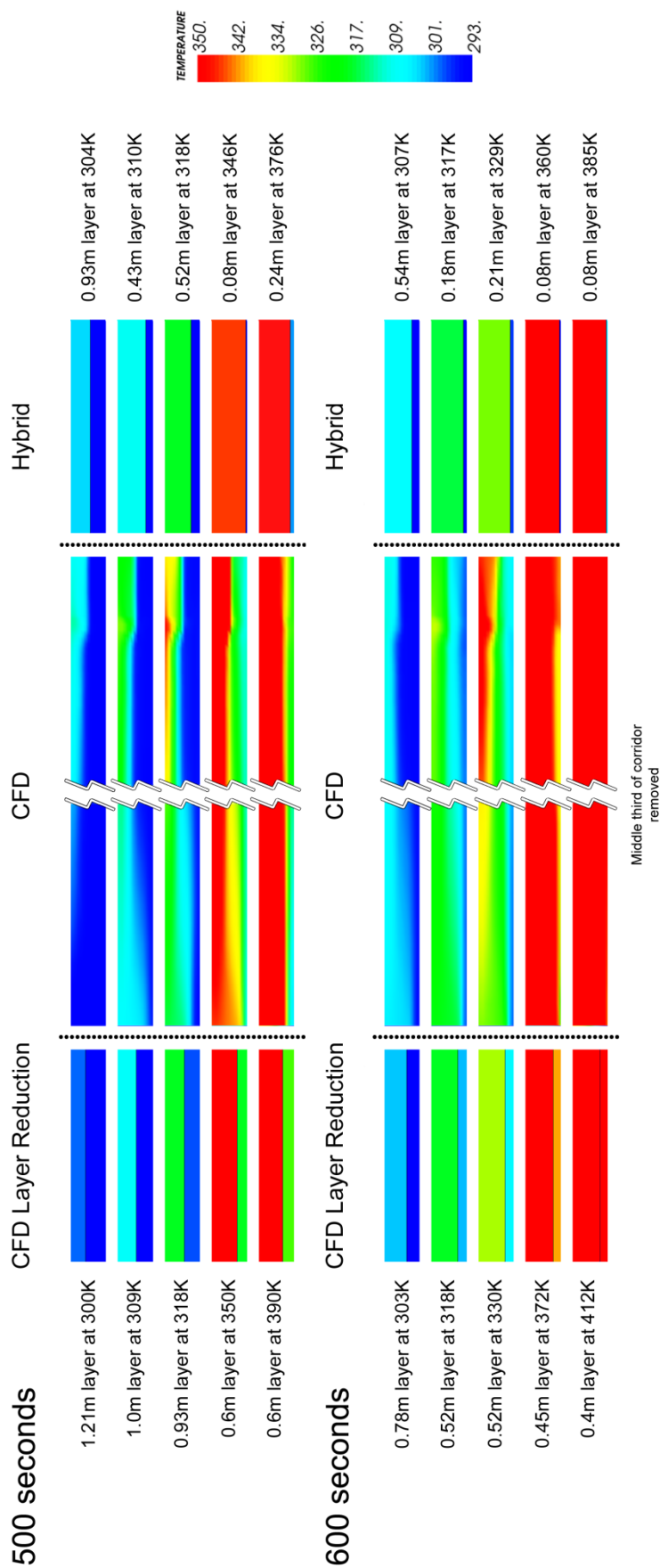
Figure 7-38. Temperature comparisons at 500 and 600 seconds.

Results

Comparisons for layer temperatures and height are shown in figures 7-36, 7-37 and 7-38 on the previous pages. Comparisons are provided at 100, 200, 300, 400, 500 and 600 seconds. The middle section of the figures are visualisations of the full resolution CFD results. The left section shows the results of the layer reduction method as applied to this CFD data. The right section shows the results form the FSEG-ZONE model from the hybrid simulation.

The results demonstrate that despite the limited suitability of the case (involving long corridors) for simulation by the hybrid model, agreement for layer temperatures and height is reasonable. Naturally, the spatial variation seen in the full resolution CFD corridors make it difficult to even pick a location to make the comparisons at. Certainly, the FSEG-ZONE results are no worse than the layer reduction method applied to the CFD data. If the average nature of the results is deemed a valid representation then the FSEG-ZONE model can indeed be considered to provide satisfactory results.

The CFD simulation took 102 hours 31 minutes and 40 seconds; the hybrid simulation took 44 hours 29 minutes and 53 seconds. This results in a saving in computational time of almost 57%, compared to a reduction in cells of almost 53%.

7.7.14 Test case – Experimental Comparison

The final test case considers the simulation of a fire experiment performed for a University of Canterbury report into data reduction techniques as a means of zone model validation [Weaver2000]. For this test case a second CFD simulation is run using a coarse mesh for comparison with the FSEG-ZONE model. Since the layer reduction method biases with CFD simulations this comparison is only valid when experimental results are available, such as the present case.

The setup consists of two compartment geometry of approximate ISO-9705 dimensions [ISO1993]. The case consists of a fire room (360cm long, 240cm wide, 240cm tall), with centrally positioned fire source, connected to a second room (same dimensions as first) through a centrally placed door (76cm wide, 198.5cm tall) . The second room is connected to the exterior by the absence of a wall (in effect a door spanning the wall dimensions), see figure 7-39 for clarification.

This open wall is likely to cause some problems for the zone model since the absence of a soffit will seriously affect the development of an upper layer. This is a fairly extreme situation for the FSEG-ZONE model to handle since the equations are derived from consideration of a contained volume. The absence of one wall is a significant deviation from this assumption, and the zone model will have to contend with balancing its pressure with the exterior CFD domain across the whole of this interface.

The floor was lined with a sheet of plywood and the walls were constructed of 'Gib' fibre line board, both 12.5mm thick. In addition, to prevent leaks the walls were further plastered with Gib paste. The report states that to allow multiple runs without damage to the Gib borad a layer of Intermediate Service Board (ISB; produced by Inzco, New Zealand) 25mm thick was screwed on to the wall surfaces, with 30mm washers. The intermediate service board was of the glass wool insulation type, and was rated for temperatures up to 450°C. After the above lining of surfaces the experimental compartments both measured 360cm long, 237cm wide and 236cm high.

In addition to this discrepancy with the ISO standard, a few of the measurements stated in the report are inconsistent. The dimensions employed in the present simulation to best take account of these measurement issues are shown in figure 7-39 below.
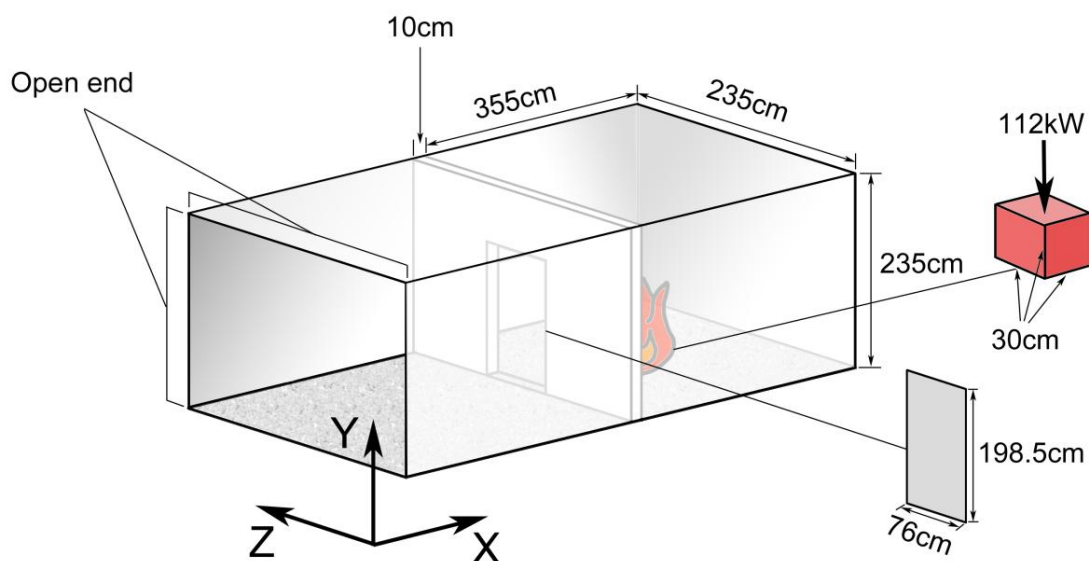
Figure 7-39. Setup for simulation.

The report does not state the thermal properties of materials used, and it has proven difficult to trace the exact materials used. An ISB board with similar specifications has been sourced, as has properties for plywood; these are displayed in table 7.2 below.

	Specific Heat J/kgK	Density kg/m^3	Conductivity W/Km	Emissivity
ISB	1200	45	0.033	0.95
Plywood	1210	600	0.13	0.83

Table 7.2. Thermal properties of intermediate service board and plywood.

The discrete transfer radiation model with 24 ray radiation model was enabled in SMARTFIRE and the simulations were run for 300 seconds using 100 sweeps per time-step. For this simulation a second CFD simulation is run where the room being replaced by the FSEG-ZONE model is also modelled using a coarse CFD mesh to test the performance of both methods (the rest of the domain remains identical). Due to limitations with the meshing tool available in SMARTFIRE, which requires a 1-to-1 cell correspondence, the cell mesh can only be made coarser in the X direction (see figure 7-39). In effect the length of the second room is spanned by a single cell, yet the width and height maintain the same cell resolution as in the original simulation. It should be noted that while this is indeed coarse in relation to what is deemed suitable for CFD simulations in general, it is a significantly better quality mesh than that which would be obtained from reducing the cell resolution in all three dimensions. The 648 cells (24 in Y, 27 in Z) used by the coarse simulation are significantly more than the 2 layers considered by the FSEG-ZONE model.

The standard CFD simulation uses 69,471 cells; the coarse CFD simulation uses 45,198 cells; the hybrid simulation uses 46,872 cells. This results in an approximate reduction of 35% for both methods (the slightly higher number of cells in the hybrid model originate from a solid obstacle used to separate the two sections of CFD domain.)

Results

From figure 7-40 it can be seen that the FSEG-ZONE model over estimates the pressure and underestimates the mass, although the range of values is small with a maximum difference of around 0.1Pa. This is a highly commendable performance from the FSEG-ZONE model considering the nature of the open wall. The reduction in accuracy from performing a coarse CFD simulation is clearly seen in the over estimation in temperature and underestimation in mass.
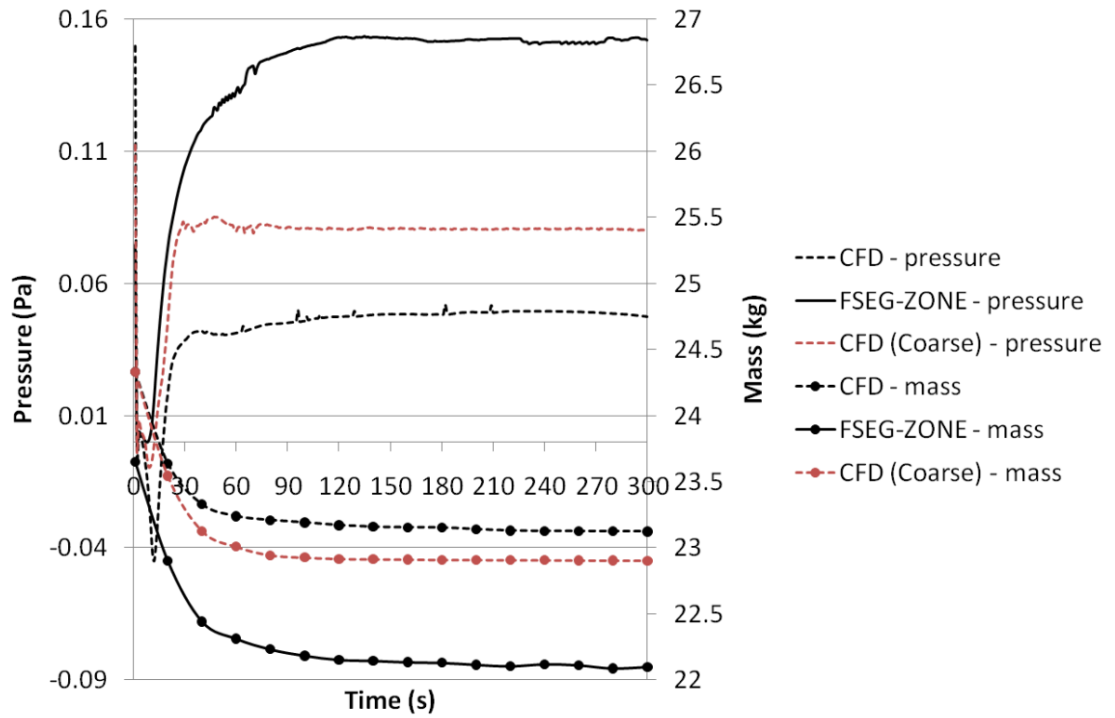
Figure 7-40. Compartment pressure and mass comparisons.
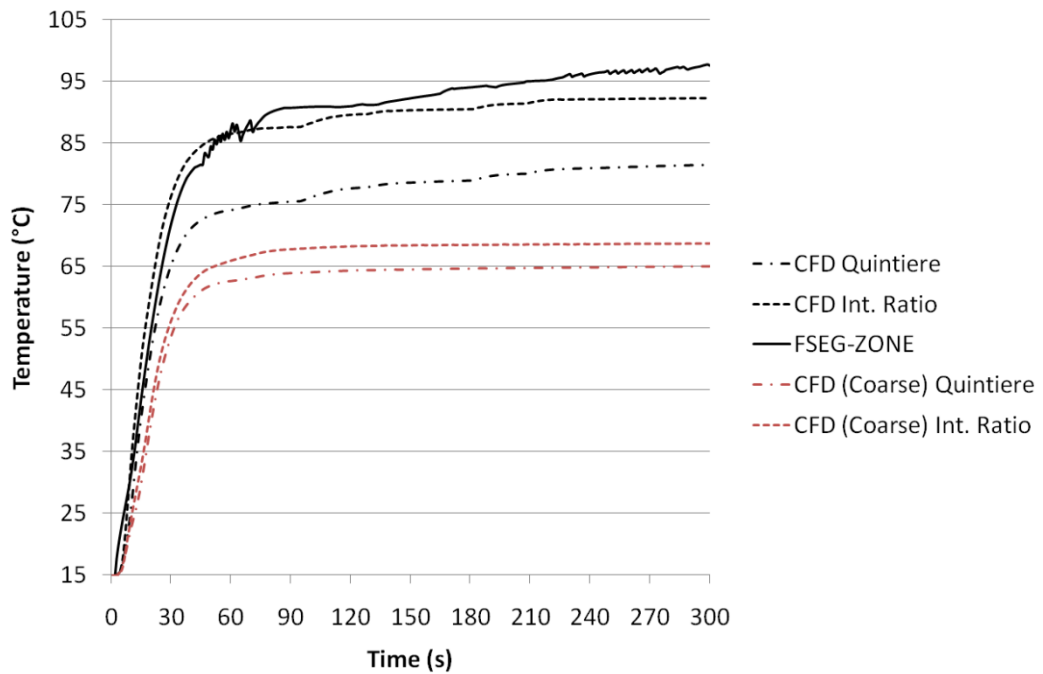
Figure 7-41. Upper layer temperature comparisons.

Figure 7-41 above shows the upper layer temperature for the FSEG-ZONE model along with the two reduction methods for both the standard and coarse CFD simulations. For the first 60 seconds, the FSEG-ZONE model is in close agreement with the standard CFD simulation, and for the remainder of the simulation has a slightly higher temperature but is always within 5°C of the integral ratio reduction value. In comparison to this, the reduction methods of the coarse CFD simulation significantly underestimate the upper layer temperature for the vast majority of the simulation. It appears that the FSEG-ZONE model out performs a coarse CFD compartment in this regard.

Figure 7-42 below demonstrates that all three simulations report similar values for the lower layer temperature, although this is expected from the extremely small range of temperatures on display (within 5°C of ambient). The FSEG-ZONE model again experiences a slight delay in heating up, although the results are in good agreement with the Quintiere method of the standard CFD simulation.
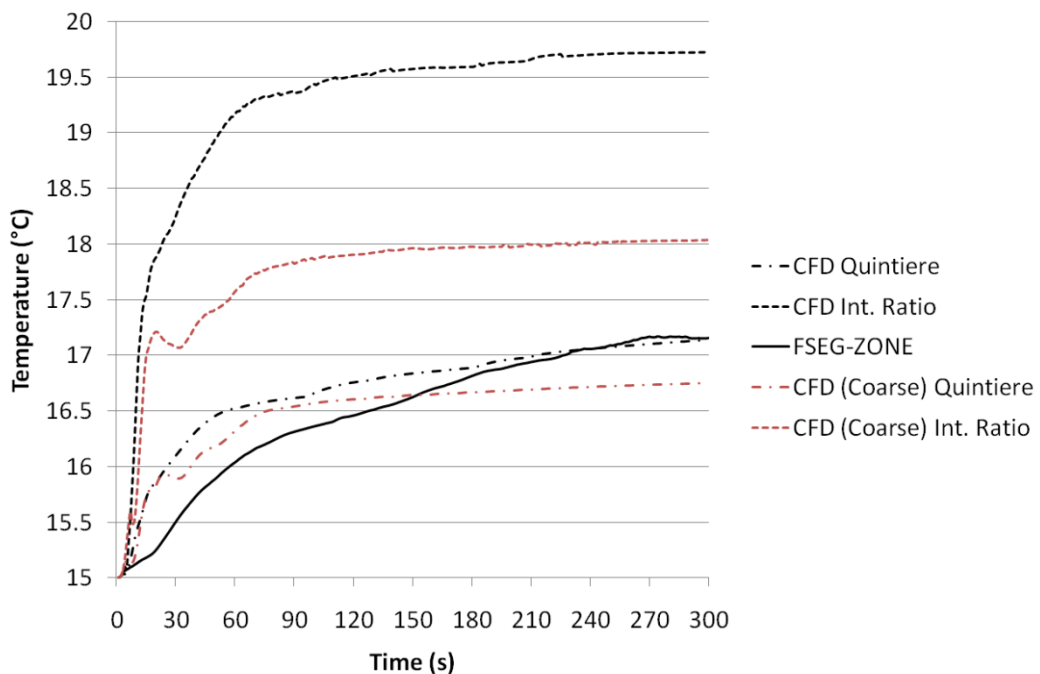
Figure 7-42. Lower layer temperature comparisons.
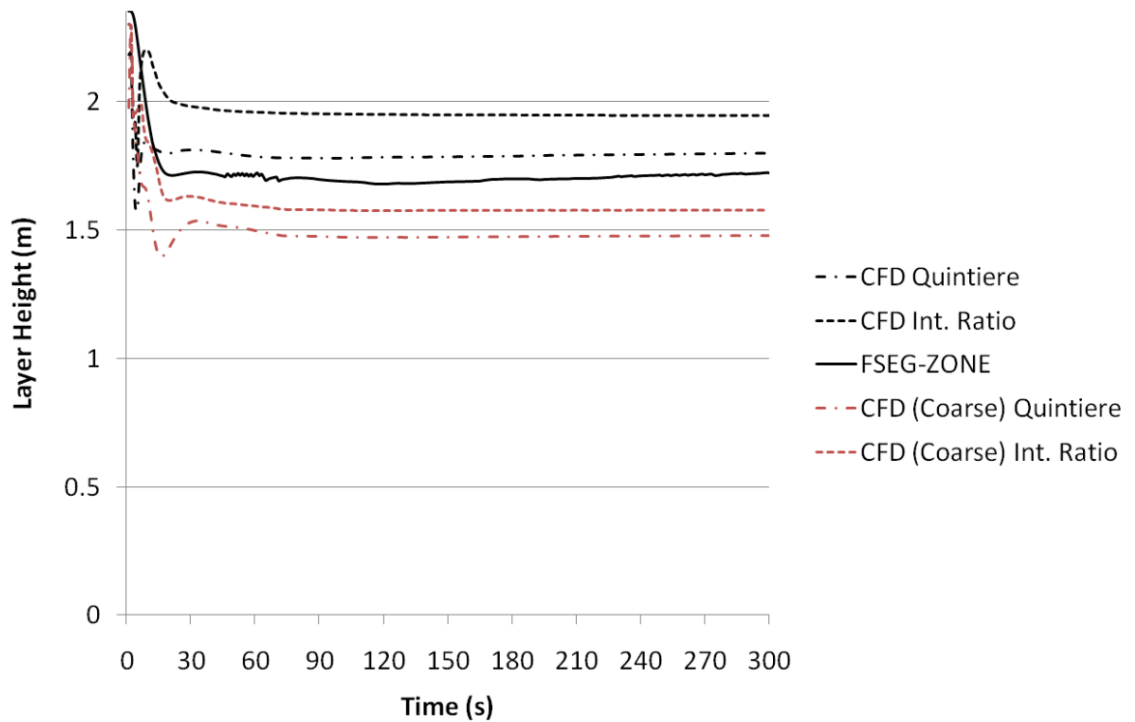
Figure 7-43. Layer height comparisons.

Figure 7-43 above shows the layer height development, and confirms that the FSEG-ZONE method again outperforms the coarse CFD compartment in this regard. Still, the open wall clearly has a detrimental effect on the FSEG-ZONE model since on this occasion the layer does not remain between the bounds set by the two reduction methods of the standard CFD simulation.

Finally, figure 7-44 below once again demonstrates the performance of the FSEG-ZONE model in accurately capturing the radiative flux, although there is an overestimation from 60 seconds onwards which can be explained by the higher layer temperature observed in figure 7-41. The coarse CFD model reports a comparatively much greater underestimation of this value, which again is explained by a corresponding underestimation in figure 7-41.
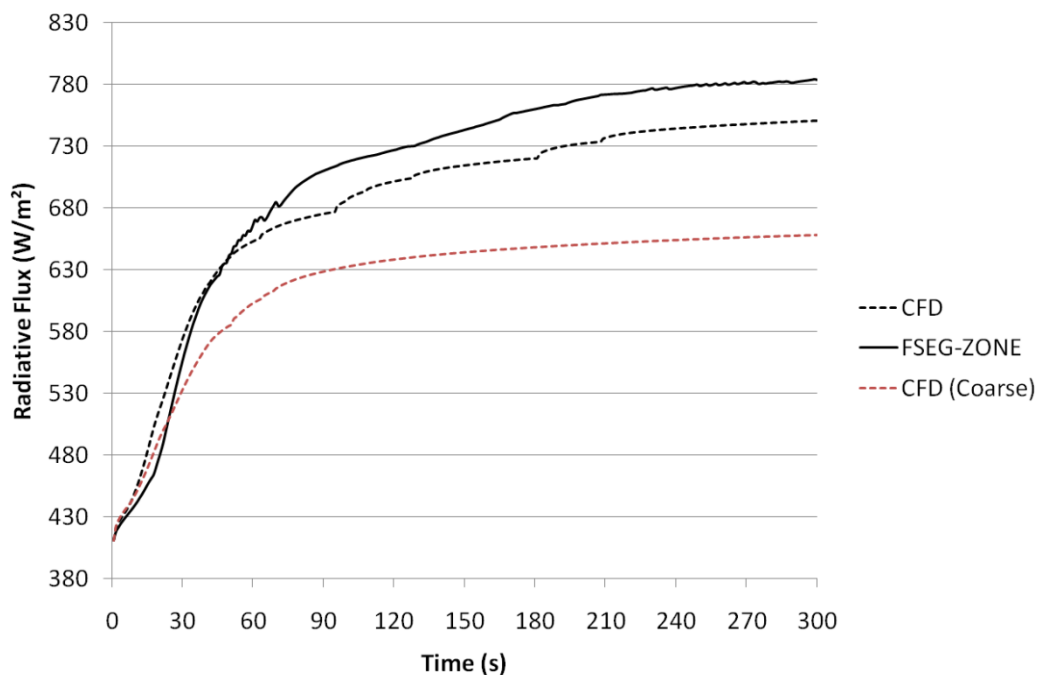
Figure 7-44. Radiative flux comparisons.

Comparisons with experimental results

Figures 7-45 to 7-47 display comparisons of the temperature profile observed at the end of the simulations with actual results obtained from thermocouples during the experiment. In addition to a thermocouple stack situated in the centre of the second room, one was also placed in the corner adjacent to the fire room; these are plotted as Exp. Corner and Exp. Centre. The FSEG-ZONE results are presented as a two piece step profile, as are the reduction methods of both the standard and coarse CFD simulations. These are compared in figure 7-45 below. The reduction is not performed for the experimental data since it is localised, as opposed to the compartment-wide 'super-cell' averages considered in the CFD simulations.

Since these values are obtained at the end of the simulation, they summarise the results seen toward the end of figures 7-41 to 7-43, namely that the coarse

CFD model performs less favourably than the FSEG-ZONE model by significantly underestimating both layer height and temperatures. From this plot alone it may be tempting to conclude that all three simulations provide acceptable results depending on the definition of the layer, e.g. the coarse CFD profiles appear to be consistent with the assumption of an ambient lower layer.
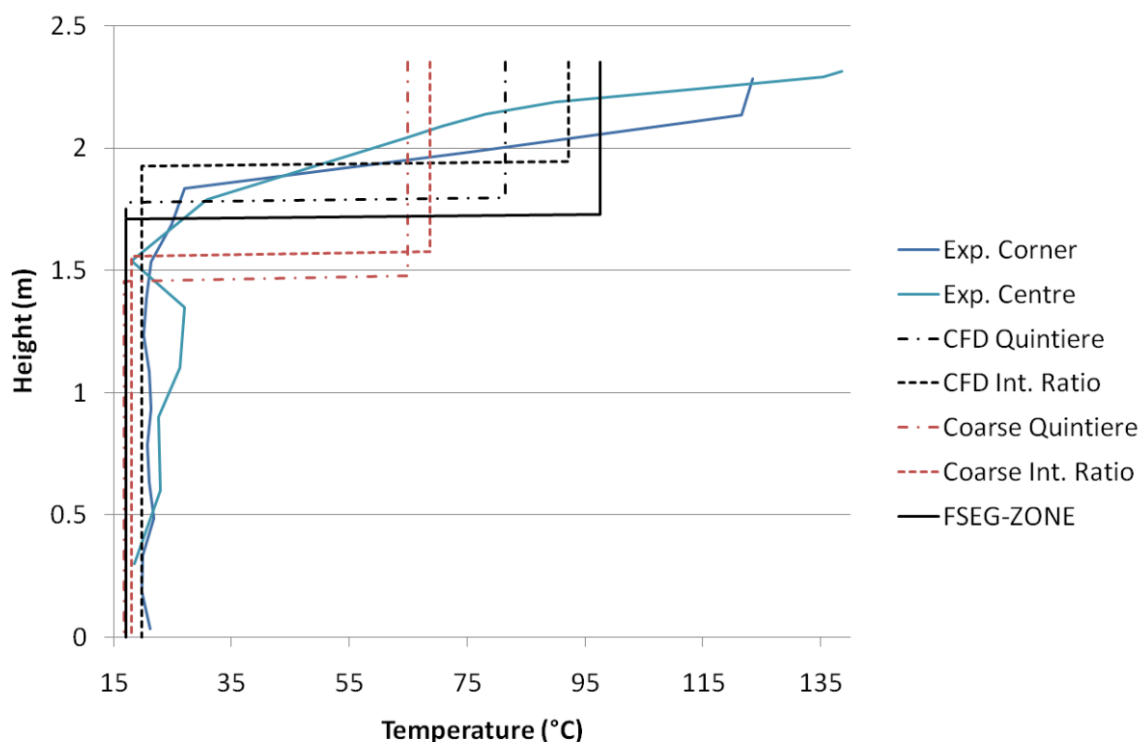
Figure 7-45. Temperature profile comparisons between FSEG-ZONE, CFD reduction methods and experimental results.

In this way the reduction methods can mask the true nature of results and used alone can result in incorrect conclusions. Figure 7-46 below demonstrates this through avoiding the reduction methods by using the actual results from the CFD cells. These were obtained from monitor lines located in the same location as the thermocouples in the experiment. It can be seen that while the reduction methods provided plausible results for the coarse CFD simulation in the previous figure, here it is obvious that it is in fact underestimating the true values. This is most clearly seen in the 'Coarse

Centre' plot which begins to deviate from ambient more than half a metre below the other profiles.

Finally, figure 7-47 plots the CFD 'super-cell' values used in the layer reduction calculations (see section 4.6.2), representing the average total room quantities. Here it is immediately clear that in this situation the FSEG-ZONE model performs better than a coarse CFD compartment and provides admirable results considering the countless concessions that have been made in its development.
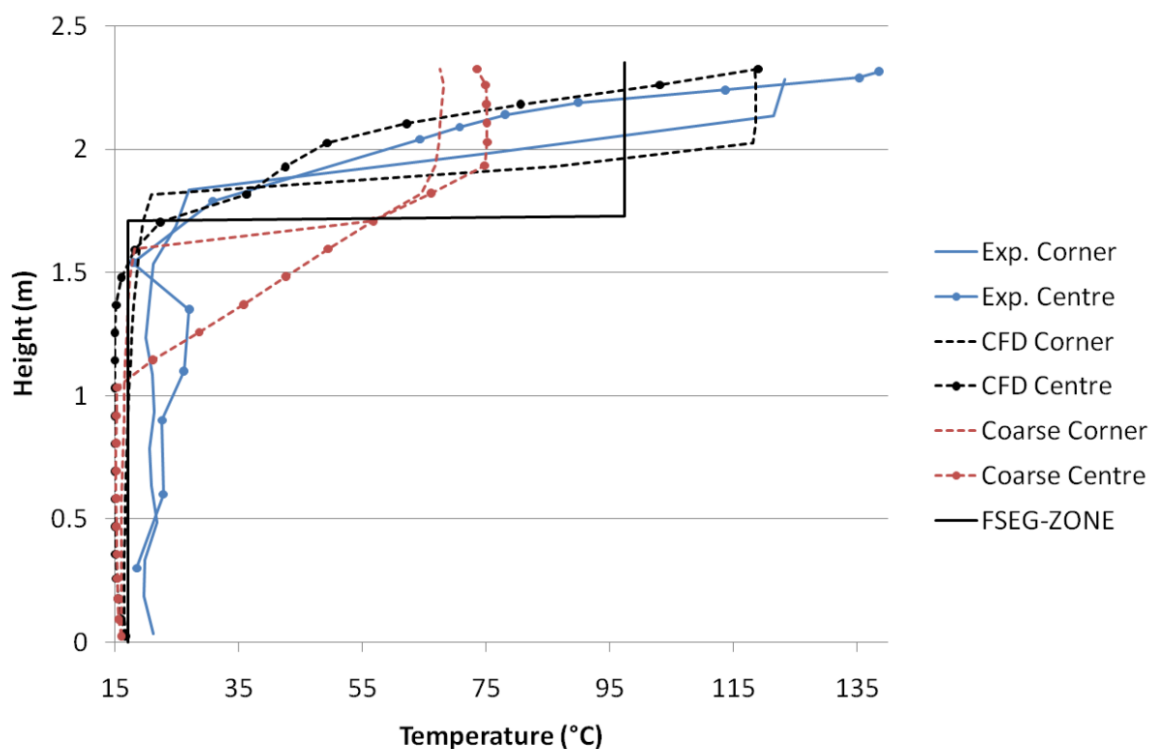
Figure 7-46. Temperature profile comparisons between FSEG-ZONE, CFD monitor lines and experimental results.

Despite this, the coarse CFD simulation took 17 hours and 50 minutes to complete, whereas the hybrid model took 18 hours and 36 minutes; the standard CFD simulation took 28 hours and 40 minutes. This means the coarse CFD simulation actually made a slightly greater saving in

computational time of 38%, compared to the 35% saving made by the hybrid model. This is possibly due to the difficulties presented to the FSEG-ZONE model by the open wall configuration, since in previous test cases it has been demonstrated that the hybrid model achieves savings equivalent to a wall patch which relates to simply removing the room from a simulation (see section 6.3.2). Also, due to the nature of the geometry and interfacing between models, the hybrid simulation considered an extra layer of solid cells, although the effect of this is unlikely to be as significant as to explain the discrepancy seen.
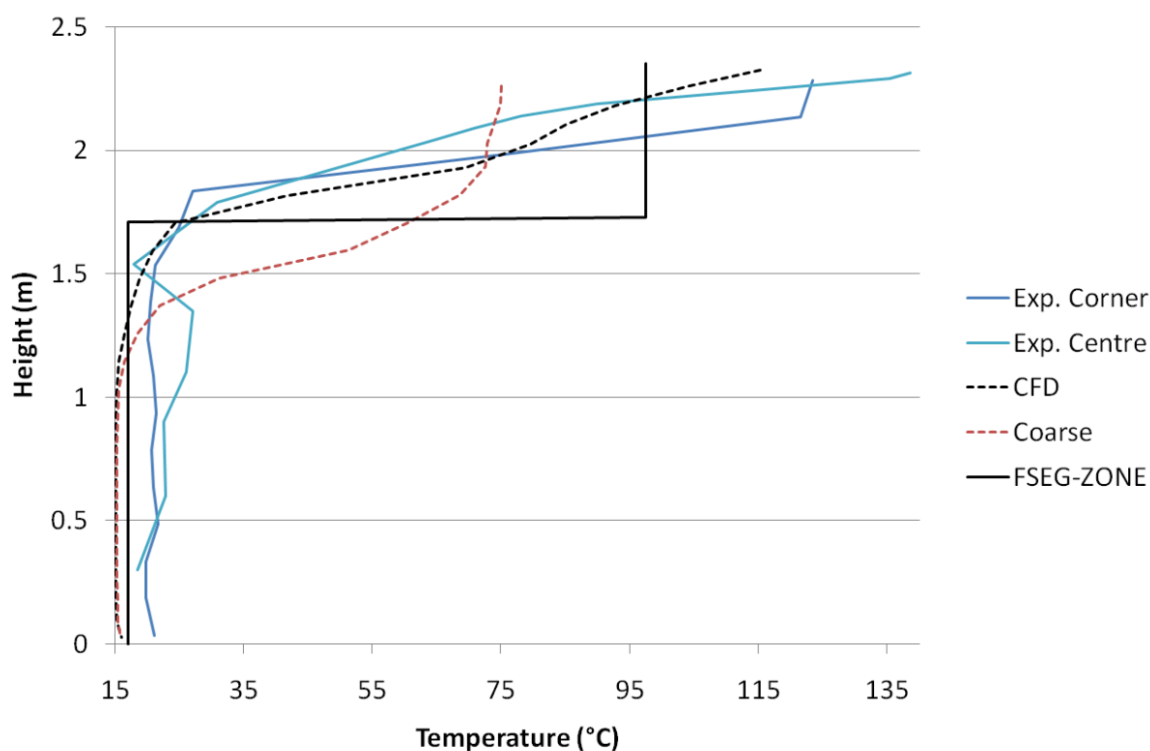
Figure 7-47. Temperature profile comparisons between FSEG-ZONE, CFD 'super-cell' values and experimental results.

Issues with coarse CFD simulations

The coarse simulation used in the present test case was obtained by reducing the mesh resolution in the direction normal to the connecting doorways/vents. The resolution in the vertical and remaining horizontal direction had to

remain the same due to limitations with the basic SMARTFIRE meshing tool. This was discussed earlier where it was suggested that, due to the vertical resolution remaining constant, the coarse simulation will actually perform better than a true coarse simulation which has reduced resolution in all directions. Additionally, there is a further issue with reducing the resolution in a single direction, since doing so can severely elongate mesh cells, leading to aspect ratios that fall outside accepted ranges. For this reason a further simulation was run using a coarsened CFD mesh (as far as was possible) whilst maintaining an aspect ratio of at most 3:1. Corresponding reproductions of figures 7-40 to 7-44 are given below as figures 7-40a to 7-44a where this new data is referred to as semi-coarse for clarity.
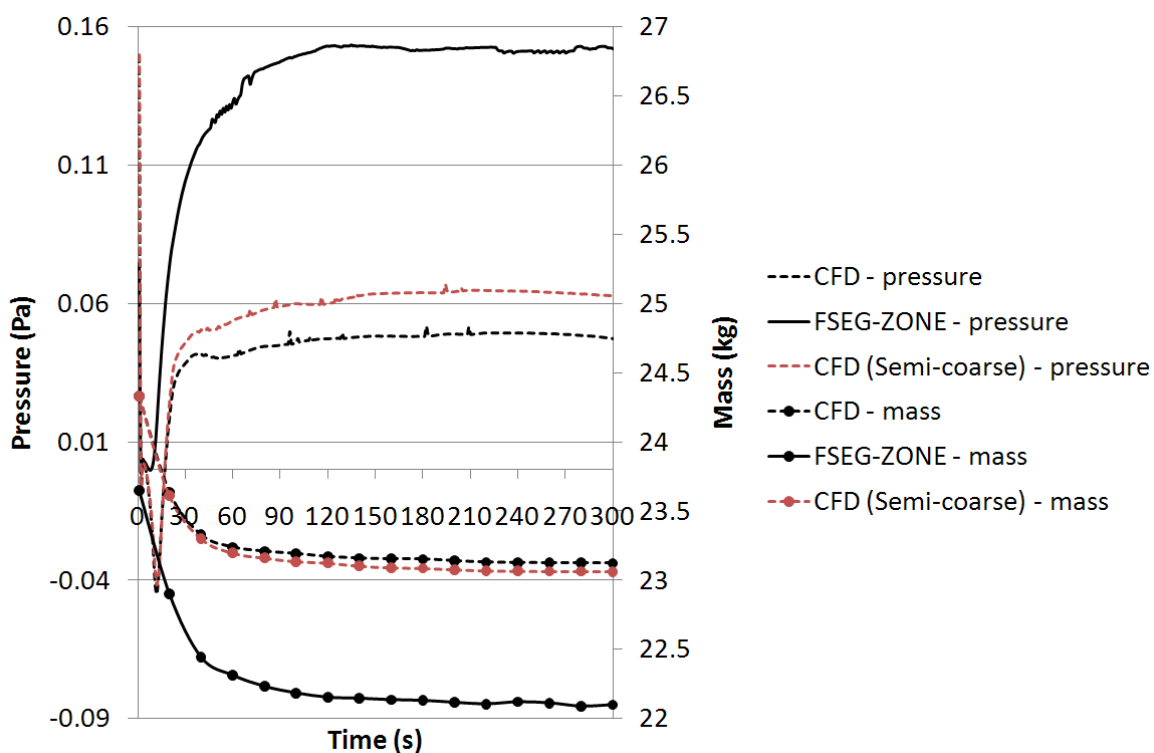
Figure 7-40a. Compartment pressure and mass comparisons.
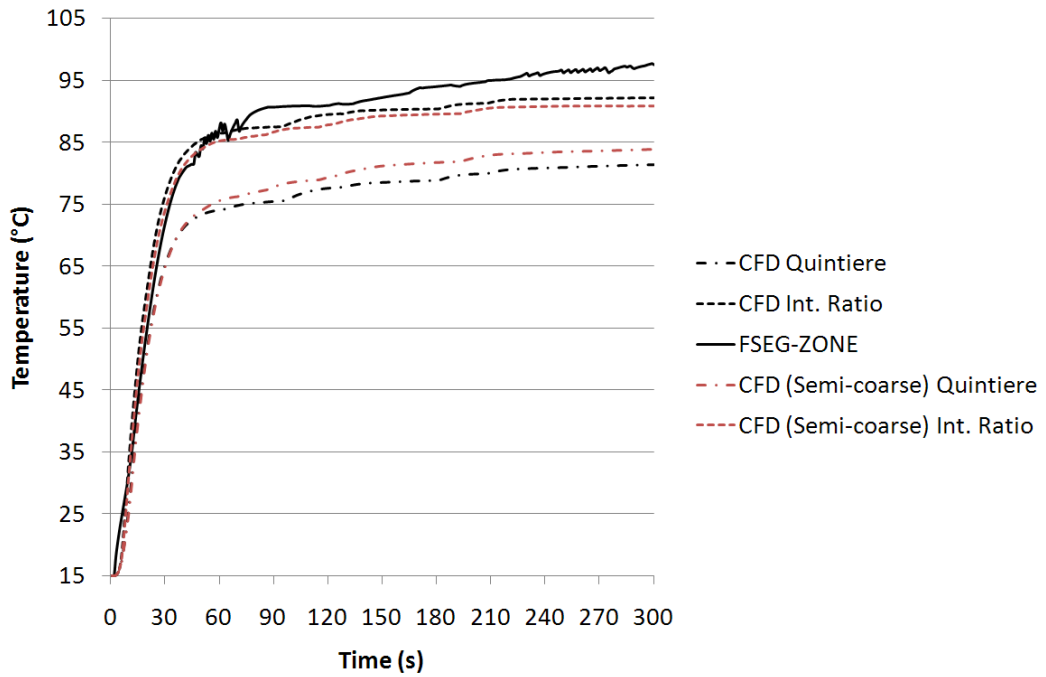
Figure 7-41a. Upper layer temperature comparisons.
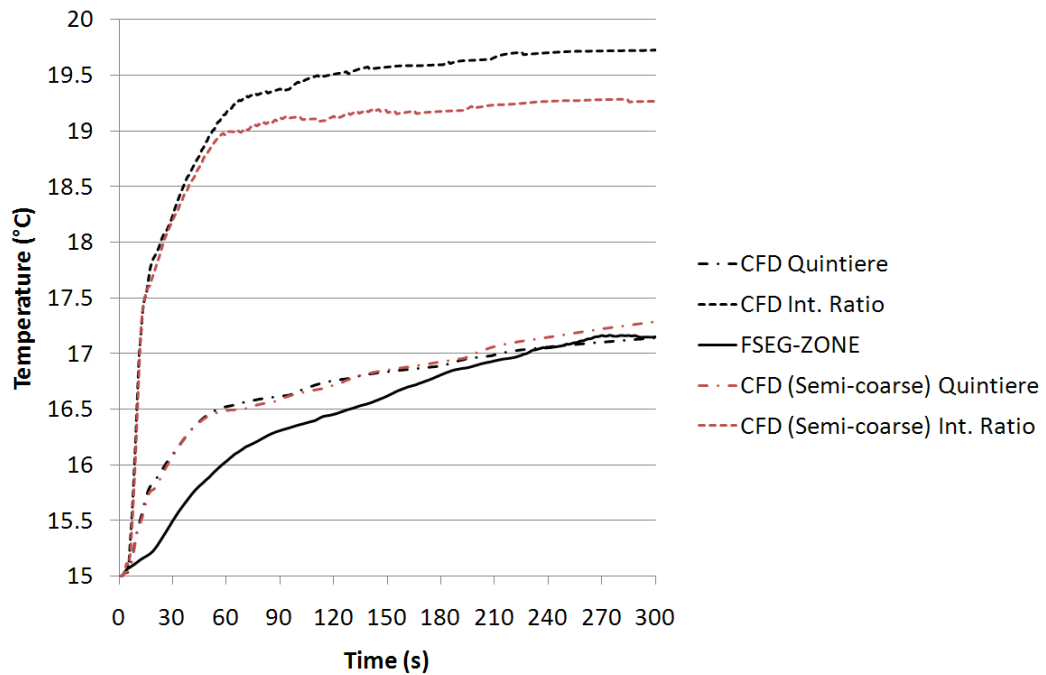
Figure 7-42a. Lower layer temperature comparisons.
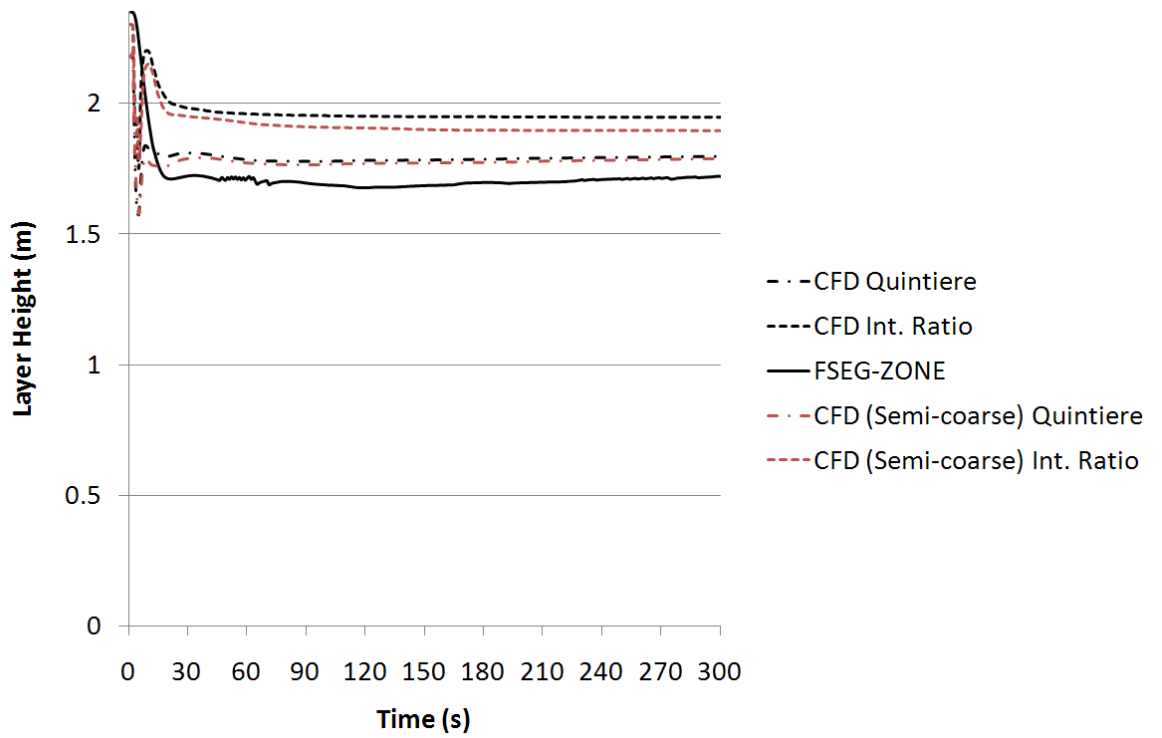
Figure 7-43a. Layer height comparisons.
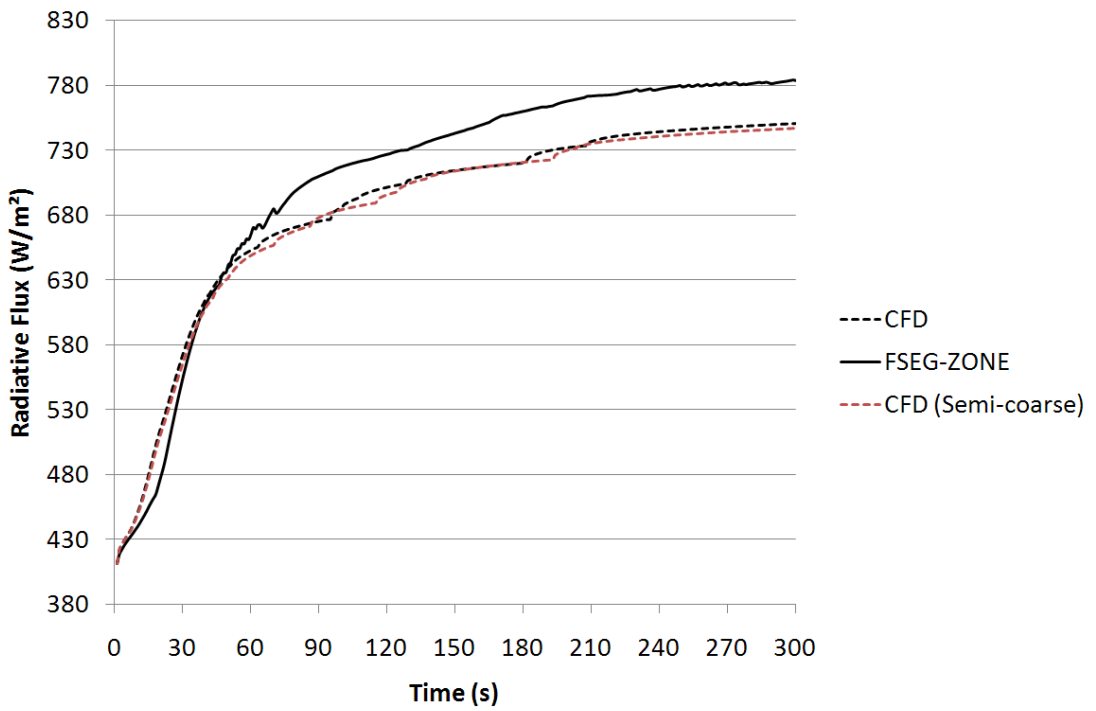
Figure 7-44a. Radiative flux comparisons.

What is immediately clear from the above comparisons is that the semi-coarse CFD simulation out-performs the hybrid model. In fact, the semi-coarse results are in exceptional agreement with the full resolution data, with only the range spanned by the layer reduction methods showing any noticeable differences (this is to be expected due to the reduced number of cells).

Despite being subjected to a (limited) reduction in resolution, the semi-coarse mesh is not really very coarse, and certainly not of a sufficient coarseness to compare with the timings of a zone model. In fact, the semi-coarse mesh still takes over three hours longer to complete (21 hourse 43 minutes) than both the previous coarse and hybrid simulations. An in-depth discussion of mesh quality is beyond the scope of this work, yet it is clear that significant savings in computational time can indeed be achieved whilst maintaining accuracy. Such considerations are extremely risky since sub-standard meshes clearly have grave consequences for accurate results, yet evaluating the magnitudes of such effects is not trivial. The hybrid model differs in this regard because there is no choice to be made of coarseness with its use, and therefore no potential of going 'too coarse'.

What is clear, and certainly of more interest to the present work, is that it is apparent that there is some point between the coarse and semi-coarse simulations at which the hybrid model begins to perform better than a coarse CFD simulation. The large wall-sized vent in this case posed some problems for the convergence in the hybrid model, but for the remainder of the test cases seen the hybrid model takes negligible time when compared to the CFD model. In this way it is reasonable to expect the hybrid model to out-perform a coarse CFD simulation at a point where the CFD model is still requiring a non-negligible excess of computational time. At this point the hybrid model can therefore simultaneously provide more accurate results whilst realising a saving in computational requirements.

8. Conclusions and Further Work

The development and implementation of a fully functional novel hybrid field/zone fire model has been comprehensively discussed, and numerous test cases have been performed and analysed. It is clear that such a hybrid model can provide accurate results whilst delivering substantial savings in the computational time required in performing simulations.

Summary

The thesis began by discussing at length the two existing fire models in common use today, and analysed their relevant advantages they bring as methodologies. It is clear that CFD modelling provides the most accurate results due to its basis on the actual physical phenomena concerned, yet can prove inhibitive with regards to the computational time required to run simulations. In comparison, the zone model has been demonstrated to have the capability to provide accurate results, but its basis on two, uniform layers means it leaves much to be desired with regards to phenomena that depend on spatial variation; also, it is simply not valid for use on certain geometries that inhibit an appreciable amount of stratification. The advantage of accepting these limitations is that the computational times required by zone model simulations are negligible in comparison to CFD models.

The idea of a hybrid field/zone fire model is deceptively simple. Is it possible to replace certain rooms in a CFD fire simulation with the zone model? The

answer to this question has been shown to be in the affirmative in this thesis and also in the publications by Burton et al. [Burton2007] [Burton2011], yet considerable effort has been required in doing so.

Initially a hybrid model combining the SMARTFIRE CFD model and the CFAST zone model was developed. In chapter 5 it was demonstrated that such a model was capable of providing acceptable results, although simultaneously highlighted a fundamental issue that changed the direction of the research. The different nature of these two models (implicit and explicit) and the corresponding difference in the time-steps required meant that the zone model could only be used if it had opportunity to equalize pressure with regards to its much finer resolution of time. Effectively the zone compartment needed to be exposed to a fixed pressure with which it could exchange mass and enthalpy, without consideration of the interface connecting it to the CFD domain. In practice this meant that the SMARTFIRE/CFAST hybrid model was only suitable for use when the zone compartments included vents (doors or windows) that were exclusively contained in the zone domain. Since these rooms already had at least one vent in the form of the hybrid interface, the condition above meant that single vent rooms were simply not suitable for simulation. The problem is that the majority of rooms of interest, especially those suitable for treatment with the zone model, are of the single door type, and windows cannot always be assumed to be open if indeed the room actually has any.

To counter this problem it was decided to develop a custom zone model to allow both a semi implicit formulation and greater control over the solution routine. The algorithm focussed on the use of a velocity correction term that allowed the interface velocities calculated by the CFD model to be modified between iterations.

The next issue centred on the comparisons that would naturally be required in validating the FSEG-ZONE model with CFD results. Since the two models presented data in different ways, it was necessary to somehow reduce the

CFD data to an equivalent data set. It became apparent that there was no objectively 'correct' way of doing this, and the performance of different methods was closely related to how the layer height was actually defined. As a result, two reduction methods were proposed that were expected to define an interval, in which the FSEG-ZONE results were likely to lie. Chapter 6 demonstrated that the FSEG-ZONE model performed surprisingly well on the various test cases considering its simple nature. It was also shown to perform better than either of the two simplistic alternatives of replacing the compartment in question with either an outlet or a wall patch.

The FSEG-ZONE model was then extended to address important phenomena of direct interest in fire simulations. First the model was modified to allow multiple interfaces on a single FSEG-ZONE room, meaning that two disjoint sections of the CFD domain could be connected by the zone model. This provided some encouraging results, although it was clear that the absence of momentum in the zone model meant that the transient nature of flow passing through the zone room was neglected; this resulted in the upper layer cooling quicker.

The next model development was the inclusion of convective heat transfer to surfaces, along with the necessary conduction within these solids. This highlighted an important difference between the models, specifically in their individual calculations of the convective coefficient. The effect of this was to ensure that more energy was removed from the layers of the FSEG-ZONE model, as compared to the SMARTFIRE field model, yet neither treatment is necessarily more correct. At present it is simply necessary to realise this discrepancy between the models, and to ensure that analysis of results is performed in full appreciation of the fact that neither method is inherently more accurate. Regardless of the differences observed in temperature, the layer height remained in close agreement.

The final additions of species transport, combustion, smoke and radiation culminated in a test case performed over a multi-room geometry. It was

shown that the FSEG-ZONE model demonstrated exceptional agreement with regards to the radiative flux considering its relatively simple nature. One weakness that was noted was that the re-ascension of a layer resulted in some premature surface cooling in the FSEG-ZONE model caused by the discrete treatment of its surfaces. The effect of this was to slightly underestimate the value of radiative flux, but only once the heat source had been removed (extinguished). The Multiroom case demonstrated that the hybrid model experienced no problems in dealing with multiple FSEG-ZONE compartments in close proximity. The species, combustion and smoke model additions were again demonstrated to be capable of providing results that were surprisingly very similar to those of the pure CFD simulation in SMARTFIRE.

Finally, the FSEG-ZONE model was compared with experimental results obtained from a physical fire simulation, and provided good results despite the unsuitability of the open wall configuration for treatment with a zone model. During this test case, the FSEG-ZONE model was also simultaneously compared to a coarse CFD simulation. From the results it was apparent that the FSEG-ZONE model outperformed the coarse CFD simulation which consistently underestimated all the variables. This was despite the fact that the level of coarseness used was limited by the meshing within SMARTFIRE, and the cell resolution was actually maintained in both the Y and Z directions. The one redeeming feature of the coarse CFD simulation was that it realised a saving in computational time of approximately 38%, compared to the 35% achieved through the FSEG-ZONE model. The likely reason for this difference was that the open wall configuration proved troublesome for the FSEG-ZONE model to achieve convergence over, resulting in slightly more work having to be performed during individual iterations.

Regardless, when considering the quality of the results, it would be prudent to accept the 3% differencing in timing to achieve the accuracy of the results provided by the FSEG-ZONE model.

Contribution to Knowledge

During the course of this work a novel 'integral ratio' reduction method, used to obtain a two layer equivalent data set from a CFD compartment, has been developed and employed in the comparisons that were made. The method itself appears to give more accurate results than the majority of existing methods, with the possible exception of He et al's reduction [He1998], although the stability and consistency of the integral ratio method was seen to be much better in this regard.

Previous work in the area of hybrid field/zone fire modelling has been limited and little detail of the implementations has been published. Of those results that have been published most are simply demonstrative and there is little or no comparison to either full-field or experimental results. The single comparison that is made in the work discussed in chapter two is for layer height alone, and is based on a simple visual check which is inherently subjective.

The details are sparse, but it appears that previous hybrid models have been written such that both field and zone model have been developed in parallel as part of a single entity. The difference between this approach and the alternative of combining a zone model with an existing CFD code was mentioned in chapter two, but it is safe to assume that fashioning a hybrid model in the former way can avoid many of the problems that will be experienced by the latter. The most obvious advantage is that the variables, by definition, will be identical thus avoiding issues of conservation. Possibly of greater importance to developing a perfect coupling is that the two models would naturally be part of the same solution structure, sharing both time-step and iteration regimes, and being simultaneously solved in a true fashion.

The work contained in this thesis developed a hybrid field and zone model that combined the zone model with an existing CFD code. This meant that a significant portion of work was required to address the issues inherent in this

approach, but the final result is a methodology that may prove more fruitful since it can be used to extend an in-use CFD code, making use of existing knowledge, previous work and the advantages that this can bring.

The first implementation discussed combined the explicit CFAST zone model with the implicit SMARTFIRE field model. Chapter 5 demonstrated that reasonable results can be obtained for 'open' situations, but that it is apparent that the combination of explicit and implicit models is not suitable for consideration of 'closed' cases.

To address this issue, a proprietary semi-implicit zone model was developed that allowed a novel solution method, based on a velocity correction, to be employed to solve 'closed' cases. It appears that the SMARTFIRE/FSEG-ZONE implementation is the first hybrid field/zone fire model to be functional in a practical sense, allowing simulations of general cases to be run in a simple and user-friendly manner, by making use of the existing SMARTFIRE GUI and the CFD engine. It is also the first time that a significant amount of results have been obtained and compared to full-field data, and the final test case was the first time that a hybrid model has been compared against experimental data. The comparisons have shown that the hybrid method compares very favourably considering the simplifications and assumptions made in employing a zone model.

The FSEG-ZONE model was extended, described in chapter seven, to include further phenomena of interest in a fire situation. This functionality is available in certain existing zone models, but the luxury of having the zone timing judged in relation to the CFD timing has meant that some of these considerations have been open to a more complex/accurate treatment than has previously been made. The semi-implicit nature of the FSEG-ZONE model has meant that it was necessary to develop and employ several novel approaches in the implementation that are not required by the explicit zone models that are available.

Finally, the hybrid model developed in this work has been the first to demonstrate consistent speed ups of the order expected in replacing sections of domain with the zone model without having a significant impact on solution consistency.

Further Work

In this section ideas for further work and model development that could not be fully explored due to time constraints are suggested.

- Any new model requires a significant amount of verification and validation if they are to be confidently used by third parties. A large portion of verification has been performed in this thesis, yet the cases required for validation work are limited. The next body of work with regards to the SMARTFIRE/FSEG-ZONE hybrid model should sensibly involve a substantial validation effort, along with a comprehensive analysis of configurations and geometries that are suitable for consideration. Again, the present work has been focused on the development and implementation of the model and its robustness with respect to the inclusion of all the sub-models.

- The developmental path of the FSEG-ZONE model was dictated by the realization that certain cases (closed rooms) were unsuitable for hybrid treatment through the earlier SMARTFIRE/CFAST hybrid model. This resulted in the development of the FSEG-ZONE model in order to address these compartments. Later developments have allowed the FSEG-ZONE model to act as a link between CFD domains, yet modelling an 'open' room in this manner is surely an unnecessary indulgence. The implementation of a link to the exterior, be it a window or door, should be developed within the FSEG-ZONE model to allow such an entity to exist exclusively within the zone domain. This

will naturally rely on a Bernoulli representation of velocity and the basis for such a method has already been developed.

- Although the FSEG-ZONE model at present allows the simulation of multiple single compartments connected to a CFD region it cannot address multiple interconnected zone compartments. This situation is addressed by the CFAST/SMARTFIRE hybrid model discussed in chapter 5, although this is limited to cases where the zone domain is itself directly connected to a fixed pressure (e.g. the exterior). The true strength of a hybrid model would be realised when the zone model is used to replace such large sections (legs/wings) of domain, consisting of multiple interconnected zone compartments. The solution method discussed in section 6.1.1 of this thesis has been based on a bisection solver, which is unsuited to the multi-dimensional nature of such configurations. Logically, the most substantial technical development to be made in the FSEG-ZONE model would be the implementation of a new solver capable of simultaneously solving such problems. The modular fashion of the FSEG-ZONE model should significantly reduce the amount of work required to do this. Both this and the previous point, along with the hybrid model in general, could benefit from a simplified treatment of momentum conservation within the zone portion of the domain. Whether such a treatment would be valid is uncertain, yet this development, if possible, could improve a fundamental limitation of the zone model.

- The method developed to address conduction within solids is capable of addressing complex conduction problems consisting of composite materials to a high degree of accuracy. The basis for the consideration of composite materials has already been developed, with the only required addition being a method to correctly calculate the conductivity at material discontinuities; this method requires verification. The solver used at present is simple since the requirements made of it have been minimal, and this can certainly be improved to achieve higher accuracy if necessary. Certainly the

implementation of a TDMA solver is the next natural step, although the timing benefits may not be so relevant in a hybrid environment. If significant levels of accuracy are required it may be necessary to develop a solution method that circumvents the numerical issues associated with very fine partitions of the solid.

- The hybrid model should be further developed to provide the same capability as the original CFD room being replaced by FSEG-ZONE model. One example would be the inclusion of relevant detectors within the zone model that can trigger secondary events, or even a primitive sprinkler system within the zone model itself. The action of opening or closing a door can theoretically be achieved at present through the use of time activated/deactivated obstruction in front of the hybrid interface. It would useful to implement this directly within the FSEG-ZONE model to maintain full control, and also to allow further capabilities. One of these would be the dynamic transition of CFD rooms to zone rooms and vice versa. It would be extremely useful if a CFD room that has reached a prescribed condition could be converted into the relevant zone compartment, and then progress in such a manner for the duration of the simulation. Conversely, it may prove useful to have the capability of converting a zone room into an equivalent CFD room if the potential for complex flow conditions begins to develop.

References

[Abanto2007]   Abanto, J., Reggio, M., Barrero, D., Petro, E., 2007. "Prediction of fire and smoke propagation in an underwater tunnel", *Tunnelling and Underground Space Technology*, 22(1), pp.90-95. doi:10.1016/j.tust.2005.10.006

[Arvidson2008]   Arvidson, M., Axelsson, J., Hertzberg, T., 2008. "Large-scale fire tests in a passenger cabin," *Fire Technology*, SP Report 2008:33.

[Atreya1992]   Atreya, A., 1992. "Convection Heat Transfer," *SFPE Handbook of Fire Protection Engineering*, DiNenno, P.J., ed., National Fire Protection Association and The Society of Fire Protection Engineers, Quincy, MA, 2003, ch.1-3.

[Babrauskas1978]   Babrauskas, V., Williamson, R., 1978. "Post-flashover compartment fires: Basis of a theoretical model," *Fire and Materials*, 2(2), pp.39–53. DOI: 10.1002/fam.810020202

[Babrauskas1981]   Babrauskas, V., 1981. "A Closed-form Approximation for Post Flashover Compartment Fire Temperatures," *Fire Safety Journal*, 4, pp.63-73.

[Babrauskas1991]   Babrauskas, V., Levin, B.C., Gann, R.G., Paabo, M., Harris, R. H., Peacock, R.D., Yusa, S., 1991. "Toxic potency measurement for fire hazard analysis", Special Pub. 827, NIST.

[Babrauskas1995]   Babrauskas, V., 1995. "The Generation of CO in Bench-scale Fire Tests and the Prediction for Realscale Fires", *Fire and Materials*, 19, pp.205-213.

References

[Boris1992] Boris, J.P., Grinstein, F.F., Oran, E.S., Kolbe, R.L., 1992. "New insights into large eddy simulation", *Fluid Dynamics Research*, 10(4-6), doi:10.1016/0169-5983(92)90023-P

[Boussinesq1877] Boussinesq, J., 1877. "Théorie de l'Écoulement Tourbillant," *Academie Royale des Sciences de l'Institut de France*, 23, pp.46-50.

[Brenan1989] Brenan, K.E., Campbell, S.L., Petzold, L.R., 1989 "Numerical Solution of Initial-Value Problems in Differential-Algebraic Equations," Elsevier Science Publishing, New York.

[Brent1973] Brent, R.P., 1973. "Algorithms for Minimization without Derivatives," Chapter 4, Prentice-Hall, Englewoods Cliffs, NJ, ISBN 0-13-022335-2

[Brushlinsky2006] Brushlinsky, N.N., Sokolov, S.V., Wagner, P., Hall, J.R., 2006. "World fire statistics," Report No 10 of Centre of Fire Statistics, International Association of Fire and Rescue Services, Moscow - Berlin June 2006.

[Bukowski1996] Bukowski R., 1996. "Applications of FASTlite," Proceedings of Computer Applications in Fire Protection Engineering, Technical Symposium, June 20-21, 1996, Worcester, MA.

[Burton2007] Burton, D.J., Grandison, A.J., Patel, M.K., Galea, E.R., Ewer, J.C., 2007. "Introducing a hybrid field/zone fire modelling approach for fire simulation, " *Interflam 2007*, Interscience Communications, 2007, pp.1491-1497.

[Burton2011] Burton, D.J., Grandison, A.J., Patel, M.K., Galea, E.R., Ewer, J.C., 2011 (in press). "Development of a Hybrid Field/Zone Fire Model," *IAFSS Symposium Proceedings,* 10, http://iafss.haifire.com/html/iafss/symposium/10/abstracts/10-126.htm

[Chen2011] Chen, F., Leong, J.C., 2011. "Smoke flow phenomena and turbulence characteristics of tunnel fires," *Applied Mathematical Modelling*, 35(9), pp.4554-4566. doi:10.1016/j.apm.2011.03.033

References

[Chow1995]   Chow, W.K., 1995. "A comparison of the use of fire zone and field models for simulating atrium smoke-filling processes," *Fire Safety Journal*, 25(4), pp.337-353. doi:10.1016/0379-7112(96)00001-X

[Chow1996]   Chow, W.K., 1996. "Simulation of tunnel fires using a zone model," *Tunnelling and Underground Space Technology*,
11(2), pp.221-236. doi:10.1016/0886-7798(96)00012-0

[Colella2010]   Colella, F., 2010. "Multiscale Modelling of Tunnel Ventilation Flows and Fires," PhD thesis, Politecnico di Torino, Dipartimento di Energetica.

[Cooper1982]   Cooper, L., Harkleroad, M., Quintiere, J., Rinkinen, W., 1982. "An Experimental Study of Upper Hot Layer Stratification in Full-Scale Multiroom Fire Scenarios," *Journal of Heat Transfer*, 104, pp.741-749.

[Courant1928]   Courant, R., Friedrichs, K., Lewy, H. 1928. "Über die partiellen Differenzengleichungen der mathematischen Physik," *Mathematische Annalen*, 100(1), pp.32-74. doi:10.1007/BF01448839

[Cox1995]   (Ed)Cox, G., 1995. "Combustion Fundamentals of Fire", Academic Press. ISBN-10: 0121942304

[DCLG2010]   Fire statistics monitor. April 2009 to March 2010. Issue No. 03/10. Department for Communities and Local Government: London.

[DCLG2011]   The economic cost of fire: estimates for 2008. Fire research report 3/2011. Department for Communities and Local Government: London.

[Dembsey1995]   Dembsey, N.A., Pagni, P.J., Williamson, R.B., 1995. "Compartment fire experiments: Comparison with models," *Fire Safety Journal*, 25(3), pp.187-227. doi:10.1016/0379-7112(96)00002-1

[Edwards1985]   Edwards, D.K., 1985. "Radiation Properties of Gases," *Handbook of Heat Transfer Fundamentals*, Rohsenow, W.M., ed., McGraw-Hill Book Company, pp.74-75.

[Emmerich1998]   Emmerich, S.J., McGrattan, K.B., 1998. "Application of

Large Eddy Simulation Model to Study Room Airflow," *ASHRAE Transactions*, 104(1), pp.1-9.

[Emmons1989]   Emmons, H. W., 1989. Vent Flows. SFPE Handbook for Fire Protection Engineering, 2, pp.40-49

[Esmaeilz.2011]   Esmaeilzadeh, H., Blem, E., St. Amant, R., Sankaralingam, K., Burger, D., 2011, "Dark Silicon and the End of Multicore Scaling," *Proceedings of the 38th International Symposium on Computer Architecture*, San Jose, California, USA.

[Ewer2008]   Ewer, J., Jia., F., Grandison, A., Galea, E., Patel, M., 2008. "SMARTFIRE V4.1, Technical Reference Manual," Fire Safety Engineering Group, University of Greenwich, United Kingdom.

[Fan1992]   Fan, W., Yan, Z., Huo, R., Chen, Y., Zhao, H., 1992. "A Combined Field-Zone Model for Compartment Fire," *Proceedings of the first Asia-Oceania Symposium on Fire Safety Science and Technology*, pp.300-305.

[Fan1997]   Fan, W., Wang, X., 1997. "A New Numerical Calculation Method for Zone Modelling to Predict Smoke Movement in Building Fires," *Proceedings of the Fifth International Symposium*, International Association of Fire Safety Science, pp.487-598.

[Floyd2009]   Floyd, J.E., McGrattan, K.B., 2009. "Extending the mixture fraction concept to address under-ventilated fires," *Fire Safety Journal*, 44(3), pp.291-300. doi:10.1016/j.firesaf.2008.07.002

[Galaj2009]   Galaj, J., 2009. "A General Concept of Fire Hybrid Modelling in Compartments," *Journal of Civil Engineering and Management*, 15(3), pp.237-245.

[Galea1989]   Galea, E.R., 1989. "On the field modelling approach to the simulation of enclosure fires", *Journal of Fire Protection Engineering*, 1(1), pp.11-22.

[Galea2004]   Galea, E.R., Gwynne, S., Lawrence, P.J., Filippidis, L., Blackshields, D., Cooney, D., 2004. *buildingEXODUS V4.0 User Guide and Technical Manual*, University of Greenwich.

[Grandison2003]   Grandison, A.J., Galea, E.R., Patel M.K., Ewer, J.,

References

2003-2004. "The Development of Parallel Implementation for a CFD based fire field model utilising conventional office based PCs", *Journal of Applied Fire Science*, 12(2), pp.137-157.

[Grandison2003b]   Grandison, A., 2003. "Improving the regulatory acceptance and numerical performance of CFD based fire modelling software," PhD Thesis, University of Greenwich, London.

[Grandison2007]   Grandison, A.J., Galea, E.R., Patel, M.K., Ewer, J., 2007. "Parallel CFD fire modelling on office PCs with dynamic load balancing", *International Journal for Numerical Methods in Fluids*, 55(1), pp.29–39. doi: 10.1002/fld.1278

[Gutiérrez 2009]   Gutiérrez-Montes, C., Sanmiguel-Rojas, E., Viedma, A., Rein, G., 2009. "Experimental data and numerical modelling of 1.3 and 2.3 MW fires in a 20 m cubic atrium", *Building and Environment*, 44(9), pp.1827-1839. doi:10.1016/j.buildenv.2008.12.010

[Hadjisoph.2005]   Hadjisophocleous, G.V., McCartney, C.J., 2005. "Guidelines for the use of CFD simulations for fire and smoke modelling," *ASHRAE Transactions*, 111(2), pp.583-594.

[He1998]   He, Y., Fernando, A., Luo, M., 1998, "Determination of Interface Height from Measured Parameter Profile in Enclosure Fire Experiment," *Fire Safety Journal*, 31, pp.19-38.

[Hostikka2006]   Hostikka, S., McGrattan, K., 2006. "Numerical modeling of radiative heat transfer in water sprays", *Fire Safety Journal*, 41, pp.76-86. doi:10.1016/j.firesaf.2005.09.003

[Howell1982]   Howell, J.R., "A Catalogue of Radiation Heat Transfer Configuration Factors." Available in web format at http://www.engr.uky.edu/rtl/Catalog/.

[Hua2005]   Hua, J., Wang,. J., Kumar, K., 2005. "Development of a hybrid field and zone model for fire smoke propagation simulation in buildings," *Fire Safety Journal*, 40, pp.99-119.

[Hurst2004]   Hurst-Clark, N.M., Ewer, J., Grandison, A.J., Galea,

E.R., 2004. "Group Solvers: A Means of Reducing Run-Times and Memory Overheads for CFD Based Fire Simulation Software", *Interflam'04 Conference Proceedings*, 1, pp.659-664.

[Incropera2006]   Incropera, F.P., DeWitt, D.P., Bergman, T.L., Lavine, A.S., 2006. "Fundamentals of Heat and Mass Transfer, Sixth Edition," John Wiley & Sons, New Jersey, USA.

[ISO1993]   ISO 9705, 1993. *Full Scale Room Test for Surface Products*, International Standards Organisation, Geneva, Switzerland.

[Janssens1992]   Janssens, M., Tran, H., 1992, "Data Reduction of Room Tests for Zone Model Validation," *Journal of Fire Sciences*, 10(6), pp.528-555.

[Jia1997]   Jia, F., Galea, E.R., Patel, M.K., 1997. "Simulating Flashover and Backdraft Type Events Using Fire Field Models - A First Approximation", *Journal of Fire Protection Engineering*, 9, pp.1-17.

[Jia2006]   Jia F., Patel, M.K., Galea, E.R., Grandison, A., Ewer, J., 2006. "CFD Fire Simulation of the Swissair Flight 111 In-flight Fire – Part II: Fire Spread within the Simulated Area", *The Aeronautical Journal of the Royal Aeronautical Society*, 110(1107), pp.303-314.

[Jones1985]   Jones, W.W., 1985. "A multicompartment model for the spread of fire, smoke and toxic gases," *Fire Safety Journal*,
9(1), pp.55-79. doi:10.1016/0379-7112(85)90030-X

[Jones1992]   Jones, W.W., Matsushita, T., Baum, H.R., 1992. "Smoke Movement in Corridors: Adding the Horizontal Momentum Equation to a Zone Model," U.S./Japan Government Cooperative Program on Natural Resources, Fire Research and Safety. 12th Joint Panel Meeting. October 27-November 2, 1992, Tsukuba, Japan, Building Research Institute, Ibaraki, Japan Fire Research Institute, Tokyo, Japan, pp.42-54.

[Jones2001]   Jones, W.W., 2001. "State of the Art in Zone Modeling of Fires," *Proceedings of the 9th International Fire Protection Seminar, Engineering Methods for Fire Safety*. Munich, Germany, A.4/pp.89-126.

References

[Jones2009]	Jones, W.W., Peacock, R.D., Forney, G.P., Reneke, P.A., 2009. "CFAST – Consolidated Model of Fire Growth and Smoke Transport (Version 6), Technical Reference Guide," NIST Special Publication 1026, National Institute of Standards and Technology.
[Kawagoe1958]	Kawagoe, K., Fire Behaviour in Rooms, Building Research Institute, Ministry of Construction (Japan), Report No.27, Tokyo.
[Kerrison1994]	Kerrison, L., Galea, E.R., Hoffmann, N., Patel, M. K., 1994. "A Comparison of a FLOW3D Based Fire Field Model with Experimental Room Fire Data," *Fire Safety Journal*, 23, pp.387-411.
[Kerrison1994b]	Kerrison, L., Mawhinney, N., Galea, E.R., Hoffmann, N., Patel, M.K.; "A Comparison of Two Fire Field Models with Experimental Room Fire Data."; *Proceedings of the 4th International Symposium on Fire Safety Science*, pp.161-172.
[Keski2002]	Keski-Rahkonen, O., Hostikka, S., 2002. "Zone Model Validation of Room Fire Scenarios," International Collaborative Project to Evaluate Fire Models for Nuclear Power Plant Applications, Gaithersburg, MD, May 2-3, 2002.
[Lecocq2011]	Lecocq, G., Richard, S., Colin, O., Vervisch, L., 2011. "Hybrid presumed pdf and flame surface density approaches for Large-Eddy Simulation of premixed turbulent combustion: Part 1: Formalism and simulation of a quasi-steady burner," *Combustion and Flame*, 158(6), pp.1201-1214. doi:10.1016/j.combustflame.2010.09.023
[Lee2010]	Lee, Y.H., Kim, J.H., Yang, J.E., 2010. "Application of the CFAST zone model to the Fire PSA," *Nuclear Engineering and Design*, 240(10), pp.3571-3576. doi:10.1016/j.nucengdes.2010.04.035
[Liu2002]	Liu, F., Wen, J.X., 2002. "The effect of turbulence modelling on the CFD simulation of buoyant diffusion flames", *Fire Safety Journal*, 37(2), pp.125-150. doi:10.1016/S0379-7112(01)00022-4

References

[Luo1994]	Luo, M., Beck, V., 1994. "The fire environment in a multi-room building— comparison of predicted and experimental results", *Fire Safety Journal*, 23(4), pp.413-438. doi:10.1016/0379-7112(94)90006-X
[Luo1996]	Luo, M., Beck, V., 1996. "Flashover fires in a full scale building: prediction and experiment", *Proceedings Interflam'96*, Compiled by C.Franks and S Grayson, pp.361-370. ISBN: 0 9516320 9 4
[Markatos1984]	Markatos, N.C., Cox, G., 1984. "Hydrodynamics and Heat Transfer in Enclosures", *Physicochemical Hydrodynamics*, 5, pp.53-66.
[McCaffrey1981]	McCaffrey, B.J., Quintiere, J.G., Herkleroad, M.F., 1981. "Estimating Room Fire Temperatures and the Likelihood of Flashover Using Fire Test Data Correlations," *Fire Technology*, 17(2), pp.98-119.
[McGrattan1998]	McGrattan, K.B., Baum, H.R., Rehm, R.G., 1998. "Large Eddy Simulations of Smoke Movement," *Fire Safety Journal*, 30, pp.161-178.
[McGrattan2001]	McGrattan, K. B., Baum, H. R., Rehm, R. G., Hamins, A., Forney, G. P., Floyd, J. E., Hostikka, S., 2001. "Fire Dynamics Simulator (Version 2) – Technical Reference Guide", NISTIR 6783.
[McGrattan2010]	McGratten, K., Hostikka, S., Floyd, J., McDermott, R., 2010. "Fire Dynamics Simulator (Version 5) – Technical Reference Guide, Volume 3: Validation", NIST Special Publication 1018-5.
[Miles2004]	Miles, S., 2004, "International Panel Report on Benchmark Exercises # 2 – Pool Fires in Large Halls," International Collaborative Project to Evaluate Power Plant Applications, BRE client report number 212214.
[Milne1973]	Milne-Thomson, L.M., 1973. "Theoretical Aerodynamics", Dover Publications. ISBN: 048661980X
[Mitler1987]	Mitler, H.E., Rockett, J.A., 1987. "Users' Guide to FIRST, A Comprehensive Single-Room Fire Model," National Bureau of Standards, Gaithersburg, MD CIB W14/88/22, NBSIR 87-3595.

References

[Nelson1991]	Nelson, H.E., Deal, S., 1991. "Comparing Compartment Fires with Compartment Fire Models," *Proceedings of the 3rd International Symposium on Fire Safety Science*, 719.
[Pape1981]	Pape R., Waterman T.E., Eichler T.V., 1981. "Development of a Fire in a Room from Ignition to Full Room Involvement – RFIRES," National Bureau of Standards, NBS-GCR-81-301, Washington.
[Patankar1980]	Patankar S.V., 1980. "Numerical Heat Transfer and Fluid Flow", Taylor & Francis Publishing. ISBN-10: 0891165223
[Peacock1988]	Peacock, R.D., Davis, S., Lee, B.T., 1988. "An Experimental Data Set for the Accuracy Assessment of Room Fire Models," National Bureau of Standards, NBSIR 88-3752, pp.12
[Peacock1993]	Peacock, R.D., Jones, W.W., Bukowski, R.W., 1993. "Verification of a Model of Fire and Smoke Transport," *Fire Safety Journal*, 21(2), pp.89-129. doi:10.1016/0379-7112(93)90038-R
[Peacock2008]	Peacock, R.D., Jones, W.W., Reneke, P.A., Forney, G.P., 2008. "CFAST – Consolidated Model of Fire Growth and Smoke Transport (Version 6) User's Guide," NIST special Publication 1041.
[Pitts1995]	Pitts, W.M., 1995. "The Global Equivalence Ratio concept and the formation mechanisms of carbon monoxide in enclosure fires," *Progress in Energy and Combustion Science*, 21, pp.197-237.
[Powell1988]	Powell, M.J.D., 1988. "A hybrid method for non-linear equations," *Numerical Methods for Nonlinear Algebraic Equations*, P. Rabinowitz, ed., Gordon and Breach, New York.
[Purser2003]	Purser, D., Purser, J., 2003. "The potential for including fire chemistry and toxicity in fire safety engineering", BRE Client report 202804.
[Quintiere1977]	Quintiere, J., 1977. "Growth of Fires in Building Compartments," ASTM STP 614, American Society for Testing and Materials, Philadelphia, PA

References

[Quintiere1984]   Quintiere, J.G., Steckler, K.D., Corley, D., 1984. "An Assessment of Fire Induced Flows in Compartments," *Fire Science and Technology*, 4(1).

[Reynolds1894]   Reynolds, O., 1894. "On the Dynamical Theory of Incompressible Viscous Fluids and the Determination of the Criterion," *Philosophical Transactions of The Royal Society of London*, 186, pp.123-164.

[Keski2002]   Keski-Rahkonen, O., Hostikka, S., 2002. "Zone Model Validation of Room Fire Scenarios," International Collaborative Project to Evaluate Fire Models for Nuclear Power Plant Appplications, Gaithersburg, MD.

[Rosten1983]   Rosten, H.I., Spalding, D.B., Tatchell, D.G., 1983. "PHOENICS: A General-Purpose Program for Fluid-Flow, Heat-Transfer and Chemical-Reaction Processes", *Proceedings of the 3rd International Conference on Engineering Software*, pp.639-655.

[Rubini1997]   Rubini, P.A., 1997. "SOFIE - Simulation of Fires in Enclosures", *Proceedings of 5th International Symposium on Fire Safety Science*, International Association for Fire Safety Science, ISBN: 4-9900625-5-5.

[SFPE2010]   Guidelines for Substantiating a Fire Model for a Given Application, Society of Fire Protection Engineers, 2010.

[Simcox1992]   Simcox, S., Wilkes, N.S., Jones, I.P., 1992. "Computer Simulation of the Flows of Hot Gases from the Fire at Kings Cross Underground Station", *Fire Safety Journal*, 18, pp.49-73.

[Spearpoint2003]   Spearpoint, M.J., 2003. "Integrating the IFC Building Product Model with Zone Fire Simulation Software," Department of Civil Engineering, University of Canterbury, Christchurch, New Zealand.

[Spearpoint2006]   Spearpoint, M.J., 2006. "Fire Engineering Properties in the IFC Building Project Model and Mapping to Branzfire," Department of Civil Engineering, University of Canterbury, Christchurch, New Zealand.

[Steckler1982]   Steckler, K.D., Quintiere, J.G., Rinkinen, W.J., 1982. "Flow Induced by Fire in a Compartment," NBSIR 82-

References

2520, National Bureau of Standards.

[Tanaka1980]	Tanaka, T., (1977,1978,1980). "A Mathematical Model of a Compartment Fire," Building Research Institute (Japan) Reports 70, 79, 84.
[Thomas1963]	Thomas, P.H., Hinkley, P.L., Theobald, C.R., Simms, D.L., 1963. "Investigations into the flow of hot gases in roof venting," Fire Research Technical Paper No. 7, London, UK: ministry of Technology.
[Tien2002]	Tien, C.L., Lee, K.Y., Stretton, A.J., 2002. "Radiation Heat Transfer," *SFPE Handbook of Fire Protection Engineering*, DiNenno, P.J., ed., National Fire Protection Association and The Society of Fire Protection Engineers, ch.1-4.
[Versteeg2007]	Versteeg, H.K., Malalasekera, W., 2007. "An introduction to computational fluid dynamics, the finite volume method," 2nd ed. Pearson Prentice Hall, Glasgow.
[Wade2004]	Wade, C.A., 2004 (revised). "BRANZFIRE Technical Reference Guide," BRANZ Study Report No 92, Building Research Association of New Zealand, Judgeford.
[Wang1996]	Wang, J., Fan, W., 1996. "Numerical Simulation of Fire Process of Multi-rooms," *Journal of University of Science and Technology*, 26, pp.204-209.
[Wang2001]	Wang, Z., Jia, F., Galea, E.R., Patel, M.K., Ewer, J,, 2001. "Simulating one of the CIB W14 round robin test cases using the SMARTFIRE fire field model", *Fire Safety Journal*, 36, pp.661-677.
[Wang2007]	Wang, L., Chen, Q., 2007. "Theoretical and Numerical Studies of Coupling Multizone and CFD Models for Building Air Distribution Simulations," *Indoor Air*, 17, pp.348-361.
[Wang2007b]	Wang Z., Jia F., Galea, E.R., 2007. "Predicting toxic gas concentrations resulting from enclosure fires using local equivalence ratio concept linked to fire field models," *Fire and Materials*, 31(1), pp.27-51.
[Wang2011]	Wang, G., Boileau, M., Veynante, D., 2011.

References

"Implementation of a dynamic thickened flame model for large eddy simulations of turbulent premixed combustion," *Combustion and Flame*, Article in Press, Corrected Proof. doi:10.1016/j.combustflame.2011.04.008

[Weaver2000]   Weaver, S., 2000, "A Comparison of Data Reduction Techniques for Zone Model Validation," Fire Engineering Research Report 2000/12, ISSN 1173-5996, University of Canterbury, Christchurch, New Zealand.

[Wilcox1994]   Wilcox, D.C., 1994. "Turbulence Modeling for CFD," DCW Industries, Inc., La Cañada, California.

[Xu1991]   Xu, T., Wang, J., Fan, W., 1991. "A New Method of Modeling of a Fire – Combination of Field Modeling and Zone Modeling," *Proceedings of the Symposium on Engineering Thermophysics*, ZhenJiang, China.

[Xue2001]   Xue, H., Ho, J.C., Cheng, Y.M., 2001. "Comparison of different combustion models in enclosure fire simulation" *Fire Safety Journal*, 36(1), pp.37-54. doi:10.1016/S0379-7112(00)00043-6

[Yan2001]   Yan, Z., Holmstedt, G., 2001. "Investigation of the dance hall fire in Gothenburg, October 1998 – a comparison between human observation and CFD simulation", *Proceedings of the 9th International Symposium on Fire Safety Science*, pp.951-963.

[Yang2005]   Yang, R., Weng, W.G., Fan, W.C., Wang, Y.S., 2005. "Subgrid scale laminar flamelet model for partially premixed combustion and its application to backdraft simulation," *Fire Safety Journal*, 40(2), pp.81-98. doi:10.1016/j.firesaf.2004.09.004

[Yao1999]   Yao, J., Fan, W., Kohyu, S., Daisuke, K., 1999. "Verification and application of field-zone-network model in building fire," *Fire Safety Journal*, 33, pp.35-44.

[Yeoh1995]   Yeoh, G.H., Chandrasekaran, V., Leonardi, E., 1995. "Numerical Prediction of Fire and Smoke," *AIRAH Journal*, 49, pp13-18.

[Yeoh2003]   Yeoh, G.H., Yuen, R.K., Lo, S.M., Chen, D.H., 2003. "On numerical comparison of enclosure fire in a multi-

compartment building", *Fire Safety Journal*, 38(1), pp.85-94. doi:10.1016/S0379-7112(02)00032-2

Appendix 1 – View Factor Formulas

The calculations for view factors in this section are taken from 'A Catalogue of Radiation Heat Transfer Configuration Factors' by J.R. Howell, available in web format at http://www.engr.uky.edu/rtl/Catalog/.

Equal, directly opposed surfaces

For two equal sized and perfectly opposite parallel surfaces as in figure A1-1
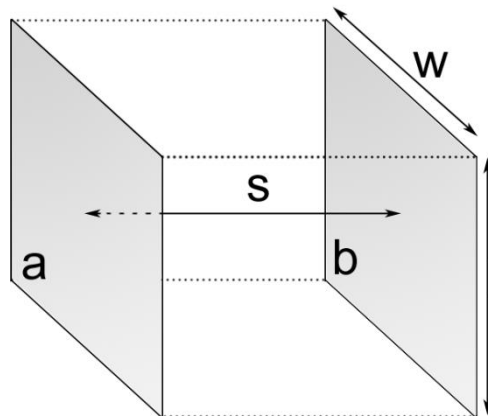
Figure A1-1. Equal, directly opposed surfaces

letting

$$x = \frac{w}{s} \quad , \quad y = \frac{l}{s} \tag{A1.1}$$

the view factor can be calculated from

$$F_{a,b} = \frac{2}{\pi xy} \left[ln \sqrt{\frac{(1+x^2)(1+y^2)}{1+x^2+y^2}} - y \tan^{-1} y - x \tan^{-1} x \right.$$
$$+ y\sqrt{1+x^2} \tan^{-1} \frac{y}{\sqrt{1+x^2}}$$
$$\left. + x\sqrt{1+y^2} \tan^{-1} \frac{x}{\sqrt{1+y^2}} \right]$$

(A1.2)

Arbitrary parallel surfaces

For two arbitrary parallel surfaces as in figure A1-2
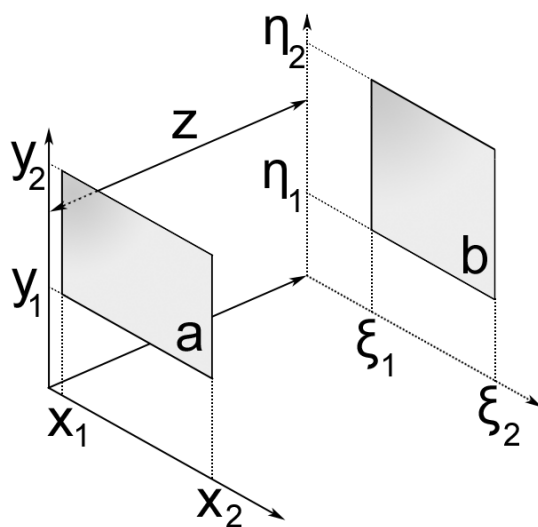
Figure A1-2. Arbitrary parallel surfaces.

the view factor can be calculated from

$$F_{a,b}$$

$$= \frac{1}{(x_2 - x_1)(y_2 - y_1)} \sum_{l=1}^{2} \sum_{k=1}^{2} \sum_{j=1}^{2} \sum_{i=1}^{2} (-1)^{(i+j+k+l)} G(x_i, y_j, \eta_k, \xi_l) \quad \text{(A1.3)}$$

where

$$G(x, y, \eta, \xi)$$

$$= \frac{1}{2\pi} \left[(y - \eta)\sqrt{(x - \xi)^2 + z^2} \tan^{-1}\left(\frac{y - \eta}{\sqrt{(x - \xi)^2 + z^2}}\right) \right.$$

$$+ (x - \xi)\sqrt{(y - \eta)^2 + z^2} \tan^{-1}\left(\frac{x - \xi}{\sqrt{(y - \eta)^2 + z^2}}\right)$$

$$\left. - \frac{z^2}{2} ln((x - \xi)^2 + (y - \eta)^2 + z^2) \right] \quad \text{(A1.4)}$$

Perpendicular surfaces with a common edge

For two perpendicular surfaces that share one edge of equal length as in figure A1‑3
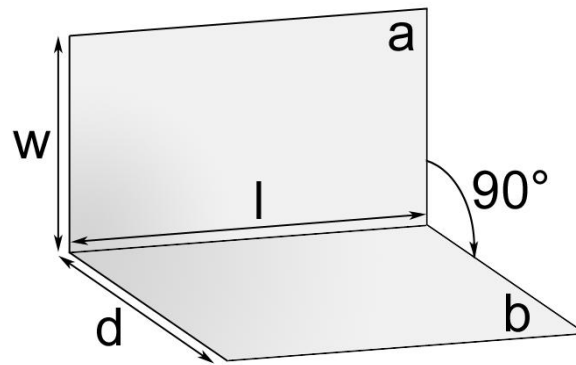
Figure A1-3. Perpendicular surfaces with common edge

letting

$$x = \frac{d}{l} \quad , \quad y = \frac{w}{l}$$ (A1.5)

the view factor can be calculated from

$F_{a,b}$

$$= \frac{1}{y\pi}\left(y\tan^{-1}\frac{1}{y} + x\tan^{-1}\frac{1}{x} - \sqrt{x^2+y^2}\,\tan^{-1}\sqrt{\frac{1}{x^2+y^2}} \right.$$

$$\left. + \frac{1}{4}\ln\left(\frac{(1+y^2)(1+x^2)}{1+y^2+x^2}\left[\frac{y^2(1+y^2+x^2)}{(1+y^2)(y^2+x^2)}\right]^{y^2}\left[\frac{x^2(1+y^2+x^2)}{(1+x^2)(y^2+x^2)}\right]^{x^2} \right)\right)$$ (A1.6)

Arbitrary perpendicular surfaces

For two arbitrary perpendicular surfaces as in figure A1-4
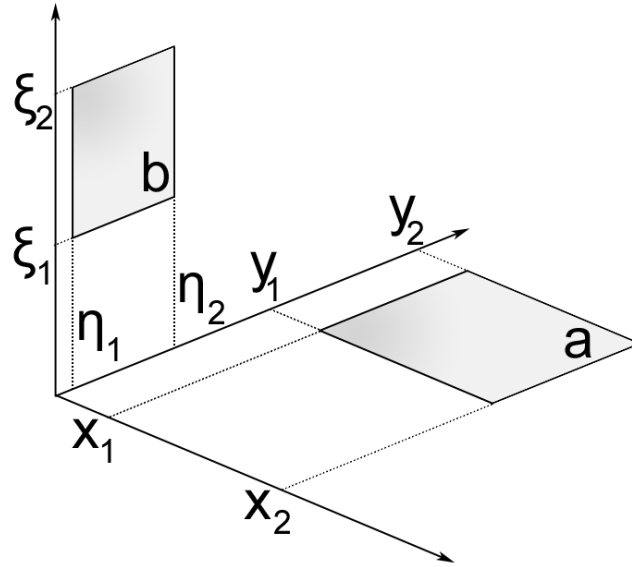
Figure A1-4. Arbitrary perpendicular surfaces.

the view factor can be calculated from

$$
\begin{aligned}
&F_{a,b} \\
&= \frac{1}{(x_2 - x_1)(y_2 - y_1)} \sum_{l=1}^{2} \sum_{k=1}^{2} \sum_{j=1}^{2} \sum_{i=1}^{2} (-1)^{(i+j+k+l)}\, G\left(x_i, y_j, \eta_k, \xi_l\right)
\end{aligned}
\qquad \text{(A1.7)}
$$

where

$$G(x,y,\eta,\xi) = \frac{1}{2\pi}\left[(y-\eta)\sqrt{x^2+\xi^2}\tan^{-1}\frac{(y-\eta)}{\sqrt{x^2+\xi^2}}\right.$$

$$-\frac{1}{4}\left[(x^2+\xi^2)ln\left(1+\frac{(y-\eta)^2}{x^2+\xi^2}\right)\right.$$

$$\left.\left.-(y-\eta)^2 ln\left(1+\frac{x^2+\xi^2}{(y-\eta)^2}\right)\right]\right]$$

(A1.8)

Note that A1.8 fails to hold if the surfaces touch at the intersection of their perpendicular planes $(x = \xi = 0)$, since an evaluation of $G(x,y,\eta,\xi)$ at this location will contain a division by zero. Also, if the surfaces are situated such that any of their edges lie in a common 3rd plane perpendicular to the others $(y = \eta)$, the last term in $G(x,y,\eta,\xi)$ will involve a division by zero.

For the first situation where $x = \xi = 0$, the first term in $G(x,y,\eta,\xi)$ includes a $x^2 + \xi^2$ term that goes toward zero whereas heuristically $\tan^{-1}\infty = \pi/2$, and the product can therefore be equated to zero. The second term includes a $x^2 + \xi^2$ term that again goes towards zero but does so quicker than the $ln\left(1 + \frac{(y-\eta)^2}{x^2+\xi^2}\right)$ term goes toward infinity, again heuristically this product can be equated to zero. Finally the third term will contain an $ln(1)$ term which is itself zero. Therefore, for perpendicular surfaces meeting at the plane intersection, A1.8 can still be used by simply letting $G(x,y,\eta,\xi) = 0$ for the relevant evaluation.

For the second situation where $y = \eta$ the only issue is the final term which will include a division by zero. As above, the $(y-\eta)^2$ term will go to zero much quicker than the logarithm term will go to infinity and so this product can again be equated to zero. In this way A1.8 can still be used for arbitrary perpendicular surfaces with a common edge if during the relevant evaluations of $G(x,y,\eta,\xi)$ this final term is neglected

Appendix 2 – LU Decomposition Example

A simple example with a 3 by 3 matrix is given to illustrate the method used by the hybrid model's solver. Consider the system

$$\begin{bmatrix} 2 & 2 & 1 \\ 1 & 2 & 1 \\ 1 & 2 & 4 \end{bmatrix} \cdot \begin{bmatrix} x \\ y \\ z \end{bmatrix} = \begin{bmatrix} 3 \\ 2 \\ 3 \end{bmatrix}$$

First the upper matrix U is found through row operations, making a note of the factors used during this procedure as follows.

First take the first row multiplied by 0.5 away from the second and third rows, causing their first column values to become zero,

$$\begin{bmatrix} 2 & 2 & 1 \\ 0 & 1 & 0.5 \\ 0 & 1 & 3.5 \end{bmatrix} \cdot \begin{bmatrix} x \\ y \\ z \end{bmatrix} = \begin{bmatrix} 3 \\ 0.5 \\ 1.5 \end{bmatrix}$$

next take the second row away from the third (using a factor of 1), causing its second column value to become zero,

$$\begin{bmatrix} 2 & 2 & 1 \\ 0 & 1 & 0.5 \\ 0 & 0 & 3 \end{bmatrix} \cdot \begin{bmatrix} x \\ y \\ z \end{bmatrix} = \begin{bmatrix} 3 \\ 0.5 \\ 1 \end{bmatrix}$$

Note here, that since the row operations have also been performed on the solution vector, it is now possible to find the solution through back substitution. Beginning with the third row, $3z = 1 \Rightarrow z = 0.33\dot{3}$, plug this value into the second row to find y and similarly into the first to get x.

Instead, the lower triangular matrix is instead formed from the factors used in the eliminations just performed, giving

$$A\bar{x} = \begin{bmatrix} 2 & 2 & 1 \\ 1 & 2 & 1 \\ 1 & 2 & 4 \end{bmatrix} . \bar{x} = LU\bar{x} = \begin{bmatrix} 1 & 0 & 0 \\ 0.5 & 1 & 0 \\ 0.5 & 1 & 1 \end{bmatrix} . \begin{bmatrix} 2 & 2 & 1 \\ 0 & 1 & 0.5 \\ 0 & 0 & 3 \end{bmatrix} . \bar{x} = \bar{b}$$

where $\bar{b}$ is the original solution vector, not the modified version that would be used in back substitution. Next, $L\bar{y} = \bar{b}$ is solved for $\bar{y}$,

$$\begin{bmatrix} 1 & 0 & 0 \\ 0.5 & 1 & 0 \\ 0.5 & 1 & 1 \end{bmatrix} . \bar{y} = \begin{bmatrix} 3 \\ 2 \\ 3 \end{bmatrix}$$

$$y_1 = 3$$

$$y_2 = 2 - 0.5(3) = 0.5$$

$$y_3 = 3 - 0.5(3) - 1(0.5) = 1$$

finally $U\bar{x} = \bar{y}$ can now be solved for $\bar{x}$,

$$\begin{bmatrix} 2 & 2 & 1 \\ 0 & 1 & 0.5 \\ 0 & 0 & 3 \end{bmatrix} . \bar{x} = \begin{bmatrix} y_1 \\ y_2 \\ y_3 \end{bmatrix} = \begin{bmatrix} 3 \\ 0.5 \\ 1 \end{bmatrix}$$

$$x_3 = {}^1\!/_3$$

$$x_2 = 0.5 - 0.5 \left(\tfrac{1}{3} \right) = {}^1\!/_3$$

$$x_1 = \left(\tfrac{1}{2} \right) \left(3 - 2 \left(\tfrac{1}{3} \right) - 1 \left(\tfrac{1}{3} \right) \right) = 1$$

giving a final solution $\bar{x} = [1, {}^1\!/_3, {}^1\!/_3]$.

Appendix 3 – Paper published in Interflam 2007

INTRODUCING A HYBRID FIELD/ZONE MODELLING APPROACH FOR FIRE SIMULATION

D.J.Burton, A.J.Grandison, M.K.Patel, E.R.Galea and J.A.C.Ewer.
Fire Safety Engineering Group, University of Greenwich, U.K.
http://fseg.gre.ac.uk

ABSTRACT

This paper describes the design and implementation of a novel hybrid field/zone fire model linking SMARTFIRE to CFAST. The intention of the hybrid model is to reduce the amount of computation incurred in using field models to simulate large geometries. Using the hybrid model only the most important parts of the geometry are fully modelled using the field model. Other less important parts of the geometry which would otherwise be needlessly modelled using the field model are modelled using the zone model. From the field models perspective, the zone model is used to represent parts of the geometry as an accurate boundary condition. Using this approach many computational cells are replaced by a simple zone model saving computational time. In the test case used in this paper it is shown that the reduction in computational time realised is proportional to the percentage of domain replaced by the zone portion of the Hybrid model.

INTRODUCTION

The use of fire field modelling based on computational fluid dynamics (CFD) has become increasingly popular over the past 20 years and has been used in a number of different scenarios[1-4]. One of the major disadvantages of CFD modelling is the time necessary to run the models[5]. There are a number of potential ways of reducing runtimes for CFD based fire simulations. Parallel Processing has been applied to fire modelling to reduce run times[6], and although these have been successful, many engineers may not have access to more than a single computer. Another methodology for reducing runtime is to make use of group solvers[7]; in combining cells/regions into logical groups, it is possible to significantly reduce computational requirements by setting solver criteria on a group by group basis. In this way, regions requiring less computation can be lowered in priority, allowing computational effort to be focused as required. Another methodology, which is explored in this paper is to combine the field modelling and zone modelling approach in the one simulation to produce a Hybrid model methodology. While the field model can

be used to represent all areas of the domain, this can be computationally expensive leading to long run times. Replacing the field model with a zone model in appropriate parts of the geometry could lead to a considerable saving in run time while not reducing the accuracy of the simulations within the relevant portions of the solution domain. Previous work[8-10] on the implementation of Hybrid models focussed initially on two-dimensional problem domains[8]. This was expanded to three dimensions[9] and later work allowed for simulations across different floors[10] of a multi-floor domain. The hybrid model proposed here will utilise the zone model representation to replace the field calculation in relatively small compartments not directly involved in the scenario or regions of large solution domains which are far from the region of fire origin and of little direct interest. The approach will couple the CFAST[13] zone model with the SMARTFIRE[3,4,15] CFD fire model.

Zone Modelling

Fire zone models have been extensively used to model a variety of fire scenarios for around 40 years[11,12]. The basic assumption of the zone model is that a room can be divided into a number of distinct zones with the temperature, density and other attributes (e.g. product concentrations) assumed to be uniform within each layer at any time. For a large number of fire scenarios, experimental data supports the assumption that fire gases within the fire compartment stratifies into distinct layers, and while conditions within the layers are not strictly uniform, the variation through the layer, compared with that between the layers, is small enough to be assumed negligible. Indeed, in many circumstances a two layer zone model provides a good approximation to reality. Further compartments connected to the initial fire compartment can also be modelled, with the flow through connecting vents usually being found from the horizontal pressure differences across the vent. The conservation equations of mass and energy are applied to each zone, and the system of differential equations constructed is solved discretely in time giving the values of the variables in each layer, the height of the interfaces between the layers and the compartment pressures. As the approach relies on a well stratified environment, it is not suitable for use in situations with complex/quickly changing fluid flow. Current zone models don't take into consideration the conservation of momentum, and so the flow field is never calculated. The main advantage of using a zone model is the sheer speed of the calculations and the small requirement on memory, simulations usually taking less than a minute to complete. The CFAST[13] zone model, written in Fortran, is one of the most widely used, best validated zone models available and so was selected to form the zone component of the Hybrid model.

Field Modelling

Field modelling is more mathematically complex than its zone modelling counterpart, and is based on the actual physics of the fluid flow. Due to its reduced reliance on empiricism the range of applicability is generally far greater for the field modelling approach compared to the zone modelling approach. For example a zone model would not usually be considered appropriate for modelling fire conditions within tall atria. In fire field modelling, the fluid flow is governed by a set of three-dimensional partial differential equations. This set consists of the continuity equation, the momentum equations in three space dimensions, the energy equation, the user equations for mass and mixture fraction, and the equations for the turbulence model, in this case the k-ε model which incorporates buoyancy modification. The generalised governing equation for all variables is expressed in the form of equation (1);

$$\frac{\partial \rho \phi}{\partial t} + \nabla(\rho \bar{U} \phi) = \nabla(\Gamma_\phi \nabla \phi) + S_\phi \tag{1}$$

where ϕ is the particular fluid variable under consideration; ρ is the density; $\bar{U}$ is the local velocity vector; Γ_ϕ is the effective exchange coefficient for ϕ, and S_ϕ is the source term. These partial differential equation cannot generally be solved analytically and must be solved numerically by discretisation[14]. Discretisation leads to the creation of a number, thousands to perhaps many millions, of computational cells to represent the solution within the computational domain. As the discretisation process creates a large number of cells and a large amount of iteration is required to achieve a converged solution for each time step of the calculation and many time steps are required to solve the whole problem then a huge amount of computation is necessary. Large cases can take a number of days to run limiting the usability of fire field modelling due to time and fiscal constraints. The field model used in the work presented here is SMARTFIRE[3,14,15], which is written in C++.

Hybrid Model

The remainder of this paper considers the design and implementation of a novel hybrid field/zone model. The intention is to combine the two separate models to take advantage of their various benefits whilst minimising the effects of their shortcomings. Use will be made of the field model's ability to supply accurate results in all situations, while the zone model's speed will be exploited to greatly reduce computational time in suitable areas of the domain. To achieve this the field model will be used in regions where accuracy of results is paramount as well as in regions with complex/rapidly changing flow patterns and geometry, e.g. the fire room, stairwells, long corridors etc. The zone model can then be confidently used in the remaining geometry, which will be well suited to its methods. The focus of attention is the interface between the two models, through which data will be passed and iterated. The mechanism of the interface will be invisible to the end user. It is intended that the end result will be a model that appeals to all individuals involved with practical fire engineering to whom time and efficiency are significant issues.

THe HYBRID INTERFACE

The interface between the two models is where the bulk of the work involved with implementing the hybrid model lies, and there are several issues that need to be addressed:

- Modelling the interface,
- Converting data values between the two models,
- Ensuring the conservation of mass and energy,
- Consistency,
- Correct handling of pressure,
- Mixed programming language issues.

Within the field section of the hybrid model, the interface will be modelled as a dynamic fixed pressure and temperature boundary condition, the values for which are obtained from the zone model. Within the zone model, the interface will not be visible per-se, but will simply be implemented by creating a source/sink in each layer. In both cases there is

an issue of converting the different forms of data the respective models use so that they can interact correctly. The field model provides as many points of data as there are cells neighbouring the particular boundary we are adding, whereas the zone model simply has two sets of values belonging to the upper and lower layers. In the present implementation, when communicating data from the field to the zone, a simple sum/average will be used; in the other direction the two values will be applied directly to the boundary condition. The pressure for the boundary condition is calculated from a hydrostatic pressure distribution as follows:

$$P = \begin{cases} -g\rho_l h \ + \ P_Z, & \text{if } h \le l \\ -g(\rho_l l + \rho_u (h-l)) \ + \ P_Z, & \text{if } h > l \end{cases} \tag{2}$$

where g is gravity, ρ_l and ρ_u are the densities of the lower and upper layers respectively, l is the layer height, h is the height at which the pressure is required, and P_Z is the floor pressure of the adjoining zone region. The temperature distribution at present is simply calculated as follows,

$$T = \begin{cases} T_l, & \text{if } h \le l \\ T_u, & \text{if } h > l \end{cases} \tag{3}$$

When these values are applied as a boundary condition, and the field model is run for a single iteration, a flow is calculated across the interface, and it is from this flow that the values to be communicated back to the zone model can be found. At each cell-face lying on the boundary, the mass and enthalpy fluxes across the interface are calculated. These fluxes are grouped depending on which layer of the zone model they are entering/leaving, and are then applied to the appropriate layers as source/sink terms; the layers are selected according to the following rules. For a flow from field to zone, the two fluxes are deposited in a layer according to the temperature of the flow. If the flow is hotter than the upper layer, then they are deposited in their entirety in the upper layer. Similarly, if the flow is colder than the lower layer, they are totally deposited in the lower layer. For flow with a temperature between the two layer temperatures, the fluxes are divided linearly between the two layers, e.g.,

$$R_L = \frac{T_U - T}{T_U - T_L} \quad , \quad R_U = 1 - R_L \tag{4}$$

where R_U and R_L are the proportions of the flow going to the upper and lower layers respectively.

For a flow from zone to field, again there are two fluxes, although in this case there is the issue of which layers these are to be removed from. For flow in this direction, the layer is decided on by considering the height at which the flow is occurring; this height is taken to be the mid-point of the cell-face that is under inspection. If this height is above the layer

interface height, then the fluxes are removed from the upper layer, on the other hand, for flow below the layer interface, the fluxes are removed from the lower layer. The use of the boundary condition means that there is no need to consider any further the flow across the interface for this iteration; as the field model is left to calculate the flow, any issues with fluxes entering/leaving the field side are dealt with automatically. This methodology ensures the conservation of mass and energy due to the fact that everything that leaves/enters the field model over the interface is accounted for in the zone model, and vice versa.

The one issue that can cause problems in this area is the consistency between the two models. Two different models have differences in their formulations, e.g. physical constants, assumptions etc., but in this case, where the two models are written in different programming languages, we also experience round-off errors when passing variables between the different instances of code. The consistency, although having a small effect on accuracy, does need to be addressed fully and further work is required to ensure that all possible areas of discrepancy are rectified.

TEST CASE

The test case comprises three rooms in series; a middle fire room which is vented to two side rooms, these side rooms being further vented to the exterior. The case is symmetrical about the centre of the fire room; refer to Figure 1 below. The line P in Figure 1 indicates the location where comparisons between the full field, hybrid, and zone models are made.
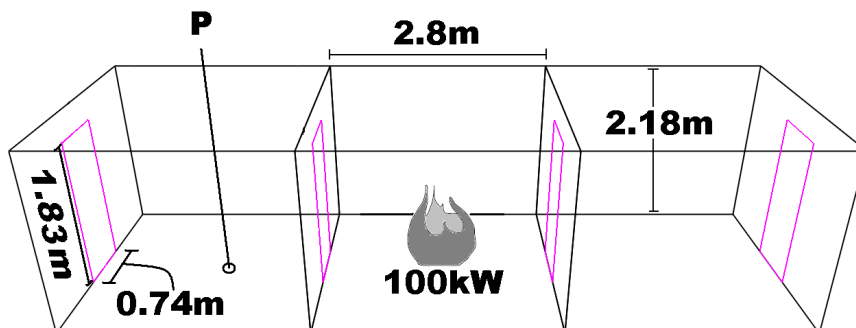
Figure 1. Test case configuration and data comparison location

All rooms have equal dimensions: width 2.8m, depth 2.8m, and height 2.18m. Also all vents are doorways of height 1.83m and width 0.74m and centrally located on their respective walls. The vents/doorways are open for the entire duration of the simulation. The fire is modelled as a simple heat source of a constant 100kW heat release rate, and is located centrally on the floor of the fire room. The simulation was run for 100 seconds using one second time steps, and was run in SMARTFIRE (full-field), CFAST (full-zone), and the Hybrid model, where the right side room was replaced by a zone model; for the field and hybrid simulations 50 iterations were performed over each time step. The case was run full field to provide an upper bound to accuracy and computational time, and the Hybrid model was expected to perform proportionally quicker than the full-field simulation. The case was run in CFAST to provide an indicator of the computational resources required by the zone aspect of the hybrid model, and the Hybrid was expected

to give more accurate results than the CFAST simulation. The cell budget was 9261 cells for each room; the total cell budget for the full field simulation was 33,957 cells (including extended regions), and the total cell budget for the Hybrid simulation was 21,609 cells (after removal of one side room and the respective extended region).

RESULTS

The first comparisons are between the field section of the Hybrid model and the full field results. Depicted in Figure 2 is a 90°C iso-surface at three different times of the simulation, along with the velocity field; on the left is the full field simulation, and on the right the field model part of the Hybrid model.

10 seconds
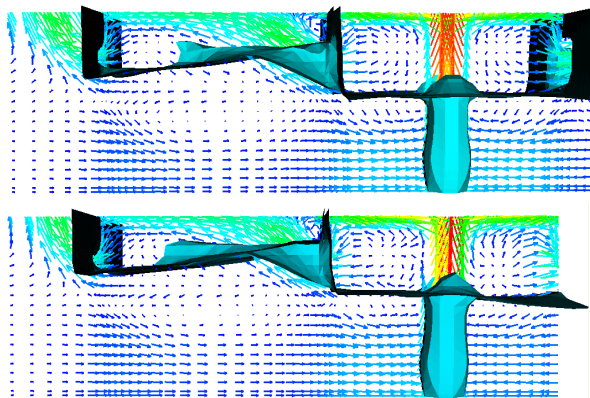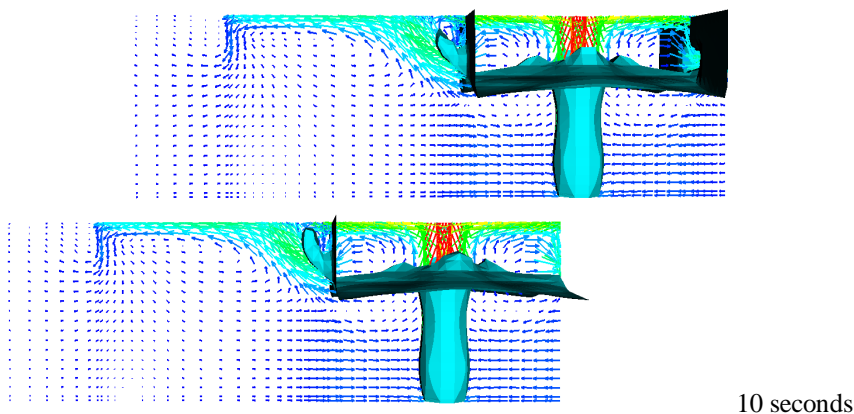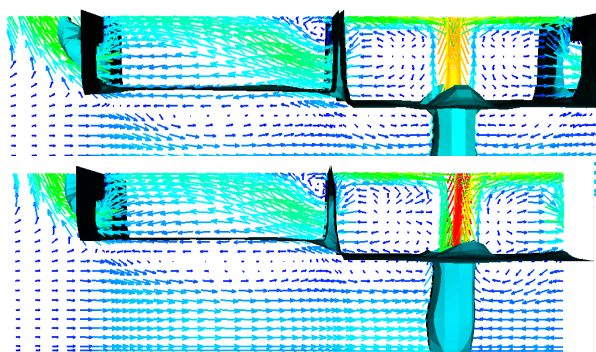
30 seconds

50 seconds

Figure 2. The 90°C iso-surface and velocity vectors in a vertical plane passing through the fire produced by the full-field (left) and Hybrid models (right) for three times.

Depicted in Figure 3 are the vertical temperature distributions at location P over time. These comparisons highlight the effect that the implementation of a Hybrid zone model has on the field results. As can be seen, there is good conformity between the two different models, with the temporal temperature values and velocity vectors being in excellent agreement. From the final comparison at 50s it can be seen that there is a slight plume lean in the hybrid model. This is to be expected due to the close proximity of the interface to the fire due to the reduction in data at the interface compared to the full field model.
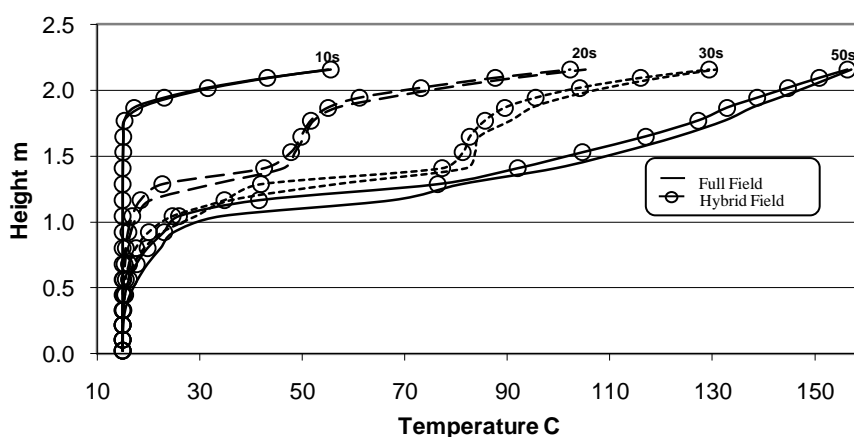
Figure 3. Vertical temperature distribution at location P for times 10s, 20s, 30s and 50s

The next comparison illustrates the agreement between the zone section of the Hybrid model and the full field model. Presented in Table 1 are the upper and lower layer temperatures for SMARTFIRE, the Hybrid zone and CFAST, along with the percentage change over SMARTFIRE. To enable this comparison the data from the full field model was reduced to a two zone form equivalent to the zone model using a mass equivalency method[16,17]. Using these values for the full field, a comparison can now be made between the three different models. Looking at Table 1, we can see that after an initial period, the Hybrid model agrees more closely with the full field model than does CFAST. One assumption of the zone model is that the interface height is accurate to within a spatial error of approximately 10%. Taking this into account, it can be seen that the Hybrid model produces some very satisfactory results. The computational time for the full field model was approximately 3 hrs 33 mins while the computational time for the Hybrid model was approximately 2 hs 24 mins. This is a reduction of around 33% as is to be expected with the removal of a third of the solution domain.

Table 1. Upper and lower layer temperatures, interface height and a percentage difference for the Hybrid and CFAST results over the full field (SMARTFIRE) at different times.

Time	Model	Upper Layer Temp (C)	Change over SMARTFIRE	Lower Layer Temp (C)	Change over SMARTFIRE	Interface Height (m)	Change over SMARTFIRE
	SMARTFIRE	86.3	-	14.9	-	1.1	-
30s	Hybrid	106.4	23.29%	16.6	11.41%	1.4	21.62%
	CFAST	82.9	-3.94%	16.9	13.42%	1.3	16.22%
	SMARTFIRE	90.9	-	14.9	-	1.1	-
40s	Hybrid	108.4	19.25%	17.2	15.44%	1.3	20.56%
	CFAST	97.9	7.70%	18.9	26.85%	1.3	19.63%
	SMARTFIRE	98.4	-	14.9	-	1.1	-
50s	Hybrid	108.4	10.16%	17.8	19.46%	1.3	21.70%
	CFAST	120.0	21.95%	21.9	46.98%	1.3	24.53%
	SMARTFIRE	116.0	-	14.9	-	1.1	-
80s	Hybrid	114.1	-1.64%	18.4	23.49%	1.3	16.67%
	CFAST	131.0	12.93%	24.9	67.11%	1.4	25.00%
	SMARTFIRE	118.0	-	14.9	-	1.1	-
100s	Hybrid	115.4	-2.20%	18.1	21.48%	1.3	16.51%
	CFAST	137.0	16.10%	26.9	80.54%	1.4	24.77%

CONCLUSION

It has been demonstrated that a Hybrid model can be a viable option when the computational resources demanded by a field model are too 'expensive'. It has been shown that the implementation of a zone model interface has a small effect on the final field results, even when the interface is situated in close proximity to the fire. It has also been shown that the results reported by the Hybrid's zone are in good agreement with the SMARTFIRE (full field) results. The decrease in computational time required was equivalent to the percentage of CFD domain replaced by the zone model, which is in agreement with the methodology. As expected, the Hybrid model shows an improvement

in computational time taken over the full field simulation, and also produces more accurate results than the full zone model. Future work is directed at implementing different aspects within the Hybrid frame, such as radiation, species flow, and turbulence. These will hopefully increase the accuracy of the method without significantly increasing the computational time required.

ACKNOWLEDGEMENT

REFERENCES

1. Yan, Z. and Holmstedt, G., 2001, "Investigation of the dance hall fire in Gothenburg, October 1998 – a comparison between human observation and CFD simulation", Fire Safety Science – Proceedings of the 9th International Symposium, pp 951-963.
2. Luo, M. and Beck, V., 1996, Flashover fires in a full scale building: prediction and experiment, Proceedings Interflam'96, Compiled by C.Franks and S Grayson, ISBN 0 9516320 9 4, pp. 361-370.
3. Wang, Z., Jia, F., Galea, E.R., Patel, M.K., Ewer, J , 2001, Simulating one of the CIB W14 round robin test cases using the SMARTFIRE fire field model. *Fire Safety Journal*, **36**, pp661-677.
4. Jia F., Patel M.K., Galea E.R., Grandison A. and Ewer J., 2006, CFD Fire Simulation of the Swissair Flight 111 In-flight Fire – Part II: Fire Spread within the Simulated Area, The Aeronautical Journal of the Royal Aeronautical Soc, Vol 110, Nr 1107, pp 303-314.
5. Chow, W. K., 1995. A Comparison of the Use of Fire Zone and Field Models for Simulating Atrium Smoke-Filling Processes. *Fire Safety Journal*, **25**, pp.337-353.
6. Grandison, A.J., Galea, E.R., Patel M.K., Ewer, J., 2003-2004. The Development of Parallel Implementation for a CFD based fire field model utilising conventional office based PCs. *Journal of Applied Fire Science*, **12(2)**, pp.137-157.
7. N.M. Hurst-Clark, J.A.C. Ewer, A.J. Grandison and E.R. Galea, 2004. Group Solvers: A Means of Reducing Run-Times and Memory Overheads for CFD Based Fire Simulation Software. *Interflam 2004 Conference Proceedings*, **1**, pp.659-664
8. Xu T., Wang J., Fan W., 1991. A new method of modelling of a fire–combination of field modelling and zone modelling. *Proceedings of the Symposium on Engineering Thermophysics*, ZhenJiang, China.
9. Wang J., Fan W., 1996. Numerical simulation of fire process of Multi-rooms. J Univ Sci Technol China, **26**, pp.204-9
10. Hua J., Wang J., Kumar K., 2005. Development of a hybrid field and zone model for fire smoke propagation simulation in buildings. *Fire Safety Journal,* **40**, pp.99-119
11. Quintiere J, 1977. Growth of Fires in Building Compartments. ASTM STP 614, American Society for Testing and Materials, Philadelphia, PA
12. Pape R., Waterman T.E., Eichler T.V., 1981. Development of a Fire in a Room from Ignition to Full Room Involvement – RFIRES. National Bureau of Standards, NBS-GCR-81-301, Washington

13. CFAST, 2007, BFRL, NIST, <u>U.S. Commerce Department's</u> Technology Administration

14. Patankar S.V., 1980. Numerical Heat Transfer and Fluid Flow. Taylor & Francis Publishing. ISBN-10: 0891165223

15. Wang Z., Jia F. and Galea E.R., 2007, Predicting toxic gas concentrations resulting from enclosure fires using local equivalence ratio concept linked to fire field models. Fire and Materials, Vol 31, Issue 1 pp 27-51.

16. Emmons, H. W., 1989. Vent Flows. *SFPE Handbook for Fire Protection Engineering*, **2**, pp.40-49

17. Janssens, M., Tran, H. C., 1992. Data Reduction of Room Tests for Zone Model Validation. *Journal of Fire Sciences*, **10**, (6), pp.528-555.

Appendix 4 – Paper published in IAFSS 2011

Development of a Hybrid Field/Zone Fire Model

DANIEL Burton, ANGUS Grandison, MAYUR PATEL, EDWIN Galea, and JOHN Ewer
Fire Safety Engineering Group
The University of Greenwich
30 Park Row, Greenwich, London SE10 9LS, UK

ABSTRACT

A novel hybrid field/zone fire model, coupling the SMARTFIRE CFD fire model to both the CFAST zone model and a custom zone model is presented. The intention of the hybrid model is to reduce the computational overheads incurred in using fire field models to simulate large geometries such as large buildings or large passenger ships, while maintaining the accuracy of the fire field model. In using the hybrid model, only the most important parts of the geometry are fully modeled using the field model. Other less important parts of the geometry are modeled using the zone model. From the field model's perspective, the zone model is used to represent parts of the geometry as an accurate boundary condition. By using this approach, many computational cells are replaced by a simple zone model, saving computational costs. Two tests cases demonstrating the technique are presented. It is shown that the hybrid approach is capable of producing reasonably accurate predictions of fire development while substantially reducing computational costs. It is shown that by removing some 56% of the CFD solution domain, the hybrid case can achieve a saving of 48% in the run time.

KEYWORDS: modeling, compartment fires, CFD, zone, hybrid, simulation.

Nomenclature Listing

C_P	specific heat, constant pressure ($J \cdot kg^{-1} \cdot K^{-1}$)	V	volume (m^3)
C_V	specific heat, constant volume ($J \cdot kg^{-1} \cdot K^{-1}$)	v	velocity ($m \cdot s^{-1}$)
g	acceleration due to gravity ($m \cdot s^{-2}$)	**Greek**	
h	enthalpy (J)	Γ	effective exchange coefficient
I	interface height (m)	γ	ratio of specific heats (C_P/C_V)
m	mass (kg)	ρ	density ($kg \cdot m^{-3}$)
P	pressure (Pa)	Φ	fluid field variable
R	gas constant ($m^2 \cdot K^{-1} \cdot s^{-2}$)	**Subscripts**	
S	source term	u	upper zone layer
T	temperature (K)	l	lower zone layer
t	time (s)	ref	reference or ambient condition
U	local velocity vector ($m \cdot s^{-1}$)		

INTRODUCTION

The use of computational fluid dynamics (CFD) based fire field modeling has become increasingly popular over the past twenty years and has been used in a number of different scenarios [1–4]. One of the major disadvantages of fire field modeling is the time required to run the models [5]. Parallel processing is one way of reducing run times associated with running fire models [6], and while successful, many engineers may not have access to more than one or two computers. Another methodology for reducing runtime is to make use of advanced solver technology such as group solvers [7]. Using this approach cells/regions are combined into logical groups, making it possible to significantly reduce computational requirements by setting solver criteria on a group-by-group basis. In this way, regions requiring less computation can be lowered in priority, allowing computational effort to be focused as required. In this paper we explore a novel methodology which combines the CFD fire field model approach to that of the zone modeling approach [11] within the simulation environment to produce a hybrid modeling methodology. Within the hybrid approach, areas of the solution domain that would normally be modeled using the expensive field modeling approach are replaced with a zone model representation. Replacing the field model with a zone model in appropriate parts of the geometry could lead to a considerable saving in run time, whilst maintaining the accuracy of the simulations within the relevant portions of the solution domain. The hybrid approach would be particularly suited to larger domains containing numerous small compartments where large speed ups in solution time could be realized. Large passenger ships such as modern cruise ships are one example of such environments. The work described in this paper forms part of the EU Framework 7 project FIREPROOF, which is investigating the use of fire modeling for large passenger ships. The hybrid modeling technology described in this paper is being developed to reduce the run time associated with detailed fire simulations required for risk assessment analysis of passenger ship designs. Previous work on the implementation of hybrid models focused initially on two-dimensional problem domains [8]; this was expanded to three dimensions [9], and later work allowed for simulations across different floors of a multi-floor domain [10]. The hybrid model proposed here utilizes the zone model representation to replace the field calculation in relatively small compartments not directly involved in the scenario, or regions of large solution domains which are far from the region of fire origin and of little direct interest. The hybrid model utilizes two approaches, the first approach couples the CFAST [11] zone model with the SMARTFIRE [3,4,12] CFD fire model; the second approach couples a custom zone model with the SMARTFIRE CFD fire model. An earlier version of the hybrid model presented here was discussed in a previous paper [13]. In this earlier work the hybrid approach was restricted to compartments in which the zone model component was open to the outside and utilized the CFAST zone model. In the current implementation this restriction has been lifted allowing zone model compartments with no external vent of their own. This was achieved via the implementation of a custom zone model which is the focus of this paper. In this case, zone pressure release *must* occur through the CFD domain. In addition, hybrid simulation consisting of multiple zone rooms independently connected to the CFD domain is now addressed.

FIRE MODELLING APPROACHeS

Zone Modeling

Computer-based zone models were first developed in the early seventies and have been used extensively over the years in modeling a large catalogue of fire scenarios [14–16]. The underlying assumption of zone models is that a room can be divided into a number of distinct horizontal zones or layers, and the temperature, density and other attributes (e.g. product concentrations) are assumed to be uniform within each layer at any point in time, i.e. the layers are fully mixed. Experimental fire data suggests that fire gases stratify into these distinct layers, and while these values are never in reality uniform the variations through the layer, compared with those between

the layers, are small enough to be assumed negligible. Due to stratification between the existing ambient 'cold' air and the fire affected 'hot' gases, a two layer zone model is generally accepted as a valid assumption allowing the prediction of reasonably accurate layer temperatures and the interface height. The mathematical model describing the zone model consists of a set of ordinary differential equations derived from conservation equations of mass and energy.

Zone models continue to be popular and effort is being invested to improve zone modeling capabilities; for example Li and Chow [17] have developed a water suppression capability within a single-zone zone model, Konecki and Pólka [18] have developed complex species transfer mechanisms, and Chen et al. [19] have developed zone models which make use of multiple layers (>2) within a single compartment. The main advantage of zone modeling is the comparatively small computational requirements compared to CFD models. Zone model calculations typically require only minutes rather than the many hours associated with CFD fire modeling.

Fire Field Modeling

Field modeling is more computationally demanding than its zone modeling counterpart, and is based on the more fundamental physics of the fluid flow [20]. Due to its reduced reliance on empiricism, the range of applicability is generally far greater for the field modeling approach compared to that of the zone model. In fire field modeling, the fluid flow is governed by a set of three-dimensional partial differential equations. This set consists of the continuity equation, the momentum equations in three space dimensions, the energy equation, the user equations for mass and mixture fraction, and the equations for the turbulence model; in this case the k-ε model which incorporates buoyancy modification. The generalized governing equation for all variables is expressed in the form shown in Eq. 1,

$$\frac{\partial \rho \phi}{\partial t} + \nabla(\rho \bar{U} \phi) = \nabla(\Gamma_\phi \nabla \phi) + S_\phi \qquad (1)$$

This collection of partial differential equations is solved numerically, usually using iterative methods [20].

The Hybrid Model

The basic premise of the hybrid model is to combine the use of the two fire modeling approaches to benefit from each of the models' strong points whilst minimizing their respective disadvantages. The CFD model would be used primarily in compartments where accuracy is essential, such as the room of fire origin and regions where detailed analysis is required. It would also be used in compartments not adequately represented by zone models, such as long corridors or tall compartments. Finally, the CFD model would also be used in compartments containing complex flow qualities, such as strong turbulence and curl of the velocity field, which can have a significant effect on the simulation. The zone model would then be used in the remaining compartments.

Use of the zone model within these compartments allows parameters such as layer height and average temperature to be determined. This information is extremely useful when performing evacuation simulation or risk analysis. The real strength of the hybrid model is realized in situations containing many such compartments, each of which may be insignificant in isolation but together having a very large cumulative effect. Environments especially suited to hybrid treatment are large domains with numerous small compartments such as hotels, prisons and passenger ships.

The majority of the research effort involved in developing hybrid field/zone models focuses on the interface connecting the two separate models. These models have been individually validated, therefore any errors or inconsistencies will stem from how the interface is handled, both in the way it is represented within the models themselves and in how calculations and conversions are performed across it.

THe HYBRID MODEL IMPLEMENTATION

Within the field model portion of the hybrid model, the interface is modeled as a dynamic fixed pressure and temperature boundary condition, the values for which are obtained from the zone model results. This is performed by enhancing the code's existing treatment of fixed-pressure boundary conditions, by allowing variation of pressure, temperature and density across the interface (see Fig. 1). Within the zone model the interface will not be visible per-se nor modeled along with its internal connections, but will simply be implemented by creating a source/sink term in each layer to represent the net flow between the models.

The pressure for the boundary condition is calculated from a hydrostatic pressure distribution similar to the treatment of pressure within the zone model itself; the applied temperatures and densities are calculated based on flow direction and height. When these values are applied on the boundary condition, and SMARTFIRE is run for a single iteration, a flow is calculated across the interface. It is from this flow that the summed values to be communicated back to the zone model are found. At each cell-face lying on the boundary, the mass and enthalpy fluxes across the interface are calculated. These fluxes are grouped depending on which layer of the zone model they are depositing/extracting from, and are then applied to the appropriate layers as source/sink terms respectively.

In both directions there is an issue of converting the different forms of data that the respective models use so that they can interact correctly. The field model provides as many sets of data as there are cells neighboring the boundary condition in question (typically around 50–200 cells), whereas the zone model simply has two sets of values belonging to the upper and lower layers. When communicating data from SMARTFIRE to the zone model, a simple sum is used to reduce the resolution of the data to values for each of the two layers. In the reverse direction there is the issue of taking the sparse data of the zone model and applying it to the numerous CFD cells on the interface.
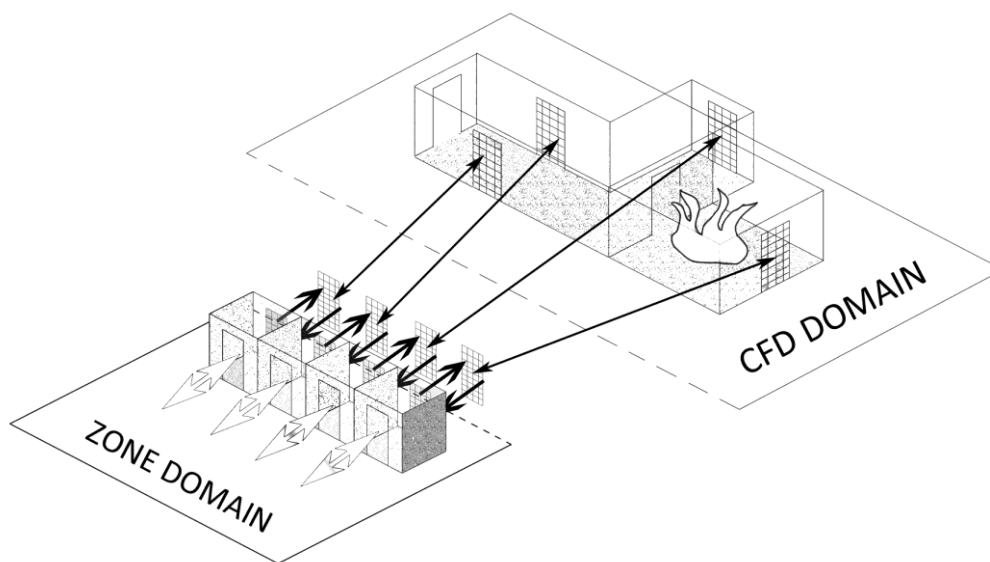
Fig. 1. Replacing CFD compartments with zone model representations.

Passing fluxes from a CFD to a zone model (and pressures from zone to CFD) ensures conservation across the interface; if instead pressure was passed from SMARTFIRE the calculation of fluxes for conversion to layer sources would have to be performed within the zone model itself. The zone model calculation for fluxes is fundamentally different to that of SMARTFIRE, and would result in discrepancies between the net flux leaving the CFD domain at the boundary and the net flux being accounted for by the sources within the zone model. With differing representation of fluxes it would be possible to create and destroy both enthalpy and mass across the interface, invalidating the very conservation principle the two models are based on.

Pressure Boundary Condition

The hybrid interface is represented within SMARTFIRE as a pressure boundary condition having variation in the vertical direction. Along with a value for pressure, accurate treatment of the hybrid interface also requires temperature and density to be declared at the boundary condition. These values are used to address convected quantities for flow entering the CFD domain from the zone model; the temperature values can also contribute to diffusion at the interface.

The value of pressure assigned at any point on this interface consists of three components: the room pressure supplied by the zone model, a hydrostatic term representing changes in pressure for varying height and density, and a dynamic term representing the variation in pressure over the hydrostatic value for flow speed.

$$P_{room} = P_{zone} \tag{2}$$

$$P_{static} = \begin{cases} -g\rho_l h & : h \le I \\ -g\left(\rho_l l + \rho_u\left(h - I\right)\right) : h > I \end{cases} \tag{3}$$

$$P_{dynam} = -\frac{\rho v^2}{2} \tag{4}$$

where v is the component of velocity normal to the interface.

The first component of room pressure (Eq. 2) corresponds to the total enthalpy contained within a zone compartment and represents the notion of a room being pressurized. Because the hydrostatic pressure manifests as a reduction with increasing height, this floor pressure is the highest value attained within the room. In this way it forms the basis for comparisons between rooms and differences in this value are the main driving force of flow. The zone model lacks any variation in pressure throughout the rooms but the consequences of layers of differing depth, temperature and density need to be accounted for. Due to the absence of momentum and velocities, dynamic pressure is not represented within the zone model itself and a standard hydrostatic treatment is used; this treatment is extended to the interface through the second pressure component (see Eq. 3). Despite the absence of momentum and dynamic pressure within the zone model, accurate treatment at the interface still requires inclusion of this term. This is addressed through the final component which is a pressure drop term representing the dynamic variation in pressure, due to flow speed, over the zone hydrostatic pressure where flow is assumed to have come to a state of rest (see Eq. 4). This drop term represents the pressure observed at a point on a streamline that comes to rest at the zone pressure value, and it accounts for the pressure gradient applying over the length of a streamline, not instantaneously at a point.

Calculating the values of temperature and density to apply to the boundary condition in SMARTFIRE is a straightforward matter. For flow from CFD to zone, these values are obtained directly from the boundary cell at which the flow leaves the CFD domain. For flow from zone to CFD, the values of temperature and density at a face are taken from the layers in which the flow

originates. Flow is assumed to have originated from the layer that shares its vertical displacement, i.e. the layer making contact with the face being considered. It is generally the case that the zone interface (layer) height falls midway along a face, causing both upper and lower layers to be in contact with the row of faces at that height. By using the midpoint of the face as the comparison height, this issue is consistently dealt with by assigning the layer that makes the majority of contact with each face.

A significant difference between the field and zone models is the size of time step used in the solution procedure. Zone models tend to use extremely small time steps which allow them to proceed to a solution in an explicit manner. In comparison, implicitly discretized field models such as SMARTFIRE can be solved over a wide range of time step values. Handling species flux across the hybrid interface in a summed/averaged manner can maintain conservation and ensure accurate results, but the time step discrepancy has implications for the solution of pressure within the zone model whose equations are extremely stiff with regards to this variable. A net change in enthalpy in a compartment results in a corresponding change in pressure; when this net change is caused by an enthalpy flux applying over the length of a comparatively 'large' field model time step, the resulting pressure change can be excessive. Simply using this value of zone pressure for the next iteration would result in an even greater change in values, and the solution procedure would quickly diverge to failure; this issue does not affect the accuracy of the solution, but makes reaching a solution much more difficult.

An interesting consequence of the above issue is that it differentiates between two possible configurations that define all cases applicable to treatment by the hybrid model; namely 'open' and 'closed' cases. The fundamental difference is that for the open case, the compartment or section of building being replaced by the zone model has its own vent to the outside; in other words from any point in the zone domain, it is possible to find a path to the external domain without having to first pass through any section of the CFD domain. The closed case on the other hand is characterized by the zone portion of the domain itself having no vent to the outside; any flow reaching the external domain, or any pressure release required by the zone section, would first have to pass through the hybrid interface into the CFD section. In essence, a domain having a link to the outside manifests itself as an opportunity for pressure release; this is due to the infinite nature of the 'outside', meaning that despite net flows in or out the external pressure remains at the reference pressure throughout the simulation. In this way, any simulation with an 'open' configuration circumvents the pressure/time step issue by allowing venting of any pressure build up; in effect, the value of pressure is kept within sensible limits, allowing iteration to proceed. Consequently, the hybrid implementation discussed to this point can be applied to cases of an 'open' nature.

For 'closed' cases there is no option of pressure release within the zone model domain, therefore any release must be performed through the CFD domain (via the hybrid interface) and only with respect to the time step size dictated by the CFD model. To handle these issues a custom zone model has been implemented within the hybrid model, allowing both the CFD and zone model to run over identically sized time steps. The issue of stability of the zone model over these comparatively larger time steps has been addressed by solving the zone model equations fully (to convergence) at the end of each CFD iteration, as opposed to allowing both models to iterate with the intention of reaching convergence solely at the last iteration of the present time step. This is in comparison to the usual 'coupling' (as used in the open case) where the zone model is also solved with respect to the current CFD iteration, but where this solution will contain an error term that tends to zero as the solution proceeds through the iterations. In essence, for the open case a residual will exist between the two models until convergence is reached (to within some tolerance); for the closed case, extra work is done in solving the zone model to ensure this residual is within the specified tolerance for each and every iteration. This clearly affects the computational effort required to solve the hybrid model, although the inherently low requirements of the zone model solution procedure results in this method remaining viable.

This pseudo-converged solution at the end of each iteration will consist of a value of pressure for the zone compartment along with the corresponding fluxes at each CFD face on the hybrid

interface. Flow variables and the calculation of the zone layer sources are performed in the same manner as the open formulation [13] where variables are assigned depending on flow direction and layers assigned based on temperature and height. The mass and enthalpy sources are then used to evaluate the variables for layer i as follows (subscript 0 indicates 'old' values from the previous time step),

$$V_i = \frac{(m_{i,0} + \dot{m}_i)}{\rho_i} \tag{5}$$

$$T_i = \frac{T_{i,0} m_{i,0} + \dot{h}_i / C_P}{m_{i,0} + \dot{m}_i} + \frac{1}{C_P (m_{i,0} + \dot{m}_i)} \cdot \frac{V_i}{V_{room}} \cdot (\gamma - 1) \left(\sum_j \dot{h}_j \right) \tag{6}$$

$$\rho_i = \frac{P_{ref} + P_{zone}}{R T_i} \tag{7}$$

The pressure boundary condition is updated with these newly calculated values and the CFD model is run for the next iteration.

TEST CASES

As use of the hybrid model on the 'open' type of case has been demonstrated in previous work [13], the two test cases herein will focus on use of the hybrid model in a 'closed' situation. The first test case presents a situation where the zone room has two interfaces to the CFD domain; despite this it remains classified as 'closed' as it is only indirectly connected to the exterior through the second CFD room. Both cases below present instances where the zone model is in close proximity to the fire-room, testing both the stability of the hybrid implementation itself, along with its effect on the remaining CFD domain. Realistically, locations of such complex, large pressure driven flows would be reserved for the CFD model for an accurate treatment, but testing the hybrid model at its limits will provide both confidence and an idea of its limitations. In comparing between CFD and zone data, use has been made of the mass equivalency method outlined by Janssens and Tran [21] to produce approximations for the layer height and average zone temperatures based on CFD data.

Test Case 1

This case consists of three identically sized rooms (each sized 2.8 m × 2.8 m × 2.18 m) connected via centrally located doorways (0.74 m × 1.83 m) in series. The first room contains a centrally placed 62.9 kW heat source and is vented to the second room; the second room is then vented to the third which in turn is vented to the exterior (see Fig 2). The heat source is active for the first 60 s of the simulation, at which point it is turned off (i.e. 0 kW). This particular value of heat release rate corresponds to one of the four fire sizes used by Steckler et al during their experiments on compartment opening flows. This case will test the hybrid model's capability in handling transient changes in simulation factors, along with its capacity to share the zone model with separated sections of the CFD domain. It also serves as a strong test of the hybrid implementation's stability and the effect the interface has on the CFD domain due to it being the sole means of venting available to the CFD fire room (both in the release of pressure and hot gases, and in allowing the drawing of ambient air from the exterior towards the bottom of the fire). The hybrid interface is also much closer to the fire origin than would be typically applied and this is therefore a hard test for the accuracy of the method.
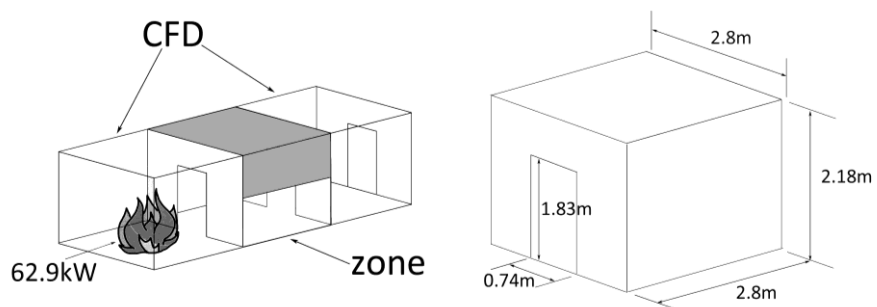
Fig. 2. Setup for Test Case 1.

The first set of comparisons is for the side rooms that remain modeled by field model in both the CFD and hybrid simulations, see Fig. 3 to Fig. 8. Results for all the CFD cases are shown at the top of each figure while results for the hybrid case are shown at the bottom of each figure.
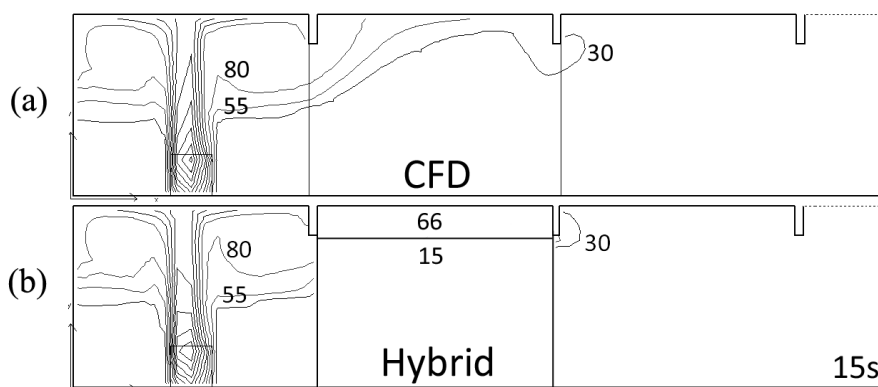
Fig. 3. Temperature (ºC) comparisons between CFD (a) and hybrid (b) at 15 s.
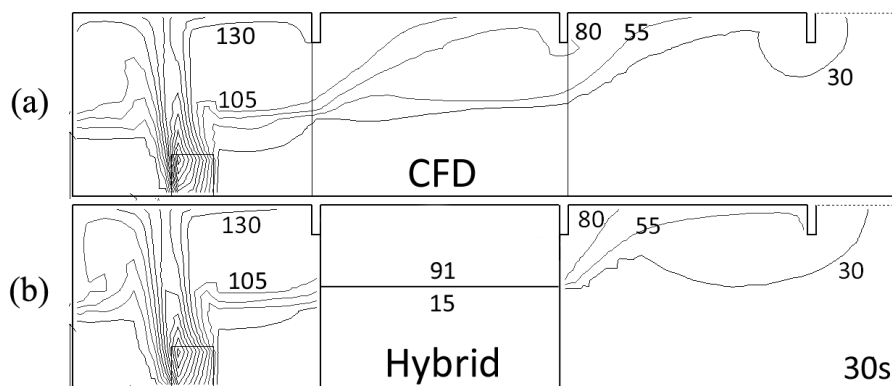
Fig. 4. Temperature (ºC) comparisons between CFD (a) and hybrid (b) at 30 s.

In the results for the hybrid model, the middle compartment is modeled using the zone model while the compartments at either side are modeled using the CFD approach. Within each compartment modeled using the CFD approach temperature iso-contours (ºC) are depicted while in the compartment modeled using the zone approach a visual representation of the layer height and the average upper and lower layer temperatures (ºC) are shown. Results are presented at 15, 30, 45, 60, 90 and 180 s after fire initiation in Fig. 3 to Fig. 8 respectively. Note that the fire is deactivated after 60 s and so there is no fire plume evident in Fig. 7 and Fig. 8.
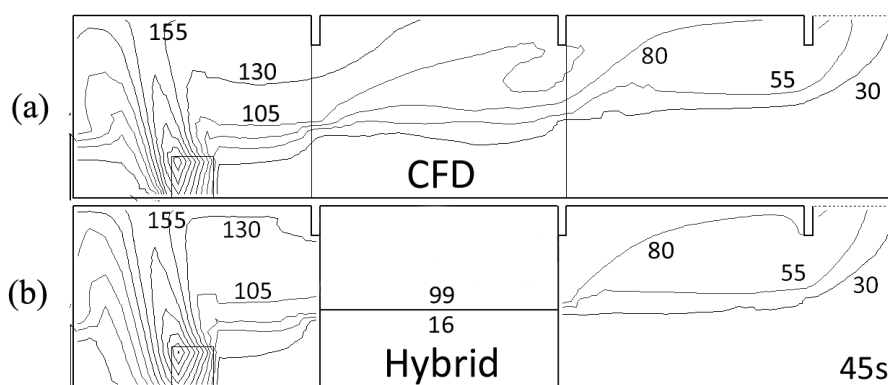
Fig. 5. Temperature (ºC) comparisons between CFD (a) and hybrid (b) at 45 s.
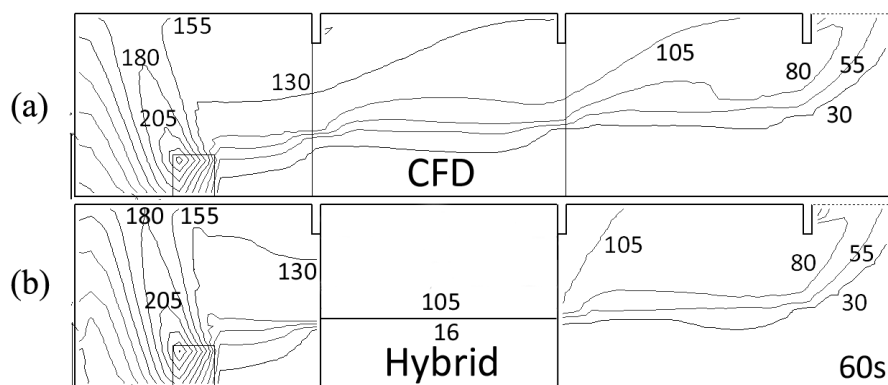
Fig. 6. Temperature (ºC) comparisons between CFD (a) and hybrid (b) at 60 s.
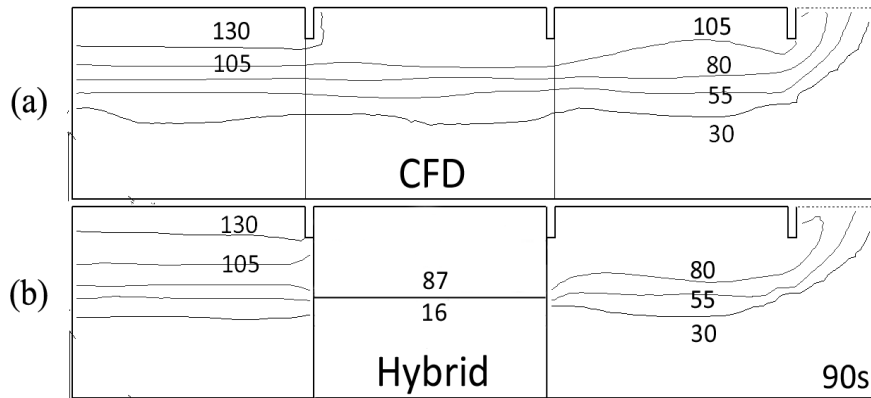
Fig. 7. Temperature (°C) comparisons between CFD (a) and hybrid (b) at 90 s.
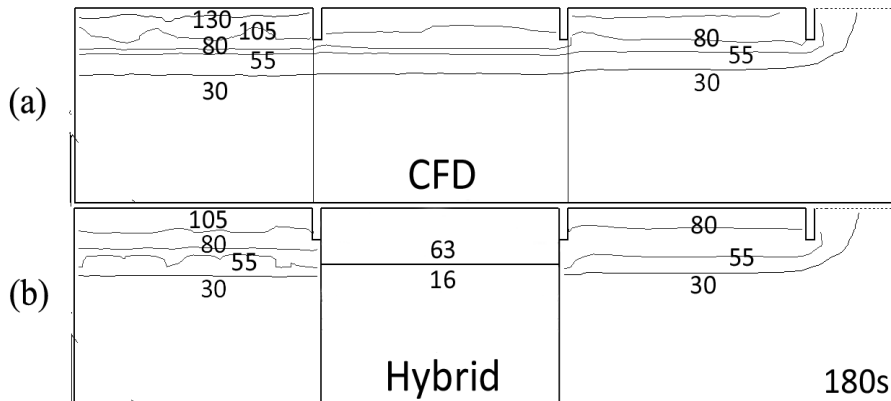
Fig. 8. Temperature (°C) comparisons between CFD (a) and hybrid (b) at 180 s.

From Fig. 3 to Fig. 8 it is noted that there is good agreement between the results produced by both models for both the qualitative characteristics, such as layering and the shape of the fire plume, and the quantitative values of temperature. Slight differences exist in the values of temperature observed in the compartment on the far right. This is to be expected as the upper layer temperatures at the interface that are obtained from the zone room are uniform throughout the layer, whereas the CFD simulation maintains the resolution of the temperature data. After the fire is deactivated, the rooms proceed to partially cool and again good agreement is seen between the results for this portion of the simulation, especially with regard to the heights of the layers. Figure 9 presents detailed results for the upper layer temperature and layer height for the central room that has been removed from the CFD domain and replaced with the zone model representation.

Good agreement is seen for the general trend of the upper layer temperature. Initially approximated upper layer temperatures are in good agreement, although after the fire (heat source) has been deactivated, the hybrid model appears to cool down quicker and therefore predicts lower temperatures than the CFD model. Despite this, agreement with respect to the layer height is very encouraging.
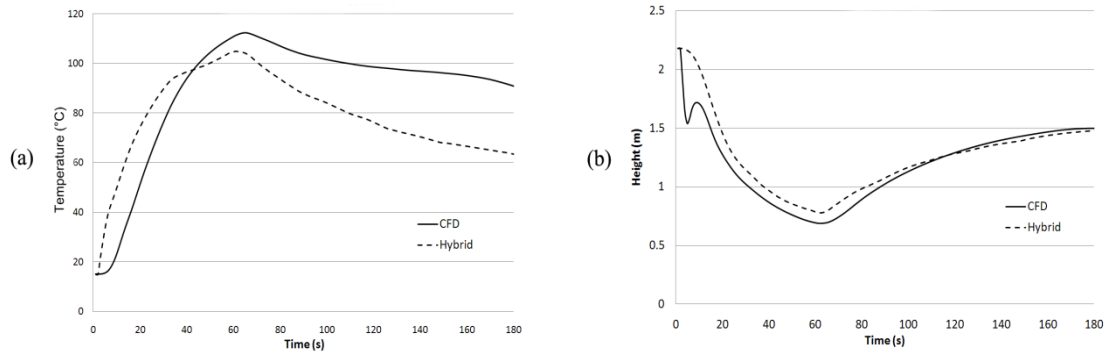
Fig. 9. Upper layer temperature (℃) (a) and layer height (b) for the central room.

Test Case 2

The second test case consists of six identically sized compartments opening on to a common corridor that is vented to the exterior at one end (see Fig. 10). One of these compartments, situated at the closed end of the corridor, contains a centrally placed 500 kW heat source to represent a fire. In the hybrid model representation for this case, the remaining five compartments are modeled using the zone model approach. As a result, the hybrid model contains 56% fewer computational cells than the full CFD simulation.
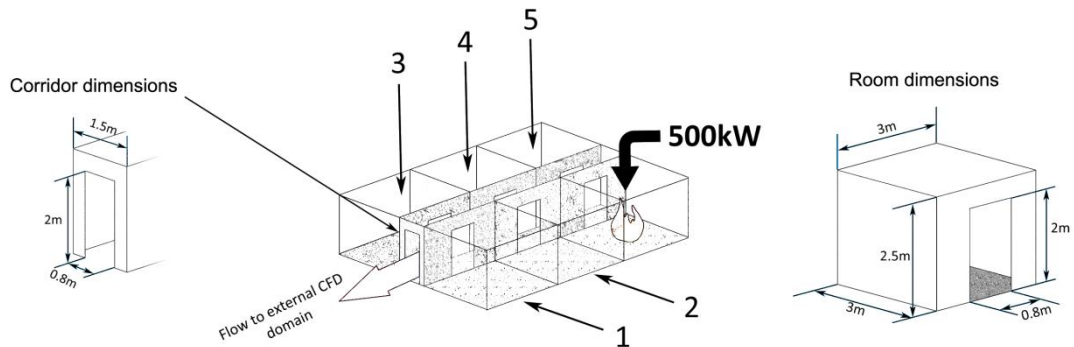
Fig. 10. Setup for Test Case 2.

The first set of results is for the sections of domain that remain modeled by the field model in both simulations (see Fig. 11 and Fig. 12). The first set of comparisons are for a cross-section through the fire room including the door leading out into the corridor (see Fig. 11) and a central cross-section along the length of the corridor itself (see Fig. 12). The contours shown are at the end of the simulation at 120 s.
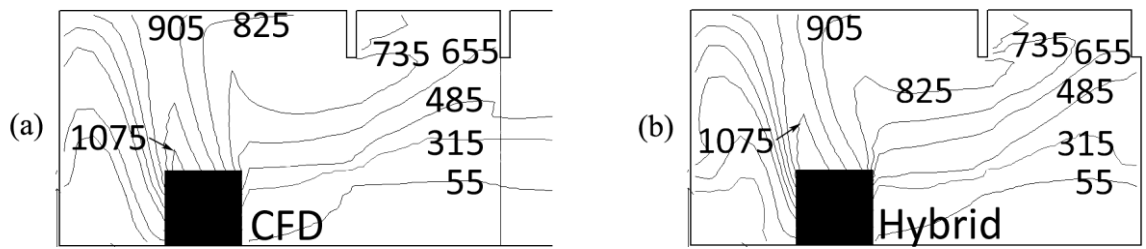
Fig. 11. Temperature (°C) distribution within the fire room for the full CFD case (a) and the hybrid case (b) at 120 s.
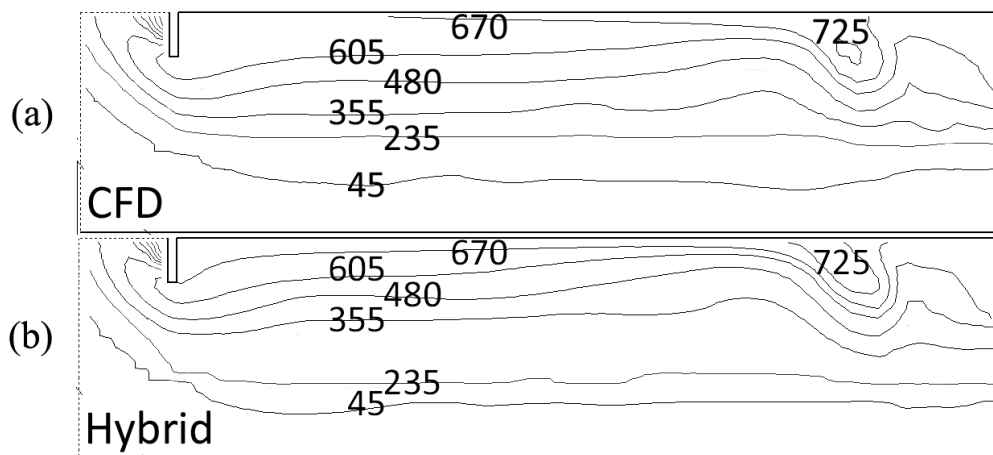
Fig. 12. Temperature (°C) distribution within the corridor for the full CFD case (a) and the hybrid case (b) at 120 s.

Good agreement is observed for temperatures throughout the length of the corridor (see Fig. 12). The interface height separating the ambient air and hot fire gases is also in agreement to within less than 4% of the corridor height. Again, slight banding is present in the hybrid temperatures due to the uniform layer data being applied at the interface representing each doorway. Fluxes at the external doorway at the left end of the corridor are also in agreement implying equivalent net mass balances between the two simulations.

Presented in Fig. 13 and Fig. 14 are results for two of the four rooms modeled using the zone model approach; room 1 at the external end of the corridor and room 5 opposite the fire room. Figure 13 shows that there is good agreement in the trends of the upper layer temperature (°C) development between the two simulations. It is noted that the hybrid model predicts higher upper layer temperatures at the start of the simulation and lower temperatures towards the end of the simulation as compared to the CFD results.
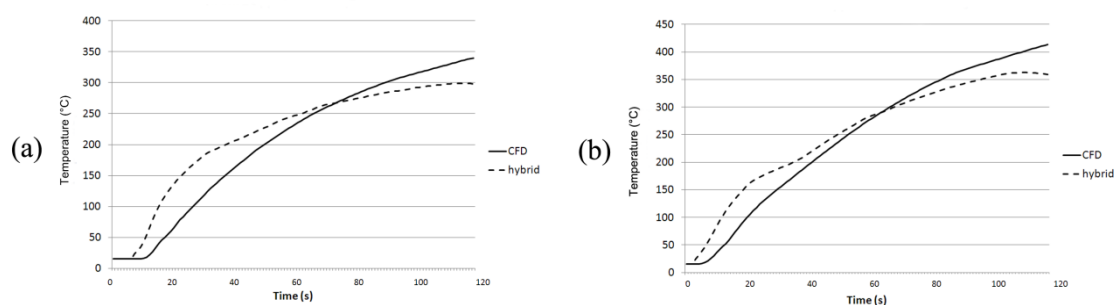
Fig. 13. Temperature comparisons for rooms 1 (a), and 5 (b), replaced by the zone model.
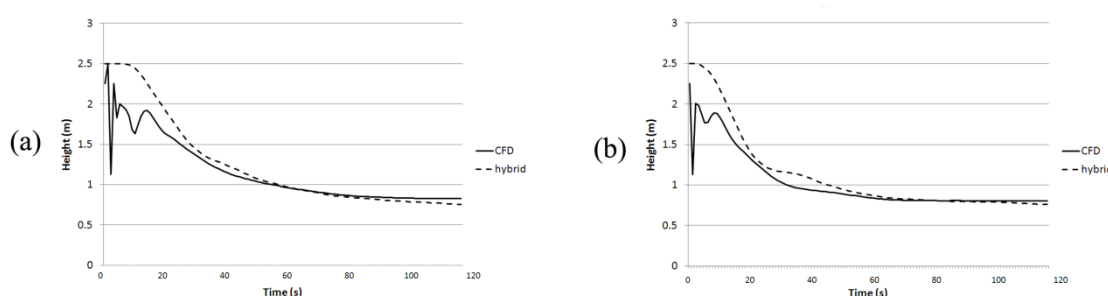
Fig. 14. Layer height comparisons for rooms 1 (a), and 5 (b), replaced by the zone model.

Figure 14 shows the layer height for the two rooms with better agreement between the two models. The hybrid model agrees well in both the size and transient development of the layers, reporting a slightly deeper layer towards the end of the simulation.

In both test cases, the method reported by Janssens and Tran [21] was used to determine average layer temperature and height based on data from a CFD fire model. This approach has produced some favourable comparisons in the two test cases, particularly with regard to layer height. It is worth noting that a positive (or negative) error in layer depth can be 'explained' somewhat by a negative (or positive) error in the layer temperature in so far as these values can vary without the total enthalpy of a layer being affected. These opposing errors are clearly apparent in Fig. 13 and Fig. 14, where an increasing disparity between the hybrid and CFD temperatures towards the end of the simulation could be explained by the fact that the hybrid layer continues to descend somewhat, as compared to that reported by the present CFD approximation. During the first 20 s there are fluctuations in the layer height for the CFD results; these are due to difficulties in the reduction method's ability to accurately determine the layer height when there are small temperature differences between the upper and lower layers. These fluctuations are not directly observed from the field values and is a numerical artefact of the method when a layer is not properly established. This suggests that a different method of obtaining layer averages from CFD data may produce more favourable comparisons than noted using the method of Janssens and Tran.

It is noted that for these simulations, the time required by the CFD simulation was 13 h 8min 38 s while the time required by the hybrid simulation was 6 h 51 min 29 s, a 48% reduction in run time. Thus, by removing some 56% of the CFD solution domain, the hybrid case achieved a saving of 48% in the run time. This suggests that the hybrid model is returning an 86% computational efficiency (i.e. the model achieves a 86% (0.48/0.56) saving of the maximum expected savings to be made through removal of part of the domain). While this is a considerable saving in run time, by optimizing the hybrid code, it is felt that this can be further improved. However, the hybrid

approach can only decrease the computational requirements of a simulation through reducing the size of the solution matrix within the CFD code. Since the run time required to perform the CFD solution procedure is not exclusively spent on operations on the system matrix, this percentage reduction in computational time cannot be expected to be directly proportional to the reduction of the computational mesh. It is worth noting that the total simulation time also includes time required by procedures external to the solution routine itself, such as GUI considerations or data print export, which are not affected by the hybrid implementation. It is also noted that the hybrid model can also be made to run in parallel, further reducing the run time assocated with the CFD component of the hybrid model.

CONCLUSION

A hybrid fire model has been developed that directly couples CFD fire simulation with zone modeling. The coupling is two-way with temperature and flow data passing from the field model to the zone model and from the zone model to the field model. The hybrid fire model makes use of the CFD fire model SMARTFIRE and two zone models, CFAST and an in-house zone model. The use of the hybrid model with CFAST was demonstrated in a previous publication [13] while the use of the in-house zone model within the hybrid model has been demonstrated in this paper.

Two test cases were demonstrated, one involving a situation in which a single compartment was replaced by a zone model representation and another more complex example where five compartments off a corridor were replaced by a zone model representation. In both cases the fire compartment is modeled using the CFD approach. The results demonstrate that the temperatures and layer height within the zone modeled compartments are in good agreement with the full CFD solution and the zone modeled compartments have only a minor effect on the remaining CFD domain. These results demonstrate that the hybrid model is a viable approach, and is capable of accurately replacing compartments within the field model computation domain with compartments that are modeled using the zone model approach. It is noted that making comparisons between regions modeled using the zonal and field approach are not straight forward. Disparities between the forms of data generated by the respective models means that conversion of some form is required before equivalent comparisons can be made. Essentially, this means that it is necessary to reduce the resolution of the CFD data to that equivalent to a two layer uniform zone; clearly this must be performed through averaging of some kind. The choice of an appropriate method to use is not trivial and small differences in the averaged results can be expected based on the averaging scheme selected. It is thus difficult to be precise concerning the level of agreement achieved between the zone results and the CFD results.

The reduction in run time achieved by the hybrid approach represents 86% of the saving that could be expected for the associated reduction in the CFD computational domain. While the savings in computational time achieved by the hybrid model cannot be expected to scale directly to the reduction in the CFD computational domain, further improvements are expected through optimisation of the hybrid code. Further work is required to improve both the accuracy and convergence of the hybrid model and to test the approach on more complex cases. In addition, further developments of the hybrid approach will include radiation handling and transportation of species.

ACKNOWLEDGEMENT

REFERENCES

[1]   Yan, Z., and Holmstedt, G., "Investigation of the dance hall fire in Gothenburg, October 1998 - a comparison between human observation and CFD simulation," *Interflam 2001*, Interscience Communications, 2001, pp. 951-963.

[2]   Luo, M., and Beck. V., "Flashover fires in a full scale building: prediction and experiment," *Interflam 1996*, Interscience Communications, 1996, pp. 361-370.

[3]   Wang, Z., Jia, F., Galea, E.R., Patel, M.K., and Ewer, J., (2001) Simulating one of the CIB W14 round robin test cases using the SMARTFIRE fire field model, Fire Safety Journal 36(7): 661-677, http://dx.doi.org/10.1016/S0379-7112(01)00018-2.

[4]   Jia, F., Patel M.K., Galea E.R., Grandison, A., and Ewer, J., (2006) CFD Fire Simulation of the Swissair Flight 111 In-flight Fire - Part II: Fire Spread within the Simulated Area, The Aeronautical Journal of the Royal Aeronautical Society 110(1107): 303-314.

[5]   Chow, W.K., (1995) A comparison of the use of fire zone and field models for simulating atrium smoke-filling processes, Fire Safety Journal 25(4): 337-353, http://dx.doi.org/10.1016/0379-7112(96)00001-X.

[6]   Grandison, A.J., Galea, E.R., Patel, M.K., and Ewer, J., (2003) The development of parallel implementation for a CFD based fire model utilising conventional office based PCs, Journal of Applied Fire Science 12(2): 137-157, http://dx.doi.org/10.2190/AGH5-EXUR-J110-HPHe.

[7]   Hurst-Clark, N.M., Ewer, J.A.C., Grandison, A.J., and Galea, E.R., "Group Solvers: A Means of Reducing Run-Times and Memory Overheads for CFD Based Fire Simulation Software," *Interflam 2004*, Interscience Communications, 2004, pp. 659-664.

[8]   Xu, T., Wang, J., and Fan, W., "A new method of modelling of a fire - combination of field modelling and zone modelling," *Symposium on Engineering Thermophysics*, ZhenJiang, China, 1991, pp. 33-45.

[9]   Wang, J., and Fan, W., (1996) Numerical simulation of fire process of multi-rooms, J Univ Sci Technol 26: 204-209.

[10]   Hua, J., Wang, J., and Kumar, K., (2005) Development of a hybrid field and zone model for fire smoke propagation simulation in buildings, Fire Safety Journal 40(2): 99-119, http://dx.doi.org/10.1016/j.firesaf.2004.09.005.

[11]   Jones, W.W., Peacock, R.D., Forney, G.P., and Reneke, P.A., "CFAST – Consolidated Model of Fire Growth and Smoke Transport (Version 6), Technical Reference Guide," National Institute of Standards and Technology Special Publication 1026, Gaithersburg, MD, 2009.

[12]   Wang, Z., Jia, F., and Galea, E., (2007) Predicting toxic gas concentrations resulting from enclosure fires using local equivalence ratio concept linked to fire field models, Fire and Materials 31(1): 27-51, http://dx.doi.org/10.1002/fam.924.

[13]   Burton, D.J., Grandison, A.J., Patel, M.K., Galea, E.R., and Ewer, J.C., "Introducing a hybrid field/zone fire modelling approach for fire simulation," *Interflam 2007*, Interscience Communications, 2007, pp. 1491-1497.

[14]   Quintiere, J., "Growth of fires in building compartments," American Society for Testing and Materials, ASTM STP 614, Philadelphia, PA, 1977.

[15]   Pape, R., Waterman, T.E., and Eichler, T.V., "Development of a fire in a room from ignition to full room involvement - RFIRES," National Bureau of Standards, NBS-GCR-81-301, Washington, 1981.

[16]   Galea, E., (1989) On the Field Modelling Approach to the Simulation of Enclosure Fires, Journal of Fire Protection Engineering 1(1): 11-22, http://dx.doi.org/10.1177/104239158900100103.

[17] Li, Y.F., and Chow, W.K., (2004) Modelling of water mist fire suppression systems by a one-zone model, Combustion Theory and Modelling 8(3): 567-592, http://dx.doi.org/10.1088/1364-7830/8/3/008.

[18] Konecki, M., and Pólka, M., (2009) Extension of the fire zone model with some detailed mass and heat transfer mechanisms, Journal of Applied Sciences Research 5(2): 212-220.

[19] Chen, X., Yang, L., Deng, Z., and Fan, W., (2004) A multi-layer zone model for predicting temperature distribution in a fire room, Progress in Natural Science 14(6): 536-540, http://dx.doi.org/10.1080/10020070412331343901.

[20] Patankar, S.V., *Numerical Heat Transfer and Fluid Flow*, McGraw-Hill, New York, 1980.

[21] Janssens, M. and Tran, H., (1992) Data Reduction of Room Tests for Zone Model Validation, Journal of Fire Sciences 10(6): 528-555, http://dx.doi.org/10.1177/073490419201000604.